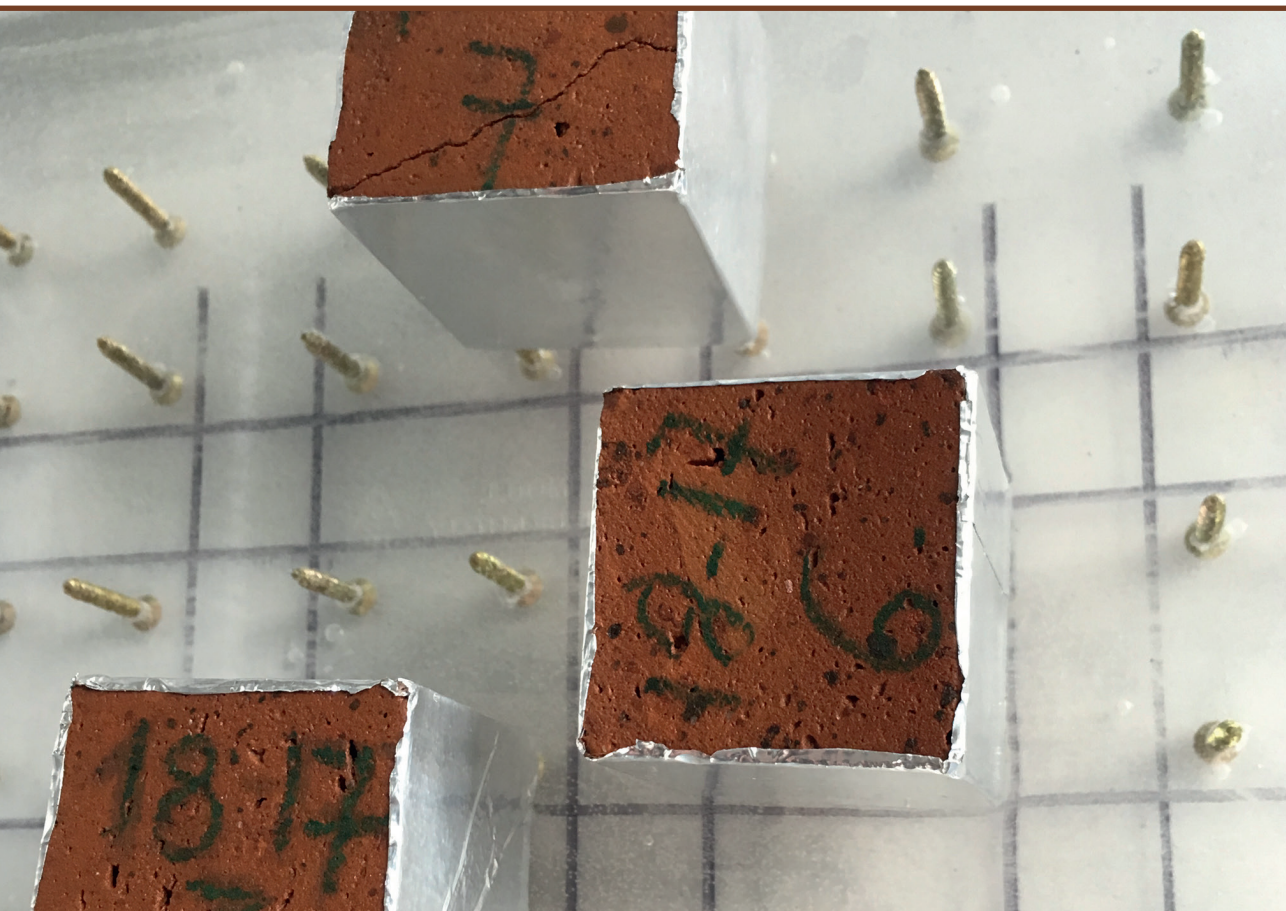**Ritvars Freimanis**

HIGROTERMĀLIE PROCESI PORAINOS MATERIĀLOS

Promocijas darbs

RĪGAS TEHNISKĀ UNIVERSITĀTE

Elektrotehnikas un vides inženierzinātņu fakultāte
Vides aizsardzības un siltuma sistēmu institūts

Ritvars Freimanis

Doktora studiju programmas "Vides inženierija" doktorants

HIGROTERMĀLIE PROCESI PORAINOS MATERIĀLOS

Promocijas darbs

Zinātniskā vadītāja
profesore *Dr. sc. ing.* ANDRA BLUMBERGA

RTU Izdevniecība
Rīga 2023

**PROMOCIJAS DARBS IZVIRZĪTS
ZINĀTNES DOKTORA GRĀDA IEGŪŠANAI
RĪGAS TEHNISKAJĀ UNIVERSITĀTĒ**

Promocijas darbs zinātnes doktora (*Ph. D.*) grāda iegūšanai tiek publiski aizstāvēts 2023. gada 21. decembrī plkst. 14.00 Rīgas Tehniskās universitātes Elektrotehnikas un vides inženierzinātņu fakultātē, Āzenes ielā 12/1, 212. telpā.

OFICIĀLIE RECENZENTI

Ph. D. Pål Ingebrigt Davidsen,
Bergenas Universitāte, Norvēģija

Dr. sc. (tech.) Peter D. Lund,
Ālto Universitāte, Somija

Dr. sc. ing. Gatis Bažbauers,
Rīgas Tehniskā universitāte

APSTIPRINĀJUMS

Apstiprinu, ka esmu izstrādājusi šo promocijas darbu, kas iesniegts izskatīšanai Rīgas Tehniskajā universitātē zinātnes doktora (*Ph. D.*) grāda iegūšanai. Promocijas darbs zinātniskā grāda iegūšanai nav iesniegts nevienā citā universitātē.

Ritvars Freimanis ……………………….. (paraksts)

Datums: ………………….

Promocijas darbs ir uzrakstīts latviešu valodā, tajā ir ievads, trīs nodaļas, secinājumi, literatūras saraksts, 36 attēli, četras tabulas, 10 pielikumu, kopā 213 lappuses. Literatūras sarakstā ir 59 nosaukumi.

ANOTĀCIJA

Lielākais enerģijas patērētājs Eiropā ir ēku sektors, kas izmanto aptuveni 40 % no kopējā enerģijas patēriņa un rada aptuveni 36 % no kopējām CO_2 emisijām Eiropas Savienībā. No kopējā EU ēku fonda, tikai 25 % ēku tiek klasificētas kā energoefektīvas un tiek prognozēts, ka 85 % – 95 % no esošā ēku fonda 2050. gadā vēl būs ekspluatācijā [1]. Iedzīvotāju prasības pēc paaugstināta komforta, plašāks elektroiekārtu lietojums u. c. ir iemesli, kas veicina enerģijas patēriņa pieaugumu. Enerģijas patēriņa pieaugums ir viens no klimata pārmaiņu veicinātājiem. Ir vairākas jomas, kur būtu iespējams izmantot enerģiju efektīvāk, tā samazinot patēriņu, kā rezultātā samazināt siltumnīcefekta gāzu emisijas. Lai Eiropas Savienība 2050. gadā sasniegtu oglekļa neitralitāti, ir izvirzīti ambiciozi mērķi, kuri ietver ēku energoefektivitātes paaugstināšanu, atjaunojamo energoresursu lietošanu un siltumnīcefektu gāzu emisiju samazināšanu [2]. Ēku siltināšana ir efektīvs ēku energoefektivitātes paaugstināšanas pasākums, bet lai to īstenotu ir jāpārvar vairākas barjeras, kuras var būt gan finansiālas, gan sentimentālas. Lai sasniegtu mērķus ir jārod risinājums dilemmai starp vidi kurā dzīvojam, kas sevī ietver kultūrvēsturiskā mantojuma saglabāšanu un energoefektivitātes paaugstināšanu. Apbūvētā vide ir viena no būtiskām kultūras vērtībām – tā veido dzīvošanai nepieciešamo vidi un ir būtiska dzīves kvalitātei [3]. Šī dilemma parāda, ka no vienas puses, esošajā ēku fondā slēpjas liels energoefektivitātes potenciāls, bet, no otras puses, jānodrošina kultūras vērtību saglabāšana. Viens no šīs dilemmas risinājumiem ir vēsturisko ēku siltināšana no iekšpuses, kas ļauj saglabāt vēsturisko ēku fasādes izskatu-vidi, vienlaikus paaugstinot ēkas energoefektivitāti. Tomēr šāds risinājums veicina izmaiņas ēkas higtrotermālajos procesos, kas var veicināt nevēlamas sekas – pelējums, ķieģeļu drupšana, sāls pleķi u. c.

Darba mērķis ir novērtēt iespējas izveidot pozitīvas energobilances kvartālu kultūrvēsturiskā pilsētvidē, izmantojot mitruma drošu ēku siltināšanu no iekšpuses.

Promocijas darbs ir izstrādāts kā desmit savstarpēji saistītu starptautisku zinātnisku publikāciju kopa. Promocijas darbs sastāv no ievada, trīs nodaļām, secinājumiem un publikāciju pielikuma.

Darbā izvirzītas četras hipotēzes, kas pētītas ar dažādām zinātniskās izpētes metodēm, tajā skaitā, mērījumi reālos objektos, mērījumu veikšana laboratorijas apstākļos, multikritēriju analīze un higrotermālo procesu datorsimulācija. Darbs sākas ar ievadu, kam seko literatūras apskats un nodaļa par metodiku. Trešajā nodaļā ir aprakstīti iegūtie rezultāti. Darbs noslēdzas ar secinājumiem un publikāciju pielikumu.

ANNOTATION

The biggest consumer of energy in Europe is the building sector, which uses about 40 % of the total energy consumption and generates about 36 % of the total CO_2 emissions in the European Union (EU). Of the total EU building stock, only 25 % of buildings are classified as energy efficient and it is predicted that 85 % – 95 % of the existing building stock will still be in operation in 2050 [1]. Residents' demands for increased comfort, wider use of electrical equipment, etc., contribute to the increase in energy consumption. The increase in energy consumption is one of the contributors to climate change. There are several areas where it would be possible to use energy more efficiently, thus reducing consumption and, as a result, reducing greenhouse gas emissions. In order for the EU to achieve carbon neutrality in 2050, ambitious goals have been set – which include increasing the energy efficiency of buildings, using renewable energy resources and overall reducing greenhouse gas emissions [2]. Building insulation is an effective measure for increasing the energy efficiency of buildings, but in order to implement it, several barriers must be overcome, which can be both financial and sentimental. In order to achieve the goals, it is necessary to find a solution to the dilemma between the environment in which we live, which includes preserving the cultural and historical heritage and increasing energy efficiency. The built environment is one of the essential cultural values – it forms the environment necessary for living and is essential for the quality of life [3]. This dilemma shows that, on the one hand, there is great potential for energy efficiency in the existing building stock, but on the other hand, the preservation of cultural values must be ensured. One of the solutions to this dilemma is insulating of historic buildings from the inside, which allows preserving the built environment, e.g. the facade of historic buildings, while increasing the building's energy efficiency. However, such a solution contributes to changes in the hygrothermal processes of the building, which can contribute to undesirable consequences, such as mold, brick deterioration, salt stains, etc.

The aim of the work is to assess the possibilities of creating a positive energy balance quarter in a cultural and historical urban environment, using moisture-proof building insulation from the inside.

The thesis is developed as a set of ten interrelated international scientific publications. The thesis consists of an introduction, three chapters, conclusions and an appendix of publications.

Four hypotheses are put forward in the work, which have been studied with various scientific research methods, including measurements in real objects, measurements in laboratory conditions, multi-criteria analysis and computer simulation of hygrothermal processes. The work begins with an introduction, followed by a literature review and a chapter on methodology. The third chapter describes the obtained results. The work ends with Conclusions and an appendix of publications.

SATURS

Promocijas darbā izmantotie zinātniskie raksti

- A publikācija. Freimanis R., Zundans Z., Balins R., Blumberga A. un Vanaga R. (2021). Hygrothermal Properties of Historic Bricks From Various Sites of Latvia [Data set]. *Zenodo. https://doi.org/10.5281/zenodo.5575101*
- B publikācija. Freimanis R., Blumberga A., Vanaga R., Zundāns Z., Evaluation of the Impact of Bricks of Various Characteristics on Internally Insulated Masonry Walls in Cold Climate*, Buildings 2023, 13 (10), 2529, https://doi.org/10.3390/buildings13102529*
- C publikācija. Freimanis, R., Zundans, Z., Balins, R., Vanaga, R., Blumberga, A., Finding the Generic Hygrothermal Properties of Historical Bricks by Supervised Agglomerative Clustering*, Environmental and Climate Technologies, 2022, 26 (1), pp. 1234–1243. https://doi.org/10.2478/rtuect-2022-0093*
- D publikācija. Biseniece, E., Freimanis, R., Purvins, R., .Pumpurs, A., Blumberga, A., Study of Hygrothermal Processes in External Walls with Internal Insulation*, Environmental and Climate Technologies, 2018, 22 (1), pp. 22–41. https://doi.org/10.1515/rtuect-2018-0002*
- E publikācija. R. Freimanis, R. Vanaga, V. Balodis, Z. Zundans, A. Blumberga, Hygrothermal assessment of insulation systems for internal insulation of solid masonry walls under various conditions, *Buildings 2023, 13 (10), 2511; https://doi.org/10.3390/buildings13102511*
- F publikācija. Blumberga A., Freimanis R., Muizniece I., Spalvins K., Blumberga D., Trilemma of historic buildings: Smart district heating systems, bioeconomy and energy efficiency, *Energy 2019, 186, art. no. 115741. https://doi.org/10.1016/j.energy.2019.07.071*
- G publikācija. Blumberga, A., Freimanis, R., Biseniece, E., Kamenders, A., Hygrothermal Performance Evaluation of Internally Insulated Historic Stone Building in a Cold Climate*, Energies, 2023, 16 (2), 866. https://doi.org/10.3390/en16020866*
- H publikācija. Freimanis, R., Vaiskunaite, R., Bezrucko, T., Blumberga, A., In-situ moisture assessment in external walls of historic building using non-destructive methods*, Environmental and Climate Technologies, 2019, 23 (1), pp. 122–134. https://doi.org/10.2478/rtuect-2019-0009*
- I publikācija. Blumberga, A., Vanaga, R., Antuzs, J., .Bondars, E., Treija, S., Is the High Quality Baukultur a Monkey Wrench in the Global Climate Challenges? *Environmental and Climate Technologies, 2019, 23 (3), pp. 230–244. https://doi.org/10.2478/rtuect-2019-0092*
- J publikācija. Blumberga, A., Vanaga, R., Freimanis, R., Bondars, E., Treija, S., Transition from traditional historic urban block to positive energy block, *Energy, 2020, 202, 117485. https://doi.org/10.1016/j.energy.2020.117485*

Lietotie saīsinājumi

SET plāns – Eiropas energotehnoloģiju stratēģiskais plāns;
EPS – ekspandētais putupolistirols;
SEG – siltumnīcefekta gāzes;
IKT – informācijas un komunikāciju tehnoloģijas;
AER – atjaunojamie energoresursi;
skat. – skatīt;
t. sk. – tai skaitā;
et.at. – un citi;
Att. – attēls;
ML – mašīnmācība;
XPS – ekstrudētais putupolistirols;
PIR – poliizocianurāts;
TDR – laika domēna reflektometrs;
VWC – tilpuma ūdens saturs;
Sd – tvaika difūzijas pretestība;
ZA – ziemeļaustrumi;
DA – dienvidaustrumi;
DR – dienvidrietumi;
CO_2 – Oglekļa dioksīds;
PV – fotoelements;
RVC – Rīgas vēsturiskais centrs;
UNESCO – Apvienoto Nāciju Izglītības, zinātnes un kultūras organizācija;
ES – Eiropas Savienība;
PFA – teflons

IEVADS

Aktualitāte

Viens no lielākajiem enerģijas patērētājiem Eiropā ir ēku sektors. Tas rada aptuveni 40 % no kopējā enerģijas patēriņa un aptuveni 36 % no kopējajām CO_2 emisijām Eiropas Savienībā. Turklāt tikai 25 % no Eiropas Savienības ēku fonda tiek klasificētas kā energoefektīvas, un prognozes rāda, ka 2050. gadā 85–95 % esošo ēku joprojām būs ekspluatācijā [1]. Iedzīvotāju pieprasījums pēc paaugstināta komforta un pieaugošā elektroiekārtu izmantošanas tendence, kā arī citi faktori veicina enerģijas patēriņa pieaugumu, kas ir viens no klimata pārmaiņu iemesliem. Ir vairākas jomas, kurās būtu iespējams izmantot enerģiju efektīvāk, samazinot patēriņu un tādējādi arī siltumnīcefekta gāzu emisijas. Tāpēc, lai sasniegtu oglekļa neitralitāti līdz 2050. gadam, Eiropas Savienība ir definējusi ambiciozus mērķus, kas ietver ēku energoefektivitātes paaugstināšanu, atjaunojamo energoresursu lietošanu un siltumnīcefekta gāzu emisiju samazināšanu [2].

Ēku siltināšana ir efektīvs pasākums ēku energoefektivitātes uzlabošanai, taču, lai sasniegtu šos mērķus, būtiski ir rast risinājumu dilemmai starp kultūrvēsturisko mantojumu un energoefektivitāti, jo apbūvētā vide ir būtiska kultūras vērtība, kas veido nepieciešamo dzīves vidi un ietekmē dzīves kvalitāti [3]. Viens šīs dilemmas risinājums varētu būt vēsturisko ēku siltināšana no iekšpuses, saglabājot fasādes izskatu un vienlaikus paaugstinot energoefektivitāti. Tomēr šāds risinājums var izraisīt nevēlamas, neparedzētas izmaiņas ēkas higrotermālajos procesos, kas potenciāli var radīt problēmas, piemēram, pelējumu, ķieģeļu drupšanu, sāls pleķus u. c.

Apsverot iekšējo siltināšanu, ir svarīgi veikt higrotermisko novērtējumu. Detalizēta plānošana samazina risku, kas saistīts ar izmaiņām higrotermiskajā uzvedībā. Plānojot jāņem vērā dažādi faktori, piemēram, ķieģeļu īpašības oriģinālajā mūrī, siltumizolācijas materiāli, āra un iekštelpu robežapstākļi. Kvantitatīvā saistība starp dažādiem faktoriem un to kopējo ietekmi uz mitruma risku joprojām nav skaidra, un faktoru sarežģītās mijiedarbības ietekmē mitruma riska izvērtēšana ir sarežģīta. Tā rezultātā vēsturisko ēku un vēsturisko ēku pilsētas kvartālu energoefektivitātēs pasākumu risinājumu plānošana un izvēle ir sarežģīts process, kas ietver nepieciešamību ēku īpašniekiem un apsaimniekotājiem novērtēt riskus un ieguvumus, siltinot ēkas no iekšpuses.

Izpētes jautājumi

1. Vai ir iespējams sasniegt pozitīvu energobilances kvartālu vēsturiskā pilsētas apbūvē.
2. Kādas ir mitruma drošas iekšējās siltumizolācijas sistēmas, ko var iekļaut energoefektivitātes renovācijas projektos, lai palīdzētu sasniegt pozitīvas energobilances vēsturiskās apbūves pilsētas kvartālu.

Darba mērķis un uzdevumi

Darba mērķis ir novērtēt iespējas izveidot pozitīvas energobilances kvartālu kultūrvēsturiskā pilsētvidē, izmantojot mitruma drošu ēku siltināšanu no iekšpuses.

Lai sasniegtu mērķi, definēti vairāki uzdevumi.

1. Veikt vēsturisko mūra un akmens ārsienu materiālu higrotermisko parametru novērtējumu.
2. Novērtēt vēsturisko ārsienu materiālu higrotermisko parametru ietekmi uz higrotermālajiem procesiem sienā, kas siltināta no iekšpuses.
3. Veikt siltumizolācijas materiālu un sistēmu lietojuma novērtēšanu izmantošanai siltināšanai no iekšpuses.
4. Veikt novērtējumu par siltināšanas no iekšpuses ietekmi uz higrotermiskajiem procesiem un potenciālo enerģijas ietaupījumu dabīgā akmens mūra sienā un ķieģeļu sienā, kas siltinātas ar tvaika necaurlaidīgu siltumizolāciju.
5. Novērtēt pozitīva energobilances kvartāla izveidi vēsturiskā pilsētvides apbūvē.
6. Novērtēt energoefektivitātes risinājumu potenciālu vēsturiskā pilsētas kvartālā.

Izvirzītās hipotēzes

1. **hipotēze.** Vēsturiskiem ķieģeļiem ir atšķirīgas higrotermālās īpašības, un tās ietekmē higrotermālos procesus no iekšpuses siltinātās masīvās mūra sienās.
2. **hipotēze.** Klimatiskie āra apstākļi ietekmē higrotermālos procesus no iekšpuses siltinātās masīvās mūra sienās.
3. **hipotēze.** Vēsturiskās mūra un akmens sienu siltināšana no iekšpuses ar tvaika necaurlaidīgu siltumizolāciju aukstā klimatā ir drošs energoefektiviātes paaugstināšanas pasākums.
4. **hipotēze.** Vēsturiskās apbūves saglabāšana neļauj sasniegt pozitīvu energobilanci vēsturiskajos pilsētas kvartālos.

Iepriekšminētās hipotēzes tika pētītas ar dažādām zinātniskās izpētes metodēm, kas sīkāk atspoguļotas zinātniskajās publikācijās.

1. hipotēze. Vēsturiskiem ķieģeļiem ir atšķirīgas higrotermālās īpašības, un tās ietekmē higrotermālos procesus no iekšpuses siltinātās masīvās mūra sienās.

1. Zinātniskās literatūras analīze.
2. 40 vēsturisko ķieģeļu paraugu savākšana un higrotermālo īpašību testēšana.
3. Datorsimulācijas rīka *Delphin* failu izveidošana.
4. Testēto ķieģeļu klasteru veidošana.
5. Datorsimulācija ar mūra ārsienām no testētajiem ķieģeļiem un siltināšanu no iekšpuses ar kapilāri aktīvu siltumizolācijas materiālu.

Izmantotās izpētes metodes un iegūtie rezultāti ir aprakstīti šādās publikācijās.

- A publikācija (Freimanis R., Zundans Z., Balins R., Blumberga A. un Vanaga R. (2021). Hygrothermal Properties of Historic Bricks From Various Sites of Latvia

[Data set]. *Zenodo. https://doi.org/10.5281/zenodo.5575101*) Publikācija ir datu kopa, kurā ir iekļauti 40 dažādu Latvijas vēsturisko ķieģeļu (no 17. līdz 20. gadsimtam) paraugu higrotermiskos parametru testēšanas rezultāti. Ķieģeļu paraugu higrotermisko parametru noteikšanai tika izmantotas standarta mērījumu metodes ar dažiem pielāgojumiem. Iegūtie parametri izmantoti, lai izveidotu materiālu failus simulācijas rīkā *Delphin*.

- B publikācija (Freimanis R., Blumberga A., Vanaga R., Zundāns Z., Evaluation of the Impact of Bricks of Various Characteristics on Internally Insulated Masonry Walls in Cold Climate*, Buildings 2023, 13 (10), 2529, https://doi.org/10.3390/buildings13102529*). Šī pētījuma galvenais mērķis bija klasterēt Latvijā atrastos 40 vēsturiskos ķieģeļus, kas tika testēti iepriekšējā publikācijā. Tas tika veikts, izmantojot ķieģeļu higrotermiskās īpašības un *Delphin* simulācijas rezultātus. Higrotermisko īpašību klasterizācijas rezultāti tika savstarpēji pārbaudīti ar *Delphin* simulācijas datu klasterizācijas rezultātiem. Divas no deviņām kopām ietver 67,5 % no visiem paraugiem, četros klasteros bija tikai viens paraugs, citās kopās – divi, trīs un četri paraugi.

- C publikācija (Freimanis, R., Zundans, Z., Balins, R., Vanaga, R., Blumberga, A., Finding the Generic Hygrothermal Properties of Historical Bricks by Supervised Agglomerative Clustering*, Environmental and Climate Technologies, 2022, 26 (1), pp. 1234–1243. https://doi.org/10.2478/rtuect-2022-0093*). Šī pētījuma mērķis bija novērtēt tvaika caurlaidīgas kapilāri aktīvās kalcija silikāta siltumizolācijas sistēmas ietekmi uz dažādu vēsturisku ķieģeļu mūra higrotermisko uzvedību aukstā klimatā ar līmi un bez tās, ja siltināšana tiek veikta no telpas puses. Skaitliskajos eksperimentos tika izmantoti A un B publikācijās aprakstīto testu rezultāti par 40 vēsturisko ķieģeļu higrotermālajām īpašībām. Pētījumā tika novērtēta ķieģeļu veida, kalcija silikāta lietošanas kvalitātes un aukstā klimata ietekme uz higrotermisko uzvedību. Rezultāti rāda, ka temperatūras uzvedība ir līdzīga visiem sienu tipiem, turpretim mitruma uzvedībā ir vērojama liela atšķirība.

2. hipotēze. Klimatiskie āra apstākļi ietekmē higrotermālos procesus no iekšpuses siltinātās masīvās mūra sienās.
1. Zinātniskās literatūras analīze.
2. Siltināšanas sistēmu laboratorijas testi un datorsimulācijas konstantos apstākļos.
3. Siltināšanas sistēmu laboratorijas testi un datorsimulācijas dinamiskos apstākļos.
4. Jauna siltumizolācijas materiāla testēšana izmantošanai siltināšanai no iekšpuses.

Izmantotās metodes un iegūtie rezultāti ir publicēti šādās publikācijās.
- D publikācija (Biseniece, E., Freimanis, R., Purvins, R., .Pumpurs, A., Blumberga, A., Study of Hygrothermal Processes in External Walls with Internal Insulation*, Environmental and Climate Technologies, 2018, 22 (1), pp. 22–41. https://doi.org/10.1515/rtuect-2018-0002*). Šajā pētījumā tika veikta higrotermālās simulācijas rezultātu salīdzināšana ar eksperimentālajiem rezultātiem, kas iegūti

no iekšpuses siltināta vēsturisko ķieģeļu mūra testēšanā. Pētījums veikts ar četriem siltumizolācijas materiāliem (minerālvate, *EPS*, kokšķiedra un granulēts aerogēls) aukstā klimatā (vidēji 4000 apkures grādu dienu). Rezultāti rāda, ka ir atšķirības starp izmērītajiem un simulētajiem pētīto konstrukciju higrotermiskajiem rādītājiem, un to cēlonis ir atšķirības starp izmantoto materiālu parametriem un sākotnējiem apstākļiem.

- E publikācija (R. Freimanis, R. Vanaga, V. Balodis, Z. Zundans, A. Blumberga, Hygrothermal assessment of insulation systems for internal insulation of solid masonry walls under various conditions, *Buildings 2023, 13 (10), 2511; https://doi.org/10.3390/buildings13102511*). Šajā pētījumā novērtēta masīvu mūra sienu higrotermiskā veiktspēja ar 17 siltumizolācijas sistēmām, kas pakļautas dažādiem ārējiem robežapstākļiem, ieskaitot līdzsvara stāvokļa ciklu, dinamisku sausuma ciklu, vēja virzītu ciklu un žāvēšanas ciklu. Eksperimentu laikā tika mērīts relatīvais mitrums un temperatūra zem izolācijas. Papildus tika mērītas relatīvās mitruma izmaiņas mūrī. Rezultāti liecina, ka testētajām siltumizolācijas sistēmām ir līdzīga siltuma veiktspēja, vienlaikus atšķirīga mitruma veiktspēja. Tvaika necaurlaidīgām un tvaiku necaurlaidīgām izolācijas sistēmām dažādos testa ciklos ir atšķirīga higrotermiskā uzvedība atkarībā no materiāla tvaika difūzijas pretestības. Skaitliskās simulācijas ir jutīgas pret materiālu higrotermālajām īpašībām.
- F publikācija (Blumberga A., Freimanis R., Muizniece I., Spalvins K., Blumberga D., Trilemma of historic buildings: Smart district heating systems, bioeconomy and energy efficiency, *Energy 2019, 186, art. no. 115741. https://doi.org/10.1016/j.energy.2019.07.071*). Šajā pētījumā ir novērtēta inovatīva priežu skuju siltumizolācijas materiāla kā iekšējās siltumizolācijas materiāla lietojamība vēsturiskām masīvām sienām. Rezultāti rāda, ka pētītais materiāls ir ļoti porains, tam ir augsta mitruma pārnese, mitruma akumulācijas spēja.

3. hipotēze. Vēsturiskās mūra un akmens sienu siltināšana no iekšpuses ar tvaika necaurlaidīgu siltumizolāciju aukstā klimatā ir drošs energoefektiviātes paaugstināšanas pasākums.

1. Zinātniskās literatūras analīze.
2. Mērījumu veikšana divās ēkās, kas siltinātas no iekšpuses ar tvaika necaurlaidīgu barjeru.
3. Higrotermālo procesu datorsimulācija divu ēku ārsnienās, kas siltinātas no iekšpuses ar tvaika necaurlaidīgu barjeru.
4. Enerģijas patēriņa analīze divās ēkās, kas siltinātas no iekšpuses ar tvaika necaurlaidīgu barjeru.

Izmantotās izpētes metodes un iegūtie rezultāti ir aprakstīti šādās publikācijās.

- G publikācija (Blumberga, A., Freimanis, R., Biseniece, E., Kamenders, A., Hygrothermal Performance Evaluation of Internally Insulated Historic Stone Building in a Cold Climate, *Energies, 2023, 16 (2), 866. https://doi.org/10.3390/en16020866*). Šī pētījuma mērķis bija veikt higrotermālās uzvedības ilgtermiņa monitoringu no iekšpuses siltinātai vēsturiskai dolomīta akmens sienai. Monitoringa rezultāti salīdzināti ar 1D higrotermiskām simulācijām un ēkas

enerģijas patēriņa simulāciju. Mērījumu rezultāti un higrotermiskais novērtējums liecina, ka enerģijas patēriņš ir samazinājies par 55 %, relatīvajam mitrumam zem izolācijas lielāko daļu laika saglabājoties 60 %, bet īslaicīgi pieaugot par 80 %. Enerģijas patēriņa simulācija parāda enerģijas ietaupījuma potenciālu līdz pat 72 % pareizas enerģijas pārvaldības gadījumā.

- H publikācija (Freimanis, R., Vaiskunaite, R., Bezrucko, T., Blumberga, A., In-situ moisture assessment in external walls of historic building using non-destructive methods, *Environmental and Climate Technologies, 2019, 23 (1), pp. 122–134. https://doi.org/10.2478/rtuect-2019-0009*). Šajā pētījumā ir veikti *in situ* mitruma un temperatūras mērījumi no iekšpuses siltinātā ķieģeļu mūrī vēsturiskā ēkā Vecrīgā. Rezultāti liecina, ka gada aukstajos mēnešos mitruma problēmas nepalielinās – zem iekšējās siltumizolācijas neveidojas kondensāts un nepastāv pelējuma veidošanās risks. Tomēr ēkas fasādi būtiski ietekmē klimatiskie laikapstākļi, un lietus laikā palielinās mūra mitrums.

4. hipotēze. Vēsturiskās apbūves saglabāšana neļauj sasniegt pozitīvu energobilanci vēsturiskajos pilsētas kvartālos.
1. Zinātniskās literatūras analīze.
2. Daudzkritēriju analīze par vēsturiskā kvartāla pāreju uz pozitīvu enerģijas kvartālu no arhitektūras un ēku energoefektivitātes aspektiem.
3. Enerģijas bilances vērtējums vēsturiskā kvartāla pārejai uz pozitīvu enerģijas kvartālu.
Izmantotās metodes un rezultāti ir atspoguļoti šajā publikācijā.

- I publikācija (Blumberga, A., Vanaga, R., Antuzs, J., .Bondars, E., Treija, S., Is the High Quality Baukultur a Monkey Wrench in the Global Climate Challenges? *Environmental and Climate Technologies, 2019, 23 (3), pp. 230–244. https://doi.org/10.2478/rtuect-2019-0092*). Šajā rakstā ir aprakstīta dubultā daudzkritēriju analīze, novērtējot pilsētu kvartālus gan no energoefektivitātes, gan kultūras mantojuma perspektīvas. Piedāvātie daudzkritēriju analīzes kritēriji, lai novērtētu kultūras mantojumu, dzīvotspēju un energoefektivitātes potenciālu, raksturo pilsētas kvartāla specifiskās īpašības. Iegūtie rezultāti liecina, ka kvartāliem ar augstāku kultūrvērtību ir mazāks energoefektivitātes potenciāls, un otrādi.

- J publikācija (Blumberga, A., Vanaga, R., Freimanis, R., Bondars, E., Treija, S., Transition from traditional historic urban block to positive energy block, *Energy, 2020, 202, 117485. https://doi.org/10.1016/j.energy.2020.117485*). Pētījums ir vērsts uz pāreju no tradicionālā pilsētas kvartāla uz pozitīvās enerģijas kvartālu pilsētas vēsturiskā centra vidē. Tajā analizēti enerģijas patēriņa dati un izstrādāta koncepcija par iespējām samazināt enerģijas patēriņu, kā arī kvartālā ražot atjaunojamo enerģiju un atgūt siltumenerģiju no datu centriem un dzesēšanas blokiem. Rezultāti liecina, ka, lai sasniegtu pozitīvu enerģijas kvartālu, nepieciešami ļoti ambiciozi energoefektivitātes uzlabošanas mērķi.

Darba zinātniskā novitāte

- Veikta Latvijas vēsturisko ēku ķieģeļu higrotermisko parametru testēšana un klasteru veidošana.
- Veikta dažādu siltumizolācijas materiālu un sistēmu testēšana laboratorijas apstākļos par izmantošanu siltināšanai no iekšpuses vēsturiskās mūra ēkās aukstā klimatā
- Veikti ilgtermiņa *in-situ* mērījumi par vēsturisko akmens ārsienu siltināšanu reālā ēkā aukstā klimatā.
- Izstrādāta dubultā daudzkritēriju analīze, ar kuru veikta vēsturiska pilsētas kvartāla atlasīšana pēc kultūrvēsturiskajiem un energoefektivitātes kritērijiem
- Veikts novērtējums par pozitīvas enerģijas bilances kvartāla izveidi kultūrvēsturiskā pilsētvides apbūvē.

Darba praktiskais lietojums

Darbā iegūtie rezultāti ir būtiski būvinženieriem, arhitektiem un citiem speciālistiem, kas saistīti ar ēku renovāciju un siltināšanu. Darbā iegūtie mērījumu un dati atvieglo vēsturisko ēku un vēsturisko ēku pilsētas kvartālu energoefektivitātēs pasākumu risinājumu plānošanu un izvēli. Darbā izveidotie Latvijā iegūto vēsturisko ķieģeļu higrotermālo parametru faili ir pieejami ikvienam speciālistam, kas plāno veikt siltināmās konstrukcijas matemātisko modelēšanu. Pētījumā iegūtie secinājumi un atziņas var palīdzēt ēku īpašniekiem un apsaimniekotājiem novērtēt riskus un ieguvumus, siltinot ēkas no iekšpuses. Darbā iegūtie rezultāti ir būtiski arī politiku veidotājiem ne tikai valsts, bet arī pašvaldību līmenī, jo ļaus veidot ar ēku renovāciju saistītus normatīvos dokumentus, kas ir zinātnē balstīti. Tie var būt saistīti gan ar dažādiem konstruktīviem ēku siltināšanas risinājumiem, gan arī ar pilsētu kvartālu pārveidošanu par pozitīvas energobilances kvartāliem.

Darba rezultātu aprobācija

Zinātniskās publikācijas par tēmu
1. Freimains R., Zundans Z., Balins R., Blumberga A., un Vanaga R. (2021). Hygrothermal Properties of Historic Bricks From Various Sites of Latvia [Data set]. *Zenodo. https://doi.org/10.5281/zenodo.5575101.*
2. Freimanis R., Blumberga A., Vanaga R., Zundāns Z., Evaluation of the Impact of Bricks of Various Characteristics on Internally Insulated Masonry Walls in Cold Climate, *Buildings 2023, 13 (10), 2529, https://doi.org/10.3390/buildings13102529*
3. Freimanis, R., Zundans, Z., Balins, R., Vanaga, R., Blumberga, A., Finding the Generic Hygrothermal Properties of Historical Bricks by Supervised Agglomerative Clustering, *Environmental and Climate Technologies, 2022, 26 (1), pp. 1234–1243. https://doi.org/10.2478/rtuect-2022-0093.*

4. Biseniece, E., Freimanis, R., Purvins, R., Pumpurs, A., Blumberga, A. Study of Hygrothermal Processes in External Walls with Internal Insulation, *Environmental and Climate Technologies, 2018, 22 (1), pp. 22–41. https://doi.org/10.1515/rtuect-2018-0002.*

5. Freimanis R., Vanaga R., Balodis V., Zundans Z., Blumberga A. Hygrothermal assessment of insulation systems for internal insulation of solid masonry walls under various conditions, *Buildings 2023, 13 (10), 2511; https://doi.org/10.3390/buildings13102511.*

6. Blumberga A., Freimanis R., Muizniece I., Spalvins K., Blumberga D. Trilemma of historic buildings: Smart district heating systems, bioeconomy and energy efficiency, *Energy 2019, 186, art. no. 115741. https://doi.org/10.1016/j.energy.2019.07.071.*

7. Blumberga, A., Freimanis, R., Biseniece, E., Kamenders, A. Hygrothermal Performance Evaluation of Internally Insulated Historic Stone Building in a Cold Climate, *Energies, 2023, 16 (2), 866. https://doi.org/10.3390/en16020866.*

8. Freimanis, R., Vaiskunaite, R., Bezrucko, T., Blumberga, A. In-situ moisture assessment in external walls of historic building using non-destructive methods, *Environmental and Climate Technologies, 2019, 23 (1), pp. 122–134. https://doi.org/10.2478/rtuect-2019-0009.*

9. Blumberga, A., Vanaga, R., Antuzs, J., .Bondars, E., Treija, S. Is the High Quality Baukultur a Monkey Wrench in the Global Climate Challenges? *Environmental and Climate Technologies, 2019, 23 (3), pp. 230–244. https://doi.org/10.2478/rtuect-2019-0092.*

10. Blumberga, A., Vanaga, R., Freimanis, R., ...Bondars, E., Treija, S. Transition from traditional historic urban block to positive energy block, *Energy, 2020, 202, 117485. https://doi.org/10.1016/j.energy.2020.117485.*

Promocijas darba rezultāti prezentēti trīs starptautiskajās zinātniskajās konferencēs.

1. Starptautiskā zinātniskā konference "Vides un klimata tehnoloģijas", CONECT, 2022, Rīga, Latvija.
2. Starptautiskā zinātniskā konference "Vides un klimata tehnoloģijas", CONECT, 2020, Rīga, Latvija.
3. Starptautiskā zinātniskā konference "Vides un klimata tehnoloģijas", CONECT, 2019, Rīga, Latvija.

Darba struktūra un apjoms

Promocijas darba pamatā ir 10 tematiski vienotas zinātniskās publikācijas. Šīs publikācijas ir prezentētas un pētījumu rezultāti aprobēti vairākās starptautiskās konferencēs, kā arī tās ir pieejams zinātniskajās informācijas krātuvēs un ietvertas starptautiskajās datubāzēs. Promocijas darbs rakstīts latviešu valodā, tā struktūra ir balstīta izpētē par vēsturisko ēku energoefektivitāti, ko veido četras galvenās tēmas (1. att.).

1. Vēsturisko ēku būvmateriāli un konstrukcijas.
2. Siltumizolācijas materiāli un sistēmas.
3. Iekšējās siltināšanas lietojums vēsturiskās ēkās.
4. Pozitīvas enerģijas bilances kvartāls vēsturiskā pilsētvidē.

1. att. Promocijas darba tematiskā struktūra.

Promocijas darbā ir ievads, trīs nodaļas, secinājumi, izmantotās literatūras saraksts. Promocijas darba ievadā definēts darba mērķis un tā īstenošanai veicamie uzdevumi, aprakstīta pētījuma zinātniskā un praktiskā nozīme. Pirmajā nodaļā sniegts literatūras apskats par pētāmajām tēmām. Otrajā nodaļā izklāstītas pētījumu metodes, kas saistītas ar vēsturisko ēku energoefektivitāti un četrām izpētes apakštēmām (1. att.). Trešajā nodaļā apskatīti pētījumu rezultāti. Promocijas darba noslēgumā apkopoti gūtie secinājumi atbilstoši definētajām hipotēzēm. Promocijas darba literatūras sarakstā ir 59 nosaukumi.

1.   IZMANTOTĀ METODIKA

Šajā nodaļā aprakstītas darbā izmantotās zinātniskās izpētes metodes. Tās detalizēti ir atspoguļotas zinātnisko žurnālu publikācijās un prezentētas starptautiskās konferencēs, un atsauces uz šīm publikācijām (skat. publikāciju sarakstu ievada nodaļā) ir izmantotas visā nodaļā. Darbā izmantotas dažādas zinātniskās izpētes metodes, t. sk. matemātiskā modelēšana, materiālu un konstrukciju testēšana laboratorijā un mērījumu veikšana reālās ēkās, kā arī daudzkritēriju analīzes metode.

1.1.   Vēsturisko ēku materiāli un konstrukcijas

Lai varētu veikt datorsimulācijas ārsienu siltināšanai no iekšpuses, nepieciešami izejas parametri par katra simulācijā izmantotā materiāla higrotermālajām īpašībām. Simulācijas rezultātu precizitāte ir atkarīga no ievades datu atbilstības konkrētajai sienai, tāpēc materiālu parametru vērtībām jābūt pēc iespējas tuvākiem pētāmās sienas parametru vērtībām. Šajā pētījumā izmantota datorprogramma *Delphin*, kas izstrādāta Drēzdenes Tehniskajā universitātē.

Pētījuma gaitā tika veikta 40 vēsturisko ķieģeļu paraugu vākšana no dažādiem Latvijas reģioniem. Paraugi tika vākti, meklējot ēkas, kas tiek renovētas vai nojauktas, vai arī ir sabrukušas. Paraugu maksimālo skaitu noteica laboratorijas testēšanas kapacitāte.

Pētījuma pirmajā posmā tika veikta savākto paraugu higrotermālo īpašību testēšana. 1.1. tabulā apkopotas savākto ķieģeļu paraugu standartizētās testēšanas metodes, kas izmantotas pētījumā [4].

1.1. tabula

**Ķieģeļu paraugu testēšanas metodes, kas izmantotas pētījumā**

Blīvums	*EN 772-13:2000*. Mūra elementu testēšanas metodes. Mūra elementu (izņemot dabīgā akmens) neto un bruto sausā blīvuma noteikšana
Porainība	*EN 772-3:1998*. Mūra elementu testēšanas metodes. Māla mūra elementu neto tilpuma un procentuālo tukšumu īpatsvara noteikšana, veicot higrostatisko svēršanu
Tvaika caurlaidība	*CUP* testi (μ vērtības). *EN ISO 12572:2001* – Būvmateriālu un izstrādājumu higrotermiskās īpašības – Ūdens tvaika caurlaidības īpašību noteikšana
Ūdens uzsūce	*ISO 15148:2002, 2002*. Būvmateriālu un izstrādājumu higrotermiskā veiktspēja – ūdens absorbcijas koeficienta noteikšana ar daļēju iegremdēšanu

Lai varētu izveidot nepieciešamos failus datorprogrammai *Delphin*, tika veiktas dažas novirzes no testēšanas standartiem saskaņā ar Drēzdenes Tehnoloģiju universitātes izstrādātajiem testēšanas aprakstiem. Izmantotās metodes aprakstītas 1.2. tabulā.

Testēšanas metodes saskaņā ar Drēzdenes Tehniskās universitātes testēšanas aprakstiem

Mitruma akumulācija	Higroskopiskās sorbcijas un ūdens akumulācijas īpašības tiek testētas pēc Drēzdenes Tehnoloģiju universitātē izstrādātās metodes, tās pamatā ir *DS/EN ISO 12571:2013* Būvmateriālu un izstrādājumu higro-termiskās īpašības – Higroskopisko sorbcijas īpašību noteikšana un *DS/EN ISO 11274* Augsnes kvalitāte – Ūdens aizturēšanas īpašību noteikšana – Laboratorijas metodes
Žūšanas līkne	Drēzdenes Tehnoloģiju universitātē izstrādāta neizotermiskā kombi-nētā tvaika un šķidruma pārneses testēšanas metode
Siltumietilpība un siltumcaurlaidība	Siltuma impulsu tehnoloģija ar *ISOMET* iekārtu

Nākamajā solī iegūtie testēšanas rezultāti tika izmantoti klasteru veidošanā, izveidojot hierarhijas klasterizācijas dendrogrammu, kas veidota ar aglomeratīvās klasterizācijas metodi. Paraugu klasterēšanai tika izmantota mašīnmācības (*ML*) klasterizācijas analīze ar *Jupyter Lab* [5]. Klasterizācijas veikšanai tika izmantotas *Python* bibliotēkas no *SciKit Learn*. Izmantotas *Python* bibliotēkas, tostarp *Sklearn* un *Matplotlib*. *Sklearn* pamatā ir *NumPy* un *Scipy*, un to izmanto klasterizācijas pro-cesa aprēķiniem [6]. *Matplotlib* tiek izmantots rezultātu vizualizācijai, ieskaitot dendrogrammu. Pirms klasterizācijas visi datu ieraksti tiek normalizēti ar *Stan-dardScaler* funkciju, kas iebūvēta *Sklearn* bibliotēkā. Datu normalizēšana ir nepie-ciešama, lai dažiem datiem nebūtu lielāks svars nekā citiem rezultātiem. Veicot klasterizācijas analīzi, tiek ģenerēti visi iespējamie klasteru skaitīšanas risinājumi, kas nozīmē, ka spektra vienā galā visi paraugi atrodas vienā lielā klasterī, bet spek-tra otrā pusē katrs paraugs veido atsevišķu klasteru [7].
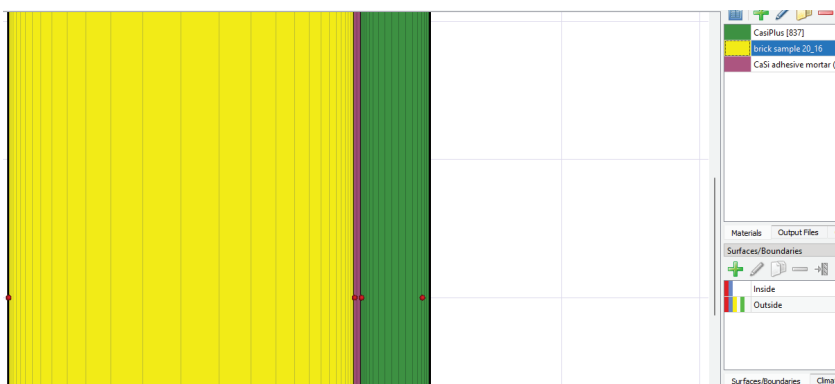

1.1. att. Simulācijas modelis, kas izmantots 40 sienu veidu salīdzinājumam.

Izveidotie *Delphin* faili tika izmantoti nākamajā pētījuma solī, lai varētu veikt datorsimulāciju programmatūrā *Delphin* ar 40 testētajiem ķieģeļiem, no kuriem veidots mūris, kas no iekšpuses siltināts ar kalcija silikātu. 1.1. attēlā redzama modelētā ārsienas struktūra ar ķieģeļu mūri (0,25 m) un kalcija silikāta siltumizolāciju (0,05 m). Tika veiktas divas simulācijas katram no 40 mūra veidiem ar un bez līmes zem izolācijas materiāla [8].

Āra klimatam izmantoti Latvijas Vides, ģeoloģijas un meteoroloģijas centra apkopotie dati par 2022. gadu, kas iegūti no Latvijas Universitātes meteoroloģiskās stacijas [9]. Iekštelpu klimata apstākļi tiek iestatīti kā āra temperatūras funkcija. Simulācijas periods ir trīs gadi.

1.2. Siltumizolācijas materiāli un sistēmas

Šajā pētījuma apakšnodaļā veiktie laboratorijas testi veikti klimata kamerās (āra klimata kamera un telpas klimata kamera), kas atrodas laboratorijā [10], [11]. Testa paraugi ir iebūvēti testa sienā, kas testēšanas laikā tiek novietota starp abām kamerām, lai kontrolētos apstākļos varētu veikt testus (1.2. att.). Āra klimata kamera simulē āra apstākļus, dinamiski kontrolējot kameras temperatūru, relatīvo mitrumu, vēja dzītu lietu un saules starojumu. Telpas klimata kamera simulē iekštelpu apstākļus, šajā kamerā tiek nodrošināts nepieciešamais mikroklimats, mainot relatīvo mitrumu un temperatūru. Āra klimata kamera ir aprīkota ar ūdens izsmidzināšanas un savākšanas sistēmu konstrukcijas ārējā pusē, lai simulētu vēja dzīta lietus ietekmi (kad lietu dzen vējš, liels ūdens daudzums iedarbojas uz vertikālām virsmām). Sistēmā ir deviņas sprauslas, pa vienai katram sienas paraugam, sūknis, plastmasas caurules ūdens sadales sistēmai un ūdens savākšanas sistēmas. Saules starojuma simulācijas lampas imitēja saules iedarbību.
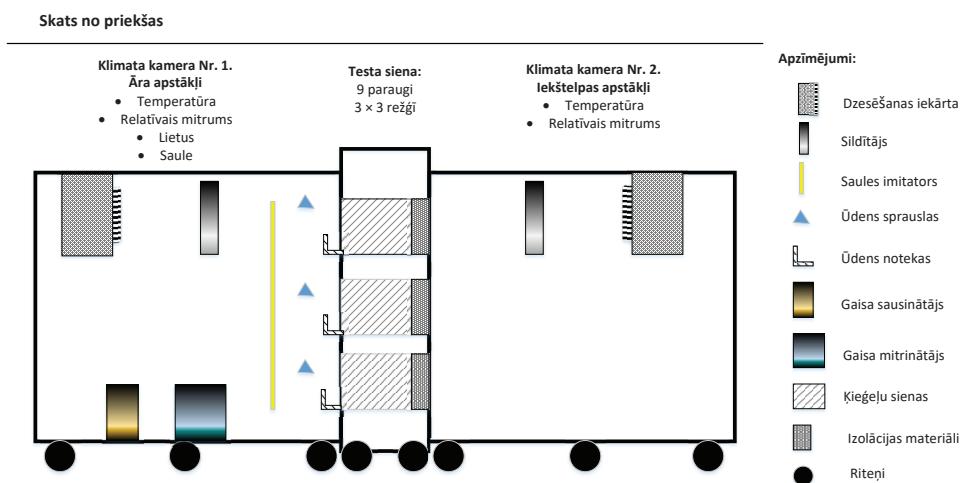

1.2. att. Klimata kameru shematiskais attēlojums.

Relatīvais mitrums starp izolācijas slāni un mūri tika mērīts, izmantojot *Honeywell HIH 4000* sērijas mitruma sensorus. Zem izolācijas slāņa tika uzstādīti mitruma sensori kopā ar K tipa termopāriem. Katra parauga sensori mēra apstākļus starp izolācijas slāni un mūra sienu, kur pastāv ievērojams kondensācijas risks. *Campbell Scientific CR1000* datu reģistrētājs ieraksta datus datorā. Mērījumu laika intervāls ir 1 min.

Vienā no pētījuma posmiem tika testētas 18 siltumizolācijas sistēmas. Katra sistēma sastāv no siltumizolācijas materiāla ar tvaika barjeru vai bez tās, līmes un ārējās apdares (dažām sistēmām tās nav). Dažas sistēmas tika uzbūvētas pēc ražotāja norādījumiem (minerālvate ar tvaika barjeru, *EPS* (divi veidi), *XPS*, *PIR* ar *Sika* cementa kārtu un stikla šķiedras tīklu, korķis, aerogela sega). Citas sistēmas ar nolūku tika veidotas atšķirīgi no instrukcijām, lai pārbaudītu materiālu higrotermisko uzvedību, piemēram, tvaika caurlaidīgi materiāli tika uzstādīti bez tvaika barjeras: akmens vate, keramzīts, celuloze, trīs veidu kokšķiedras plāksnes ar dažādu blīvumu un ēveļskaidu plāksne bez ārējās apdares. Siltumizolācijas materiāliem ir dažāda izcelsme, un tie ietver gan tvaika necaurlaidīgus, gan tvaiku necaurlaidīgus materiālus. Ģipša apmetums tika izslēgts no rezultātiem, jo relatīvā mitruma sensors testu laikā nedarbojās. Testos izmantotās siltumizolācijas sistēmas ir no neorganiskiem minerāliem iegūti materiāli: minerālvate ar tvaika barjeru, akmens vate, keramzīts, ģipša apmetums un aerogela sega. Materiāli, kas ir atvasināti no organiska fosilā kurināmā, ir *EPS* (divi veidi), *XPS*, *PIR* ar *Sika* cementa slāni un stikla šķiedras tīklu (no ārpuses), *PIR* ar alumīnija segumu un *VIP*. Bioloģiskie augu/dzīvnieku izcelsmes materiāli ir celuloze, trīs veidu kokšķiedras plātnes ar dažādu blīvumu: korķa, keramzīta un ēvelēšanas skaidu plāksne. Materiālu īpašības tika iegūtas no ražotāja tehniskajām datu lapām vai tieši sazinoties ar ražotājiem. Pieejamā informācija bija par materiāla siltuma īpašībām, piemēram, siltumvadītspēju λ, citu parametru, piemēram, īpatnējo siltumu vai tvaika pretestību, dažu izstrādājumu tehniskajās datu lapās trūka.

Katra siltināšanas sistēma tika piestiprināta pie mūra parauga, kas būvēts no rūpnieciski ražotiem jauniem ķieģeļiem (1.3. att.). Lai samazinātu materiāla īpašību nenoteiktības ietekmi, tika izmantoti jauni ķieģeļi. Pirms mērījumu sākšanas tika veikta ķieģeļu nostādināšana telpas apstākļos, lai sienu paraugi izžūtu.
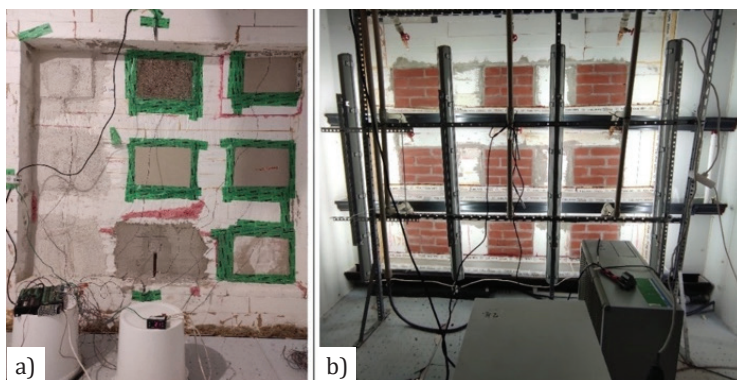
1.3. att. Testa siena ar deviņiem mūra sienas paraugiem: a) no siltās puses; b) no aukstās puses.

Āra klimata kameras parametru vērtības visiem cikliem tika balstītas 2014.–2018. gada laikapstākļu datos, lai atdarinātu āra vides apstākļus. Tie iegūti no publisko novērojumu datubāzes. Kritērijs mēneša izvēlei temperatūras svārstību cikla modelēšanai bija dienas temperatūras svārstību lielākā amplitūda, tāpēc āra gaisa parametri atbilst maijam (1.4. att.). Eksperimentālā plāna pamatā bija šādi apstākļi kamerās:

- telpas klimata kameras temperatūra +20 °C, relatīvais mitrums 50 %;
- āra klimata kameras temperatūra līdzsvara apstākļos +10 °C, relatīvais mitrums 50 %; dinamiskajiem cikliem temperatūra un relatīvais mitrums atbilst āra ikdienas svārstībām maijā (1.4. att.); vēja virzīts lietus 0,278 l/m^2·s (piecas minūtes katru dienu), saules starojums 300 W/m^2 (astoņas stundas dienā).
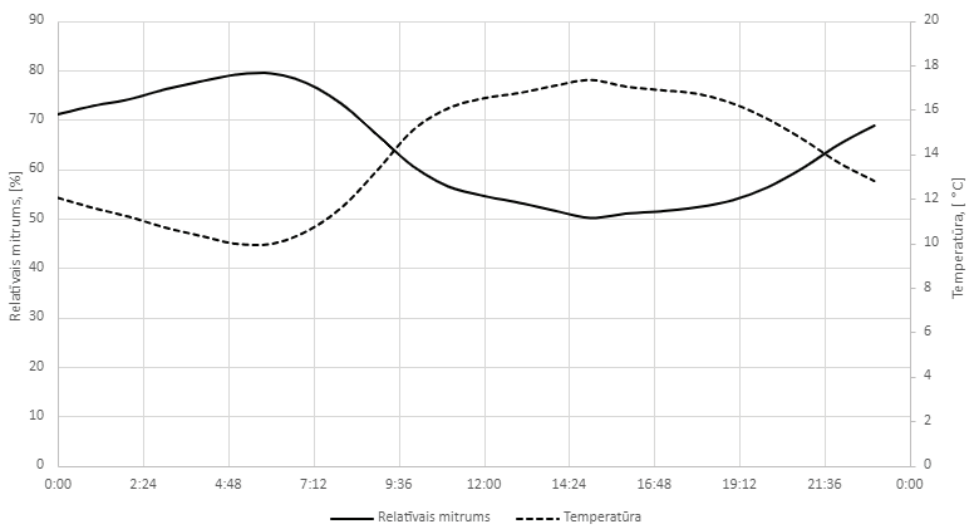

1.4. att. Diennakts klimata svārstības maijā, kas izvēlētas par pamatu dinamiskajam testēšanas ciklam.

Šajā pētījuma posmā papildus relatīvā mitruma un temperatūras mērījumiem zem izolācijas tika veikti mūra mitruma mērījumi ar neinvazīvām mērīšanas metodēm (dielektrisko un mikroviļņu zondi). Neinvazīvi mitruma mērījumi testa laikā tika veikti piecas reizes pirms un pēc katra testa cikla. Mērījumiem tika izmantots *Trotec T3000*. Mitruma mērīšanai 20 cm dziļumā tika izmantota mikroviļņu zonde, 2 cm dziļumā – ar dielektriskā zonde.

Pirmās deviņas laboratorijā testētās sistēmas tika simulētas programmā *Delphin* līdzsvara stāvokļa apstākļos, izmantojot līdzīgus materiālus no esošās materiālu datubāzes. Materiāli tika izvēlēti, pamatojoties uz norādījumiem specifikācijās, ko ražotāji nodrošina laboratorijas eksperimentā izmantotajiem oriģinālajiem materiāliem. Šīs simulācijas tika veiktas gan atbilstoši mainīgiem āra klimata apstākļiem, gan nemainīgiem apstākļiem, lai iegūtu datus un salīdzinātu tos ar mērījumu datiem, kas iegūti laboratorijas eksperimentā. Simulāciju sākotnējie

temperatūras un relatīvā mitruma apstākļi tika iestatīti tā, lai tie atbilstu eksperimenta sākumā izmērītajiem, un āra relatīvais mitrums tika palielināts līdz 93 %, lai tas atbilstu apstākļiem, kas tiek uzturēti klimata kamerā. Simulāciju laika posms tika iestatīts uz vienu stundu. Katra izolācijas sistēma tika modelēta arī programmatūrā *Delphin* (1.5. att.). *Delphin* fails tika izveidots testa sienās izmantoto ķieģeļu higrotermiskajām īpašībām.
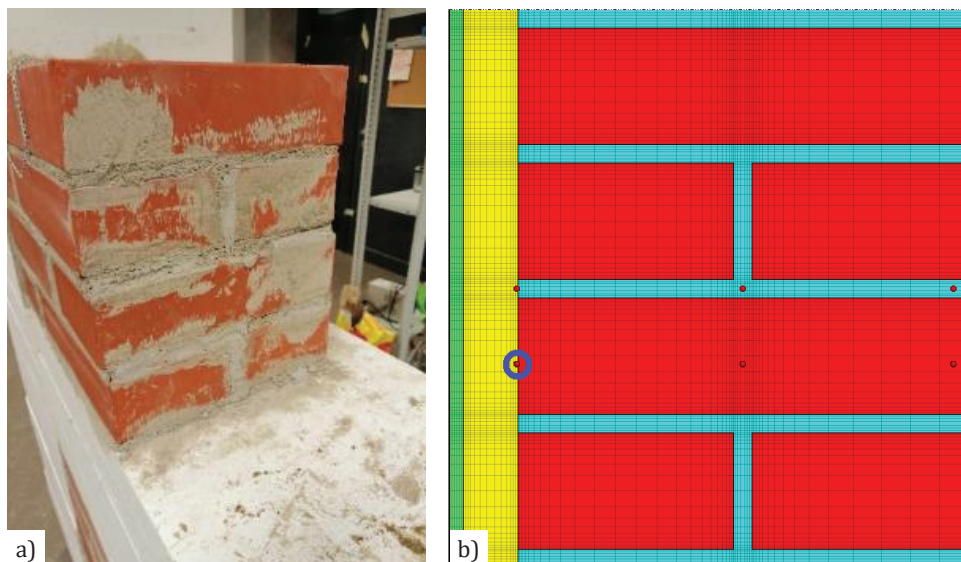

1.5. att. Testa sienas paraugs: a) laboratorijā; b) *Delphin* modelī.

1.3. Iekšējās siltināšanas lietojums vēsturiskās ēkās

Pirmais pētījums veikts vienģimeņu ēkā Seces pagastā, Aizkraukles novadā, Latvijā [12]. Tā celta 1893. gadā kā lauku māja. Pēc Otrā pasaules kara līdz 21. gadsimtam ēka bija slikti uzturēta; pagrabs tika izmantots kā lopu novietne, un tā rezultātā tika nopietni bojātas koka sijas un pirmā stāva segums. 1992. gadā ēka tika denacionalizēta, un īpašumtiesības uz ēku atguva ēkas sākotnējā īpašnieka ģimene.

Ēkai ir divi stāvi ar kopējo apsildāmo platību 339 m^2 un tilpumu 870 m^3. Pagrabstāvs (stāva platība 68 m^2, tilpums 130 m^3) aizņem pusi no ēkas platības dienvidaustrumu fasādē un netiek apsildīts. Fasādes kopējā platība ir 274 m^2, ieskaitot logus un durvis, bet neskaitot pagraba daļu.

Ārsienas ir būvētas no vietējas izcelsmes dolomīta akmens, kas iestrādāts javā. Pagraba sienām izmantoti arī granīta akmeņi. Granīta šķembas izmantotas arī javas šuvju pārklāšanai starp dolomīta akmeņiem (1.6. att.).
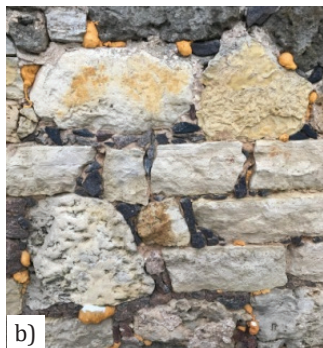
1.6. att. Dolomīta akmeņu vēsturiskā ēka Seces pagastā: a) ēkas galvenā fasāde; b) akmens sienas ārējā virsma.

Dolomīta paraugi no ēkas tika iegūti un pārbaudīti laboratorijā, lai noteiktu to galvenās īpašības – blīvumu, īpatnējo siltumietilpību, siltumvadītspēju, kopējo porainību, kapilāru piesātinājumu, ūdens tvaika pretestības koeficientu, ūdens uzņemšanas koeficientu un mitruma uzglabāšanu. Šīs vērtības tika tālāk izmantotas kā ievades dati, lai raksturotu materiāla īpašības simulācijas programmā *Delphin*.

Laboratorijas dati tika noteikti, izmantojot virkni testu. Atkarībā no testa tika sagatavoti 3–22 paraugi. Papildus standarta pārbaudes metodēm tika izmantotas arī citas metodes.

Ēkas energobilances aprēķināšanai tika izmantots dinamiskās simulācijas rīks *TRNSYS Type 56* (2016). Tika simulēti trīs scenāriji.
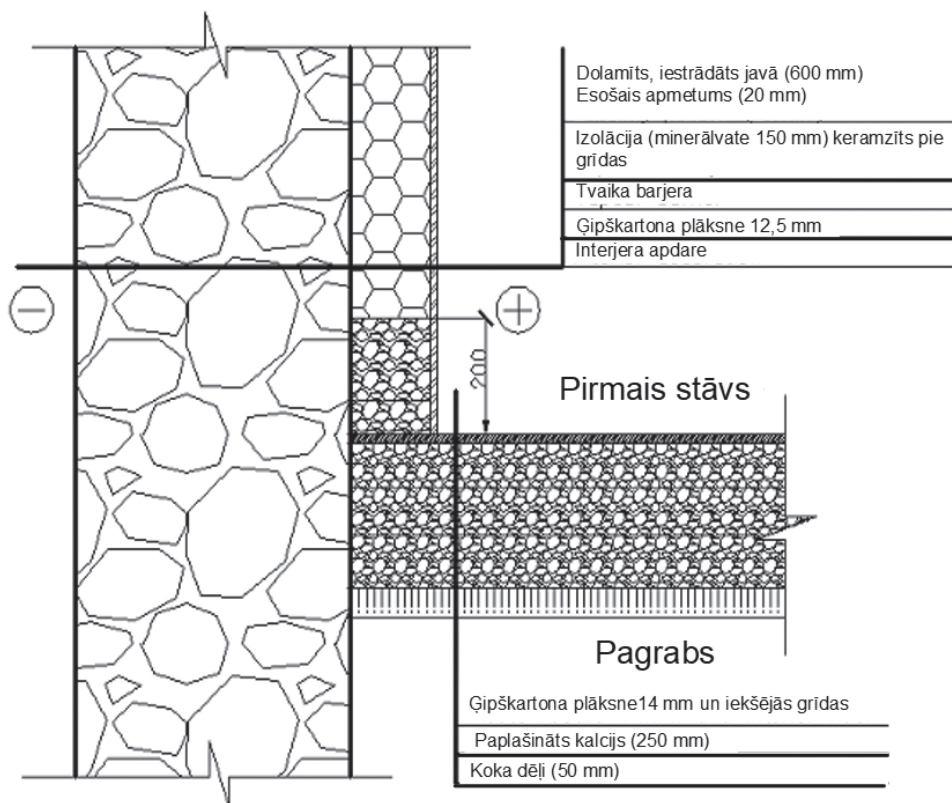
- Bāzes līnija. Ēka pirms abām renovācijām.
- Ēka ar iekšējo izolāciju uz zemes un pirmā stāva sienām.
- Ēka ar papildu energotaupības pasākumiem (pagraba griestu un jumta siltināšana, logu nomaiņa).

Visu scenāriju simulācijas balstījās šādos pieņēmumos:

- tika izmantoti Latvijas klimatiskie dati;
- iekštelpu temperatūra +20 °C, kad ēka tiek izmantota, piemēram, darba dienās no rīta (no plkst. 6 līdz plkst. 8) un vakarā (no plkst. 16 līdz plkst. 23) un pilnas dienas brīvdienās, un +18 °C pārējā laikā;
- iekštelpu relatīvais mitrums 50 %; infiltrācija 0,05 h^{-1}, ar papildu dabisko ventilāciju logu atvēršanas laikā 0,5 h^{-1}; siltuma ieguvumi ir balstīti vērtībās, kas noteiktas standartā *EN ISO 13790:2008*, visi siltuma ieguvumi ir plānoti.

2017. gada decembrī ziemeļaustrumu fasādes ārsienās tika uzstādīti temperatūras, relatīvā mitruma, tilpuma ūdens satura un siltuma plūsmas sensori. Viens sensoru komplekts tika uzstādīts dzīvojamās istabas sienā, otrs – vannasistabas sienā. Abas sienas tika modernizētas 2015. gadā (1.7. att.).

Dolamīts, iestrādāts javā (600 mm)
Esošais apmetums (20 mm)

Izolācija (minerālvate 150 mm) keramzīts pie grīdas

Tvaika barjera

Ģipškartona plāksne 12,5 mm

Interjera apdare

200

Pirmais stāvs

Pagrabs

Ģipškartona plāksne14 mm un iekšējās grīdas

Paplašināts kalcijs (250 mm)

Koka dēļi (50 mm)

1.7. att. Dzīvojamās istabas ārsienas un grīdas šķērsgriezums pēc 2015. gada renovācijas.

Papildus uz ziemeļaustrumu fasādes tika uzstādīts piranometrs *Campbell CMP3 060271* ar jutību $11{,}72 \cdot 10^{-6}$ [V/(W·m^{-2})]. Sensoru uzstādīšana viesistabai un vannasistabai ir vienāda, izņemot saules starojuma sensoru. Viens saules starojuma sensors tika uzstādīts 5 m no zemes līmeņa. Iekštelpu temperatūras mērījumi tika veikti ar vītā pāra T veida termopāriem – *Labfacility XE-2342*. Temperatūras sensors t1 mēra temperatūru starp dolomīta sienu un izolācijas slāni, t2 mēra temperatūru starp izolācijas slāni un tvaika barjeru. Šie sensori tika uzstādīti 1,8 m augstumā no grīdas, kas atbilst 4 m no zemes līmeņa. *RH1-2* mēra relatīvo mitrumu tajās pašās vietās, kur temperatūras sensori. *Honeywell HIH-4000-002* mērījumu *RH* precizitāte bija ± 3,5 %. Siltuma plūsma sienās tika mērīta ar *Hukseflux* siltuma plūsmas sensoriem. Tilpuma ūdens saturs tiek mērīts, izmantojot laika domēna (*TDR*) reflektometru *Campbell CR616*, ar precizitāti ± 2,5 % no tilpuma ūdens satura (*VWC*) un darba temperatūru no 0 °C līdz 70 °C. *CR616* ir uzstādīts 3,5 m no zemes līmeņa. Datu reģistrēšanai tika izmantoti trīs datu reģistrētāji: divi *Campbell Scientific CR1000* datu reģistrētāji (viens viesistabā, viens vannasistabā); viens *Campbell Scientific CR800* datu reģistrētājs (ārpusē). Visiem mērījumiem tika veikts 30 minūšu laika posms. Dati no datu reģistrētājiem tika periodiski savākti.

Lai novērtētu ēkas ārsienu higrotermisko uzvedību ar iekšējo izolāciju, tika izmantota simulācijas rīka *Delphin* 6.1. versija un Glāzera metode. *Delphin* programmatūra ir simulācijas programma viendabīgiem slāņiem, lai modelētu siltuma un mitruma masas transportēšanu un uzglabāšanu materiālos. Glāzera metodi izmanto, lai noteiktu apstākļus dažādos sienas slāņos konkrētos iekštelpu un āra apstākļos. Simulācijā tika izmantoti programmatūras lietotāja ievadītie klimatiskie dati. Iekštelpu robežapstākļiem (temperatūra un relatīvais mitrums) tika izmantoti dati, kas iegūti no *in-situ* mērījumiem. Laikapstākļu dati, piemēram, āra temperatūra, relatīvais mitrums, vēja ātrums un virziens, stundas lietus summa un gaisa spiediens, tika ņemti no meteoroloģiskās stacijas "Skrīveri", kas atrodas 20 km attālumā no gadījuma izpētes ēkas, savukārt saules starojuma dati tika ņemti no meteoroloģiskās stacijas "Rīga–Universitāte", kas atrodas 100 km no gadījuma izpētes ēkas. Abas meteoroloģiskās stacijas apkalpo valsts SIA "Latvijas Vides, ģeoloģijas un meteoroloģijas centrs". Ģipškartona un minerālvates materiālu īpašības tika importētas no *Delphin* materiālu datubāzes. Kā pretestība starp materiāla slāņiem tika pievienota tvaika barjera (S_d = 2,3 m). Dolomīta īpašības tika importētas modelī kā jauna materiāla fails, izmantojot laboratorisko pārbaužu laikā iegūtās vērtības. Taču jāņem vērā tas, ka sienu nesošā daļa ir veidota no neviendabīgiem dabas materiāliem. Par to šī pētījuma laikā liecina arī laboratorisko pārbaužu rezultāti.

Otrais pētījums tika veikts trīsstāvu dzīvojamā ēkā ar papildu bēniņu stāvu un vienu pazemes stāvu [13]. Ēka celta 1880. gadā un atrodas Rīgas vēsturiskajā centrā, aptuveni 150 m no Daugavas (1.8. att.). Ēkas platība ir 120,9 m^2, būves tilpums – 1511 m^3. Ēkai ir divas blakus esošās ēkas, viena – ēkas ziemeļrietumu (ZA), otra – ēkas ziemeļaustrumu (ZA) pusē. Abas blakus esošās ēkas ir par vienu stāvu augstākas nekā gadījuma izpētes ēka. Ēkas dienvidrietumu (DR) pusē ir galvenā fasāde ar ieeju no ielas. Uz DA vērstā fasāde ir lielākā atvērtā zona āra laikapstākļiem, piemēram, vēja izraisītam lietum, saules starojumam un vējam. Brīvā telpa starp DA fasādi un nākamo ēku šajā virzienā ir 15 m, šai blakus ēkai ir vienāds augstums ar gadījuma izpētes ēku. Apmēram pirms 10 gadiem pirmā stāva dzīvokļa īpašnieks uz DA sienas ir ierīkojis iekšējo izolāciju no stikla vates (0,05 m).
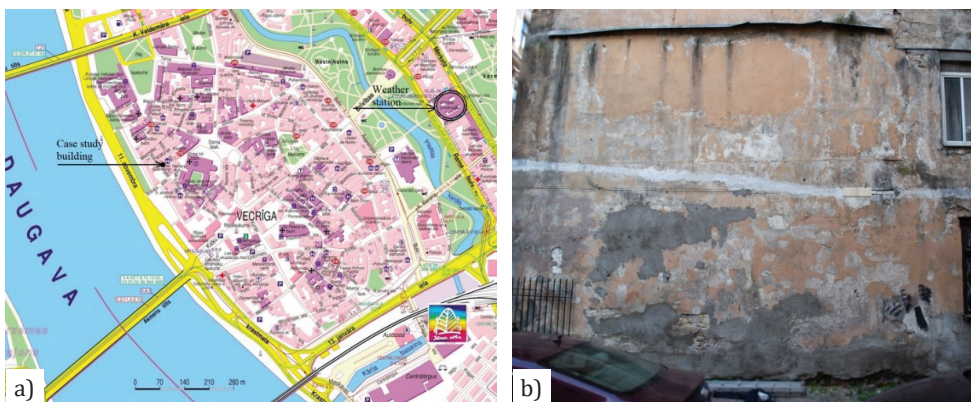
1.8. att. Vēsturiskā ķieģeļu ēka Vecrīgā: a) atrašanās vieta; b) dienvidaustrumu fasāde.

Iespējamo mitruma avotu noteikšanai ārsienu mūrī izmantotas kvalitatīvās un kvantitatīvās metodes. Kvalitatīvā analīze ietver tiešu ēkas novērošanu, lai identificētu esošās sabrukšanas pazīmes un mitruma radītos bojājumus. Kvantitatīvā metode ietver mitruma sadalījuma novērtēšanu ēkas ārsienu relatīvajās skalās. Sienas mitrums tika mērīts no ārpuses. Sienu mitruma mērījumi no iekšpuses bija ierobežoti iekšējās izolācijas dēļ. Mitruma novērtējums tika veikts divos dziļumos – 2 cm un 20 cm dziļumā mūrī (ieskaitot apmetumu). Šiem mērījumiem tika izmantota daudzfunkcionāla mērierīce *Trotec T3000*. *Trotec T3000* tika izmantots ar divu veidu mērīšanas zondēm dažādiem mērījumu dziļumiem: dielektrisko zondi *TS 660 SDI* – 2 cm dziļumam; mikroviļņu zondi *TS 610 SDI* – 20 cm dziļumam. Gan dielektrisko, gan mikroviļņu zondi izmanto mitruma sadalījuma mērījumiem relatīvā mērogā un nevar tieši salīdzināt viens ar otru. Monitoringa nolūkos izmērītā dienvidaustrumu virziena siena tika sadalīta mazākos kvadrātos, veidojot režģi, katrs no tiem – aptuveni 0,4 m līdz 0,4 m. Tas pats režģis tika izmantots atkārtotiem mitruma mērījumiem noteiktā laika periodā.
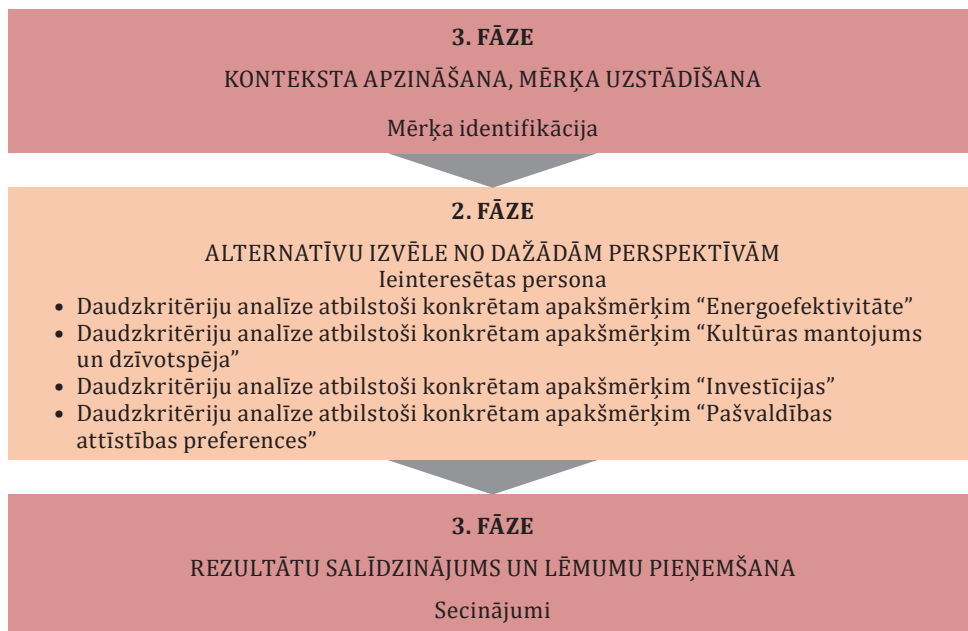
Sienu mitruma mērījumi tika iesākti rudenī (2018. gada 21. septembrī) un turpinājās līdz pavasarim (2019. gada 5. martam). Monitoringa periodā sienu mitrums tika mērīts piecas reizes. Monitoringa sistēma sāka vākt datus 2018. gada 20. novembrī. Monitoringa sistēma ietvēra relatīvā mitruma un temperatūras monitoringu starp ārsienas izolācijas slāņiem. Relatīvā mitruma un temperatūras monitorings starp izolācijas slāņiem tika veikts, izmantojot *Honeywell HIH 4000-002* un T tipa PFA izolētu dubulto vītā pāra termopāra kabeli. Šo sensoru datu reģistrēšanai tika izmantots datu reģistrētājs *Campbell CR1000*. Monitoringa sistēmas ievietošanai iekšēji izolētajā sienā tika izurbts neliels caurums 27 mm diametrā. Kopumā izolācijas slāņos tika uzstādīti divi relatīvā mitruma un divi temperatūras sensori. Sensori tika uzstādīti pa pāriem (relatīvā mitruma sensors kopā ar temperatūras sensoru). Sensoru pāri tika uzstādīti 20 cm zem cauruma, viens pāris – starp sienu un izolāciju, otrs pāris – starp izolāciju un ģipškartona plāksni. Papildus tika mērīta temperatūra un relatīvais mitrums pie izolētās sienas iekšējās virsmas. Pēc relatīvā mitruma un temperatūras sensoru ievietošanas caurums tika atkārtoti aizpildīts ar minerālvati un ģipškartona plāksni. Lai izvairītos no papildu mitruma pievienošanas izolācijas sistēmai caur griezumu un saglabātu piekļuvi sensoriem, cauruma aizklāšanai netika izmantots apmetums. Tā vietā ģipškartona plāksne tika noslēgta ar maskēšanas lenti un papildus pārklāta ar tvaiku necaurlaidīgu alumīnija līmlenti. Tika izmantoti tuvākās meteoroloģiskās stacijas laikapstākļu dati. Meteoroloģiskā stacija atrodas Latvijas Universitātē, un datus pārvalda Latvijas Vides, ģeoloģijas un meteoroloģijas centrs.

1.4. Pozitīvas enerģijas bilances kvartāls vēsturiskā pilsētvidē

Vēsturiski celtām būvēm ir daudzi nacionāli un globāli nozīmīgi kultūras vērtību slāņi un dimensijas. Līdz ar to uzdevums pārveidot vēsturisko pilsētas kvartālu par pozitīvas energobilances kvartālu ir tikpat sarežģīts kā pats pilsētas būvapjoms. Šī pētījuma metodoloģija ir sakārtota sešos secīgos posmos: kvartāla izvēle; energoefektivitātes potenciāla novērtēšana; datu analīze; plānoto

pasākumu apzināšana un izvēle; novērtēšana; secinājumi [14]. Vēsturiskā centra pilsētas kvartāla dekarbonizācijas stratēģija pozitīvas energobilances kvartāla koncepcijā izstrādāta, ņemot vērā divus aspektus – energoefektivitāti un kultūras mantojumu. Katrā pētījuma metodoloģijas posmā ņemta vērā abu pušu perspektīva. Parasti energoefektivitātes scenāriji tiek svērti, izmantojot izmaksu un ieguvumu analīzi un CO_2 dzīves cikla analīzi. Šajā pētījumā izvērtējums papildināts ar energoefektivitātes pasākumu ietekmes uz kultūras mantojumu novērtējumu. Komforta paaugstināšana vēsturiskajās ēkās un jaunu elementu pievienošana tiek uzskatīta par ielaušanos vēsturiskajā celtnē. Tālākai diskusijai svarīgi izvērtēt, vai piedāvātais projekts paaugstina dzīves kvalitāti pilsētas kvartālā un kāda ir tā ietekme uz vēsturiskā mantojuma vērtībām. Trīs dažādas vērtēšanas analīzes metodes ilustrē dažādas iespējamās perspektīvas un kalpo par pamatu diskusijai starp profesionāļiem – vides inženieriem, arhitektiem, vietējiem pilsētplānotājiem un varas iestādēm, kā arī plašākai sabiedrībai par to, kā atrast līdzsvaru starp klimata pārmaiņu seku mazināšanas pasākumiem un kultūras mantojuma saglabāšanu, ceļā uz zemu oglekļa emisiju sabiedrību.

Pētījumā ir izstrādāta un lietota pilsētas kvartāla atlases metodika ar vislielāko potenciālu sasniegt pozitīvu gada energobilanci. Tā ir piemērojama jebkurai blīvi apbūvētai pilsētvidei. Pētījuma pirmā soļa mērķis ir izvēlēties kvartālu viedai pilsētvides atjaunošanai. Pētījumam ir divi vienlīdz svarīgi mērķi, tāpēc kvartāla izvēle tiek izskatīta no divām perspektīvām – tā energoefektivitātes potenciāla un augstas celtniecības kultūras kvalitātes un apdzīvojamības pilsētas kvartālos. Kvartāla izvēle tika balstīta daudzkritēriju analīzē, kur iespējamās alternatīvas tiek izvērtētas atbilstoši mērķim svarīgu kritēriju kopai [15], [16]. Pētījums tika veikts trīs posmos (1.9. att.).

| 3. FĀZE |
| KONTEKSTA APZINĀŠANA, MĒRĶA UZSTĀDĪŠANA |
| Mērķa identifikācija |

| 2. FĀZE |
| ALTERNATĪVU IZVĒLE NO DAŽĀDĀM PERSPEKTĪVĀM |
| Ieinteresēta persona |
| • Daudzkritēriju analīze atbilstoši konkrētam apakšmērķim "Energoefektivitāte" |
| • Daudzkritēriju analīze atbilstoši konkrētam apakšmērķim "Kultūras mantojums un dzīvotspēja" |
| • Daudzkritēriju analīze atbilstoši konkrētam apakšmērķim "Investīcijas" |
| • Daudzkritēriju analīze atbilstoši konkrētam apakšmērķim "Pašvaldības attīstības preferences" |

| 3. FĀZE |
| REZULTĀTU SALĪDZINĀJUMS UN LĒMUMU PIEŅEMŠANA |
| Secinājumi |

1.9. att. Pētījuma metodika.

Vispirms tiek apzināts lēmumu pieņemšanas konteksts, definēti mērķi un izveidota lēmumu pieņemšanas hierarhija. Pēc tam atbilstoši iesaistīto ieinteresēto personu skaitam tiek izstrādātas vairākas daudzkritēriju analīzes metodes kopas. Šajā pētījumā tiek aplūkota "Energoefektivitāte" un "Kultūras mantojums un dzīvotspēja". Alternatīvas tiek sarindotas atbilstoši katras analīzes apakšmērķiem, katrai ieinteresētajai pusei nosakot labāko alternatīvu. Noslēgumā rezultāti tiek salīdzināti un pieņemti galīgie lēmumi, pamatojoties uz otrā soļa rezultātiem, un apkopoti secinājumos.

Vienam no sarežģītākajiem pētījuma posmiem – pasākumu izvēles fāzei – tika izveidota metodoloģija [17]. Metodoloģija ietver trīs galvenos posmus – sākotnējo izpēti, konceptuālo izstrādi un kopējās enerģijas bilances aprēķinu (1.10. att.). Šajā darbā ir aprakstīts 2. solis – izvēlētā pilsētas kvartāla dekarbonizācijas potenciāla sākotnējais novērtējums, tajā skaitā provizoriskā enerģijas patēriņa datu analīze un iespējamo atjaunojamās enerģijas koncepciju izvērtēšana.
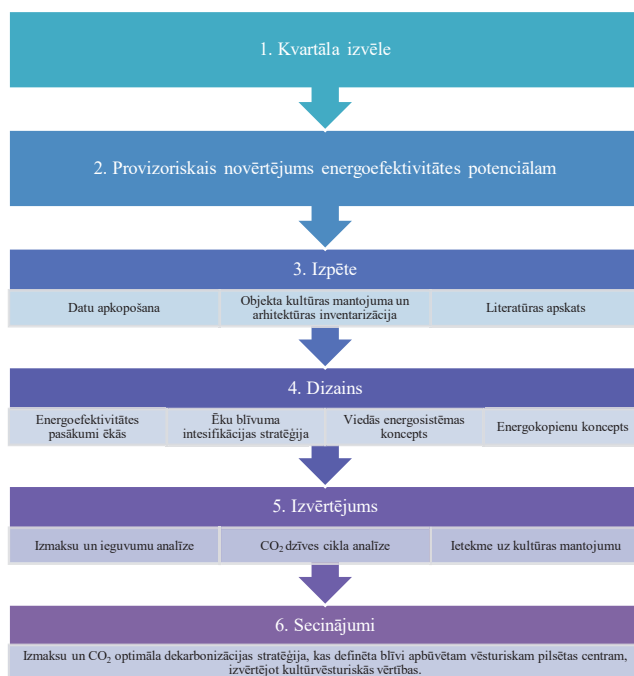
1.10. att. Pētījumā izmantotā metodika.

Dati par esošo situāciju tiek iegūti no enerģijas patērētājiem vai publiski pieejamām datubāzēm. Lai novērtētu provizorisko enerģijas ietaupījuma potenciālu izvēlētajā pilsētas kvartālā, ir veikts vienkāršots aprēķins, novērtējot: 1) ēkas dziļās renovācijas enerģijas ietaupījumu; 2) AER ražošanu ar tradicionālajām tehnoloģijām – PV un saules siltumenerģiju; 3) nelietderīgā siltuma reģenerācijas tehnoloģiju.

2. REZULTĀTI

2.1. Vēsturisko ēku materiāli un konstrukcijas

No *Delphin* rezultātiem tika iegūti 3 klasteri, kur lielākā daļa (87,5 %) paraugu atrodas vienā klasterī (B). No ķieģeļu parametriem tika iegūti 6 klasteri, kur divos no tiem (3 un 5) atrodas 70 % no visiem paraugiem (37,5 % un 32,5 %). Pēc abu klastera grupu apvienošanas šie trīs ķieģelu skaita ziņā lielākie klasteri (B, 3 un 5) izveidoja divus jaunus klasterus (B3 un B5). Kopumā 67,5 % no visiem paraugiem atrodas šajos divos klasteros, 30 % B3 un 37,5 % B5 klasterī. Paraugs (18-4) tika atzīts par vienīgo paraugu divās klasteru grupās (grupā A un grupā 2). Salīdzinot ar pārējiem ķieģeļu paraugiem pēc to apraksta, ir vēl trīs ķieģeli ar tādu pašu aprakstu (dzeltenais māla ķieģelis, ražots 20. gs. 1. pusē). Trīs citi ķieģeli pieder grupai B4, un šajā grupā ir tikai viens ķieģelis – sarkanais māla ķieģelis, ražots 20. gadsimta 2. pusē.

Lielākā daļa B5 apvienoto klasteru grupas paraugu ir sarkanā māla ķieģeli (86,7 %), un lielākā daļa no tiem ir ražoti laika posmā no 19. gadsimta 2. puses (30,8 %) līdz 20. gadsimta 1. pusei (38,5 %). Otrajā lielākajā klasteru grupā B3 gandrīz visi ķieģeli ir sarkanie māla ķieģeli, izņemot vienu ķieģeli, kas ir no betona, un šajā grupā lielākā daļa ķieģeļu ir ražoti laika posmā no 19. gs. (27,3 %) līdz 20. gadsimta 1. pusei (36,4 %).

Taču jāatzīmē, ka lielākā daļa ķieģeļu paraugu ir sarkanais māls (75 %) un 60 % ir ražoti laika posmā no 19. gadsimta 2. puses (22,5 %) līdz 20. gadsimta 1. pusei (37,5 %).

Aplūkojot klasterus, kas iegūti no *Delphin* rezultātiem, kur 35 no 40 ķieģeliem atrodas vienā klasterī, var secināt, ka dažādi parametru klasteri ģenerē līdzīgus rezultātus, šajā gadījumā 5. un 4. parametru kopas 100 % pārklājas ar rezultātu B kopu, kam seko parametru 3. kopa (92,3 % pārklāšanās) un 1. kopa (25 % pārklāšanās). Taču jāatzīmē, ka zemais klasteru skaits, šajā gadījumā – trīs, no *Delphin* rezultātu datiem ir saistīts ar lielo attālumu starp pirmo divu klasteru kombināciju ar 1. un 2. klasteri, attiecīgi 494,17 un 378,56, kam seko attālums 168 no kombinācijā ar trīs kopām. Ja pirmās divas klasteru kombinācijas tiek izslēgtas no optimālās klasteru kombinācijas aprēķiniem, tad optimālais klasteru skaits pret attālumu būtu kombinācija ar 15 klasteriem un attālumu 37,5.

P klasteru ievades dati ir balstīti skaitliskās simulācijas izvadē, tāpēc šos rezultātus lielā mērā ietekmē izvēlētā skaitliskā aprēķinu programma (*Delphin*) un veiktās simulācijas ievades dati (materiāla īpašības, izvēlētā ģeometrija, klimatiskie apstākļi, robežnosacījumi utt.), tāpēc rezultātu interpretācija aprobežojas ar konkrētajiem klimatiskajiem apstākļiem un šajā pētījumā izmantoto ķieģeļu paraugu kopumu [7].

Skaitliskie eksperimenti par 40 dažādu ķieģeļu veidu masīvu mūra sienu, visas siltinātas no iekšpuses ar kalcija silikātu (kapilāri aktīva izolācija), liecina, ka visu sienu veidiem ir loti līdzīgas temperatūras tendences, savukārt mitruma uzvedībā ir vērojama liela atšķirība. Tas atbilst (*Zhou et al.*, 2018) [18] secinājumiem, ka ķieģeļu veida ietekme uz relatīvo mitrumu un temperatūru zem siltumizolācijas ir

sarežģīta. Iegūtie rezultāti rāda, ka temperatūras svārstības starp dažādiem sienu veidiem ir atkarīgas no ķieģeļu termiskās pretestības – jo augstāka ir termiskā pretestība, jo zemāka ir temperatūra zem siltumizolācijas materiāla (2.1. att.).
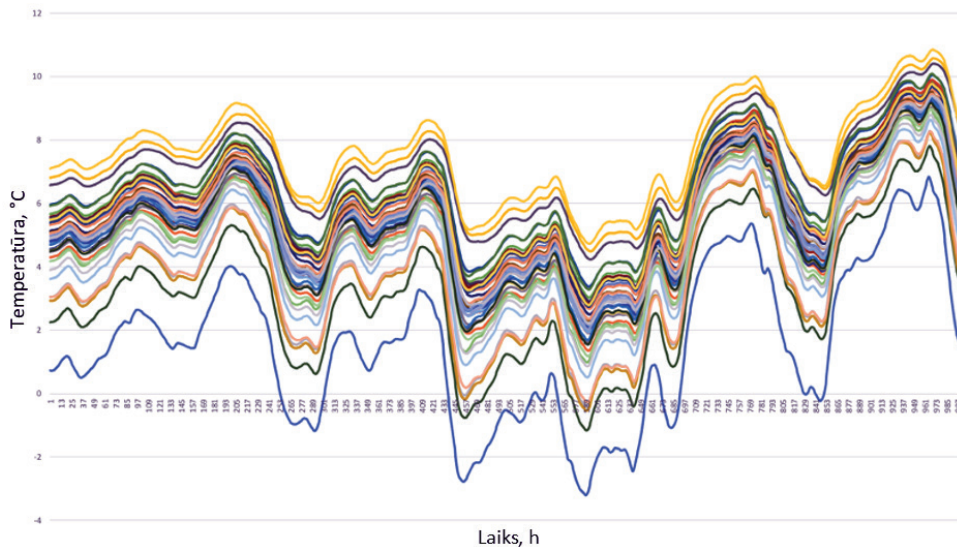
2.1. att. Temperatūra zem siltumizolācijas laika posmā starp 7800. un 8800. stundu.
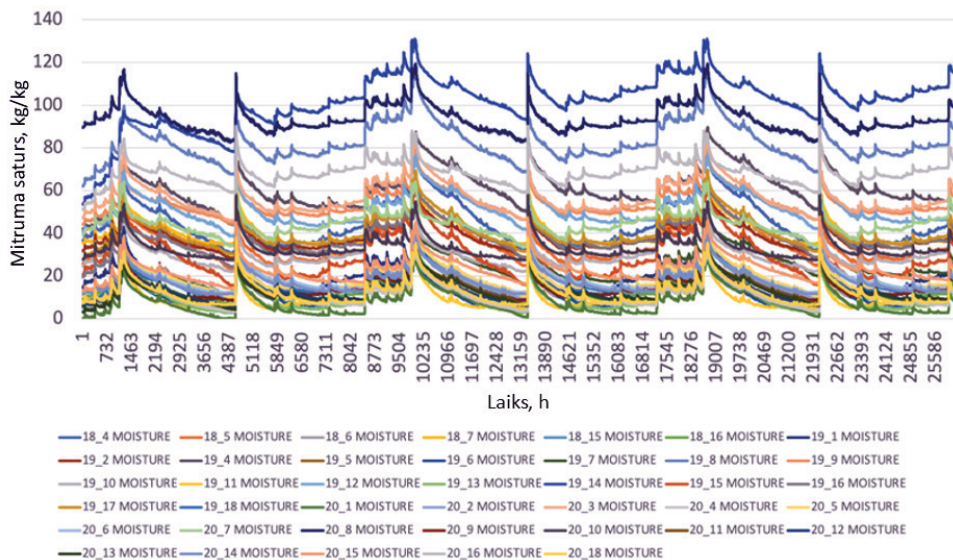
2.2. att. Mitruma saturs mūrī visiem simulētajiem sienu veidiem.

2.2 attēlā redzams, ka mitruma satura līmeņi dažādiem sienu veidiem atšķiras četras reizes. Arī mitruma satura sadalījums mūrī būtiski atšķiras. Tas ir novērojams gan kā nemainīgs mitruma līmenis visā mūrī, gan arī kā nemainīgs mitruma līmenis sienas ārējā daļā, kam seko straujš samazinājums mūra dziļākajos slāņos. Datu analīze liecina, ka šajā pētījumā nav konstatēta korelācija starp mitruma saturu, relatīvā mitruma līmeni un citiem parametriem (ūdens absorbcijas koeficients, šķidruma ūdens vadītspēja, poraininība, blīvums).

No iegūtajiem rezultātiem nevar gūt apstiprinājumu citiem pētījumos izdarītajiem secinājumiem, ka masīvas mūra sienas, kas siltinātas no iekšpuses ar tvaika caurlaidīgiem kapilāri aktīviem materiāliem, higrotermiskā veiktspēja ir atkarīga no poru izmēra sadalījuma, kas nosaka ķieģeļu šķidruma ūdens vadītspēju (jo augstāks šis parametrs, jo dziļāk mūrī iekļūst lietus) [19]. Tas neatbilst arī (*Zhou et al.*, 2018) [18] secinājumam, ka mūra sienām ar augstu kapilaritāti ir lielāki relatīvā mitruma un temperatūras rādītāji. Pētījumā nav noteikti materiāla poru izmēri, lai varētu rezultātus salīdzināt ar (*Feng et al.*, 2021) [19] pētījumu, ka tie būtiski ietekmē tā higriskās īpašības – mazas poras galvenokārt palielina higroskopiskumu (piemēram, sorbcijas izotermas), savukārt lielas poras galvenokārt uzlabo kapilaritāti (piemēram, kapilārās absorbcijas koeficientu).

Ja būvniecības kvalitāte ir zema un līme nenodrošina pilnu saskari starp mūri un siltumizolācijas materiālu, lietus mitrums var iekļūt siltumizolācijas materiālā. 2.3. attēlā redzams piemērs ar 20_18 ķieģeļa mūri ar līmi un bez tās. Ja līme nodrošina pilnu saskari starp mūri un siltumizolācijas materiālu, nav vērojam vēja dzītā lietus ietekme uz siltumizolācijas materiālu. Šie atklājumi atbilst cita pētījuma [20] secinājumiem. Līmei ir augsta mitruma buferspēja, ja tā tiek pareizi uzklāta. Līdzīgi secinājumi publicēti arī citā pētījumā [21].
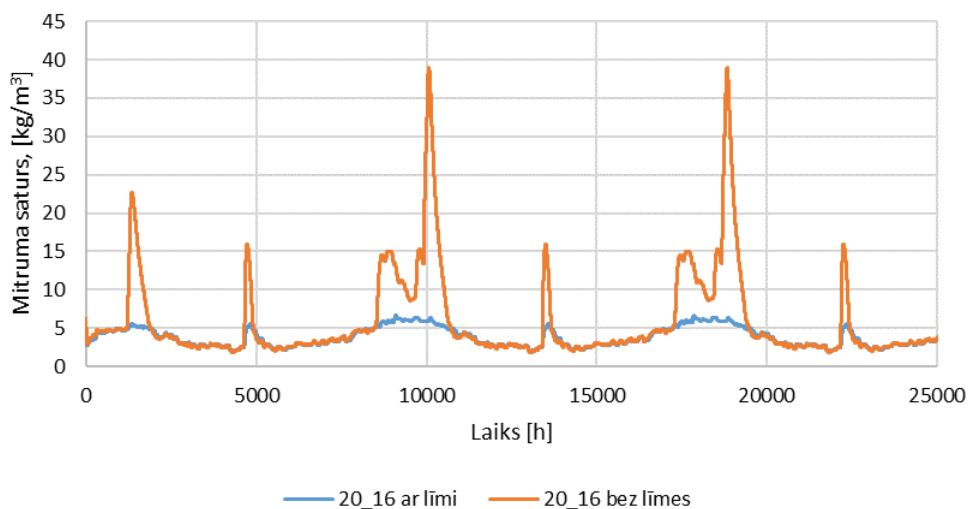

2.3. att. Mitruma saturs siltumizolācijas materiālā 20_16 ķieģeļa mūrim ar līmi un bez tās.

Simulācijas rezultāti liecina, ka, ja iekšējā siltumizolācija ar kapilāri aktīvo kalcija silikātu tiek izmantota aukstā klimatā ar normālu iekštelpu mitruma slodzi, relatīvais mitrums nepārsniedz 96 % un tiek uzskatīts par drošu [22]. Šis secinājums attiecas gan uz siltumizolāciju ar līmi, gan bez tās.

2.2. Siltumizolācijas materiāli un sistēmas

Iegūtie rezultāti liecina, ka pastāv nesakritība starp izmērīto un simulēto higrotermisko uzvedību. Testa rezultāti rāda, ka relatīvā mitruma pieauguma temps starp mūri un siltumizolācijas materiālu ir augsts pirmajās testa dienās visiem materiāliem un palēninās, tuvojoties līdzsvara apstākļiem. Temperatūra pazeminās nedaudz mazākā tempā nekā relatīvais mitrums un sasniedz līdzsvaru aptuveni piecu dienu laikā. Pirms eksperimentālā testa veiktā simulācija parādīja daudz zemāku relatīvā mitruma pieauguma un temperatūras pazemināšanās tempu, salīdzinot ar izmērīto uzvedību. 2.4. attēlā redzamā korelācijas analīze starp mērījumu un simulāciju rezultātiem parāda, ka ir cieša sakarība starp temperatūrām – korelācijas koeficients R^2 ir 0,81–0,86 diapazonā. Cieša korelācija ir koksnes šķiedras relatīvajam mitrumam ($R^2 = 0,84$), savukārt daudz vājāka tā ir EPS ($R^2 = 0,59$) un minerālvatei ($R^2 = 0,54$).
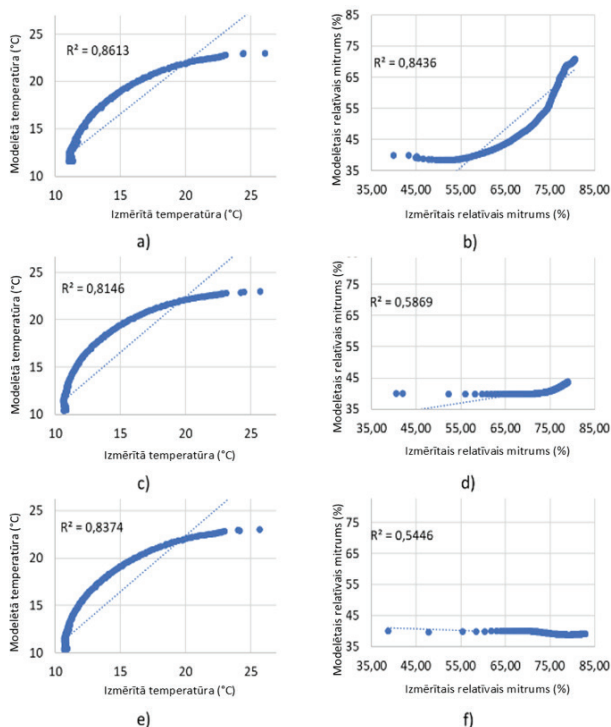
2.4. att. Korelācija starp modelēto un izmērīto temperatūru starp mūri un izolācijas slāni (a) kokšķiedra; c) EPS; e) minerālvate) un relatīvo mitrumu (b) kokšķiedra; d) EPS; f) minerālvate).

Modeļa pielāgošana izmērītajiem datiem tika uzlabota, izmantojot parametru analīzi. Tas tika veikts, mainot mūra, javas un izolācijas materiālu parametrus. Siltumvadītspēja, sausā materiāla blīvums un ūdens tvaiku difūzijas pretestības koeficients izolācijas materiāliem tika mainīti uz materiālu ražotāju norādītajām vērtībām (2.1. tab.). Ķieģeļiem un javas siltumvadītspējai tika koriģēta īpatnējā siltumietilpība, ūdens vadītspēja pie piesātinājuma, ūdens uzsūces koeficients un sākotnējais relatīvais mitrums. Koriģētās vērtības apkopotas 2.1. tabulā.

2.1. tabula

Parametriskai analīzei izmantoto materiālu īpašības

	Ķieģelis	Javas	Minerālvate	Koksnes šķiedra	*EPS*
Materiāla nosaukums *Delphin* datubāzē	Vecs celtniecības ķieģelis *Dresden ZD*	Kaļķu cementa java	Minerālvate	Kokšķiedras izolācijas plāksne	Polistirola plāksne – paplašināta
Sausā materiāla blīvums, kg/m^3	1619,51	1878,47	28 (–24 %)	50 (–67 %)	13,5 (–41 %)
Siltumvadītspēja, W/(m·K)	0,482 (+20 %)	0,5 (–38 %)	0,036 (–10 %)	0,038 (–10 %)	0,039 (+8 %)
Sausā materiāla īpatnējā siltumietilpība, J/kg	430 (–55 %)	470 (–38 %)	840	2000. gads	1500
Ūdens tvaiku difūzijas pretestības koeficients	10,4726	36,9113	1	2,1 (–30 %)	30 (–69 %)
Ūdens uzņemšanas koeficients, kg/(m^2·s^{0,5})	0,423587 (+11 %)	0,211622 (+486 %)	0	0,07	0,00001
Efektīvs piesātinājums (ilgtermiņa process), m^3/m^3	0,761043 (+111 %)	0,1 (–55 %)	0.9	0,6	0,92
Šķidrā ūdens vadītspēja pie efektīva piesātinājuma, s	0,2059E-10 (+24 %)	3,52E-10 (+3339%)	0	0,0216E-10	0
Sorbcijas izoterma — Mitruma saturs, m^3/m^3, RH 0 %	0,004030	2,83E-08		0,0000683	0,0000528
RH 30 %	0,007003	0,004542		0,0048476	0,000455
RH 50 %	0,007261	0,015729		0,0080606	0,000617
RH 80 %	0,007720	0,027090		0,0176992	0,001078
RH 95 %	0,023461	0,037559		0,0328964	0,009227
RH 100 %	0,761043	0,1		0,6	0,92
Sākotnējais relatīvais mitrums materiālā,%	65 (+62 %)*	85 (+112 %)*	40	40	40
Materiāla sākotnējā temperatūra, °C	23	23	23	23	23

* Materiāla iekšienē, sākot no 2,5…3,5 cm dziļumā no materiāla ārējām virsmām.

Pētījumā [11] secināts, ka simulācijā liela nozīme ir materiāla parametru vērtību precizitātei, kā arī materiālu sākotnējām vērtībām, taču sākotnējām vērtībām ir daudz lielāka ietekme.

Veiktā parametru analīze parādīja parametrus, kas visbūtiskāk ietekmē konstrukcijas higrotermālo uzvedību. Visu trīs testā izmantoto siltumizolācijas materiālu parametri tika pielāgoti materiālu ražotāju sniegtajām vērtībām – siltumvadītspēja *EPS* palielināta par 8 %, minerālvatei samazināta par 10 %, kokšķiedrai – par 10 %. Blīvums tika samazināts visiem trim izolācijas materiāliem: minerālvatei – līdz 24 %, kokšķiedrai – līdz 67 %, *EPS* – līdz 41 %, savukārt ūdens tvaiku difūzijas pretestības koeficients tika samazināts kokšķiedrai par 30 %, *EPS* – par 69 %.

Lai simulācijas rezultātus tuvinātu mērījumu rezultātiem, tika mainīta termiskā uzvedība, palielinot ķieģeļu siltumvadītspēju par 20 %, javai samazinot par 38 %. Īpatnējā siltumietilpība tika ievērojami samazināta gan ķieģeļiem (55 %), gan javai (38 %).

Vislielākā ietekme uz mitruma pārneses pieauguma tempu ir materiālu sākotnējam relatīvajam mitrumam – tas tika palielināts par 62 % ķieģeļiem un par 112 % javai, salīdzinot ar simulācijas vērtībām pirms testa. Pirms testiem mūris tika žāvēts 10 dienas, un tas bija pārāk īss laika posms, lai mūris izžūtu, tāpēc mitruma līmenis testu sākumā joprojām bija augstāks, nekā tika prognozēts simulācijas laikā pirms testa. Citi parametri, kas ietekmē mitruma pārnesi, ir ūdens vadītspēja pie efektīvā piesātinājuma, kas ķieģeļiem un javai tika palielināta par 24 %, līdz ar to ūdens uzsūces koeficients ķieģeļiem palielinājās par 11 %, javai – par 486 %. Efektīvais piesātinājums tika palielināts par aptuveni 111 % ķieģeļiem un samazināts par 55 % javai.

2.5. attēlā redzamas temperatūras un relatīvā mitruma izmaiņas simulācijas laikā pirms un pēc eksperimenta un mērījumu rezultāti sienai ar kokšķiedru bez tvaika barjeras. Galvenā atšķirība starp mērīto temperatūru un simulācijas temperatūru pirms testa tiek novērota pirmajās 10 dienās, kad simulācijas temperatūra pirms testa pazeminās lēnāk nekā izmērītā temperatūra. Savukārt pēc testa simulācijas rezultāti atbilst izmērītajai temperatūrai Temperatūra līdzsvara stāvoklī atšķiras tikai par 0,6 °C. Lai sasniegtu pieņemamus rezultātus simulācijas atbilstībai pēc testa, ir mainīta siltumvadītspēja, sausā materiāla blīvuma un īpatnējās siltumietilpības vērtības. Tāda pati tendence vērojama arī relatīvajam mitrumam – simulācijai pirms testa sākumā ir daudz mazāks pieauguma temps, tāpēc simulācijas periodā tā nav sasniegusi līdzsvaru. Simulācija pēc testa un izmērītais relatīvais mitrums labi korelē, un abi stabilizējas pie aptuveni 80 %. Lai sasniegtu līdzīgus rezultātus simulācijā pēc testa, ir mainīts ūdens tvaiku difūzijas pretestības koeficients, ūdens vadītspēja pie efektīva piesātinājuma, ūdens uzsūces koeficients un sākotnējais ķieģeļu un javas relatīvais mitrums.

Testu rezultāti rāda, ka līdzsvara apstākļos augstāko relatīvo mitrumu starp mūri un siltumizolāciju sasniedz minerālvate (82,9 %), kam seko kokšķiedra bez tvaika barjeras (80,5 %), *EPS* (79 %), aerogels ar tvaika barjeru (78,2 %), aerogels bez tvaika barjeras (73,3 %) un kokšķiedra ar tvaika barjeru (72,7 %). Temperatūra starp mūra sienu un visiem izolācijas materiāliem ir nostabilizējusies vidēji pie +10 °C.
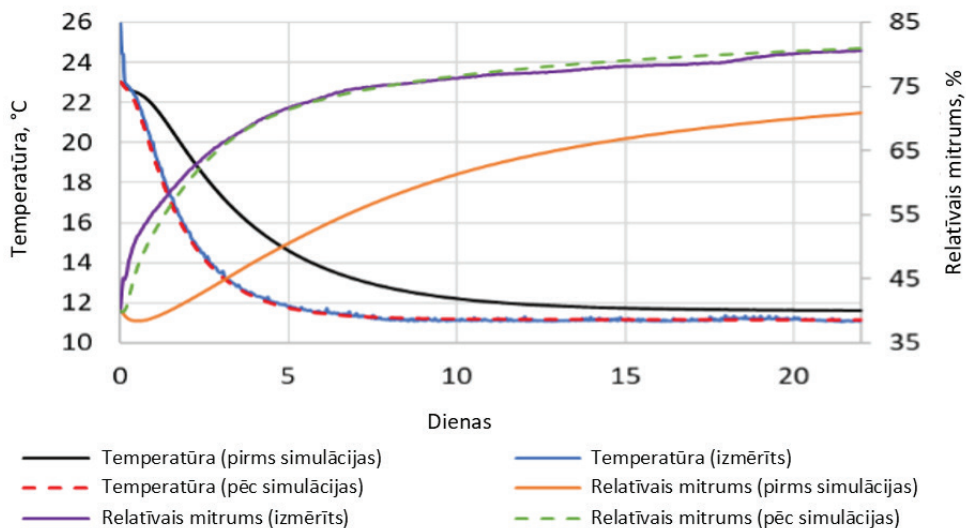
2.5. att. Temperatūras un relatīvā mitruma uzvedība starp mūri un kokšķiedru bez tvaika barjeras: simulācija pirms un pēc eksperimenta, mērījumu rezultāti.

Relatīvais mitrums nav palielinājies virs 95 % (stāvoklis, kad sākas kapilāru piesātinājums) nevienā no materiāliem, tāpēc sasalšanas risks nepastāv. Tas var mainīties, ja tiek mainīti āra robežapstākļi, piemēram, vēja dzīts lietus un saules starojums uz virsmas. Tomēr pastāv pelējuma veidošanās risks bioloģiskas izcelsmes izolācijas materiāliem, piemēram, kokšķiedrām, kā tas tika novērots testu laikā.

Šajā pētījumā tika veikts arī tests ar 18 siltumizolācijas sistēmām, taču sistēmai ar ģipša apmetumu testa sākumā tika bojāti temperatūras un relatīvā mitruma sensori, tāpēc rezultātu analīzē tiek izmantoti mērījuma dati par 17 siltumizolācijas sistēmām.

Iegūtie rezultāti rāda, ka siltināšanai no iekšpuses ir liela ietekme uz sienas higrotermisko uzvedību, jo pieaug relatīvais mitrumu starp siltumizolāciju un mūra sienu, kas savukārt palielina pelējuma rašanās, sala bojājumu un koka siju sabrukšanas risku.

Testētajām siltumizolācijas sistēmām ir līdzīga termālā uzvedība, bet atšķirīga mitruma uzvedība. 2.6. attēlā redzama simulētā un mērītā temperatūra starp siltumizolācijas materiālu un mūra sienu līdzsvara ciklā astoņām siltumizolācijas sistēmām.
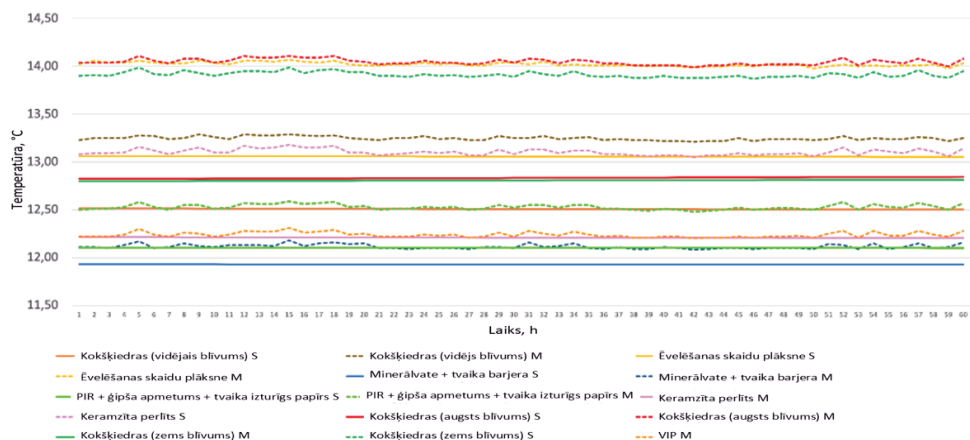
2.6. att. Simulētā (S) un mērītā (M) temperatūra starp siltumizolācijas materiālu un mūra sienu līdzsvara ciklā (laika posms starp 245. minūti un 305. minūti).

Kavējums, kas rodas no siltuma plūsmas starp konstrukcijas iekšējo virsmu un ārējo virsmu, ir novērojams visās siltumizolācijas sistēmās (2.7. att.). Vidējā laika nobīde līdzsvara stāvoklī ir atkarīga no robežnosacījumiem. Jo lielāka ir atšķirība starp iekštelpu un āra temperatūru, jo lielāka ir laika nobīde. Temperatūras samazinājuma koeficients, kas atspoguļo siltuma plūsmas viļņu amplitūdu attiecību, dažādām siltumizolācijas sistēmām atšķiras un pozitīvi korelē ar tvaika difūzijas pretestību.
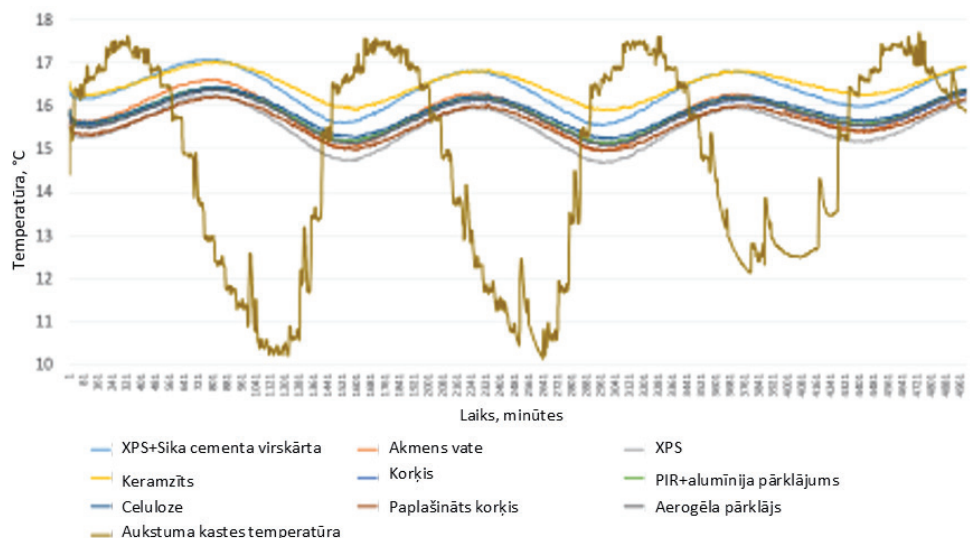
2.7. att. Temperatūras izmaiņas starp mūri un siltumizolācijas materiālu dinamiskajā testā.

Relatīvo mitrumu zem izolācijas materiāla ietekmē āra gaisa temperatūras un iekštelpu relatīvā mitruma izmaiņas. Ja āra temperatūra ir nemainīga un iekštelpu relatīvais mitrums vides apstākļos svārstās, relatīvais mitrums zem izolācijas tvaika caurlaidīgās siltumizolācijas sistēmās ar zemu tvaika difūzijas pretestību uzvedas kā iekštelpu relatīvais mitrums (2.8. att.). Kavējums ir atkarīgs no S_d vērtībām. Jo mazāka ir tvaika pretestība, jo mazāka ir laika nobīde relatīvā mitruma viļņa izplatībai no sienas ārējās virsmas uz tās iekšējo virsmu, un jo lielāka ir relatīvā mitruma viļņu amplitūdu attiecība abās sienas virsmās. Tvaika necaurlaidīgās sistēmas ar augstu tvaika difūzijas pretestību neietekmē iekštelpu relatīvais mitrums, un relatīvais mitrums starp mūri un siltumizolāciju ir atkarīgas tikai no āra gaisa temperatūras.
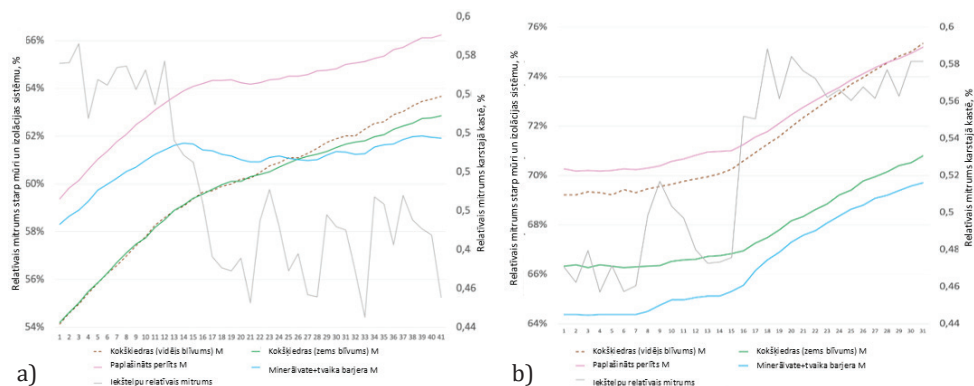

2.8. att. Relatīvā mitruma izmaiņas starp mūri un tvaika caurlaidīgu siltumizolācijas materiālu, kad telpas relatīvais mitrums: a) samazinās; b) pieaug.

Ja iekštelpu relatīvais mitrums ir stabils un āra temperatūra svārstās, tvaika caurlaidīgās siltumizolācijas sistēmās ar zemu tvaika difūzijas pretestību relatīvais mitrums zem izolācijas seko temperatūras profilam. Jo zemāka ir tvaika difūzija, jo tuvāk relatīvā mitruma viļņi zem izolācijas seko temperatūras profilam. Tvaika necaurlaidīgām sistēmām relatīvā mitruma vērtību amplitūda samazinās, kad tvaika difūzijas pretestība samazinās. 2.9. attēlā redzams, kā mainās relatīvais mitrums starp siltumizolāciju un mūri, ja iekštelpu relatīvais mitrums ir stabils un āra temperatūra svārstās.

Kad svārstās gan iekštelpu relatīvais mitrums, gan āra gaisa temperatūra, tvaika caurlaidīgās sistēmas ar zemu tvaika difūzijas pretestību vairāk seko iekštelpu relatīvā mitruma profilam.
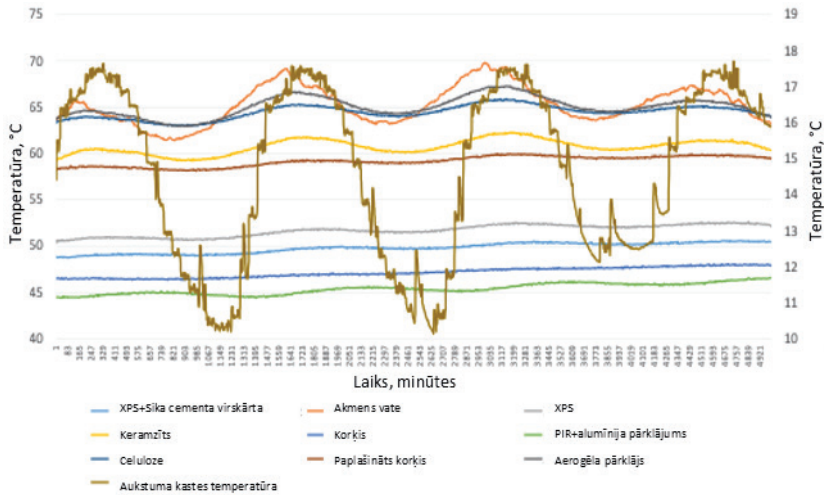
2.9. att. Relatīvais mitrums starp siltumizolāciju un mūri, ja iekštelpu relatīvais mitrums ir stabils un āra temperatūra svārstās (dinamiskais cikls).
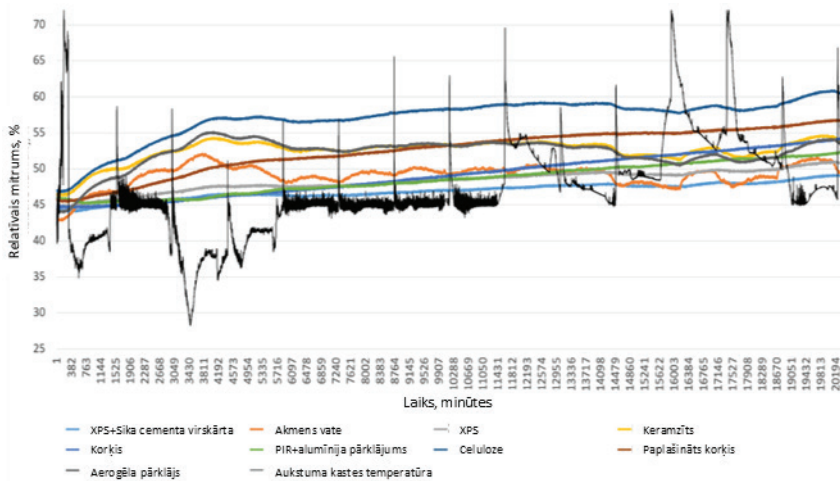
2.10. att. Vēja dzīta lietus testa rezultāti deviņām siltumizolācijas sistēmām.

2.10. attēlā redzami vēja dzīta lietus testa rezultāti deviņām siltumizolācijas sistēmām. Rezultāti liecina, ka vēja dzītā lietus apstākļos relatīvā mitruma palielināšanās zem siltumizolācijas sistēmām ir saistīta ar materiāla tvaiku difūzijas pretestību. Jo lielāka pretestība, jo lielāka ir vēja dzītā lietus ietekme, jo samazinās žūšanas iespēja uz telpas pusi.

Tvaika caurlaidīgi materiāli, piemēram, korķis, uzpūsts korķis un augsta blīvuma kokšķiedru plātnes bez tvaika barjerām, darbojas līdzīgi kā tvaika necaurlaidīgās sistēmas. Relatīvais mitrums zem izolācijas ir mazāk jutīgs pret iekštelpu

relatīvā mitruma izmaiņām un jutīgāks pret āra temperatūras svārstībām. Korķis ir mazāk jutīgs pret mitrumu nekā koks un koksnes materiāli.

Pētījums rāda, ka testēšanas periodam jābūt ilgākam, lai noteiktu mitruma uzkrāšanos mūra paraugos un tā ietekmi uz temperatūru un relatīvo mitrumu zem siltumizolācijas materiāla. Lai noteiktu mitruma uzkrāšanās ilgtermiņa ietekmi, nepieciešams veikt vai nu garākus testa ciklus, vai arī matemātiskā modeļa simulāciju, validējot modeli ar jau iegūtiem īstermiņa datiem.

Skaitliskie eksperimenti simulācijas rīkā *Delphin* parādīja, ka simulācijas kvalitāte ir atkarīga no ievades datiem. Lai simulācija nodrošinātu visprecīzākos ievades datus, visiem materiāliem, ieskaitot siltumizolāciju un javu, jābūt pēc iespējas tuvākam faktiskajām vērtībām. Materiāli ir jātestē pirms simulācijas, un katram jāizveido pielāgots materiāla fails, lai simulācija būtu pēc iespējas tuvāka realitātei. Citos pētījumos ir līdzīgi secinājumi [20], ilustrējot to ar ķieģeļu parametru nozīmību – diviem ķieģeļiem ar līdzīgu ūdens uzsūces koeficientu ir atšķirīga ūdens vadītspēja, arī higrotermālā uzvedība ir atšķirīga. (*Kloseiko et al.*, 2022) [23] secināja, ka iekšējās siltināšanas projektos katram gadījumam joprojām ir nepieciešama specifiska pieeja. Cits pētījums atklāj, ka daudzus materiālu parametrus, kas nepieciešami higrotermiskām simulācijām, ir grūti noteikt, jo īpaši tvaika vadītspēju un kapilāro vadītspēju kā mitruma satura funkciju [24]. Savukārt (*Leone et. al.*, 2019) [25] iesaka veikt detalizētu plānošanu, lai iegūtu visas parametru vērtības, kas nepieciešamas katram iekšējās siltināšanas projektam.

Šī pētījuma gaitā tika apskatīts arī inovatīvs bioloģiskas izcelsmes siltināšanas materiāls no priedes (*Pinus Sylvestris*) skujām, kas ražots pēc bioekonomikas principiem, un tā lietojums siltināšanai no iekšpuses vēsturiskām masīvām sienām [26]. Pētījums tika veikts, lai noteiktu materiāla higrotermālās īpašības un novērtētu temperatūras un relatīvā mitruma ietekmi uz mitruma transportu un uzkrāšanos, kā arī kritiskos apstākļus pelējuma augšanai. Skuju siltumizolācijas materiāls tika apstrādāts ar kaļķi, lai novērstu pelējuma veidošanos, un tika salīdzināts ar neapstrādātu materiālu. Inovatīvais bioloģiski ražotais materiāls tika sagatavots, pamatojoties uz bioekonomikas principiem un ar samazinātu dzīves cikla ietekmi. Šis augstas pievienotās vērtības produkts tika radīts no priežu skujām no meža atliekām. Skujas tika sajauktas ar kaļķi un ksantāna sveķiem, lai izvairītos no tādu produktu izmantošanas, kuru pamatā ir fosilie produkti ar lielu ietekmi uz vidi.

Iegūtie rezultāti liecina, ka pētītais materiāls ir ļoti porains un kaļķa pievienošana palielina materiāla mitruma absorbcijas ātrumu, jo palielinās poru laukums. Skuju siltumizolācijas materiālam ir lielāka mitruma pārneses un uzglabāšanas spēja, un tas ir labs higriskais regulators. Šī ir svarīga vēsturisko ēku iekšējai siltināšanai lietojama siltumizolācijas materiāla īpašība, jo, samazinoties apkārtējā gaisa relatīvajam mitrumam, tas spēj ātri izžūt. Siltumizolācijas materiāla apstrādei ar kaļķi ir neliela ietekme uz siltumvadītspēju, bet ir ietekme uz pelējuma augšanas samazināšanos (2.11. att.).
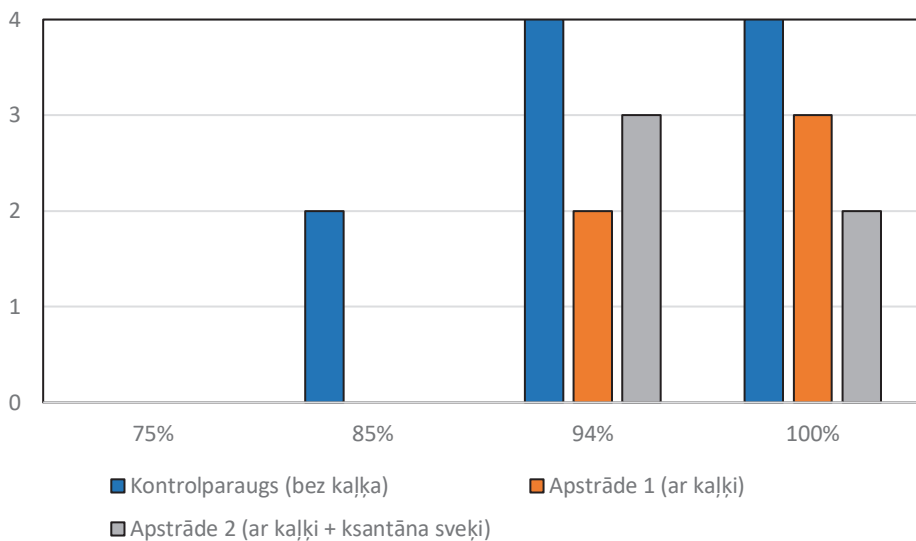
2.11. att. Pelējuma augšana uz materiālu paraugiem dažādos relatīvā mitruma apstākļos.

Ar kaļķi apstrādātam paraugam netika novērota pelējuma veidošanās 85 % relatīvajā mitrumā, savukārt pie relatīvā mitruma 94 % un 100 % pelējums tika atrasts visos paraugos (2.12. att.).
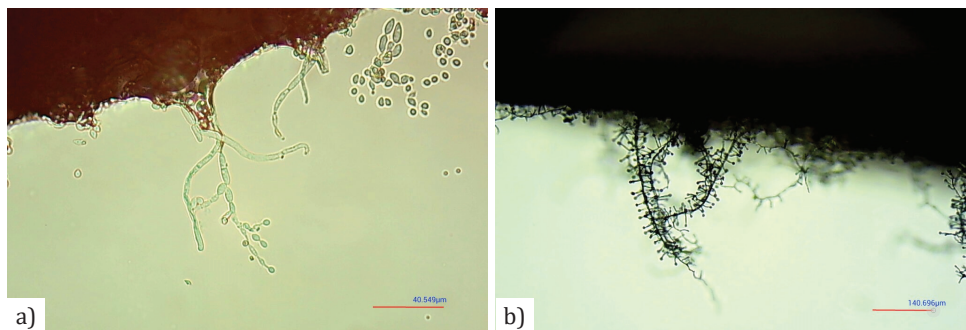
2.12. att. Pelējuma veidošanās uz paraugiem pie 100 % relatīvā mitruma: a) *Cladosporium* uz parauga virsmas bez kaļķa; b) *Trihodermija viride* uz apstrādātā parauga virsmas.

Līdzsvara apstākļos zemāka temperatūra rada augstāku relatīvā mitruma līmeni starp akmens sienu un skuju siltumizolācijas materiālu un sasniedz kritisko vērtību pelējuma augšanai. Dinamisku apstākļu testa rezultāti (2.13. att.) liecina, ka galvenais relatīvā mitruma izmaiņu virzītājspēks ir iekštelpu gaisa relatīvais mitrums, nevis temperatūras izmaiņas sienā. Pat tad, ja siltumizolācijas materiāls tiek apstrādāts ar kaļķi, ir jāupurē siltuma ietaupījumi, lai samazinātu kritiskos apstākļus pelējuma augšanai.
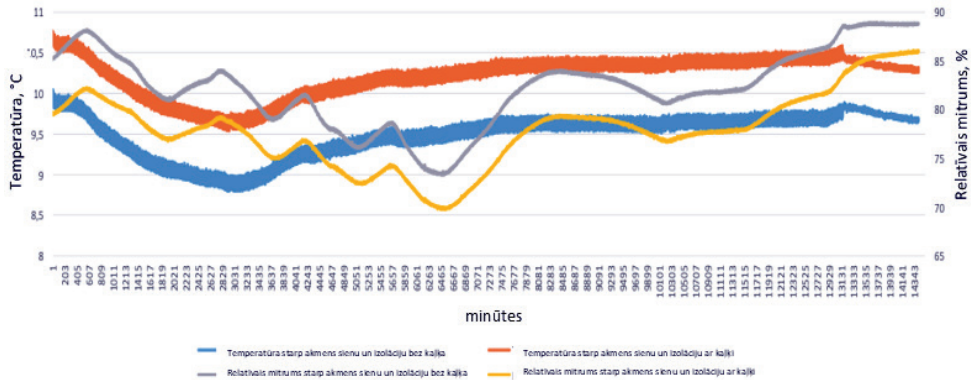
2.13. att. Relatīvais mitrums un temperatūra mainīgos apstākļos starp akmens sienu un adatas izolāciju ar kaļķi un bez tā.

Pētījumā secināts, ka turpmākajos pētījumos galvenā uzmanība jāpievērš kaļķa un izolācijas materiāla svara attiecības optimizācijai, lai uzlabotu higrotermisko uzvedību un kritiskos apstākļus riska režīmiem. Ir jāveic arī papildu testi, lai samazinātu izolācijas materiāla sablīvēšanos sienā. Jāpārbauda arī citi materiāli kaļķu putekļošanas samazināšanai.

2.3. Iekšējās siltināšanas lietojums vēsturiskās ēkās

Gan *in-situ* mērījumi, gan higrotermiskā simulācija vienģimeņu mājas (Secē) abās telpās uzrādīja apmierinošus higrotermiskos apstākļus sienā [12]. Ārsienas higrotermiskā uzvedība liecina, ka pelējuma augšanas riska nav, jo normālos ēkas ekspluatācijas apstākļos (izņemot ūdens noplūdes negadījumu) relatīvais mitrums starp siltumizolācijas slāni un ģipškartona plāksnēm ir salīdzinoši zems (zem 60 %). 2.14. attēlā redzamas mērītās relatīvā mitruma izmaiņas telpā, āra gaisā un zem siltumizolācijas, kā arī simulētās relatīvā mitruma vērtības dzīvojamā istabā.
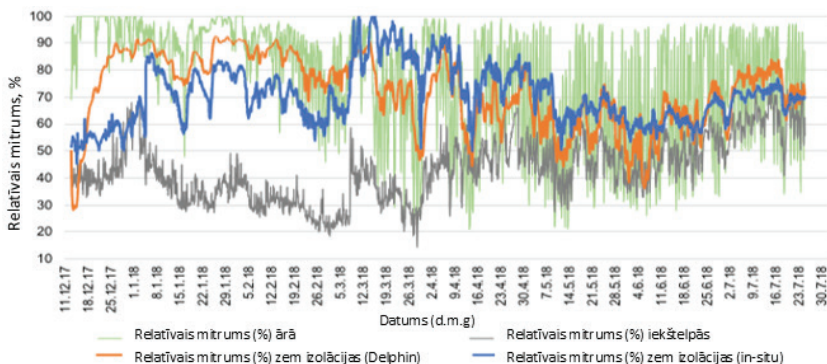
2.14. att. Mērītās relatīvā mitruma izmaiņas telpā un zem siltumizolācijas, kā arī simulētās relatīvā mitruma vērtības dzīvojamā istabā.

2.15. attēlā redzamas mērītās relatīvā mitruma izmaiņas telpā un zem siltumizolācijas, kā arī simulētās relatīvā mitruma vērtības vannasistabā.
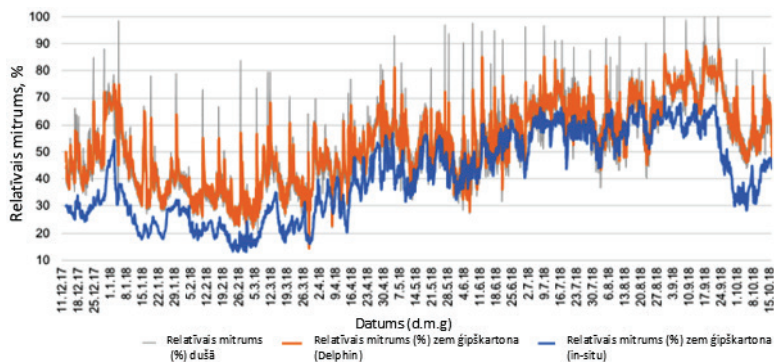
2.15. att. Mērītās relatīvā mitruma izmaiņas telpā un zem siltumizolācijas, kā arī simulētās relatīvā mitruma vērtības vannasistabā.

Relatīvais mitrums virs kritiskajiem 80 % starp dolomīta sienu un izolācijas slāni sasniedz tikai īsu laiku. Bet šajos brīžos un šajā vietā temperatūra ir zemāka nekā nepieciešama sporu dīgšanai (sākotnējai pelējuma augšanai). Pelējuma veidošanās var notikt pie 80 % augsta relatīvā mitruma, ja porainiem materiāliem temperatūra ir vismaz 20 °C. Taču, ņemot vērā to, ka 2015. gada renovācijas laikā īrnieki uz vannasistabas sienām konstatēja pelējumu, pastāv pelējuma augšanas potenciāls, ja izveidojas atbilstoši apstākļi (augsts relatīvais mitrums un temperatūra) un tie saglabājas pietiekami ilgi, jo sienu materiāli satur pelējuma sporas.

Temperatūras mērījumi liecina, ka dolomīta sienas ārējā daļa piedzīvo atkārtotus sasalšanas un atkušanas ciklus, taču sabrukšanas risks no sasalšanas un atkušanas cikliem ir ārkārtīgi mazs, jo dolomīts nesasniedz piesātinājumu.

Simulācijas rezultāti rāda, ka gada siltuma patēriņu telpu apkurei bāzes scenārijā var samazināt par 35 %, ja pirmā un otrā stāva sienas tiek siltinātas no iekšpuses. Ja tiek veikta būtiska energoefektivitātes paaugstināšana (iekšējo sienu siltināšana, pagraba griestu, jumta siltināšana, logu nomaiņa), bāzes enerģijas patēriņš var samazināties par 72 %. Faktiskais enerģijas patēriņš tiek aprēķināts, pamatojoties uz iedzīvotāju sniegtajiem datiem, kuri rēķina primāros energoresursus – malku, kas daļēji tiek piegādāta tieši no meža un žāvēta uz vietas. Ja koksnes baļķu patēriņu pārvērš gala enerģijā, enerģijas patēriņam gadā uz apsildāmo platību jābūt 87 kWh/m^2. Enerģijas ietaupījums ir par 17 % mazāks, nekā aprēķināts simulācijas modelī. Šo atšķirību var radīt vairāki iemesli, piemēram, nenoteiktība par būvdarbu kvalitāti un atlikušajiem siltuma tiltiem, modeļa ievades dati, tostarp faktori, kas saistīti ar noslogojuma biežumu (siltuma pieaugums, telpas temperatūra un ventilācijas biežums). Simulācijas rezultāti ir jutīgi pret ievades datu kvalitāti, piemēram, telpas temperatūru, relatīvo mitrumu, ventilāciju un materiāla īpašībām. Vēsturiskajās ēkās trūkst detalizētas informācijas par sienu dobumiem, akmeņu un javas attiecību un tipoloģiju, būvniecības defektiem, materiālu

specifiskajām īpašībām. Savukārt faktiskā primārās enerģijas patēriņa nenoteik-tība, tai skaitā enerģijas pārveidošanas tehnoloģiju malkas efektivitātes apjoms un kvalitāte, būtiski ietekmē galaenerģijas patēriņa vērtības.

Vēsturiskajai ēkai Bīskapa gātē Rīgā tika konstatēti būtiski bojājumi fasā-des apmetumā, un ēkai uz fasādes ir daudz plaisu un spraugu. Šīs atvērtās zonas nodrošina āra mitruma, tai skaitā vēja dzīta lietus, iekļūšanu ārsienās. Balstoties laikapstākļu datu analīzē, pētījumā tiek secināts, ka fasādi spēcīgi ietekmē āra relatīvais mitrums un lietus. Uz fasādes augošās aļģes liecina, ka uz sienu virsmas ir bijis lietusūdens. Laika apstākļu dati rāda, ka valdošais vējš monitoringa periodā ir no dienvidaustrumiem un ēkas lielākā fasāde ir pakļauta vēja dzītam lietum. 2.16. attēlā redzami temperatūras mērījumi monitoringa periodā. Telpas tempe-ratūra un temperatūra starp mūri un siltumizolāciju seko āra gaisa temperatūras profilam, jo telpā ir nepietiekama apkures radiatora jauda.
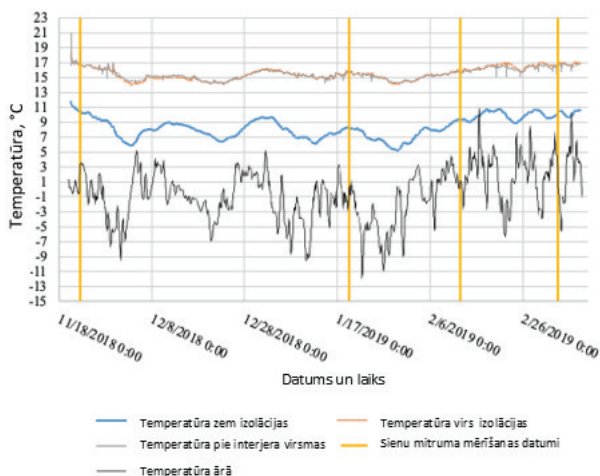


2.16. att. Temperatūras mērījumi monitoringa periodā.

Āra laikapstākļi ietekmē arī apstākļus starp siltumizolāciju un mūri, taču moni-toringa periodā intersticiāla kondensācija nav novērota. Relatīvā mitruma svārstī-bas starp mūri un siltumizolācijas materiālu (2.17. att.) ir saistītas ar temperatūras izmaiņām. Augstākais relatīvais mitrums zem izolācijas materiāla monitoringa periodā sasniedz 84 %, un lielāko daļu laika relatīvais mitrums saglabājas zem 80 %. Šādi mitruma apstākļi nerada lielu pelējuma veidošanās risku.
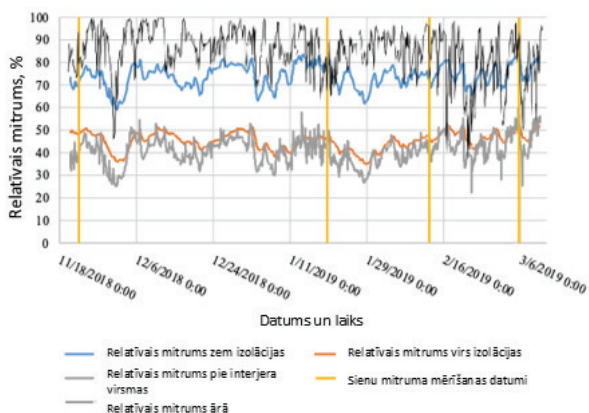
2.17. att. Relatīvā mitruma izmaiņas monitoringa periodā.

Neinvazīvie mitruma mērījumi veikti ar mikroviļņu mērījumu metodi 20 cm dziļumā un dielektrisko metodi 2 cm dziļumā. Iegūtās vērtības norāda mitrumu relatīvā mērogā – no sausākas līdz mitrai zonai, kur 0 ir sausākā, 250 – mitrākā vērtība. Sienas apakšējā mērījumu zona ir līdz 0,8 m virs zemes, vidējā daļa – no 0,8 m līdz 1,6 m virs zemes, augšējā daļa – no 1,6 m līdz 2 m virs zemes. 2.18. attēlā redzamas vidējo vērtību izmaiņas augšējā, vidējā un apakšējā daļā mikroviļņu mērījumiem 20 cm dziļumā. Mērījumu periodā ir vērojama augšupejoša tendence sienas apakšējā daļā. Arī augšējā daļa seko augšupejošai tendencei ar nelielu samazinājumu no 1. uz 2. mērījumu. Vidējā posma mitruma mērījumos janvārī bija vērojams vidējā mitruma līmeņa kritums, bet pēc tam tas sāk sekot augšupejošai tendencei.

2.19. attēlā redzamas vidējo vērtību izmaiņas augšējā, vidējā un apakšējā daļā dielektriskajiem mērījumiem 2 cm dziļumā.
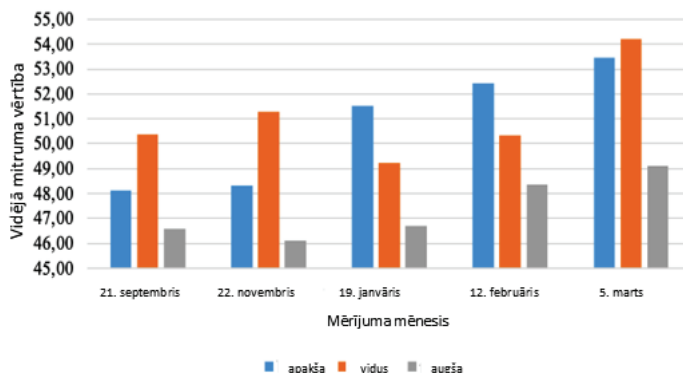
2.18. att. Vidējo vērtību izmaiņas augšējā, vidējā un apakšējā sienas daļā, mikroviļņu mērījumiem 20 cm dziļumā.
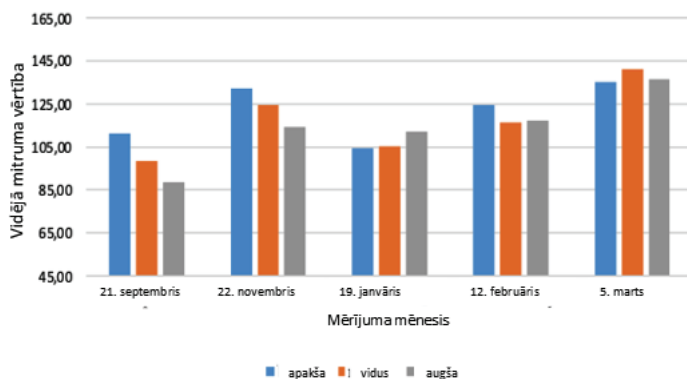
2.19. att. Vidējo vērtību izmaiņas augšējā, vidējā un apakšējā daļā, dielektriskajiem mērījumiem 2 cm dziļumā.

Pētījuma [13] veikšanas laikā netika novērotas skaidras mitruma problēmu pieauguma pazīmes, taču jāņem vērā, ka monitoringa periods bija tikai septiņus mēnešus gada aukstajā periodā, palielināta mitruma problēma varētu rasties gada siltajos mēnešos. Fasādes nviendabīgums varētu būt cēlonis mērījumu svārstībām, īpaši dielektriskajiem mērījumiem, kas veikti tuvu virsmai. Lai iegūtu pārliecinošākus rezultātus, uzraudzība jāturpina vismaz vienu pilnu gadu. Jāveic vēja lietus mērījumi uz fasādes un nepārtraukta mitruma uzraudzība dažādos mūra augstumos.

2.4. Pozitīvas enerģijas bilances kvartāls vēsturiskā pilsētvidē

Kvartāli ar energoefektivitātes potenciālu atrodas RVC ārējā perimetrā, savukārt kvartāli ar augstāku kultūrvērtību koncentrējas RVC centrālajās daļās, tāpēc lēmumu pieņemšanas hierarhijā tika noteikti divi apakšmērķi: 1) atrast RVC pilsētas kvartālu ar augstāko energoefektivitātes potenciālu; 2) atrast RVC pilsētas kvartālu, kas pārstāv kultūras mantojuma un pilsētvides dzīvotspējas augstākās kvalitātes.

Izmantojot daudzkritēriju analīzi, tika veikta "Kultūras mantojuma kvartāla" izvēle. Kritēriju svari tiek iegūti pāru salīdzināšanas matricā pēc analītiskās hierarhijas procesa metodoloģijas. 2.20. attēlā redzams kritēriju svars. Kā svarīgākie kritēriji ir noteikti kultūras nozīme un būvniecības periodu dažādība. No dzīvošanas kvalitātes viedokļa vissvarīgākā ir aizsardzība pret noziedzību, laba maņu pieredze un ēku renovācija.
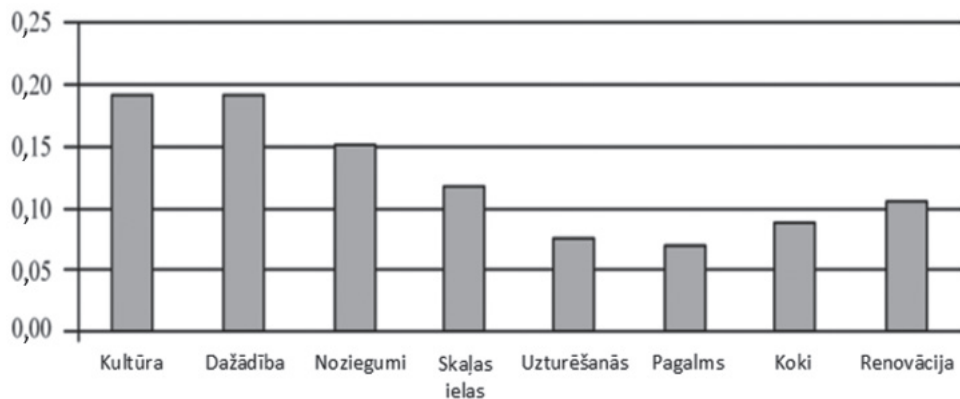
2.20. att. Kultūras mantojuma un dzīvošanas kvalitātes kritēriju svars.
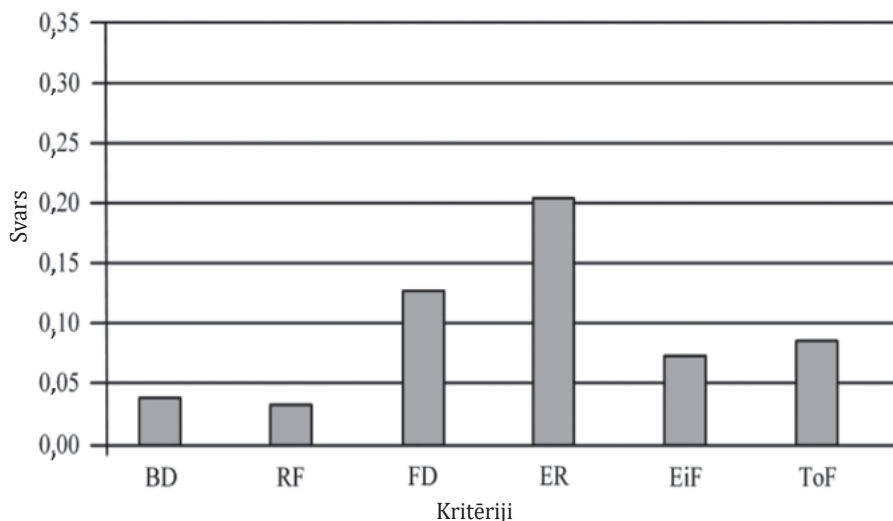
2.21. att. Enerģētikas kvartāla kritēriju īpatsvari. (BD – Apbūves blīvums; RF – Dzīvojamo
ēku blīvums; FD – Nākotnes attīstības iespējas; ER – Ēku atjaunošanas iespējas;
EiF – Energoietilpīgs uzņēmums; ToF – Energoietilpīgā uzņēmuma veids)

Pētījuma gaitā tika identificēti divi atšķirīgi kvartāli, kas ieguva visaugstāko vērtējumu kā "Kultūras mantojuma kvartāls". Pirmais kvartāls atrodas pie RVC robežas, ietver izcilas kultūras mantojuma vērtības – ievērojamākos jūgendstila paraugus Rīgas vēsturiskajā pilsētā. Pārsvaru nodrošina gan kultūras mantojums, gan dzīvošanas kvalitātes kritēriji (noziedzība, nepatīkami sajūtu pārdzīvojumi un ēku renovācija). Otrais kvartāls, kas ieņem augstāko vērtējumu no kultūras mantojuma un apdzīvojamības viedokļa, ir neliels pilsētvides kvartāls RVC iekšējā daļā.

Izmantojot daudzkritēriju analīzi, tika noteikti visatbilstošākie "Enerģētikas kvartāli". Galvenais mērķis ir noteikt kvartālus ar lielāko potenciālu pārtapšanai

par pozitīvas energobilances kvartālu. Sākotnēji kvartāli tika atlasīti, balstoties šādos izvēles kritērijos: 1) kvartālā atrodas energoietilpīgs uzņēmums; 2) kvartālam ir vismaz 10 % dzīvojamā funkcija; 3) pilsētas kvartālā ir neapbūvēts zemesgabals augsti efektīvai attīstībai. Balstoties šajos kritērijos, tika atlasīti 12 kvartāli detalizētākai izpētei un daudzkritēriju analīzei ar *TOPSIS* metodi. 2.21. attēlā redzami vērtēšanas kritēriju īpatsvari.

Pētījums liecina, ka kvalitatīvāka arhitektūra ar nozīmīgāku kultūras vērtību koncentrējas RVC centrālajos rajonos pa galvenajām trasēm, kur savulaik tai bijusi reprezentatīva funkcija – eksponēt tehnoloģiskos sasniegumus un konceptuāli jaunas idejas. Diemžēl laika gaitā galvenie maršruti ir zaudējuši savu nozīmi jaunu arhitektūras koncepciju un ideju demonstrēšanā un kļuvuši par transporta infrastruktūru. Automašīnas ņem virsroku pār cilvēkiem, un kulturāli vērtīgākās teritorijas satiksmes dēļ zaudē savu dzīvotspēju. Konstatēts, ka kvartāli ar lielāku apdzīvojamību atrodas nedaudz tālāk no galvenajām ielām, bet tomēr RVC centrālajos rajonos. Šiem kvartāliem ir zemāka kultūras vērtība, bet augstākas dzīvošanas kvalitātes īpašības. "Enerģētikas kvartāli" pārsvarā atrodas RVC malās. Lielākā daļa identificēto energoietilpīgo kvartālu ir uzbūvēti pēc Otrā pasaules kara. Pēc kara plānošanā publiskās telpas tika integrētas esošajā pilsētas struktūrā.

Pētījuma rezultāti rāda, ka abos ("Enerģētikas kvartāls" un "Kultūras mantojuma kvartāls") sarakstos bija tikai divi kvartāli, taču neviens no tiem neieņēma augstu vietu individuālajā alternatīvu reitingā un netika apspriests turpmākai izpētei. Viens no tiem tika izvēlēts tālākai analīzei. Kvartāla ilustrācijas redzama 2.22. attēlā.

2.22. att. Pētījumā izvēlētais pilsētas kvartāls, kas ir visatbilstošākais pārejai uz pozitīvu energobilances kvartālu gan no enerģētikas, gan kultūrvēsturiskā vērtības aspekta.

Tiecoties uz oglekļa neitrālu nākotni 2050. gadā, būtiska uzmanība ir jāpievērš esošajām ēkām, jo tajās ir liels CO_2 emisiju samazināšanas potenciāls. Taču jāņem

vērā tas, ka vēsturiskās pilsētbūvniecības struktūras ir sarežģītas – apbūves blīvums ir augsts, attālums starp ēkām ir mazāks nekā jaunbūvēm un saglabājama vēsturiskā vērtība, kas ierobežo energoefektivitātes pasākumus. 2.2. tabulā apkopoti pētījuma rezultāti par energoefektivitātes potenciālu, atjaunojamo energoresursu potenciālu un CO_2 samazinājumu izvēlētajā Rīgas vēsturiskā centra kvartālā. Pētījuma aprēķini par iespējamo CO_2 ietaupījumu, pārejot no tradicionālā vēsturiskā pilsētas kvartāla uz pozitīvās enerģijas kvartālu, liecina par aptuveni 45 kg/m² CO_2 ietaupījuma potenciālu gadā, samazinot CO_2 emisijas no 50 kg/m² līdz 5 kg/m² gadā un kopumā 1627 tonnas gadā. Atbilstoši aprēķinātajiem rezultātiem siltumenerģijas pieprasījumu var pilnībā segt ar uz vietas saražoto enerģiju (izmantojot akumulāciju vai pievadot centralizētās siltumapgādes tīklu), bet elektroenerģijas pieprasījuma segšanai energoietilpīgu patērētāju gadījumā nepieciešama ārēja ražošana. Rezultāti parāda potenciālu, kā sasniegt ļoti zemu enerģijas pieprasījumu kvartālā.

2.2. tabula

Pētījuma rezultāti par energoefektivitātes potenciālu, atjaunojamo energoresursu potenciālu un CO_2 samazinājumu izvēlētajā Rīgas vēsturiskā centra kvartālā

Izmantotā tehnoloģija	Enerģijas ietaupījumi			Enerģijas ražošana		CO_2
	Sil-tums	Elek-trība		Elek-trība	Siltu-menerģija	CO_2 ietau-pījumi
	MWh	MWh	m²	MWh	MWh	tonnas
Enerģijas ietaupījumi no ēku energoefektivitātes	2686	2400	–	–	–	970
Atlikumu siltuma izmantošana			–	–		
Datu centra atlikumu siltums	–	–	–	–	338	89
Izmanto dzesēšanas enerģijas patēriņu			–	–	83	22
Enerģijas ražošana						
Izmantojamā jumta platība						
Jumta platība pārklāta ar *PV*	–	–	5965	1014	–	111
Jumta platība pārklāta ar *PVT*	–	–	3895	425	1380	411
Fasādes	–	–				
Izmantojamā platība uz dienvid-austrumu fasādes	–	–	1307	135	–	15
Izmantojamā platība uz dienvidrie-tumu fasādes	–	–	835	89	–	10
				1663	1800	1627
Procentuālais īpatsvars no kopējā izvēlētā enerģijas patēriņa				69 %	100 %	

SECINĀJUMI

1. hipotēze

Vēsturiskiem ķieģeļiem ir atšķirīgas higrotermālās īpašības, un tās ietekmē higrotermālos procesus no iekšpuses siltinātās masīvās mūra sienās.

Hipotēze apstiprinājās, jo 40 vēsturisku ķieģeļu paraugu testēšanas rezultāti rāda, ka tiem ir atšķirīgas higrotermālās īpašības. Iegūtie rezultāti rāda, ka ķieģeļu paraugu sadalījums klasteros ir līdzīgs ķieģeļu paraugu tipu sadalījumam, pamatojoties uz to aprakstu, tāpēc vispārinātus secinājumus nevar izdarīt. Tomēr pētījumā novērots, ka sarkanajiem māla ķieģeļiem, kas ražoti no 19. gadsimta beigām līdz 20. gadsimta sākumam, ir izteikta atšķirība starp diviem galvenajiem klasteriem un tikai divi no paraugiem atrodas citās kopās. Lai iegūtu detalizētākus rezultātus par iespējamiem klasteriem, nepieciešams turpināt pētījumus ar lielāku paraugu skaitu. Pētījumā par 40 testēto ķieģeļu mūra siltināšanu no iekšpuses ar tvaika caurlaidīgu kapilāri aktīvu siltumizolācijas materiālu aukstā klimatā secināts, ka visos sienu paraugos ir ļoti līdzīgas temperatūras tendences, savukārt mitruma uzvedībā ir vērojama liela atšķirība. Temperatūras svārstības starp dažādiem sienu veidiem ir atkarīgas no ķieģeļu termiskās pretestības. Mitruma satura līmeņi dažādiem sienu veidiem atšķiras četras reizes, un mitruma satura uzvedība ir ļoti atšķirīga. Simulācijas rezultāti rāda, ka mitruma saturu mūrī un siltumizolācijas materiālā, kā arī relatīvo mitrumu starp mūri un siltumizolācijas materiālu ietekmē lietus un līmes uzklāšanas kvalitāte. Simulācijas rezultāti liecina, ka, ja siltināšana no iekšpuses notiek ar tvaika caurlaidīgu kapilāri aktīvu materiālu ēkā, kas atrodas aukstā klimatā un ir ar normālu iekštelpu mitruma slodzi, relatīvais mitrums starp mūri un siltumizolāciju nepārsniedz 96 % un tiek uzskatīts par drošu. Šis secinājums attiecas gan uz izolāciju ar līmi, gan bez tās.

2. hipotēze

Klimatiskie āra apstākļi ietekmē higrotermālos procesus no iekšpuses siltinātās masīvās mūra sienās.

Hipotēze apstiprinājās daļēji, jo dažādu siltumizolācijas materiālu testēšanas rezultāti rāda, ka atkarībā no siltumizolācijas sistēmas veida (tvaika caurlaidīga vai tvaika necaurlaidīga) higrotermālos procesus no iekšpuses siltinātās masīvās mūra sienās ietekmē ne tikai klimatiskie āra apstākļi, bet arī iekštelpas gaisa parametri. Turklāt tika secināts, ka testētajām siltumizolācijas sistēmām ir līdzīga termālā uzvedība, bet tām ir atšķirīga mitruma uzvedība. Siltināšanai no iekšpuses ir liela ietekme uz sienas higrotermisko uzvedību, jo pieaug relatīvais mitrumu starp siltumizolāciju un mūra sienu, kas savukārt palielina pelējuma rašanās, sala bojājumu un koka siju sabrukšanas risku. Konstrukcijās rodas siltuma plūsmas kavējums starp konstrukcijas iekšējo virsmu un ārējo virsmu, un tā lielums ir atkarīgs no robežnosacījumiem – jo lielāka ir atšķirība starp iekštelpu un āra temperatūru, jo lielāka ir laika nobīde. Temperatūras samazinājuma koeficients, kas atspoguļo

siltuma plūsmas viļņu amplitūdu attiecību, dažādām siltumizolācijas sistēmām atšķiras un pozitīvi korelē ar tvaika difūzijas pretestību.

Relatīvo mitrumu zem izolācijas materiāla ietekmē āra gaisa temperatūras un iekštelpu relatīvā mitruma izmaiņas. Ja āra temperatūra ir nemainīga un iekštelpu relatīvais mitrums vides apstākļos svārstās, relatīvais mitrums zem izolācijas tvaika caurlaidīgās siltumizolācijas sistēmās ar zemu tvaika difūzijas pretestību uzvedas kā iekštelpu relatīvais mitrums. Kavējums ir atkarīgs no S_d vērtībām. Jo mazāka ir tvaika pretestība, jo mazāka ir laika nobīde relatīvā mitruma viļņa izplatībai no sienas ārējās virsmas uz tās iekšējo virsmu, un jo lielāka ir relatīvā mitruma viļņu amplitūdu attiecība abās sienas virsmās. Tvaika necaurlaidīgās sistēmas ar augstu tvaika difūzijas pretestību neietekmē iekštelpu relatīvais mitrums, un relatīvais mitrums starp mūri un siltumizolāciju ir atkarīgas tikai no āra gaisa temperatūras. Ja iekštelpu relatīvais mitrums ir stabils un āra temperatūra svārstās, tvaika caurlaidīgās siltumizolācijas sistēmās ar zemu tvaika difūzijas pretestību relatīvais mitrums zem izolācijas seko temperatūras profilam. Jo zemāka ir tvaika difūzija, jo tuvāk relatīvā mitruma viļņi zem izolācijas seko temperatūras profilam. Tvaika necaurlaidīgām sistēmām relatīvā mitruma vērtību amplitūda samazinās, kad samazinās tvaika difūzijas pretestība. Kad svārstās gan iekštelpu relatīvais mitrums, gan āra gaisa temperatūra, tvaika caurlaidīgās sistēmas ar zemu tvaika difūzijas pretestību vairāk seko iekštelpu relatīvā mitruma profilam.

Rezultāti liecina, ka vēja dzītā lietus apstākļos relatīvā mitruma palielināšanās zem siltumizolācijas sistēmām ir saistīta ar materiāla tvaiku difūzijas pretestību. Jo lielāka pretestība, jo lielāka ir vēja dzītā lietus ietekme, jo samazinās žūšanas iespēja uz telpas pusi.

Tvaika caurlaidīgi materiāli, piemēram, korķis, uzpūsts korķis un augsta blīvuma kokšķiedru plātnes bez tvaika barjerām, darbojas līdzīgi kā tvaika necaurlaidīgās sistēmas. Relatīvais mitrums zem izolācijas ir mazāk jutīgs pret iekštelpu relatīvā mitruma izmaiņām un jutīgāks pret āra temperatūras svārstībām. Korķis ir mazāk jutīgs pret mitrumu nekā koks un koksnes materiāli.

Skaitliskie eksperimenti simulācijas rīkā Delphin rāda, ka simulācijas kvalitāte ir atkarīga no ievades datiem. Lai simulācija nodrošinātu visprecīzākos ievades datus, visiem materiāliem, ieskaitot siltumizolāciju un javu, jābūt pēc iespējas tuvākam faktiskajām vērtībām. Materiāli ir jātestē pirms simulācijas, un katram jāizveido pielāgots materiāla fails, lai simulācija būtu pēc iespējas tuvāka realitātei. Pētījums rāda, ka aukstā klimatā vēsturiskajam mūrim uzliekot iekšējo izolāciju, ir rūpīgi jānovērtē kombinētās vēsturiskā mūra un izolācijas materiālu sienu konstrukcijas higrotermiskās īpašības. Simulācijas rezultāti var nesakrist ar izmērītajiem datiem sienas sākotnējā mitruma satura vērtību dēļ, kā arī parametru vērtības ietekmes dēļ.

3. hipotēze

Vēsturiskās mūra un akmens sienu siltināšana no iekšpuses ar tvaika necaurlaidīgu siltumizolāciju aukstā klimatā ir drošs energoefektivitātes paaugstināšanas pasākums.

Hipotēze apstiprinājās, jo mērījumu un datorsimulāciju rezultāti rāda, ka ārsienu siltināšana no iekšpuses ar tvaika necaurlaidīgu siltumizolācijas sistēmu aukstā klimatā šajās divās ēkās ir drošs energoefektivitātes paaugstināšanas pasākums. Abos gadījumos relatīvais mitrums starp ārsienu un siltumizolācijas sistēmu pārsniedz 80 % salīdzinoši neilgu laika posmu gada aukstajos mēnešos un nepietuvojas kondensāta veidošanās procesam. Pelējuma veidošanās risks ir zems, jo periodā, kad ir paaugstināts relatīvais mitrums, temperatūra ir zemāka nekā nepieciešama sporu dīgšanai un sākotnējai pelējuma augšanai. Abos gadījumos relatīvais mitrums starp sienu un siltumizolācijas materiālu seko āra gaisa temperatūras izmaiņām.

4. hipotēze

Vēsturiskās apbūves saglabāšana neļauj sasniegt pozitīvu energobilanci vēsturiskajos pilsētas kvartālos.

Hipotēze apstiprinājās, jo rezultāti liecina, ka kvartāliem ar augstāku kultūrvērtību ir mazāks energoefektivitātes potenciāls, un otrādi. Pētījumā tika izmantota dubultā daudzkritēriju analīze, kas rāda, ka pilsētu kvartālus var vērtēt gan no energoefektivitātes, gan kultūras mantojuma perspektīvas. Piedāvātie daudzkritēriju analīzes kritēriji, lai novērtētu kultūras mantojumu, dzīvotspēju un energoefektivitātes potenciālu, raksturo pilsētas kvartāla specifiskās īpašības. Turklāt rezultāti liecina, ka, lai sasniegtu pozitīvu enerģijas kvartālu, nepieciešami ļoti ambiciozi energoefektivitātes uzlabošanas mērķi. Pētījums rāda, ka šādas analīzes par pāreju no tradicionālā vēsturiskā pilsētas kvartāla uz pozitīvas energobilances kvartālu, kurā jāsaskaņo divas pretrunīgas koncepcijas – kultūras mantojuma saglabāšana un koncepcija "energoefektivitāte pirmajā vietā", katram solim ir vajadzīgas zināšanas par konkrēto kvartālu: 1) energoefektivitātes pasākumi ir jāpielāgo vietējam klimatam; 2) atjaunojamās enerģijas tehnoloģijām jāizmanto īpašas vides un klimata apstākļu priekšrocības; 3) saglabājamām vēsturiskajām vērtībām arī ir lokāls raksturs.

LITERATŪRAS SARAKSTS

[1] "Factsheet – Energy Performance of Buildings," European Commission – European Commission. Accessed: Oct. 04, 2023. [Online]. Available: https://ec.europa.eu/commission/presscorner/detail/en/fs_21_6691.

[2] "EUR-Lex - L:2023:231:TOC - EN - EUR-Lex." Official Journal of the European Union, Sep. 13, 2023. Accessed: Oct. 04, 2023. [Online]. Available: https://eur-lex.europa.eu/legal-content/LV/TXT/?uri=OJ%3AL%3A2023%3A231%3ATOC.

[3] "2022-06-27-102346--davos-declaration-2018-23-01-2018-lv.pdf." Accessed: Sep. 22, 2023. [Online]. Available: https://baukultur--production--storage.s3.amazonaws.com/baukultur/2022-06-27-102346--davos-declaration-2018-23-01-2018-lv.pdf.

[4] Ritvars Freimanis, "HYGROTHERMAL PROPERTIES OF HISTORIC BRICKS FROM VARIOUS SITES OF LATVIA." Mendeley, Oct. 18, 2021. doi: 10.17632/CGP2VYRTNH.3.

[5] "Project Jupyter." Accessed: Oct. 03, 2023. [Online]. Available: https://jupyter.org.

[6] F. Pedregosa *et al.*, "Scikit-learn: Machine Learning in Python," *J. Mach. Learn. Res.*, vol. 12, no. 85, pp. 2825–2830, 2011.

[7] R. Freimanis, A. Blumberga, R. Vanaga, and Z. Zundāns, "Evaluation of the Impact of Bricks of Various Characteristics on Internally Insulated Masonry Walls in Cold Climate," *Buildings*, vol. 13, no. 10, Art. no. 10, Oct. 2023, doi: 10.3390/buildings13102529.

[8] R. Freimanis, Z. Zundans, R. Balins, R. Vanaga, and A. Blumberga, "Finding the Generic Hygrothermal Properties of Historical Bricks by Supervised Agglomerative Clustering," *Environ. Clim. Technol.*, vol. 26, no. 1, pp. 1234–1243, Jan. 2022, doi: 10.2478/rtuect-2022-0093.

[9] "Latvijas Vides, ģeoloģijas un meteoroloģijas centrs." Accessed: Sep. 06, 2023. [Online]. Available: https://videscentrs.lv.

[10] R. Freimanis, R. Vanaga, V. Balodis, Z. Zundans, and A. Blumberga, "Hygrothermal Assessment of Insulation Systems for Internal Insulation of Solid Masonry Walls under Various Conditions," *Buildings*, vol. 13, no. 10, Art. no. 10, Oct. 2023, doi: 10.3390/buildings13102511.

[11] E. Biseniece, R. Freimanis, R. Purvins, A. Gravelsins, A. Pumpurs, and A. Blumberga, "Study of Hygrothermal Processes in External Walls with Internal Insulation," *Environ. Clim. Technol.*, vol. 22, no. 1, pp. 22–41, Mar. 2018, doi: 10.1515/rtuect-2018-0002.

[12] A. Blumberga, R. Freimanis, E. Biseniece, and A. Kamenders, "Hygrothermal Performance Evaluation of Internally Insulated Historic Stone Building in a Cold Climate," *Energies*, vol. 16, no. 2, p. 866, Jan. 2023, doi: 10.3390/en16020866.

[13] R. Freimanis, R. Vaiskunaite, T. Bezrucko, and A. Blumberga, "In-Situ Moisture Assessment in External Walls of Historic Building using Non-Destructive Methods," *Environ. Clim. Technol.*, vol. 23, no. 1, pp. 122–134, Jan. 2019, doi: 10.2478/rtuect-2019-0009.

[14] A. Blumberga, R. Vanaga, J. Antuzs, R. Freimanis, E. Bondars, and S. Treija, "Is the High Quality a Monkey Wrench in the Global Climate Challenges?," *Environ. Clim. Technol.*, vol. 23, no. 3, pp. 230–244, Dec. 2019, doi: 10.2478/rtuect-2019-0092.

[15] J. Malczewski, "Multicriteria Analysis," in *Comprehensive Geographic Information Systems*, Elsevier, 2018, pp. 197–217. doi: 10.1016/B978-0-12-409548-9.09698-6.

[16] J.-J. Wang, Y.-Y. Jing, C.-F. Zhang, and J.-H. Zhao, "Review on multi-criteria decision analysis aid in sustainable energy decision-making," *Renew. Sustain. Energy Rev.*, vol. 13, no. 9, pp. 2263–2278, Dec. 2009, doi: 10.1016/j.rser.2009.06.021.

[17] A. Blumberga *et al.*, "Transition from traditional historic urban block to positive energy block," *Energy*, vol. 202, p. 117485, Jul. 2020, doi: 10.1016/j.energy.2020.117485.

[18] X. Zhou, J. Carmeliet, and D. Derome, "Influence of envelope properties on interior insulation solutions for masonry walls," *Build. Environ.*, vol. 135, pp. 246–256, May 2018, doi: 10.1016/j.buildenv.2018.02.047.

[19] C. Feng and H. Janssen, "Hygric properties of porous building materials (VII): Full-range benchmark characterizations of three materials," *Build. Environ.*, vol. 195, p. 107727, May 2021, doi: 10.1016/j.buildenv.2021.107727.

[20] T. De Mets, A. Tilmans, and X. Loncour, "Hygrothermal assessment of internal insulation systems of brick walls through numerical simulation and full-scale laboratory testing," *Energy Procedia*, vol. 132, pp. 753–758, Oct. 2017, doi: 10.1016/j.egypro.2017.10.022.

[21] E. Vereecken and S. Roels, "Capillary Active Interior Insulation Systems for Wall Retrofitting: A More Nuanced Story," *Int. J. Archit. Herit.*, vol. 10, no. 5, pp. 558–569, Jul. 2016, doi: 10.1080/15583058.2015.1009575.

[22] J. Zhao, S. Feng, J. Grunewald, F. Meissner, and J. Wang, "Drying characteristics of two capillary porous building materials: Calcium silicate and ceramic brick," *Build. Environ.*, vol. 216, p. 109006, May 2022, doi: 10.1016/j.buildenv.2022.109006.

[23] P. Klõšeiko and T. Kalamees, "Hygrothermal performance of a brick wall with interior insulation in cold climate: Vapour open versus vapour tight approach," *J. Build. Phys.*, vol. 46, no. 1, pp. 3–35, Jul. 2022, doi: 10.1177/17442591211056067.

[24] H. Hirsch, R. Heyn, and P. Klõšeiko, "Capillary condensation experiment for inverse modelling of porous building materials," *E3S Web Conf.*, vol. 172, p. 17003, 2020, doi: 10.1051/e3sconf/202017217003.

[25] D. Bottino-Leone, M. Larcher, D. Herrera-Avellanosa, F. Haas, and A. Troi, "Evaluation of natural-based internal insulation systems in historic buildings through a holistic approach," *Energy*, vol. 181, pp. 521–531, Aug. 2019, doi: 10.1016/j.energy.2019.05.139.

[26] A. Blumberga, R. Freimanis, I. Muizniece, K. Spalvins, and D. Blumberga, "Trilemma of historic buildings: Smart district heating systems, bioeconomy and energy efficiency," *Energy*, vol. 186, p. 115741, Nov. 2019, doi: 10.1016/j.energy.2019.07.071.

PIELIKUMI

HYGROTHERMAL PROPERTIES OF HISTORIC BRICKS FROM VARIOUS SITES OF LATVIA

Introduction

There are available hygrothermal simulation tools that allow to model possible scenarios for optimisation of thermal transmittance of historic wall, creating complex insulation systems. The accuracy of the results depends on the conformity of the input data to the specific design of existing wall. The properties of materials selected in the simulation tool should reflect as close as possible the properties of the wall under investigation.

For theses tools to be widely applicable the material library has to include various materials from various regions, thus allowing architects, planners, real estate developers and homeowners of Latvia to use the simulation tool with greater reliance on the accuracy of the simulation results.

In order to obtain a result in mathematical modelling programmes simulating the humidity transfer processes, which would reflect the situation as close to the real conditions as possible, the database built into the modelling programme should be supplemented with materials specific to the Latvian construction periods and obtained in different locations. Samples from different regions of Latvia were collected during brick collection (see Fig. 1 tab. 1).
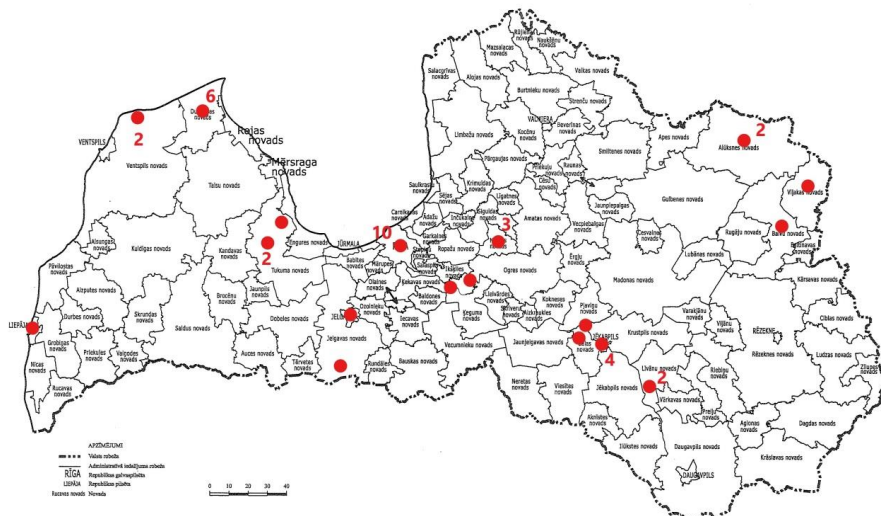
Material Samples

Figure 1. Sites of the collection of brick samples in Latvia

Table. 1. List of brick samples

Material No.	Year of construction	Address
18_4	1910- 1915	A. Briāna, Rīga
18_5	before 1960	Pulka iela 8, Rīga
18_6	19th century	Brīvības iela 78a, Rīga
18_7	18th century	Jēkaba iela 24, Rīga
18_15	1920 - 1930	Lāčplēša iela 1, Alūksne
18_16	19th century	T- Breikša iela 41, Liepāja
19_1	before 1903	Kuģu iela, Rīga
19_2	before 1903	Kuģu iela, Rīga
19_4	19th century	Irlavas pagasts, Tukuma rajons
19_5	20th century	O. Vācieša 6. Rīga
19_6	20th century	Irlavas pagasts, Tukuma rajons
19_7	18th century	Mālpils
19_8	18th century	Mālpils
19_9	19th century	Mālpils
19_10	1920 - 1930	Lāčplēša iela 1, Alūksne
19_11	20th century	O. Vācieša 6, Rīga
19_12	20th century	Pulka iela 8, Rīga
19_13	1930	Raudas pag., Tukuma rajons
19_14	1830	Dundaga
19_15	1960	Irbene
19_16	1960	Irbene
19_17	1960	Dundaga
19_18	1902 - 1903	Ogresgals
20_1	1985	Dundaga
20_2	19th century	Rožupes pagasts, Līvānu novads
20_3	1960	Upenieki
20_4	17th century	Rīgas iela 216b, Jēkabpils
20_5	1932	Cukurfabrikas iela 2, Jēkabpils
20_6	1850	Sēlpils
20_7	1940	Jēkabpils
20_8	1910	Jelgava
20_9	20th century	Kr. Valdemāra iela, Rīga
20_10	19th century	Eleja
20_11	1922	Dundaga
20_12	19th century	Talsu iela 2, Dundaga
20_13	17th century	Pils iela 14, Dundaga
20_14	-	Berkava
20_15	1900	Brīvības 120, Jēkabpils
20_16	-	Žīguri
20_18	-	Balvi

61

Methodology

Standard measurement methods with some adjustments were used (see table 2. and 3.).

Table 2. Standard measurement methods for material properties tests of historic bricks

Density	EN 772-13:2000. Methods of test for masonry units. Determination of net and gross dry density of masonry units (except for natural stone)
Porosity	EN 772-3:1998. Methods of test for masonry units. Determination of net volume and percentage of voids of clay masonry units by hygrostatic weighing
Vapor permeability	CUP-Tests (μ values). EN ISO 12572:2001 – Hygrothermal performance of building materials and products – Determination of water vapour transmission properties
Free water uptake	ISO 15148:2002, 2002: Hygrothermal performance of building materials and products – Determination of water absorption coefficient by partial immersion

The material properties were determined for a specific reason, to be used as a input data for creation of hygrothermal simulation tool material file, in this case DELPHIN simulation tool. Therefore, some deviations from the testing standards were implemented. These deviation were developed by Dresden University of Technology (also the developers of DELPHIN simulation tool) and will be described further on. Measurement methods for material properties test developed by Dresden University of Technology are compiled in Table 3.

Table 3. Measurement methods for material properties tests approved and developed by Dresden University of Technology

Moisture storage	Hygroscopic sorption and water retention properties are tested following the method developed in Dresden University of Technology based on DS/EN ISO 12571:2013 Hygrothermal performance of building materials and products – Determination of hygroscopic sorption properties and (DS/EN ISO 11274 Soil quality - Determination of the water-retention characteristic – Laboratory methods [38], [39]
Drying Curve	Non-isothermal combined vapour and liquid transfer testing method developed in Dresden University of Technology
Heat capacity and thermal conductivity	heat pulse technology by means of ISOMET equipment

Only general explanation of tests and included deviations are described, as the detailed description of all tests perfomed can be found in the corresponding standarts.

Density and porosity

Density is determined according to the standard EN 772-13:2000. Methods of test for masonry units. Determination of net and gross dry density of masonry units (except for natural stone). Porosity is determined according to the standard EN 722-3:1998. Methods of test for masonry units. Determination of net volume and percentage of voids of clay masonry units by hydrostatic weighing.

To determine bulk density, the bulk volume and the dry mass must be determined. For the determination of the dry mass, samples were oven dried in the 105 °C, until the constant mass of the samples is reached. Mass was assumed to be constant, when it doesn't change more than 0,2 % over the 24 h period. For the determination of the volume three methods were used. First method was hygrostatic weighing, second method was measurements of sample dimensions using a caliper and the third was immersion method. Hygrostatic weighing was used on the full-size bricks, and was done in three steps:

1) Brick was saturated with water;
   - This is done, to avoid water uptake by the brick during weighing;
2) Weight of the saturated brick was determined (in the air);
3) Weight of the brick was determined (immersed under the water);
   - Brick in hanged under the scale, and the determined weight is lower due to buoyance.

To determine the bulk volume of the samples, equation (1) was used:

$$V_s = \frac{(m_s - m_{sw})}{\rho_w} \qquad (1)$$

where

V_s – bulk volume of sample, cm^3

m_s - weight of the saturated sample, g

m_{sw} - weight of the saturated sample, when weighted under the water, g

ρ_w - density of the water, g/cm^3.

Immersion method was used for the cut-out samples of the brick and was performed in three steps:

1) Filling the container with water, up to the rim;
2) Immersion of the water saturated sample into the water filled container, while the overflowing water is collected, in another container;
3) The overflowing water volume equals the volume of the sample;
4) Weighing of the collected overflowing water;
5) Calculating of the overflowing water volume, (assuming that 1 g of water equals 1cm^3 of water, the mass of water in grams equals the volumes of sample in cm^3).

Prior to determination of the sample volume by immersion method, the samples had to be conditioned by saturation with water. After the samples were saturated, for determination of the volume two different size cups were used. Smaller cup was filled with the water, up to the rim and put into the larger cup, after that the brick sample was immersed into the smaller cup, with the help of an adhesive tape. The overflowing water from the smaller cup was collected into the larger cup, and the mass of overflown water was determined.

To calculate the bulk density equation (2) was used:

$$\rho_s = \frac{m_d}{V_s} \qquad (2)$$

where

m_d - Dry mass of the sample [g];

V_s – Bulk volume of sample [cm^3];

ρ_s - Bulk density of the sample [g/cm^3].

The average value of the bulk density was used for further calculations.

To determine open porosity, samples were saturated with water under the vacuum. Vacuum saturation was used to determine maximum saturation of the samples. For the vacuum saturation a desiccator filled with water and vacuum pump *CVC 3000 vacuubrand* was used (fig. 2.). The samples were kept under approximately 3 mBar pressure until the constant mass was reached. To determine open porosity, the equation (3) was used:

$$P_o = \left(\frac{m_v - m_d}{\rho_w \cdot V_s} \right) x 100\% \tag{3}$$

where
P_o – open porosity of the sample, %
m_v - mass of vacuum saturated sample, g
ρ_w - density of the water, g/cm^3
m_d - dry mass of the sample, g.
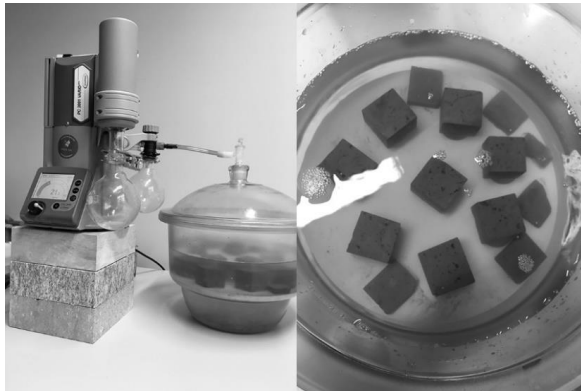
Figure 2. Vacuum saturation of brick samples

Prior to determination of the sample maximum (vacuum) saturation, the effective saturation of the material were determined by submerging the samples under the water (fig. 3.).

Figure 3. Effective saturation test

Vapor permeability

Vapor permeability test (cup test method) are performed according to the standard EN ISO 12572 Hydrothermal performance of building materials and products – Determination of water vapour transmission properties.

For the cup test method 3 samples of the brick are used in the cut sizes of 7 x 7 x 1 cm. Samples are installed in the lids of the cups, with the help of a wax (fig. 4.). Test is repeated two times, first time in low humidity conditions (Dry-cup test) and the second time in high humidity conditions (Wet-cup test).

a)   b)
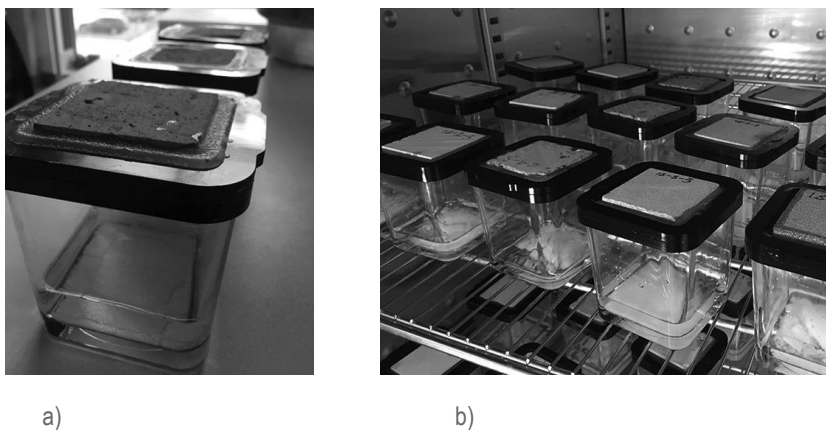
Figure 4. Cup tests a) sample installed in the lid of a cup b) cups inserted in the controlled environment

For the Dry-cup test silica gel desiccant is used, to keep low (5 %) relative humidity inside the cup. The desiccant is poured in the bottom of the cups and the cups are inserted in the climatic chamber TH-G-1000 with the constant temperature of 23 C° and relative humidity 35 %. For the Wet-cup test saturated salt solution of KH_2PO_4 is used, to keep high (96 %) relative humidity inside the cups and the cups are inserted in climatic chamber with constant temperature 23 C° and relative humidity 65 %. To calculate water vapour resistance factor, increasing mass of the cups in the case of Dry-cup test, or decreasing mass of the cups in the case of Wet-cup test, are determined, by the weighing of the cups over the period of time. Mass increase/decrease of the cup indicates how much water vapour is passed through the samples, due to the difference in the water vapour pressure in climatic chamber and cups caused by the difference in relative humidity inside the cups and in the climatic chamber. Several equations are used to calculate water vapour resistance factor. The main equations are showed below:

Density of water vapour flow:

$$g = \frac{G}{A} \tag{4}$$

where

g – density of water vapour flow, $kg/(m^2 \cdot s)$

A – surface area of the sample (exposed to vapour transfer), m^2

G – slope of the mass plotted as a function of time (cup mass increase/decrease), kg/s.

Water vapour pressure:

$$p_v = \varphi \cdot 610.5 \cdot e^{\frac{17.269\,-\theta}{237.3+\theta}} \qquad (5)$$

where
p_v – water vapour pressure, Pa
φ – relative humidity, [-]
e – base of natural logarithm (2.718...), [-]
Ө - temperature, °C.
Water vapour permeance:

$$W = \frac{g}{\Delta p} \qquad (6)$$

where
W – water vapour permeance, kg/ (m^2·s·Pa
g – density of water vapour flow, kg/(m^2·s)
Δp – pressure difference (cup, chamber), Pa.
Water vapour permeability of still air:

$$\delta_a = \frac{2.306 \cdot 10^{-5} \cdot P_0}{R_v \cdot \theta \cdot P_a} \cdot \left(\frac{\theta}{273.15}\right)^{1.81} \qquad (7)$$

where
δ_a – water vapour permeability of still air, kg/ (m·s·Pa
R_v – gas constant of water vapour (461.5), N·m/(kg·K)
Ө - temperature, °C
P_0 – standard barometric pressure (101325), Pa
P_a – pressure in climatic chamber, Pa.
Water vapour permeability:

$$\delta = W \cdot d \qquad (8)$$

where
δ – water vapor permeability of a sample, kg/(m·s·Pa)
W – water vapor permeance, kg/(m^2·s·Pa)
d – height (thickness) of a sample, m.
Water vapour resistance factor:

$$\mu = \frac{\delta_a}{\delta} \qquad (9)$$

where
μ - water vapour resistance factor, [-]
δ - water vapour permeability of still air, kg/(m·s·Pa)
δ – water vapour permeability of a sample, kg/(m·s·Pa).

Free water uptake

Free water uptake tests are performed according to the standard ISO 15148:2002, 2002: Hydrothermal performance of building materials and products – Determination of water absorption coefficient by partial immersion.

Free water uptake test are performed, to determine capillary moisture content and capillary absorption coefficient of the brick. After preparing the bricks samples for the test

and pre-conditioning, side edges of the samples are sealed with the aluminium tape, to protect samples from drying out sideways. The top and bottom part of the sample is left uncovered. The prepared samples were put into water, and only up to 5 mm of the bottom part is immersed. The sample itself is put on the pins, so that bottom plane is opened to water contact (fig. 5.).

Figure 5.. From left. Tape, sample prepared, partial immersion

During the free water uptake test mass of the samples is determined periodically with decreasing frequency of period. In the beginning of the test, when the free water uptake happens faster, the mass is determined with a higher frequency (from 5 min. interval to 1 h interval), when test progresses, the weighing interval can be as long as 24 h. Test frequency and duration of the test varies for different bricks due to different material properties.

The main results of the free water uptake test is a water uptake coefficient, capillary saturation level and suction curve, with corresponding boundary conditions.

Moisture storage

Two methods are used to determine water storage properties. In hygroscopic range a desiccator method is used to determine sorption curves, and in over-hygroscopic range, the pressure plate method is used to determine water retention curve.

Desiccator method are performed according to the standard EN ISO 12571:2013. Hydrothermal performance of building materials and products - Determination of hygroscopic sorption properties. In this test series of decreasing/increasing equilibrium relative humidity at a given temperature are established. Five different equilibrium relative humidity are established in this test. To achieve different relative humidity, individual desiccators for each relative humidity are filled with saturated salt solution and are kept at the constant temperature (23 °C), to maintain specifi relative humidity above saturated salt solution (see table 4.).

Table 4. Relative humidity above saturated salt solution at 23 °C [73]

Salt solution	Relative humidity
Potassium hydroxide (KOH)	7.38 %
Magnesium chloride (MgCl2)	32.9 %
Magnesium nitrate (MgNO3)	53 %
Potassium chloride (KCl)	84.7 %
Mono potassium phosphate (KH2PO4)	96 %

In total 10 samples with cut out size of 4 x 4 x 1 cm are used for each brick to determine sorption curves with desiccator method. Before the test samples are conditioned, by oven drying until the constant mass is reached, indicating that the samples are dry. Then the samples are divided in two groups with 5 samples in each group. One group of the samples is inserted in the desiccator with highest relative humidity (96 %) and the other group is inserted in the desiccator with the lowest relative humidity (7.38 %) (fig. 6). When the equilibrium is reached, the samples are weighed and moved to the next desiccator with lower or higher relative humidity, respectively, from 7.38 % to 32.9 %, and from 96 % to 84.7 %. The moving of the samples is continued until both groups of the samples have reached the equilibrium state in each of 5 relative humidity environments. Weighing results of the sample group moving from lowest relative humidity to higher relative humidity are used to obtain adsorption curve and the weighing results of the sample group moving from the highest relative humidity to the lower relative humidity are used to obtain desorption curve.

a)   b)
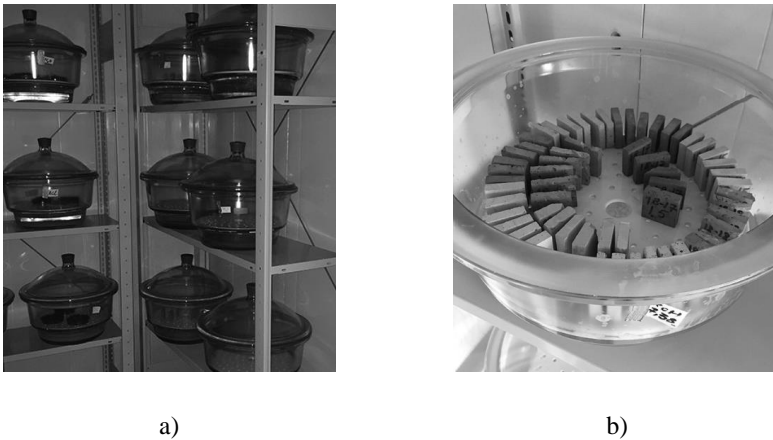
Figure 6 Setup of desiccator method a) chamber with a constant temperature of 23 °C b) desiccator filled with samples

To calculate the moisture content (MC) [g/g] of the sample, equation (10) is used:

$$MC = \frac{m - m_d}{m_d} \tag{10}$$

Where
MC –moisture content, g/g
m – mass of the weighted sample, g
m_d – dry mass of the sample, g.

Pressure plate tests are performed according to the standard DIN EN ISO 11274 Soil quality - Determination of the water-retention characteristic - Laboratory methods.

Pressure plate method is similar to desiccator method, but instead of the different relative humidity, a different pressure levels are applied to the test samples. Equilibrium of the samples is achieved when there is no water flow from the pressure chamber outlet. With the desiccator method moisture storage are expressed as the dependence of the relative humidity, but with the pressure plate method as the dependence of the capillary pressure. Both of parameters can be expressed as the other with the Kelvin equation (Eq. (11)). The

VPP-EM-EE-2018/1-0003

RĪGAS TEHNISKĀ
UNIVERSITĀTE
RTU
VASSI
Improvement of building energy efficiency technologies (I-BEET)
68

9

same formula is used to calculate MC after the equilibrium of the samples is reached at each pressure. Two pressure plate chambers are used in this test. To increase testing procedure, both pressure chambers are used in parallel with four different samples in each chamber. In total 8 samples with cut out size of 4 x 4 x 1 cm are used in pressure plate method. Before the test samples are saturated for 1 month by partially immersing them in the water. Saturated samples are placed on the ceramic plates; and the kaolin clay and the filter paper are used to provide better contact between samples and the plates. Ceramic plates together with samples are inserted into a pressure chamber and the pressure is applied (fig. 7.). When the pressure is applied to the chamber, the samples are drained until the equilibrium is reached. When the equilibrium is reached, the samples are weight and the applied pressure increased to the next step. In total 5 different pressures are applied: 0.1 bar, 0.3 bar, 4 bar, 8 bar and 15 bar.

Kelvin equation:

$$P_c(\varphi) = \rho_l \cdot R_v \cdot T \cdot ln\varphi \qquad (11)$$

where
P_c – Capillary pressure, Pa
ρ_l - Density of the liquid water, kg/m^3
R_v – Gas constant of water vapour, J/kg·K
T – Absolute (Kelvin) temperature, deg
φ – Relative humidity, [-].
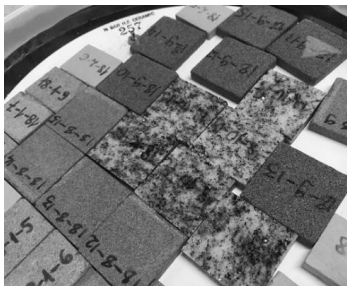
<table>
<tr><td>a)</td><td>b)</td></tr>
</table>

c)   d)

Figure 7. Pressure plate method a) saturation process of the samples b) water outlet of the pressure chamber c) pressure regulation system d) left: pressure chamber up to the 5 bar, right: pressure chamber up to the 15 bar

Drying curve

To determine a drying curve a non-isothermal combined vapour and liquid transfer testing method, developed in Dresden University of Technology, is used. In this method samples are conditioned by submerging in the water, until the effective saturation is reached. After conditioning, the brick samples are placed in the drying cabinet and measurements are made periodically to record changes in the weight and surface temperature of the samples. In the drying the cabinet flowing air above the samples is maintained, temperature and relative humidity is monitored. The placement of the samples inside the cabinet are managed in the manner, so that only the top surface of these samples are exposed to the moving air above these samples (fig. 8.).

Figure 8. Samples in drying cabinet

Results of the drying test is a drying curve and corresponding boundary conditions, that are mainly used to calibrate the relevant Delphin material file (see chapter 3.).

Specific heat capacity and heat conductivity

Thermal conductivity and specific heat capacity are determined with the *ISOMET 2114* from *Applied precision.* Surface probe IPS 1105 with the measurement range from 0.3 to 3 W/(m·K) is used. Precision of the measurements are 3 % of reading + 0.001 W/(m·K) for thermal conductivity and 3 % of reading + 1.10^3 J/(m³·K) for the volume heat capacity. Prior to the test the brick samples are oven dried in 105 C°. After preparing the bricks samples for the test, the brick samples are placed in desiccator, and measurements are performed with ISOMET 2114.

Rsults are included in separate excel file, with all the single value results in sheet1 and individual sheet for each curve.

Evaluation of the Impact of Bricks of Various Characteristics on Internally Insulated Masonry Walls in Cold Climate

Ritvars Freimanis *, Andra Blumberga, Ruta Vanaga and Zigmārs Zundāns

Institute of Energy Systems and Environment, Riga Technical University, LV1048 Riga, Latvia; ru-ta.vanaga@rtu.lv (R.V.); zigmars.zundans@rtu.lv (Z.Z.); andra.blumberga@rtu.lv (A.B.)

* Correspondence: ritvars.freimanis@rtu.lv

Abstract: Energy consumption in historic building stock is high compared to current energy efficiency standards. The heritage value of the façade and the limited space on the external surface in densely populated urban streets limit the application of external insulation. Internal insulation can be applied instead. However, it is considered to be a riskier technology due to moisture-related damage. In addition to mold growth and wood rot, frost damage should be considered in cold climates. This study aims to assess the impact of a vapor-open capillary-active calcium silicate internal insulation system with and without adhesive glue on the hygrothermal behavior of masonry from various historic bricks in cold climates by performing numerical simulations in the software Delphin. Test results of hygrothermal properties of 40 historic brick samples were used in numerical experiments to assess the impact of a brick type, the quality of the application of calcium silicate (with or without adhesive), and the impact of cold climate on the hygrothermal behavior. Results show that temperature behavior is similar to all wall types whereas a large difference is observed in moisture behavior. The application of adhesive glue tends to reduce moisture spikes caused by rain events when compared to the same samples without adhesive. Findings only partly correspond to other studies on factors affecting moisture behavior.

Keywords: internal insulation; historical bricks; capillary-active insulation; Delphin simulation; numerical experiment; digital experiment

1. Introduction

The high energy consumption in historic buildings is determined by the poor thermal properties of a building envelope. As a significant share of the thermal energy losses are through the opaque building envelope (exterior walls), the insulation of exterior walls can significantly reduce energy consumption of the building and thereby reduce greenhouse gas emissions [1]. Existing buildings can face restrictions for applying external wall insulation. First, due to the cultural heritage value of a building, and, second, technical limitations due to the geometry of the building or location within the densely built urban environment. In these cases, internal insulation should be applied. This type of energy efficiency measure has a high impact on the hygrothermal behavior of the wall, leading to a higher risk of frost damage, mold growth, and decay of embedded wooden beams [2]. If thermal insulation is applied without preliminary investigation of the existing moisture issues in the building, it can lead to increased moisture-caused problems. Moreover, if these problems are not eliminated prior to the refurbishing, they will intensify in a short period of time and can cause irreversible damage to the building's thermal envelope and construction [3].

The assessment of heat and moisture transfer in porous building materials is the central issue when internal insulation is applied in buildings. Material properties are crucial when internal insulation is considered. They include general, thermal, and hygric properties. General properties that are essential for hygrothermal behavior are bulk density

and open porosity. Thermal properties include thermal conductivity and specific heat capacity. Moisture storage in a material is characterized by saturated moisture content, capillary moisture content, sorption isotherms, and retention curves. Transport properties include the capillary absorption coefficient, vapor permeability, liquid permeability, and liquid diffusivity [4]. Various test methods are available to test the thermal and hygric properties of porous building materials in the full humidity range [5].

Existing masonry and historic bricks and their hygrothermal properties have been studied [6–12]. If historic masonry is covered with an external render, the hygrothermal performance of internally insulated walls depends mainly on the liquid permeability of the exterior finishing render [13]. De Mets et al. (2017) found that brick type and driving rain load significantly impact the moisture levels in masonry with internal insulation. They concluded that the absorption coefficient of a brick cannot be used as a single factor to assess the hygrothermal impact of interior insulation, and the liquid water conductivity has a higher impact [2]. However, the liquid water conductivity is difficult to estimate because there is a lack of a single method to directly measure the liquid permeability at low and intermediate moisture content [14]. Isothermal measurements alone are not sufficient to correctly simulate the capillary condensation process and the drying-calibrated model underestimates the moisture content [15]. A vapor-open exterior water-repellent façade impregnation or rendering is an important measure against wind-driven rain if internal insulation is applied [2]. Another study found that the pore size of a material strongly influences its hygric properties. Small pores mainly increase the hygroscopicity (e.g., the sorption isotherms), while large pores primarily enhance the capillarity (e.g., the capillary absorption coefficient). If pore size distribution is known, one can estimate the overall hygric performance of a material [14].

For capillary-active internal insulation systems, driving rain load and the drying potential of the wall are the main factors affecting their hygrothermal performance [2]. They are safe if capillary-active internal insulation is applied in spaces with low or normal occupancy with no additional moisture source. Capillary-active internal insulation is considered to be safe if the relative humidity under the insulation does not exceed 99% [16].

A capillary-active insulation system of calcium silicate insulation is adhered to the masonry wall by a glue mortar so that the interstitial condensation can be buffered [17–21]. Good contact between the masonry wall and the insulation should be provided [20]. The functionality of the system is disturbed if contact between the masonry wall and the capillary-active material is discontinued. The adhesive glue limits the redistribution of the moisture from the interstitial condensation that occurs at the warm side of the masonry wall by the capillary-active material. A low capillary absorption coefficient of the adhesive glue diminishes the risk of moisture from wind-driven rain. The glue reduces the redistribution of potential condensation toward the masonry. The absorption coefficient of the glue depends on the curing conditions. The glue mortar can capture a large amount of moisture [22]. In another study, [23] conclusions are that capillary-active interior insulation cannot be applied in a cold continental climate and vapor-tight insulation has to be applied. They found that condensation in the masonry can appear if the capillary-active interior insulation with a relatively small water vapor resistance factor, high indoor moisture load, and no adhesive glue is applied.

This study aims to assess the impact of a vapor-open capillary-active calcium silicate internal insulation system with and without adhesive glue on the hygrothermal behavior of masonry from various historic bricks in cold climates by performing numerical simulations.

2. Methodology

In this study, the simulation software Delphin 6.1 is applied. Delphin is designed to simulate the heat, moisture, and air transportation and storage processes in porous construction materials. The brick files to be used in Delphin were created during laboratory tests of hygric and thermal parameters of 40 historic bricks from Latvian historic buildings from the 17th to the 20th century (Appendix A). Tests were carried out based on the testing standards defined by Dresden Technical University and ISO standards. The following parameters were determined: density, open porosity, thermal conductivity, specific thermal capacity, sorption isotherms, retention isotherm, water absorption coefficient, capillary saturation moisture content, water vapor diffusion resistance factor, vapor diffusivity, and vapor conductivity. Tests and test results have been published [24]. A clustering analysis of tested brick samples was carried out after material tests were performed. The clustering results of hygrothermal properties were cross-examined with clustering results of the Delphin simulation data. Six and three clusters were found to be optimal, accordingly for the hygrothermal properties and the Delphin results data groups. After cross-examination, a total of nine combined clusters were recognized, with two dominant clusters containing 67.5% of all samples (30% and 37.5%), four of the clusters containing only one sample in them, and other clusters containing two, three, and four samples in them [25].

Two slightly different Delphin models were created: one for the situation where calcium silicate insulation was glued to the masonry and another where calcium silicate was not glued to the masonry. Figure 1 shows the simulated structure with masonry (0.25 m) and calcium silicate (0.05 m), with an adhesive layer of 5 mm. Simulations were carried out for each of the 40 types of masonries: with and without adhesive glue under the insulation material. For the model without adhesive, the adhesive layer was not present in the model and the gap in between the insulation and the masonry was removed.


Figure 1. Simulation model.

The properties of the insulation material and the adhesive glue are shown in Table 1.

Table 1. Properties of the insulation material and the adhesive glue.

Parameter	Calcium Silicate	Adhesive (Glue)	Unit
Bulk density	225.04	820.033	kg/m³
Specific heat capacity	1129	1306.5	J/kgK
Open porosity	0.9136	0.690553	m³/m³
Effective saturation	0.90408	0.34	m³/m³
Capillary saturation	0.7211	0.316	m³/m³

Hygroscopic sorption value at 80% relative humidity	0.00622307	0.139355	m^3/m^3
Thermal conductivity	0.061	0.216	W/mK
Water uptake coefficient	0.7831	0.00801211	$kg/m^2s^{0.5}$
Water vapor diffusion resistance factor	2.3973	18.9365	-
Liquid water conductivity	3.08745×10^{-10}	6.80328×10^{-12}	s

As there are no strict criteria or threshold values that are used to determine whether climate can be considered to be a cold climate, in this study, a cold climate is referred to as climatic conditions where four seasons can be distinguished and outdoor temperature below 0 degrees Celsius are common during one of those seasons as well as a yearly average temperature close to 0 degrees Celsius. In the simulations, the outdoor climate uses data from the year 2022 from the Riga University weather station, gathered by the Latvian Environment, Geology and Meteorology Centre. Hourly rain loads are shown in Figure 2 [26].
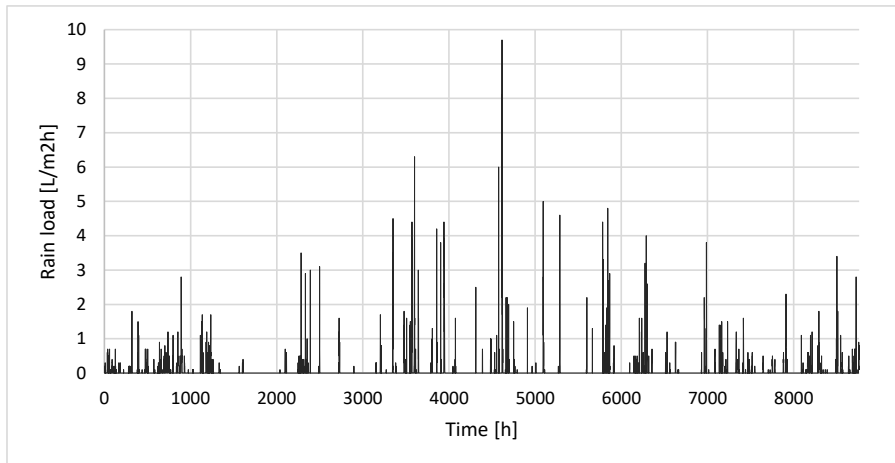
Figure 2. Hourly rain load.

Indoor climate conditions are set as a function of outdoor temperature (see Figure 3). The simulation period is set to 3 years to allow for stabilization of the initial values.
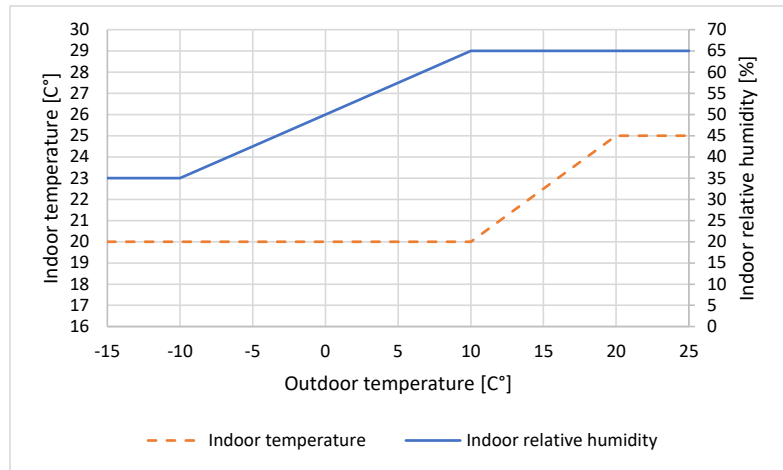
Figure 3. Indoor climate conditions functions.

3. Results

3.1. Hygrothermal Behavior of Masonry with Capillary-Active Insulation without the Adhesive Glue

Figure 4 presents temperature profiles under insulation material for each brick type. The overall trend follows outdoor temperature behavior. However, the distribution of temperature varies due to the thermal conductivity of the bricks (varies from 0.4 W/mK to 2.7 W/mK). The higher the thermal conductivity, the lower the temperature level under the insulation. Only five walls reached the freezing point during the winter months.
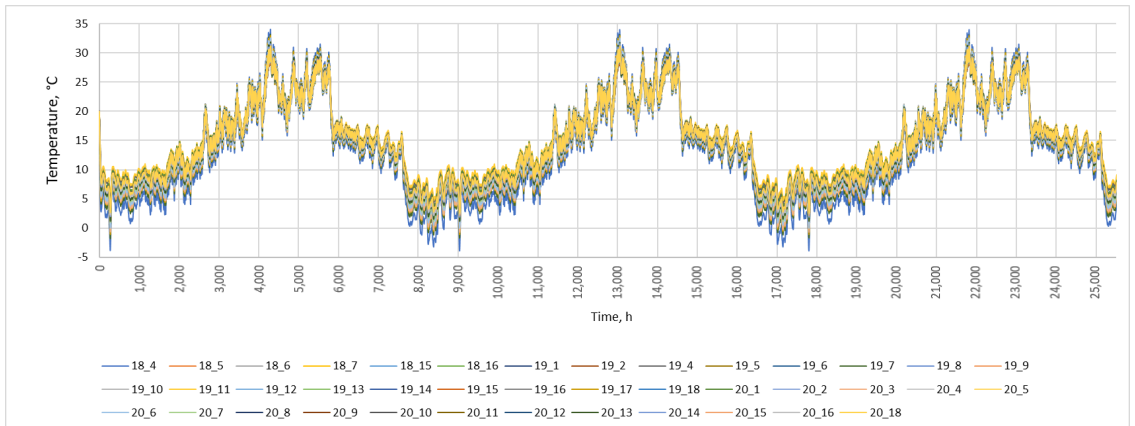
Figure 4. Temperatures under insulation.

Figure 5 illustrates that the amplitude of the temperature under the insulation is different for various bricks. The higher the temperature under the brick, the lower the amplitude is.
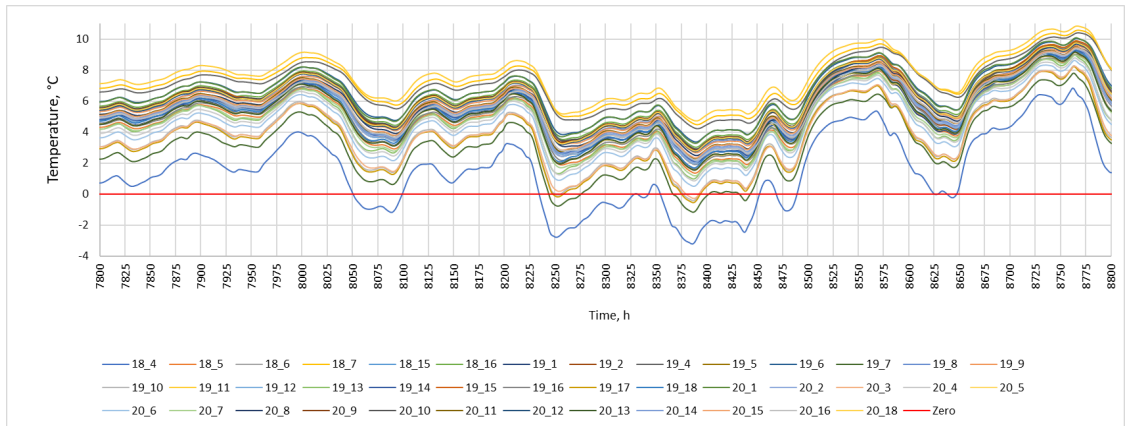
**Figure 5.** Temperature under insulation (zoomed in hours 7800 to 8800).

The relative humidity under the insulation also follows the trend of outdoor temperature (see Figure 6). The relative humidity does not exceed 96% in winter for any of the wall types. The relative humidity level reaches different values. Some walls are more susceptible to rain events than others. However, no correlation between relative humidity level and any other parameters (water absorption coefficient, liquid water conductivity, porosity, density) is seen.
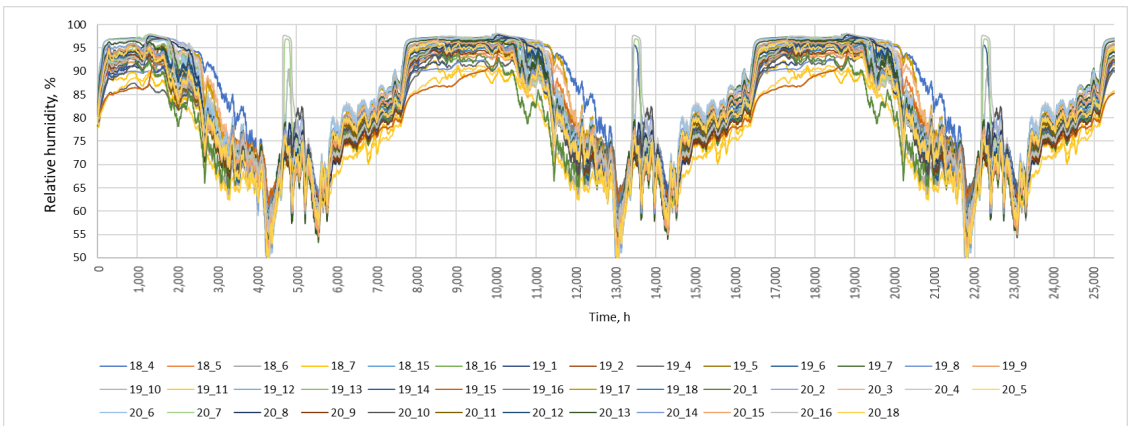
Figure 6. Relative humidity under the insulation.

Figure 7 shows the impact of rain on the relative humidity under the insulation. Before the rain, the distribution of relative humidity was 10%. During the rain, the relative humidity behavior changes: some of the bricks are more sensitive to rain, and the relative humidity level increases soon after the rain while, in other walls, it either happens with a delay or the wall does not show an impact from the rain.
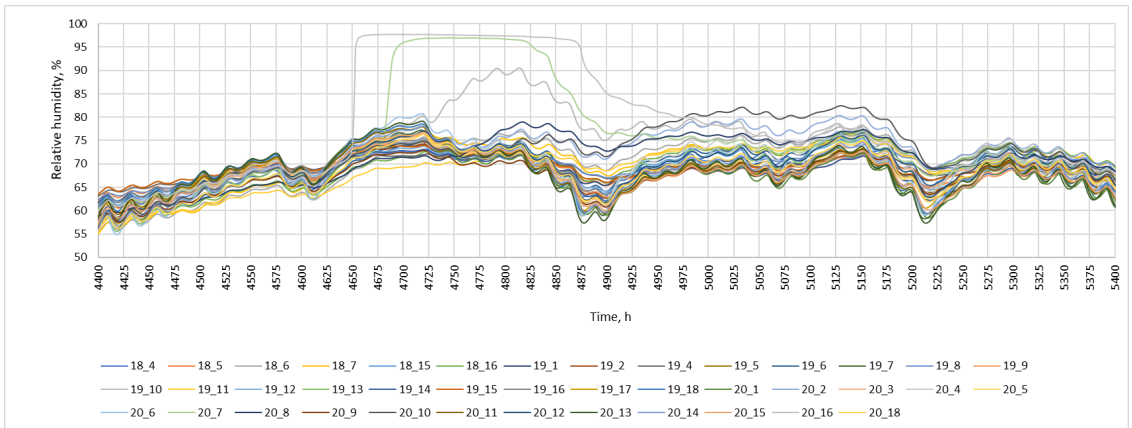
**Figure 7.** Relative humidity under the insulation for hours 4400 to 5400.

An example of relative humidity under the insulation for two wall types shows (see Figure 8) that, in wall 20_8, relative humidity increases at a slower pace during autumn and decreases at a higher rate during spring compared to wall 18_4. Wall 18_4 stabilizes at 95%, but wall 20_8 does not stabilize and it reaches 96% for a short period of time.
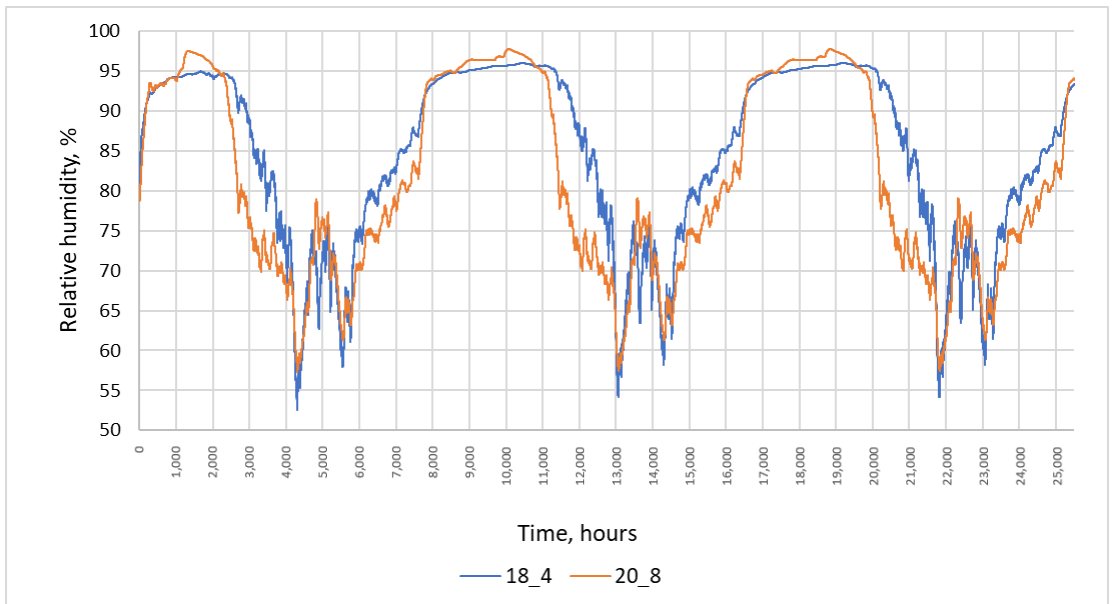
Figure 8. Relative humidity under the insulation for two wall types.

Figure 9 presents masonry moisture content in all wall types. The moisture content trend follows seasonal changes: increases during autumn and winter and decreases

during spring and summer. The difference between the lowest and the highest moisture content in walls is fourfold. Spikes in the moisture content indicate rain events (see Figure
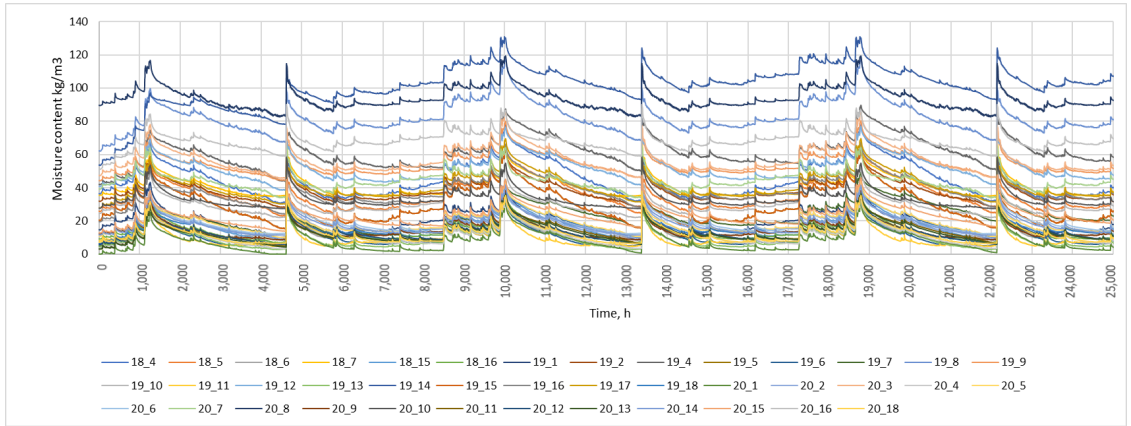
2).

Figure 9. Masonry moisture content.

For the majority of walls, the moisture under the insulation was not influenced by rain events if the adhesive glue was not applied under the insulation (see Figure 10). However, 16 walls exhibited behavior that was influenced by rain events in winter and summer.
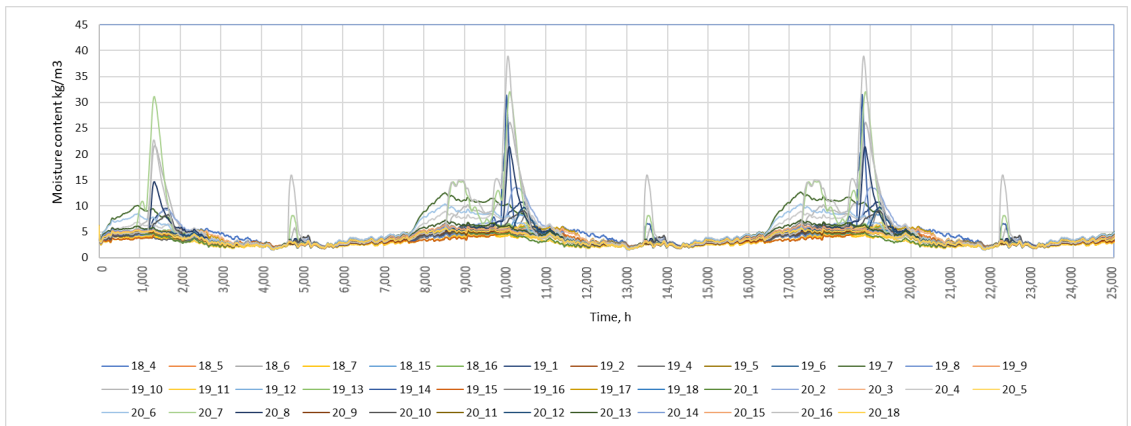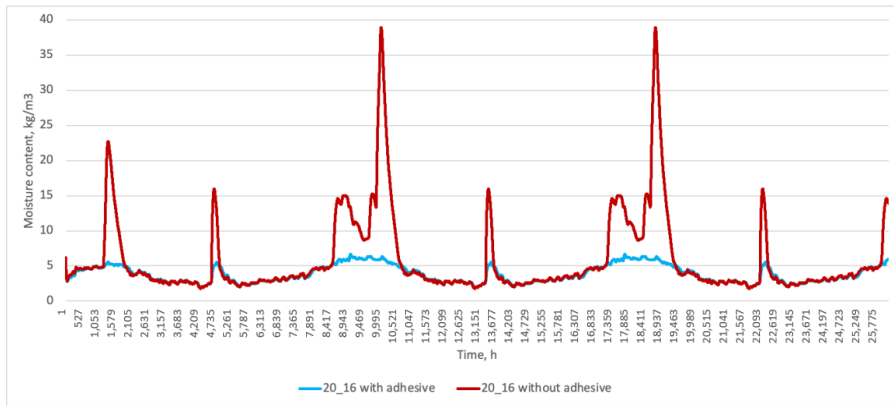

Figure 10. The moisture content of insulation material.

3.2. Hygrothermal Behavior of Masonry with Capillary-Active Insulation with the Adhesive Glue

When adhesive glue is applied under the insulation, moisture content spikes in the insulation layer are eliminated because the glue acts as a vapor barrier and a moisture buffer. Figure 11 shows the moisture content in the insulation for the wall 20_16 with and without the adhesive glue. It represents a wall type with high peaks in moisture content

after rain. Wall 20_16 has very steep and high peaks. When glue was applied, it eliminated moisture peaks.

Figure 11. Example of moisture content in insulation for the wall 20_16 with and without the adhesive glue.

When adhesive glue was applied on the walls that did not have peaks after rain, it did not affect the moisture content behavior. Figure 12 illustrates the behavior of the moisture content in the wall 20_18 with and without glue.
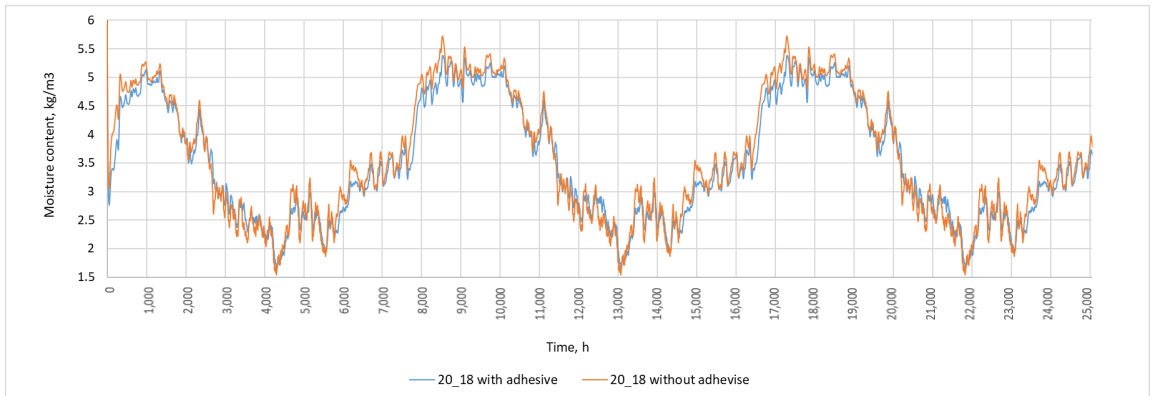

Figure 12. Moisture content in insulation for the wall 20_18 with and without the adhesive glue.

Figure 13 shows examples of the temperature, relative humidity, and moisture content distribution at the end of the simulation (in December); the integral moisture mass changed over time in the wall 20_16 when the adhesive glue was applied. The moisture content was slightly higher at the external part of the wall and was stable at a high level in the masonry in the deeper layers. It peaked in the glue and was at a very low level on the insulation side. Min and max levels during the simulation show similar trends. The relative humidity in the masonry was at a very high level at the end of the simulation and was reduced on the indoor side of the glue.
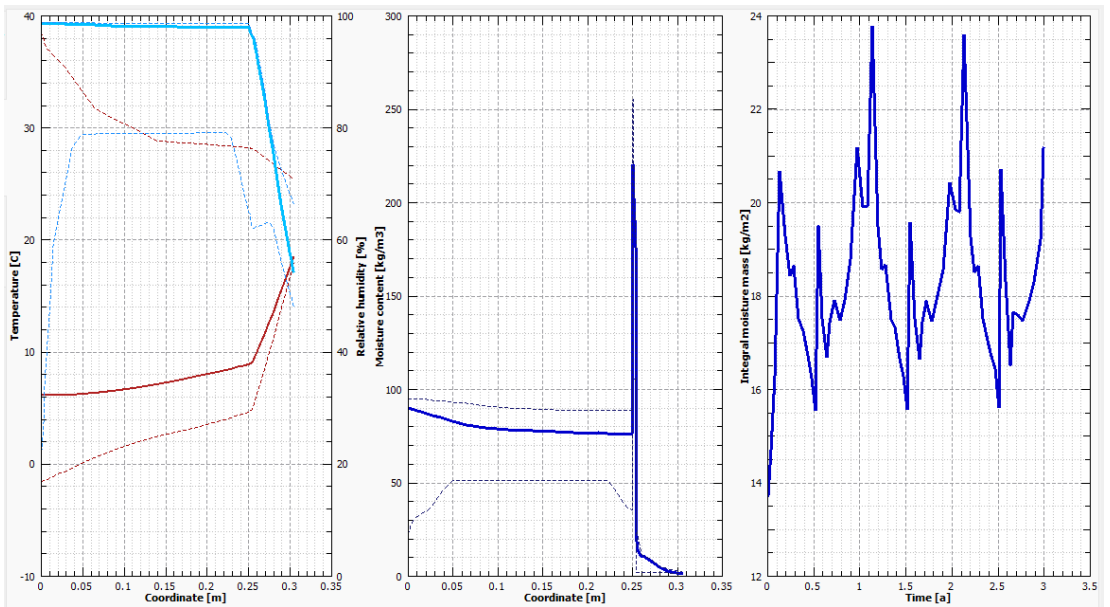
Figure 13. Example of the temperature (brown lines in the leaft side graph), relative humidity (blue lines in the left side graph), and moisture content distribution; the integral moisture mass changed over time in the wall 20_16 when the adhesive glue was applied (for the temperature and moisture content graphs, dotted lines represent the min and max values that were reached during simulation; full lines represent values at the end of the simulation).

Figure 14 presents the temperature, relative humidity, and moisture content distributions, as well as the integral moisture mass, which changed over time in the wall 20_18 when the adhesive glue was applied. The moisture content was high at the external part of the wall and was significantly reduced in the first 10 cm of the masonry and stabilized at a relatively lower level in the deeper layers. The absorbed water was transported more slowly to the inside and was stored in the exterior part of the masonry. It peaked in the glue and was at a very low level on the insulation side. Max levels during the simulation show a similar trend to the final values of the simulation. The relative humidity in the masonry was at a very high level at the end of the simulation and was reduced on the indoor side of the glue.
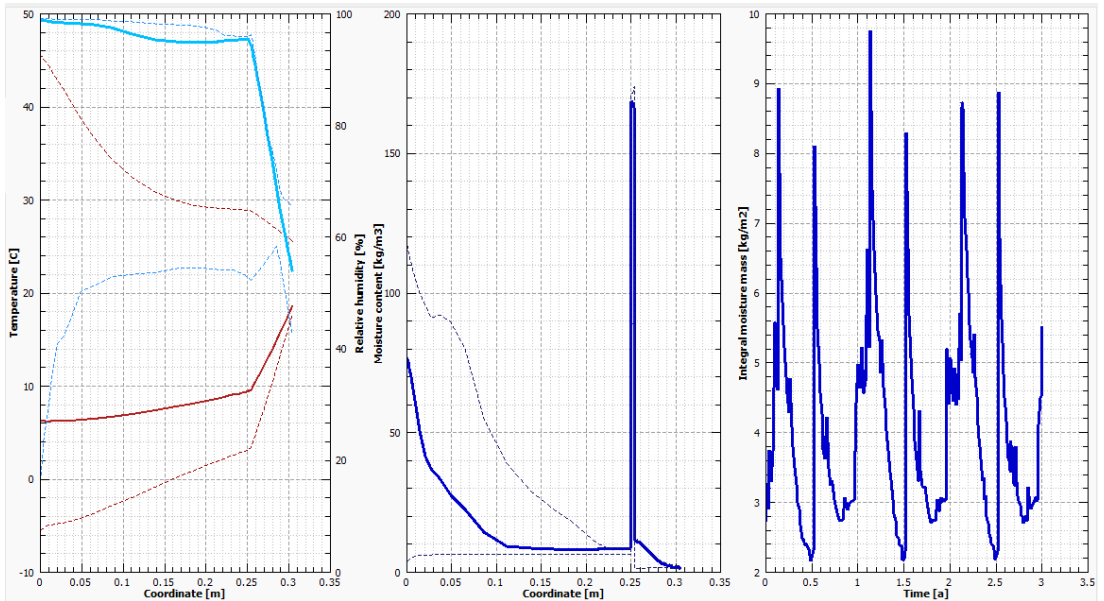
Figure 14. Example of the temperature(brown lines in the leaft side graph), relative humidity(blue lines in the left side graph), and moisture content distribution; the integral moisture mass changed over time in the wall 20_18 when adhesive glue was applied (for the temperature and moisture content graphs, dotted lines represent min and max values that were reached during simulation; full lines represent values at the end of the simulation).

The adhesive is a highly porous material (porosity 69%) and therefore can absorb a high content of water. Moreover, we can see a peak in water content for both the 20_16 and 20_18 samples (see Figures 13 and 14).

4. Discussion

The numerical experiments on the hygrothermal performance of 40 types of massive masonry walls internally insulated with vapor-open capillary-active calcium silicate in cold climates showed that all wall envelopes showed very similar temperature trends, whereas a large difference was observed in moisture behavior. This corresponds to the findings of Zhou et al. (2018) [13] that the influence of brick type on relative humidity and temperature under insulation is complex. Temperature variations between various wall types depend on the thermal resistance of the bricks.

Moisture content levels vary fourfold between wall types due to the moisture content distribution in the masonry that varies significantly between stable moisture levels throughout the masonry while also displaying stable levels at the external part of the wall followed by steep decreases in the deeper layers of masonry. At the external part of the masonry (closer to the outdoor air), the maximum masonry moisture reaches relatively similar (around 100 kg/m³) values for all the brick types. Data analysis showed that no correlation between moisture content, relative humidity level, and any other parameters (water absorption coefficient, liquid water conductivity, porosity, density) was found in this study.

The findings do not support conclusions from other studies that the hygrothermal performance of a massive masonry wall internally insulated with vapor-open capillary-active materials depends on the pore size distribution which determines liquid water conductivity of bricks: the higher this parameter, the deeper the masonry penetrates rain [14]. It also does not correspond to the finding that wall envelopes with high capillary-active

bricks show larger relative humidity and temperature indices [13]. The pore size of a material strongly influences its hygric properties. Small pores mainly increase the hygroscopicity (e.g., the sorption isotherms), while large pores primarily enhance the capillarity (e.g., the capillary absorption coefficient).

If the quality of the construction is low, and the adhesive glue does not provide full contact with the insulation material, the moisture from the rain can penetrate into the insulation material. If the adhesive glue is in full contact with the insulation material, the impact of wind-driven rain does not diffuse into insulation material. These findings correspond with conclusions from a different study [2]. The adhesive glue has a high moisture buffering capacity if properly applied. Similar conclusions were drawn by another study [22].

Simulation results showed that if internal insulation with capillary-active calcium silicate is applied in a cold climate with a normal indoor moisture load, the relative humidity does not exceed 96% and is considered safe [27]. This conclusion can be applied to both insulation with and without adhesive glue.

5. Conclusions

1. Temperature trends display practically no influences by brick type;
2. Brick type has a noticeable impact on the hygrothermal behavior of the insulated masonry wall;
3. There are no correlations between individual brick parameters and moisture dynamics within brick samples;
4. Capillary-active internal insulation use in cold climate is safe as long the indoor relative humidity does not exceed 65% in warm months and 35% in cold months;
5. The application of adhesive glue tends to reduce moisture spikes caused by rain events when compared to the same samples without adhesive.

Author Contributions:

Data Availability Statement:

Conflicts of Interest: The authors declare no conflict of interest.

Appendix A

Sample ID	Density [kg/m³]	Heat Capacity [J/kgK]	Heat Conductivity [W/mK]	Porosity [m³/m³]	Capillary Saturation [m³/m³]	Water Vapor Resistance Factor [-]	Water Uptake [kg/m²s⁰·⁵]	Liquid Water Conductivity [s]
18_4	1777.3	1181.0	2.739	0.304	0.198	18.37	0.104	1.00×10^{-10}
18_5	1516.4	1107.2	0.726	0.414	0.268	14.84	0.473	5.00×10^{-9}
18_6	1580.5	994.4	0.636	0.385	0.239	8.33	0.257	1.00×10^{-10}
18_7	1641.1	899.2	0.395	0.345	0.263	8.06	0.338	1.00×10^{-10}
18_15	1831.3	873.9	0.626	0.380	0.308	15.42	0.369	1.00×10^{-8}
18_16	1828.9	852.5	0.527	0.289	0.154	13.52	0.092	1.00×10^{-9}
19_1	1496.9	1010.1	0.686	0.427	0.387	6.82	0.744	1.00×10^{-8}
19_2	1572.4	1023.1	0.645	0.451	0.441	10.38	0.735	1.00×10^{0}
19_4	1761.9	872.1	0.411	0.297	0.216	16.49	0.158	1.00×10^{-8}
19_5	1526.0	1024.5	0.545	0.408	0.384	7.08	0.786	1.00×10^{-9}
19_6	1781.8	845.4	0.498	0.304	0.233	8.10	0.202	1.00×10^{-10}

19_7	2118.3	857.9	1.361	0.166	0.077	18.06	0.013	1.00×10^{-9}
19_8	1678.1	939.8	0.527	0.348	0.232	14.53	0.182	1.00×10^{-10}
19_9	1656.2	960.7	0.553	0.370	0.280	17.09	0.100	1.00×10^{-6}
19_10	1904.9	766.8	1.037	0.263	0.166	17.39	0.116	1.00×10^{-7}
19_11	1664.6	805.0	0.387	0.410	0.319	9.86	0.339	1.00×10^{-10}
19_12	1718.1	907.0	0.637	0.306	0.276	13.86	0.219	1.00×10^{-8}
19_13	1919.9	724.0	0.763	0.265	0.215	19.68	0.187	1.00×10^{-8}
19_14	1891.1	828.2	0.605	0.263	0.226	34.75	0.125	1.00×10^{-9}
19_15	1844.4	814.8	1.042	0.292	0.225	14.42	0.165	1.00×10^{-6}
19_16	1757.2	982.6	0.691	0.331	0.275	16.56	0.181	1.00×10^{-9}
19_17	1941.6	762.5	1.074	0.247	0.192	35.29	0.028	1.00×10^{-9}
19_18	1731.3	810.3	0.662	0.364	0.223	50.19	0.184	1.00×10^{-9}
20_1	1800.0	783.3	0.496	0.308	0.227	16.97	0.137	1.00×10^{-6}
20_2	1931.7	759.0	0.627	0.266	0.214	23.58	0.179	1.00×10^{-9}
20_3	1887.5	849.4	1.026	0.253	0.218	34.93	0.049	1.00×10^{-9}
20_4	1969.4	802.2	0.814	0.237	0.147	40.55	0.095	1.00×10^{-7}
20_5	1920.3	783.5	0.690	0.278	0.212	14.80	0.139	1.00×10^{-9}
20_6	2116.6	732.3	0.878	0.202	0.160	12.77	0.117	1.00×10^{-9}
20_7	1932.2	823.0	0.742	0.269	0.220	11.94	0.201	1.00×10^{-10}
20_8	1688.6	902.9	0.554	0.337	0.273	11.36	0.170	1.00×10^{-9}
20_9	1500.4	1011.8	0.542	0.438	0.356	6.79	0.544	1.00×10^{-9}
20_10	1685.9	941.4	0.536	0.362	0.282	10.88	0.312	1.00×10^{-9}
20_11	1862.6	820.5	0.602	0.281	0.181	19.59	0.091	1.00×10^{-9}
20_12	1954.1	787.1	0.558	0.255	0.232	21.69	0.159	1.00×10^{-6}
20_13	1886.5	793.4	0.695	0.267	0.177	23.85	0.171	1.00×10^{-9}
20_14	1755.2	874.2	0.617	0.295	0.251	14.38	0.166	1.00×10^{-9}
20_15	1623.5	998.8	0.602	0.279	0.196	16.42	0.123	1.00×10^{-9}
20_16	1846.1	878.3	0.602	0.226	0.149	33.87	0.111	1.00×10^{-9}
20_18	1787.6	851.0	0.552	0.325	0.266	10.97	0.235	1.00×10^{-9}

References

1. Adhikari, R.; Lucchi, E.; Pracchi, V. Experimental Measurements on Thermal Transmittance of the Opaque Vertical Walls in the Historical Buildings. In *PLEA 2012—28th Conference. Opportunities, Limits & Needs towards an Environmentally Responsible Architecture*; Reiser, J., Jiménez, C., Biondi Antúnez de Mayolo, S., Eds.; Lima, Peru, 2012; pp. 1248–1256.
2. De Mets, T.; Tilmans, A.; Loncour, X. Hygrothermal assessment of internal insulation systems of brick walls through numerical simulation and full-scale laboratory testing. *Energy Procedia* **2017**, *132*, 753–758. https://doi.org/10.1016/j.egypro.2017.10.022.
3. Franzoni, E. Rising damp removal from historical masonries: A still open challenge. *Constr. Build. Mater.* **2014**, *54*, 123–136. https://doi.org/10.1016/j.conbuildmat.2013.12.054.
4. Feng, C.; Janssen, H. Hygric properties of porous building materials (IV): Semi-permeable membrane and psychrometer methods for measuring moisture storage curves. *Build. Environ.* **2019**, *152*, 39–49. https://doi.org/10.1016/j.buildenv.2019.01.054.
5. Zhou, M.; Li, X.; Feng, C.; Janssen, H. Hygric properties of porous building materials (VIII): Influence of reduced air pressure. *Build. Environ.* **2022**, *225*, 109680. https://doi.org/10.1016/j.buildenv.2022.109680.
6. Oumeziane, Y.A.; Pierre, A.; El Mankibi, F.; Lepiller, V.; Gasnier, M.; Désévaux, P. Hygrothermal properties of an early 20th century clay brick from eastern France: Experimental characterization and numerical modelling. *Constr. Build. Mater.* **2021**, *273*, 121763. https://doi.org/10.1016/j.conbuildmat.2020.121763.
7. Zhou, X.; Carmeliet, J.; Derome, D. Assessment of risk of freeze-thaw damage in internally insulated masonry in a changing climate. *Build. Environ.* **2020**, *175*, 106773. https://doi.org/10.1016/j.buildenv.2020.106773.
8. Calle, K.; Van Den Bossche, N. Sensitivity of the hygrothermal behaviour of homogeneous masonry constructions: From Sobol indices to decision trees. *E3S Web Conf.* **2020**, *172*, 07001. https://doi.org/10.1051/e3sconf/202017207001.
9. Larsen, P.K. *Moisture Physical Properties of Bricks: An Investigation of Falkenløwe, Stralsund and Hartmann Bricks*; Report; Technical University of Denmark, Department of Civil Engineering: Lyngby, Denmark, 1995.
10. Vanderschelden, B.; Calle, K.; Van Den Bossche, N. On the potential of clustering approaches for hygrothermal material properties based on three degradation risks in solid masonry constructions. *J. Build. Phys.* **2022**, *46*, 36–76. https://doi.org/10.1177/17442591221085734.

11. Zhao, J.; Plagge, R.; Ramos, N.M.; Simões, M.L.; Grunewald, J. Application of clustering technique for definition of generic objects in a material database. *J. Build. Phys.* **2015**, *39*, 124–146. https://doi.org/10.1177/1744259115588013.
12. Mensinga, P.; Straube, J.; Schumacher, C. Assessing the freeze-thaw resistance of clay brick for interior insulation retrofit projects. In Proceedings of the XI International Conference Thermal Performance of the Exterior Envelopes of Whole Buildings, Clearwater, FL, USA, 15 December 2010.
13. Zhou, X.; Carmeliet, J.; Derome, D. Influence of envelope properties on interior insulation solutions for masonry walls. *Build. Environ.* **2018**, *135*, 246–256. https://doi.org/10.1016/j.buildenv.2018.02.047.
14. Feng, C.; Janssen, H. Hygric properties of porous building materials (VII): Full-range benchmark characterizations of three materials. *Build. Environ.* **2021**, *195*, 107727. https://doi.org/10.1016/j.buildenv.2021.107727.
15. Hirsch, H.; Heyn, R.; Klõšeiko, P. Capillary condensation experiment for inverse modelling of porous building materials. *E3S Web Conf.* **2020**, *172*, 17003. https://doi.org/10.1051/e3sconf/202017217003.
16. Bottino-Leone, D.; Larcher, M.; Troi, A.; Grunewald, J. Impact of climatic parameters on rain protection layer design for refurbished historic buildings. *Renew. Sustain. Energy Rev.* **2021**, *152*, 111688. https://doi.org/10.1016/j.rser.2021.111688.
17. Häupl, P.; Fechner, H. Hygric Material Properties of Porous Building Materials. *J. Therm. Envel. Build. Sci.* **2003**, *26*, 259–284. https://doi.org/10.1177/109719603032799.
18. Grunewald, J.; Ruisinger, U.; Häupl, P. The Rijksmuseum Amsterdam—Hygrothermal analysis and dimensioning of thermal insulation. In *Research in Building Physics and Building Engineering*; CRC Press: Boca Raton, FL, USA, 2006; pp. 345–352.
19. Vereecken, E.; Roels, S. A comparison of the hygric performance of interior insulation systems: A hot box–cold box experiment. *Energy Build.* **2014**, *80*, 37–44. https://doi.org/10.1016/j.enbuild.2014.04.033.
20. Scheffler, G.; Grunewald, J. Material development and optimisation supported by numerical simulation for a capillary-active inside insulation material. *Res. Build. Phys.* **2003**, Proceedings of the Second International Conference on Building Physics, Leuven, Belgium, 14-18 September 2003, 77-85.
21. Vereecken, E.; Roels, S. Capillary active interior insulation: Do the advantages really offset potential disadvantages? *Mater. Struct.* **2015**, *48*, 3009–3021. https://doi.org/10.1617/s11527-014-0373-9.
22. Vereecken, E.; Roels, S. Capillary Active Interior Insulation Systems for Wall Retrofitting: A More Nuanced Story. *Int. J. Archit. Herit.* **2016**, *10*, 558–569. https://doi.org/10.1080/15583058.2015.1009575.
23. Antolinc, D.; Černe, K.; Jagličić, Z. Risk of Using Capillary Active Interior Insulation in a Cold Climate. *Energies* **2021**, *14*, 6890. https://doi.org/10.3390/en14216890.
24. Freimanis, R.; Blumberga, A.; Zundans, Z.; Balins, R.; Vanaga, R. *Hygrothermal Properties of Historic Bricks from Various Sites of Latvia*; Rigas Tehniska Universitate: *Riga, Latvia,* 2021. https://doi.org/10.17632/CGP2VYRTNH.3.
25. Freimanis, R.; Zundans, Z.; Balins, R.; Vanaga, R.; Blumberga, A. Finding the Generic Hygrothermal Properties of Historical Bricks by Supervised Agglomerative Clustering. *Environ. Clim. Technol.* **2022**, *26*, 1234–1243. https://doi.org/10.2478/rtuect-2022-0093.
26. Latvijas Vides, Ģeoloģijas un Meteoroloģijas Centrs. Available online: https://videscentrs.lv (accessed on 6 September 2023).
27. Zhao, J.; Feng, S.; Grunewald, J.; Meissner, F.; Wang, J. Drying characteristics of two capillary porous building materials: Calcium silicate and ceramic brick. *Build. Environ.* **2022**, *216*, 109006. https://doi.org/10.1016/j.buildenv.2022.109006.

sciendo

RIGA TECHNICAL UNIVERSITY

Finding the Generic Hygrothermal Properties of Historical Bricks by Supervised Agglomerative Clustering

Ritvars FREIMANIS[1*], Zigmārs ZUNDANS[2], Roberts BALINS[3], Ruta VANAGA[4], Andra BLUMBERGA[5]

[1–5]*Institute of Energy Systems and Environment, Riga Technical University, Azenes iela 12/1, Riga, Latvia*

Abstract – **Finding the generic hygrothermal properties of historical brick for application in Heat Air and Moisture (HAM) simulation programs such as *Delphin, Wufi*, etc., is the main objective of this paper. In this paper hygrothermal properties and *Delphin* simulation results of 40 different historical brick samples from the 17th to 20th Century, were used. The clustering results of hygrothermal properties were cross-examined with the results of clustering results of *Delphin* simulation data. Six and three clusters were found to be optimal, accordingly for Hygrothermal properties and *Delphin* results data groups. After cross-examination, a total of 9 combined clusters were recognized, with two dominant clusters containing 67.5 % of all samples (30 and 37.5 %), four of the clusters had only one sample in them, and other clusters had two, three, and four samples in them. Additionally, all the resulting clusters were compared with the brick sample groups that were created based on the description of the brick: color, material type, and year of manufacturing.**

Keywords – **Agglomerative; brick; clustering; *Delphin*; generic; historical; hygrothermal; properties; supervised**

Nomenclature		
ML	Machine Learning	Method of Data Analysis
P	Parameters cluster	Cluster group from brick parameters
R	Delphin results cluster	Cluster group from Delphin results
HAM	Heat, Air, and Moisture	Type of simulation program
CT	Count	Unit for figures
FEC	Final Energy Consumption	Energy consumption by the end user

1. INTRODUCTION

The building sector accounts for one-third of the total Final Energy consumption (FEC) globally, and up to 42 % in the European Union (EU) [1], [2]. Therefore, by implementing energy efficiency measures, such as insulation of building envelope we can decrease the FEC [3]. The building envelope can be insulated either from the outside or from the inside, and in some cases, for example, for buildings with preservable façade, internal insulation is the only option. When insulating a building for the inside, the hygrothermal properties of the building envelope change and may cause durability and performance problems [4]. As the

topicality of energy efficiency increases, so is the topicality of internal insulation [5]–[11]. To avoid long and expensive experiments numeric simulations are widely used to find solutions for complex problems, including the prediction of the performance of refurbished/insulated historical masonry buildings [12]–[15]. However, these numerical calculations are based on rather complex functions that describe heat and moisture storage and transport within the materials [16]. Moreover, hygrothermal properties of the materials are used as input parameters for this calculation, therefore, accurate measurements of such parameters determine the accuracy and reliability of obtained results [17]. The amount of input parameters for such calculations is rather large and to obtain most of the data, specialized laboratory equipment and procedures must be used, which can be both, time-consuming and expensive [16]. Moreover, indoor and outdoor climatic conditions also have an impact on the output results.

By analysing multiple brick samples within one region (Latvia), it should be possible to obtain a cluster of samples that would generate similar output results. Afterward, general parameters for these clusters could be identified for use in numerical models. Such clusters are important to reduce the number of necessary parameters to be tested. With these clusters, it would be possible to include brick within a specific cluster based on a few properties or even brick types. Afterward, the numerical simulations could use general properties from specific clusters.

At the time of writing, no such clusters or attempts to generate one have been found in the scientific literature by the author. A similar study has been done by Hansen et.al. [18], where they tried to determine the key parameters that influence the outcome of the *Delphin* simulations the most, therefore minimizing the amount of necessary input data for reliable output data. In their study, they found that the water uptake coefficient has the most impact on the relative humidity results within the masonry and that water vapour diffusion factor and thermal conductivity showed seasonal impact on the results, and that density and open porosity had no significant impact on the results [18].

This study is the further research of the project 'Improvement of building energy efficiency technologies' (No. 03000–3.1.2-e/163) supported by the National Research Program of Latvia. In this study, we are trying to find one or more generic materials that could be used in the *Delphin* simulations, for the historical buildings in the region of Latvia.

2. METHODOLOGY

To analyse the Hygrothermal properties and *Delphin* simulation data [19], a Hierarchial clustering dendrogram, using an agglomerative clustering method, is created. *Jupyter Lab* [20] is used as an environment for this supervised Machine Learning (ML) clustering analysis. To perform the clustering *Python* Libraries from *SciKit Lea*rn are used [21]. Used *Python* libraries including *Sklearn* and *Matplotlib*. *Sklearn* is built on *NumPy* and *Scipy* and it is used for the calculations of the clustering process. *Matplotlib* is used for the visualization of the results, including the dendrogram.

After the initialization of the used libraries, the data for the clustering are imported and assigned to the dedicated variable 'data'. Used data can be found in the *Zenodo* data repository [22]. Before the clustering, all the data entries are normalized with the *StandardScaler* function, built into the *Sklearn* library. Data normalization is necessary to avoid some data having more weight than other data on the results.

When performing clustering analysis, all the possible cluster count solutions are generated meaning, at the one end of the spectrum all the samples are in one large cluster, and on the other side of the spectrum, each sample creates an individual cluster.

The difference between one large and many small clusters is the total distance between all the samples in the cluster. If there is data only from one sample present in the cluster, the distance is zero (the smallest possible distance). And if all the samples are combined into one large cluster, the distance between all the sample data is the largest possible. This can be shown graphically with the dendrogram (see Fig. 1).

In the hierarchical clustering dendrogram, the vertical axis represents the distance, and the horizontal lines in the graph represent the clusters. You can see from Fig. 1, that the largest possible distance for this case is around 20 (the distance has no unit – because we are using normalized data with different original units). When following the dendrogram from the top down, it can be traced how this one cluster of 40 samples starts to split into smaller clusters, containing fewer samples in each cluster, and at the same time decreasing the total distance of these new clusters.
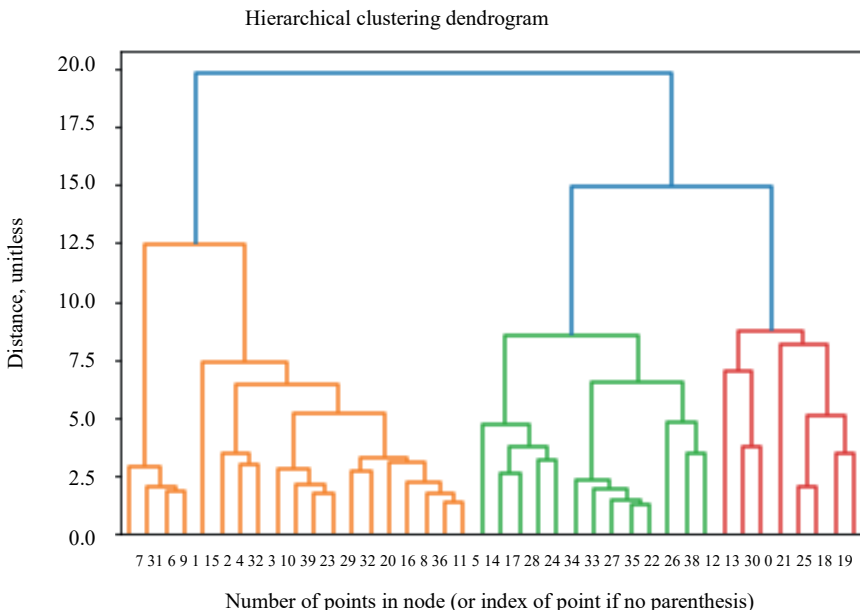

Fig. 1. Dendrogram of Hierarchical clustering.

To extract the results, all possible cluster counts (for both datasets) are generated by changing the *n_cluster* parameter in *Sklearn* and taking the array of corresponding results (in the array each number represents a cluster that the sample belongs to – the location of the number in the array correspond to the specific brick sample). Afterward, the method *model. labels_* is called to show the labels of clusters (meaning each label represents a cluster).
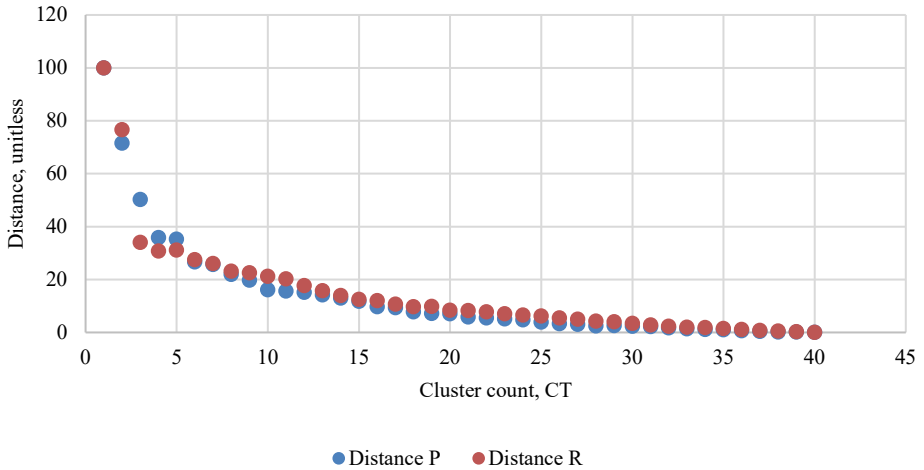
Fig. 2. Normalized Clustering results

To find the optimal combination (cluster count vs. distance) of the generated clusters, both cluster group results are normalized (see Fig. 2) and multiplied together (see Fig. 3). Afterward, for all the optimal combinations of clusters their respective average distance is compared to their cluster count (see Fig. 4).

To multiply both cluster groups from Parameters (P) and *Delphin* results (R) together, a vector of normalized distance data in descending order is created for each cluster group. These vectors are then multiplied together. All the results of the multiplied cluster results within the optimal range are shown in Fig. 3.
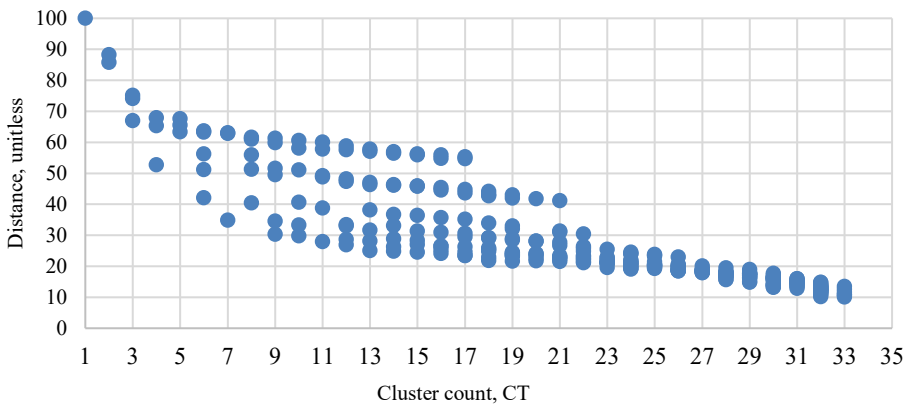
Fig. 3. Multiplied cluster results.

It can be seen in Fig. 3, that there is more than one combination of clusters for the same cluster count, and because we are looking for the most optimal combination, only the combinations with the lowest distances are used in those cases.

Afterward, the cluster count and distance of the selected combinations from Fig. 3, are normalized to the scale (0–1), with 0 being the worst case (highest cluster count; highest distance) and 1 being the best result (lowest cluster count, lowest distance), and plotted one against the other (See Fig. 4).
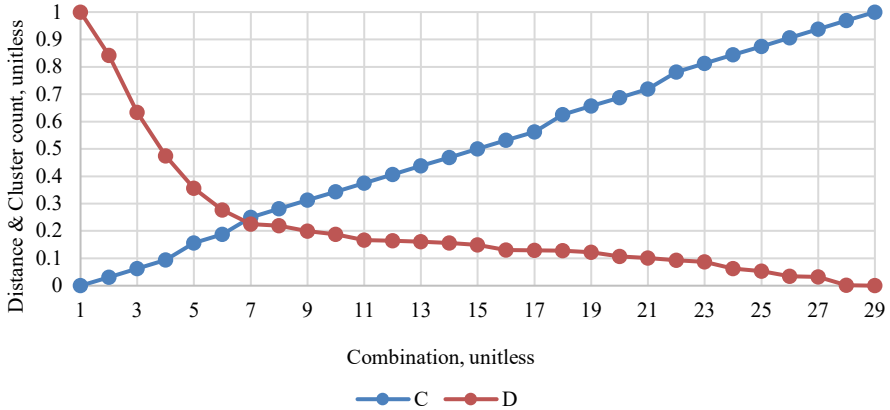

Fig. 4. Finding the optimal cluster count (C–Cluster; D–Distance).

The crossing point of Cluster and Distance lines can be considered as the optimal solution towards the smallest possible cluster count with the smallest possible distance. The resulting combination of the P and R clusters is then used to create new Combined clusters and these Combined clusters are used for further analysis, including, comparison to the clusters, based on the description of the brick samples (Year of manufacturing, colour, material type) and for the identification of the general groups/clusters of bricks.

3. RESULTS

All the possible cluster counts from *Delphin* results data, plotted against those clusters' corresponding distances, are shown in Fig. 5.
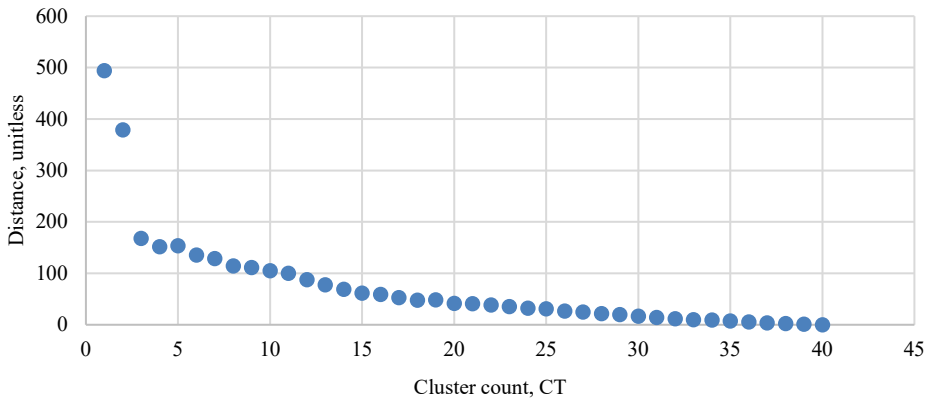

Fig. 5. Cluster combinations of *Delphin* simulations data.

1238

It can be seen if Fig. 5, that there is a significant difference in distance between a cluster count of 2 and a cluster count of 3 when comparing to the remaining cluster combinations.

All the possible cluster counts for hygrothermal properties data, plotted against those clusters' corresponding distances, are presented in Fig. 6.
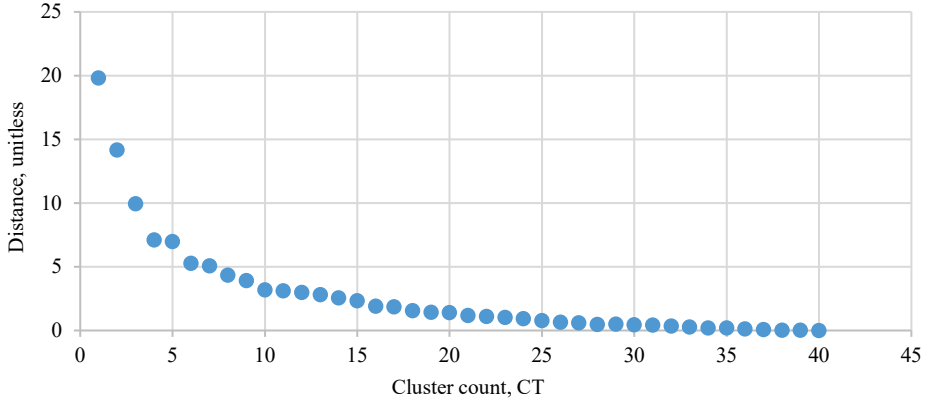

Fig. 6. Cluster combinations of hygrothermal properties data.

In Fig. 6, there is a visible exponential growth of a distance when the cluster count goes down, with the 'knee' being in a combined range of 3 to 10 clusters.

From the cluster combinations of the combined clusters, the optimal cluster combination was found to be the 7th combination, this is the combination of the P cluster of 6 and R cluster of 3, in total 9 original clusters, with the total average normalized distance of 30.3 (see Fig. 7).
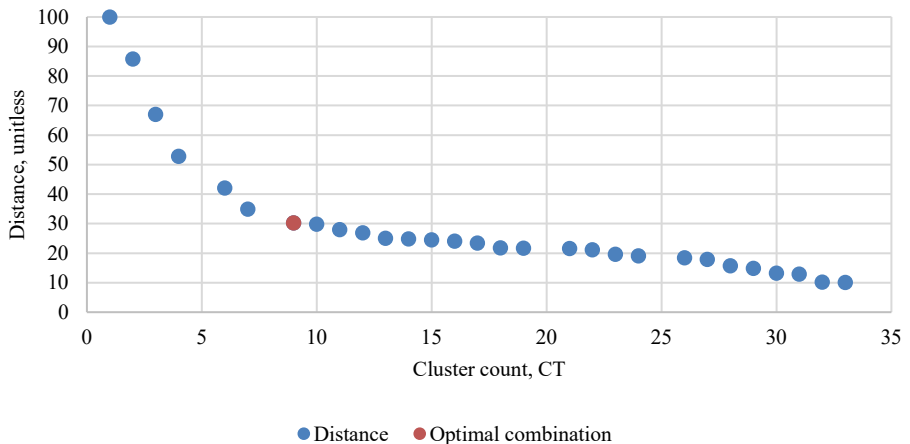

Fig. 7. Distance vs Cluster count of multiplied clusters.

From this cluster combination, 9 new clusters were created (see Table 1). If there is a zero in the box, it means that this combination of the cluster does not exist (there are any brick samples that would fit in this cluster).

1239

TABLE 1. R AND P CLUSTER OVERLAPPING (COMBINED CLUSTERS)

		P Clusters						Total samples
		0	1	2	3	4	5	
R Clusters	A	0	0	1	0	0	0	1
	B	1	3	0	12	4	15	35
	C	2	1	0	1	0	0	4
Total samples		3	4	1	13	4	15	40

In Table 1 the distribution of samples between all the clusters is shown (in total 40 samples). Clusters 'A', 'B', and 'C' are the R clusters, with 1 sample in cluster A, 35 samples in cluster B, and 4 samples in cluster C. Clusters '0', '1', '2', '3', '4', and '5' are the P clusters with 13 samples in cluster 3, 15 samples in cluster 5, etc. After combining P and R clusters new clusters 'A1', 'B0', 'B1', 'B3', 'B4', 'B5', 'C0', 'C1', and 'C3' were created.

To cross-examine created clusters groups with the types of the used brick samples, 11 clusters or groups of the brick samples were generated based on the manufacturing year, color, and material type of the brick. For each group, a unique code was generated from the denotations of description parameters. Bricks came in three colors: Yellow Pink and Red (Y, P, R). Three types of material had been used to make these bricks: Silica, Clay, and Concrete (S, C, CO). The manufacturing year was divided into the groups of 50 years period representing the half-century with the first half being (I) and the second half (II), the century is written with Greek numbers (see Table 2).

TABLE 2. CROSS-EXAMINATION OF CLUSTERS AND BRICK TYPES

		Groups of Brick Type										
		YC 20I	YS 20II	PC 19II	RC 18II	RC 20I	RC 19II	CO 20I	RC 19I	RC 20II	RC 17II	RC 17I
	A2	18-4										
	B0						19-9					
	B1		19-15 19-17 20-3									
Combined clusters	B3				19-7	19-13 19-18 20-5 20-11	18-16 20-6 20-12	19-10	20-2		20-4	20-13
	B4	19-1 19-2 19-5								20-9		
	B5		18-5	18-6	18-7	19-6 19-11 19-12 18-15 20-7	20-1 20-10 20-15 19-4		20-14 20-18	19-16		
	C0				19-8	20-8						
	C1								19-14			
	C3								20-16			

Table 2 can be read the same way as Table 1, only the brick count inside is replaced with the specific code for each brick sample group, meaning, in group B4 there are in total 4 samples (19-1, 19-2, 19-5, 20-9), in group YC20I there is also in total 4 samples (18-4, 19-1, 19-2, 19-5), but in the combination of these two clusters B4YC20I there are 3 samples (19-1, 19-2, 19-5). All the parameters for each brick sample group can be found in the *Zenodo* data repository [22].

4. DISCUSSION

Clusters generated from the *Delphin* results are creating more concise results with only three clusters, and the majority (87.5 %) of the samples being in one cluster. There are twice as many clusters (6) generated from the brick parameters with two dominant clusters containing 70 % of all the samples (37.5 and 32.5 %). After combining the cluster these three dominant clusters (B, 3, and 5) created two new dominant clusters (B3 and B5). In total 67.5 % of all samples were in these two clusters, 30 % in B3 and 37.5 % in B5.

One sample (18-4) has been recognized to be the only sample in both cluster groups. When comparing to the other brick samples based on their description, there are 3 more bricks with the same description (Yellow clay brick, manufactured in the 1st part of the 20th century). Three other bricks belong to group B4 with only one other brick being in this group, and that brick is red clay brick, manufactured in the 2nd part of the 20th century.

The majority of the samples in the largest combined cluster group of B5 are Red Clay bricks (86.7 %), with most of them being manufactured in the period from the 2nd part of the 19th century (30.8 %) to 1st part of the 20th century (38.5 %). In the second largest cluster group B3, almost all the bricks are red clay bricks, except for one brick that is made of concrete, and in this group, the majority of bricks has been manufactured in the period from the 2nd part of the 19th century (27.3 %) to 1st part of 20th century (36.4 %).

But it should be noted that the majority of the brick samples are red clay (75 %) and 60 % are manufactured in the period from the 2nd part of the 19th century (22.5 %) to the 1st part of the 20th century (37.5 %).

Looking at the *clusters from Delphin* results, where 35 of 40 bricks are in a single cluster, it could indicate, that different parameter clusters are generating similar results, in this case, parameter clusters 5 and 4 have 100 % overlap with results cluster B, followed by parameter cluster 3 with 92.3 % overlap, and cluster 1 with 25 % overlap. But it should be noted that the low number of clusters, in this case, 3, from the Delphin results data is due to the high distance of the first two cluster combination with 1 and 2 clusters, 494.17 and 378.56 accordingly, followed by a distance of 168 in combination with 3 clusters. If the first two cluster combinations are excluded from calculations of optimal cluster combination, then the optimal cluster count vs. distance would be the combination with 15 clusters and a distance of 37.5.

As the input data for P clusters are based on the numerical simulation output, these results are highly influenced by the chosen numerical calculation program (DELPHIN) and the performed simulation input data (material properties, chosen geometry, climatic conditions, boundary conditions, etc.), therefore, interpretation of the results is limited to the specific climatic condition and set of brick samples used in this study.

5. CONCLUSION

The distribution of the brick samples in the clusters, is similar to the distribution of the brick sample types, based on their description, therefore overall conclusions regarding the genericization of historical bricks cannot be made. However, regarding the red clay bricks, manufactured from the end of the 19th century till the beginning of the 20th century, there is a strong distinction between two main clusters (B3 and B5) with only two of the samples being in other clusters (B0 and C0).

The aim of the study is reached only partially, in the study 3 clusters for numerical simulation output were found, but no general brick parameters have been yet identified for those clusters, moreover, no methodology for assigning the brick sample to one of the clusters has been found.

Further research with an equal amount of brick samples with different descriptions should be carried out in a future study, moreover, different climatic conditions and geometry should be considered.

REFERENCES

[1] Freimanis R., *et al.* In-Situ Moisture Assessment in External Walls of Historic Building using Non-Destructive Methods. *Environmental and Climate Technologies* 2019:23(1):122–134. https://doi.org/10.2478/rtuect-2019-0009

[2] Zhou X., Carmeliet J., Derome D. Influence of envelope properties on interior insulation solutions for masonry walls. *Building and Environment* 2018:135:246–256. https://doi.org/10.1016/j.buildenv.2018.02.047

[3] Zhou X., Derome D., Carmeliet J. Analysis of moisture risk in internally insulated masonry walls. *Building and Environment* 2022:212:108734. https://doi.org/10.1016/j.buildenv.2021.108734

[4] Straube J., Schumacher C. Interior Insulation Retrofits of Load-Bearing Masonry Walls in Cold Climates. *Journal of Green Building* 2007:2(2):42–50.

[5] Haupl P., Jurk K., Petzold H. Inside thermal insulation for historical facades. Research in Building Physics. Boca Raton: CRC Press, 2003:463–469.

[6] Vereecken E., Roels S. Capillary active interior insulation: do the advantages offset potential disadvantages? *Materials and Structures* 2015:48:3009–3021. https://doi.org/10.1617/s11527-014-0373-9

[7] Johansson P., *et al.* Retrofitting a brick wall using vacuum insulation panels: measured hygrothermal effect on the existing structure. *Proceedings of the 10th Nordic Symposium on Building Physics* 2014:1269–1276.

[8] Kehl D., *et al.* Wooden beam ends in masonry with interior insulation–A literature review and simulation on causes and assessment of decay. *CESBP Vienna* 2013:299–304.

[9] Kohta U., Straube J., Van Straaten R. Field monitoring and simulation of a historic mass masonry building retrofitted with interior insulation. *Proceedings of the 12th International Conference on Thermal Performance of the Exterior Envelopes of Whole Buildings* 2013.

[10] Anker N., *et al.* Use of sensitivity analysis to evaluate hygrothermal conditions in solid brick walls with interior insulation. *Proceedings of the 5th International Building Physics Conference (IBPC): The Role of Building Physics in Resolving Carbon Reduction Challenge and Promoting Human Health in Buildings* 2012:377–384.

[11] Zhao J., *et al.* Evaluation of capillary-active mineral insulation systems for interior retrofit solution. *Building and Environment* 2017:115:215–227. https://doi.org/10.1016/j.buildenv.2017.01.004

[12] Sun Y., Haghighat F., Fung B. C. M. A review of the the-state-of-the-art in data-driven approaches for building energy prediction. *Energy & Buildings* 2020:221:110022. https://doi.org/10.1016/j.enbuild.2020.110022

[13] Ramirez R., *et al.* Simulation of moisture transport in fired-clay brick masonry structures accounting for interfacial phenomena. *Building and Environment* 2023:228:109898. https://doi.org/10.1016/j.buildenv.2022.109838

[14] Wasik M., Lapka P. Analysis of seasonal energy consumption during drying of highly saturated moist masonry walls in polish climatic conditions. *Energy* 2022:240:122694. https://doi.org/10.1016/j.energy.2021.122694

1242

[15] Zhou X., Carmeliet J., Derome D. Assessment of moisture risk of wooden beam embedded in internally insulated masonry walls with 2D and 3D models. *Building and Environment* 2021:193:107460. https://doi.org/10.1016/j.buildenv.2020.107460

[16] Kunzel H. M. Simultaneous Heat and Moisture Transport in Building Components. Stuttgart: Fraunhofer IRB, 1995.

[17] Freudenberg P., Ruisinger U., Stocker E., Calibration of Hygrothermal Simulations by the Help of a Generic Optimization Tool. *Energy Procedia* 2017:132:405–410. https://doi.org/10.1016/j.egypro.2017.09.645

[18] Hansen T., *et al.* Material characterization models and test methods for historic building materials. *Energy Procedia* 2017:132:315–320. https://doi.org/10.1016/j.egypro.2017.09.738

[19] Delphin Application [Online]. [Accessed 16.03.2022]. Available: https://www.bauklimatik-dresden.de/delphin/

[20] Jupyter homepage [Online]. [Accessed 16.03.2022]. Available: https://jupyter.org/

[21] Pedregosa F., *et al.* Scikit-learn: Machine Learning in Python. *Journal of Machine Learning Research* 2011:12:2825–2830.

[22] Freimanis R., *et al.* Hygrothermal Properties of historic bricks from various sites of Latvia. *Zenodo* 2021. https://doi.org/10.5281/zenodo.5656966

Study of Hygrothermal Processes in External Walls with Internal Insulation

Edite BISENIECE[1]*, Ritvars FREIMANIS[2], Reinis PURVINS[3], Armands GRAVELSINS[4], Aivars PUMPURS[5], Andra BLUMBERGA[6]

[1–4, 6] *Institute of Energy Systems and Environment, Riga Technical University*
Azenes iela 12/1, Riga, LV-1048, Latvia

[5] *Institute of Industrial Electronics and Electrical Engineering, Riga Technical University,*
Azenes iela 12/1, Riga, LV-1048, Latvia

Abstract **– Being an important contributor to the final energy consumption, historic buildings built before 1945 have high specific heating energy consumption compared to current energy standards and norms. However, they often cannot be insulated from the outside due to their heritage and culture value. Internal insulation is an alternative. However internal insulation faces challenges related to hygrothermal behaviour leading to mold growth, freezing, deterioration and other risks. The goal of this research is to link hygrothermal simulation results with experimental results for internally insulated historic brick masonry to assess correlation between simulated and measured data as well as the most influential parameters. The study is carried out by both a mathematical simulation tool and laboratory tests of historic masonry with internal insulation with four insulation materials (mineral wool, EPS, wood fiber and granulated aerogel) in a cold climate (average 4000 heating degree days). We found disparity between measured and simulated hygrothermal performance of studied constructions due to differences in material parameters and initial conditions of materials. The latter plays a more important role than material parameters. Under a steady state of conditions, the condensate tolerating system varies between 72.7 % and 80.5 % relative humidity, but in condensate limiting systems relative humidity variates between 73.3 % and 82.3 %. The temperature between the masonry wall and all insulation materials has stabilized on average at +10 °C. Mold corresponding to Mold index 3 was discovered on wood fiber mat.**

Keywords **– Energy efficiency in buildings; historic buildings; internal insulation; mold growth**

1. INTRODUCTION

With climate changes broadly witnessed, cannot afford to use more energy than we need. Today 40 % of total energy consumption in the European Union comes from the building sector [1], [2]. The European Union's research project *RIBuild* defines historic buildings as buildings built before 1945 and reports that more than 30 % of final energy consumed by the building sector is allocated to historic buildings [3]. For example, in Latvia more than 50 % of the housing stock heated area belongs to multifamily apartment buildings, and out of that about 26 % are built before 1940 [4]. Reduction of energy consumption in existing building stock is one of the European Union's energy and climate policy tools [5]. Retrofit of the existing building stock gives significant contribution in reduction of greenhouse gas emissions and overall sustainability of the building stock [6].

---

* Corresponding author.
E-mail address: edite.kamendere@rtu.lv

Insulation of external walls is an effective way to reduce energy consumption in buildings. The principles that should be followed when external walls are insulated include the air tightness of the wall, and the vapour permeability which should increase gradually towards the outside surface of the wall [7]. Although the best and the most reliable way to install external wall insulation is insulation from the outside, preservation of the facades of historic buildings prohibits external insulation in this way. Moreover, there might be other reasons why insulation from the outside is not possible such as space restrictions, aesthetic reasons, etc. An alternative solution to insulating the external wall from the outside is to insulate it from the inside. However, this is associated with risks caused by changes in the hygrothermal behaviour in the wall. When insulation is applied on the internal surface of the wall, both temperature and moisture conditions are changed within the wall, exposing it to several risks such as condensation, mold growth, freezing, deterioration, algae growth, etc. Each of these risks occurs under different hygrothermal conditions depending on the material properties, e.g. the study carried out by Purvins et al. found that fully saturated clay bricks used in historic building start to crack after two freeze-thaw cycles [8], while the study of Pasek and Kesl showed that Central Europe's climatic conditions presented high risk of structural damages for historic stone and brick masonry with internal insulation due to temperature changes [9]. Thus assessment of the technical condition of the building prior to application of internal insulation is an important activity which helps to determine the most appropriate retrofit methods and materials as well as helps to avoid or minimize problems associated with moisture [10].

Hygrothermal behaviour of internally insulated walls can be assessed either by simulation or experimentally. Mathematical models of heat and moisture transport tools, such as well know *Delphin* [11] or *WUFI* [12] can help to predict hygrothermal behaviour of building envelope. Nevertheless, accuracy of results from mathematical models depends on the quality of input data. Databases contain hygric and thermal parameters of certain materials obtained from laboratory tests and differ from other materials which are not tested in the laboratory. They also take into account parameters that are not known. Experimental tests can be carried out either in a controlled environment in a laboratory or on site in actual buildings.

A number of studies have been carried out on laboratory tests of different materials applied on the internal side of historic walls. Wurtz and Saelle tested two new types of thermal breakers designed for internal application in historical buildings, and the results showed that 60 % of heat loss reduction can be reached by using both of the thermal breakers [13]. Haupl and Fechner described the methodology on how to determine moisture storage and moisture transport properties in the capillary active insulation material which is widely used for internal insulation of historic buildings [14]. Vereecken and Roels tested eleven different types of insulation materials on the massive masonry wall under the steady-state conditions. Vapour tight systems showed the best performance and capillary active insulation systems with glue mortar showed the worse performance due to accumulation of water in the mortar [15]. Pavlik and Cerny in their study with mineral wool insulation showed that, by applying mineral wool on a brick wall, it performs well while applying it on the argillite wall, the overhygroscopic moisture is present in the wall [16]. Other research showed that vacuum panels as an internal insulation in historic buildings cause higher relative humidity in the wooden beam ends, even more so, when wind driven rain is present, the relative humidity in the wall rises substantially [17]. A non-insulated zone of 300 mm above and below the floor is proposed for buildings with floor beams. This kind of solution is proposed to avoid moisture build up for buildings located in humid climates [18].

23

A limited number of papers are available on heat transfer and moisture transport in-situ measurements in historic buildings which have internal wall insulation. In Latvia Biseniece et al., tested two types of insulation materials: aerogel and vacuum insulation panel. Test results showed that the temperature between the wall and internal insulation drop to –9.32 °C in case of vacuum panel and –7.08 °C in case of aerogel. They also concluded that energy savings cannot be reached if special attention is not paid to energy management issues, and that calcium silicate masonry faces the freeze-thaw risk if the capillary saturation reaches into the brick during the below zero outdoor conditions [19]. In Estonia Kloseiko et al., monitored a double leaf rubble exterior wall of a museum building with internal insulation. Insulation was installed during the autumn-winter period and consisted of an air cavity, mineral wool and a newly built inner leaf. During the period of monitoring, very high relative humidity was observed. The research led to the conclusion that drying of the masonry wall before insulation should be taken into account and neglect to do so will cause overall high relative humidity levels throughout the structure and potential risk of mold growth [20]. In another research carried out in Estonia by Kloseiko et al., four different insulation materials (polyurethane, polisocyanurate, aerated concrete and calcium silicate) were tested. Test results showed that calcium silicate and aerated concrete dried out faster than the other two materials, but they also showed rapid increase of moisture, when the humidity of the internal climate was increased. The main conclusion was that built in moisture of the wall during the application of the insulation is responsible for high humidity levels and can cause interstitial condensation [21]. Similar research was carried out by Pavia where seven types of insulation materials were tested on the wall of historic brick. Those materials where compared to the lime plaster finish. It was found out that by an average of 13 % to 25 % the performance of the insulation materials is overestimated by producers [22]. Bianco et al. have carried out the investigation on new thermal insulating plaster and studied this material on a historic building in Turin, Italy. The preliminary results show that thermal conductivity of proposed new plaster is 2.5 to 3 times lower than conventional plaster, but more research is needed on the long-term performance of this material [23]. Galliano et al. have carried out simulations and measurements of two new internal insulation materials [24].

Literature review on internal insulation of historic masonry walls revealed that studies are scattered and no common solution for all the different cases exists. Each of the studies have different goals mainly focusing on thermal behaviour of the wall and much less on the moisture transport. Selection of the right insulation system or material for the specific case is crucial and sometimes in order to avoid moisture problems it is better to sacrifice a bit of energy efficiency. A better understanding of the hygrothermal behaviour of internally insulated walls needs to be obtained.

The goal of this research is to link hygrothermal simulation results with experimental results for internally insulated historic brick masonry to assess correlation between simulated and measured data as well as the most influential parameters. The study is carried out through the application of both a mathematical simulation tool and laboratory tests of historic masonry built from bricks produced around 1900 with internal insulation with four insulation materials in cold climates (average outdoor temperature in heating season 0 °C and 200 heating days annually). The paper starts with an introduction, is followed by description of materials, applied methodology, analysis of results and finally, discussions and conclusions.

2. BASE WALL AND INTERNAL INSULATION MATERIALS

The experimental set-up was built in the laboratory. Four types of insulation materials, two types of vapour barriers, gypsum board and historic bricks were used in this study.

The base wall was built from historic bricks collected from the demolition site of a historic building built around 1900 at O. Vācieša iela 6, Riga, Latvia. Lime-cement mortar was used. The base wall samples were built as double leaf masonry with the size of 25 cm × 28 cm and the depth of 51 cm each.

Expanded polystyrene board, wood fiber board, mineral (rock) wool and granulated aerogel *LA1000* were used for internal insulation. Expanded polystyrene board and mineral wool are widely used and common insulation materials. Nowadays natural materials such as wood fiber board and innovative materials, e.g. granulated aerogel are becoming more popular. Vapour barriers with different equivalent air layer thicknesses (s_d values) were used. All materials and their technical parameters are listed in Table 1.

TABLE 1. TECHNICAL PARAMETERS OF TESTED INSULATION MATERIALS

Insulation material	Thickness, m	Heat conductivity, W/(mK)	Bulk density, kg/m^3	Vapour resistance coefficient μ	s_d values, m	Manufacturer
Expanded polystyrene board	0.05	0.039	13.5	30	1.5	*Tenapors (Tenax)*
Wood fiber board	0.05	0.038	50	2.1	0.105	*Steico group*
Mineral wool	0.05	0.036	28	1	0.05	*Paroc*
Granulated aerogel	0.02	0.016	65–85	N/A	N/A	*Cabot corporation*
Gypsum board	0.018	0.21	732	6.8	0.122	*Norgips*
Vapour barrier (1)	N/A	N/A	N/A	N/A	4.5	*Elkatek*
Vapour barrier (2)	N/A	N/A	N/A	N/A	12	*Jutadach*

Although many insulation materials are available on the market, it is still not clear which of them can be applied safely internally. Insulation materials can be distinguished by different parameters. In the scope of this study materials are grouped by parameters attributed to interstitial condensate. In accordance to the basic properties and following WTA 6-4 [25] and DIN 4108-3 [26], insulation materials can be divided into three groups:

- Condensate-preventing insulation systems disable vapour transfer from the room side into the construction by a vapour barrier. Vapour barriers are sealing layers with a vapour diffusion equivalent air layer thickness s_d of minimum 1500 m;
- Condensate-limiting insulation systems include a vapour brake with an s_d value of minimum 0.5 m and maximum 1500 m. Vapour control layer should reduce the vapour input from the room side into the construction and has to be combined with a sufficient wind-driven rain protection;
- Condensate-tolerating insulation systems consist of capillary active insulation material and glue mortar. The only vapour resistance in these insulation systems is given by the material itself, therefore they show very small vapour transfer resistances (s_d value < 0.5 m).

Types of insulation systems used in the tests are presented in Table 2.

25

TABLE 2. TYPES OF INSULATION SYSTEMS

Test Round	Insulation material	Vapour barrier	Finishing material	System s_d value, m	Insulation system type
Test round 1	Wood fiber	Vapour barrier (1)	Gypsum board	4.73	Condensate tolerating
Test round 1	Mineral wool	Vapour barrier (1)	Gypsum board	4.67	Condensate limiting
Test round 1	EPS	NO	Gypsum board	1.62	Condensate limiting
Test round 1	Granulated aerogel	Vapour barrier (1)	Gypsum board	N/A	N/A
Test round 2	Wood fiber	NO	Gypsum board	0.23	Condensate tolerating
Test round 2	Mineral wool	Vapour barrier (2)	Gypsum board	12.17	Condensate limiting
Test round 2	EPS	NO	Gypsum board	1.62	Condensate limiting
Test round 2	Granulated aerogel	NO	Gypsum board	N/A	N/A

3. METHODOLOGY

The study was carried out by two methods: simulation of hygrothermal behaviour with heat and transfer simulation tool *Delphin* 5.9.3. [11], and measurement of hygrothermal parameters of internally insulated masonry wall in the laboratory. The simulation was performed before and after laboratory tests to assess correlation between measured and simulated data, and perform analysis of parameters that affect the fit between the simulation results and measured results.

3.1. Tests of Bricks

Ten randomly selected bricks were tested to assess density and open porosity. Open porosity was determined based on standard EN 772-3:1998 [27]. Dry density of bricks was measured based on standard EN 772-13:2000 [28].

3.2. Heat and Moisture Transfer Model

The 2-dimensional hygrothermal behaviour in transient conditions of the base wall and three different insulation materials (granulated aerogel was not simulated as it is not available in the material database) was analyzed. The wall is composed of 2-dimensional layers (see Fig. 1).
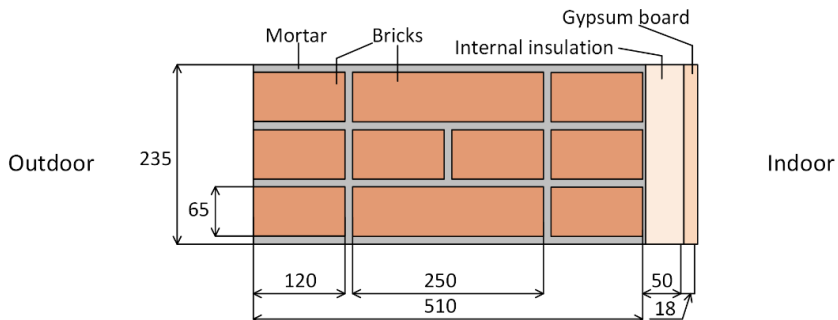

Fig. 1. 2-dimensional model of simulated masonry wall with internal insulation (all numbers are in mm).

Only density and open porosity of bricks were derived from the material tests in the laboratory prior to the experiment (see Chapter 3.1). These two parameters were used as decisive values to select brick from the *Delphin* database. Lime-cement mortar, mineral wool, wood fiber and EPS were selected from the *Delphin* database. Before the laboratory experiment the simulation was performed for insulated masonry with data from the *Delphin* database (see Table 3).

TABLE 3. PROPERTIES OF MATERIALS USED
FOR SIMULATION BEFORE LABORATORY EXPERIMENT

		Brick	Mortar	Mineral wool	Wood fiber	EPS
Name of the material in *Delphin* database		Old building brick Dresden ZD	Lime cement mortar	Mineral Wool	Wood Fiber Insulation Board	Polystyrene Board – Expanded
Density of dry material, kg/m^3		1619.51	1878.47	37	150	23
Open porosity, m^3/m^3		0.388864	0.291144	0.92	0.981	0.93
Thermal conductivity, W/(mK)		0.4025	0.803333	0.04	0.042	0.036
Specific heat capacity of dry material, J/kg		953.143	757.939	840	2000	1500
Water vapour diffusion resistance factor		10.4726	36.9113	1	3	96
Water uptake coefficient, kg/m^{2}s$^{0.5}$		0.380526	0.036085	0	0.07	0.00001
Effective saturation (long term process), m^3/m^3		0.361043	0.222606	0.9	0.6	0.92
Capillary saturation content (short term process), m^3/m^3		0.2563	0.2166	0.9	0.55	–
Liquid water conductivity at effective saturation, s		2.09E–09	1.02E–11	0	2.16E–08	0
Sorption isotherm	Moisture content, m^3/m^3 RH 0 %	0.001912	6.29E–08	N/A	0.0000683	0.0000528
	RH 30 %	0.003322	0.01011	–	0.0048476	0.000455
	RH 50 %	0.003445	0.035014	–	0.0080606	0.000617
	RH 80 %	0.003662	0.060304	–	0.0176992	0.001078
	RH 95 %	0.011130	0.083608	–	0.0328964	0.009227
	RH 100 %	0.361043	0.222606	–	0.6	0.92
Initial relative humidity within material, %		40	40	40	40	40
Initial temperature of material, °C		23	23	23	23	23

Boundary conditions used for simulation before the laboratory experiments: indoor temperature +20 °C and relative humidity 55 %, and outdoor temperature +3 °C and 85 % relative humidity. For the simulation after experiment, boundary conditions were used as in experimental test rounds.

27

3.3. Hygrothermal Behaviour Tests of the Test Wall

In the Baltic Sea region the common historic building consists of three to seven stories and has 45–90 cm thick brick wall [7]. For the hygrothermal behaviour tests of the test wall a double climatic chamber in laboratory was used. A test wall with four double leaf masonry patterns (25 cm × 28 cm × 51 cm) was built and inserted inside this chamber (see Fig. 2).
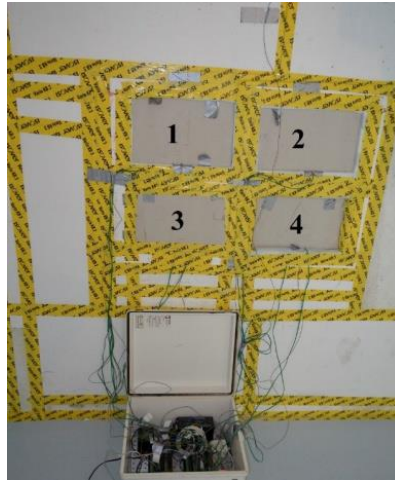

Fig. 2. Laboratory test stand with four historic masonry patterns and four insulation materials: 1 – wood fiber, 2 – mineral wool, 3 – expanded polystirene board, 4 – granulated aerogel.

Relative humidity and temperature were measured between insulation and masonry (on the middle of the brick), and in both chambers with 8 temperature sensors and 5 relative humidity sensors. Time step of both measurements is 1 minute.

Two test rounds were carried out (see Table 4). During the first test series the data monitoring equipment failed on the first day of the test run and data were collected from the second day of testing. The first test round was carried out for 22 days. The second round was carried out after drying the test wall in room condition for 8 days. The second test round took 23 days. Outdoor chamber conditions were changed for the second test round because humidifier was freezing in the first test round.

TABLE 4. TEST CONDITIONS OF TEST ROUNDS

Test conditions	Test 1	Test 2
Preconditioning period length, days	10	8
Preconditioning temperature/relative humidity	+23 °C/25 %	Room conditions
Length of the test, days	22	23
Indoor temperature/relative humidity	+19.5 °C to +20.5 °C/53–56 %	+19.5 °C to +20.5 °C/53–56 %
Outdoor temperature/relative humidity	–0.5 °C to +0.5 °C/80–90 %	+2.5 °C to +3.5 °C/80–90 %

Every masonry pattern was insulated with a different type of insulation system: expanded polystirene board, wood fiber board, mineral wool with vapour barrier (s_d in the first test round

28

was 4.5 m and in the second test round was 12 m) and translucent hydrophobic granulated aerogel (0.7–4.0 mm) (detailed information see in Table 2). The thickness of insulation materials was selected based on the average U-value of 0.35 W/(m²K) for all four patterns. All patterns were covered with gypsum board from the indoor side.

4. RESULTS

4.1. Tests of Bricks

Fig. 3 illustrates test results of density and open porosity of historic bricks used in the test wall. There is no correlation found between these two parameters with R^2 value only 0.0896. The average open porosity is 35.86 % and density is 1611.1 kg/m³.
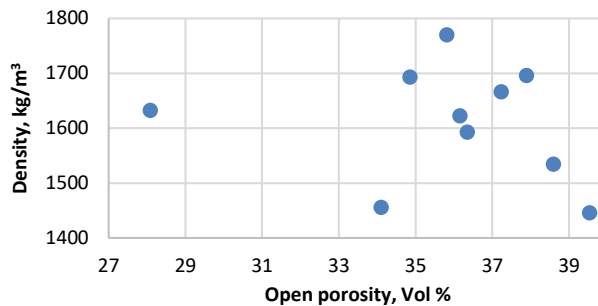
Fig. 3. Open porosity and density of tested historic bricks.

4.2. Hygrothermal Simulation before Laboratory Experiment

The relative humidity and temperature between masonry and insulation material in three simulated wall constructions are presented in Fig. 4. Both relative humidity and temperature changes at slow rate asymptotically approaching equilibrium conditions only on 14th day for mineral wool, 17th day for EPS and 21st day for wood fiber. All three samples stabilize at different temperatures: 11.55 °C for wood fiber, 10.44 °C for EPS and 10.37 °C for mineral wool. The equilibrium relative humidity also differs and is 39.1 % for mineral wool, 43.9 % for EPS and 71.4 % for wood fiber.

(a)

(b)

(c)
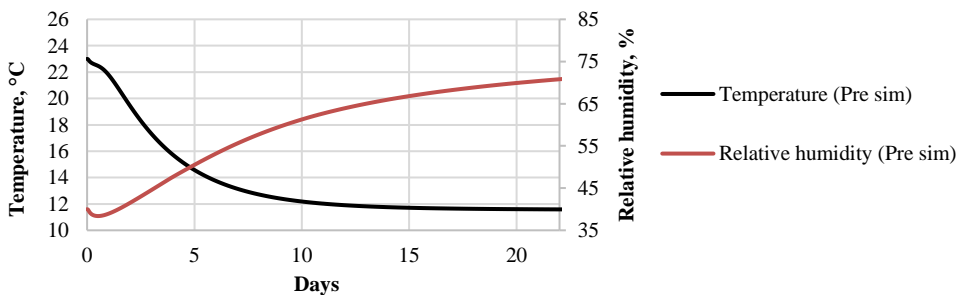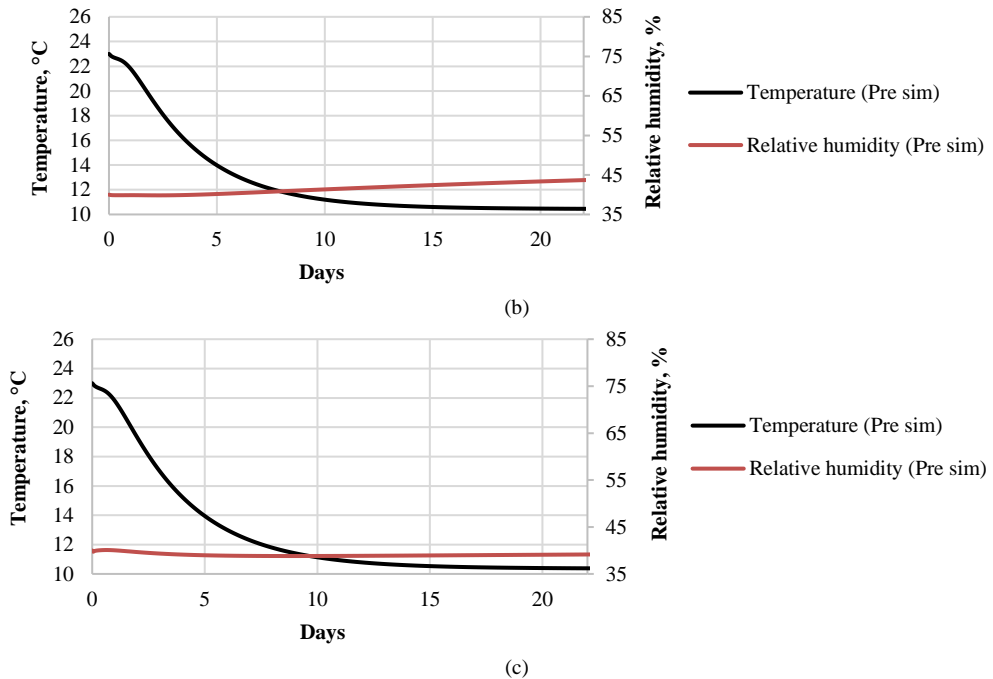
Fig. 4. Simulated temperature and relative humidity between masonry and insulation layer before experiment:
a) wood fiber, b) EPS, c) mineral wool.

4.3. Hygrothermal Behaviour of the Test Wall

The relative humidity and temperature between masonry and insulation material in four tested wall patterns measured in both test rounds is shown in Fig. 5. Relative humidity growth rate is high during first five test days for all materials and is slowing down when approaching equilibrium conditions. Temperature for all samples is reaching equilibrium in the first 5 days.

Relative humidity between masonry and the wood fiber (see Fig. 5(a)) is higher when the vapour barrier is not applied and reaches 80 % while if the vapour barrier is installed relative humidity increases up to 74 %. The growth rate of relative humidity is also higher without the vapour barrier. The initial temperatures are different for both tests but they stabilize after five days at +11.3 °C for the sample with vapour barrier and at +9.45 °C without vapour barrier.

Mineral wool with two different vapour barrier types (see Fig. 5(b)) show the same trend of behaviour of relative humidity and they both reach 83.5 % at the end of the test. The growth rate of relative humidity is very high during first two days and stabilizes thereafter. The initial temperatures are different for both tests but they stabilize after five days at +9.7 °C for the first test and at +10.8 °C for the second test.

EPS (see Fig. 5(c)) shows the same trend of behaviour of relative humidity for both tests reaching 80 % at the end of the test. The growth rate of relative humidity is very high during first two days and stabilizes after that. The initial temperatures are different for both tests but they stabilize after five days at +9 °C for the first test and at +10.7 °C for the second test.

When the vapour barrier is applied to granulated aerogel (see Fig. 5(d)) the relative humidity increases very quickly during the first two days and increases up to 79 % during the next 20
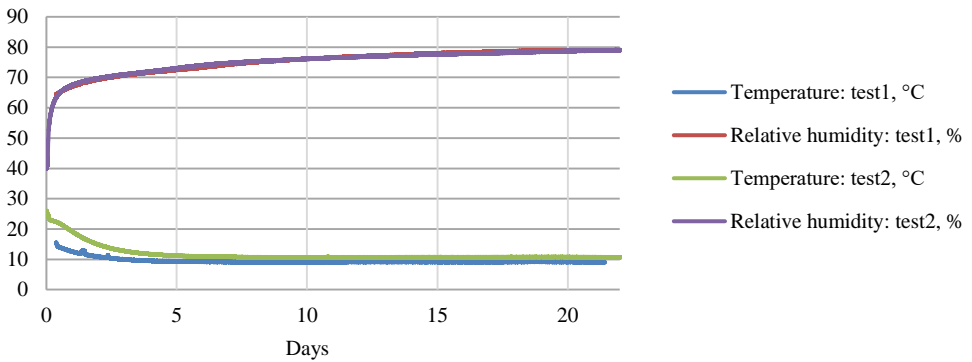
days. If aerogel is used without the vapour barrier, relative humidity is lower (74 %). Temperatures are +9.8 °C and +11 °C, respectively.
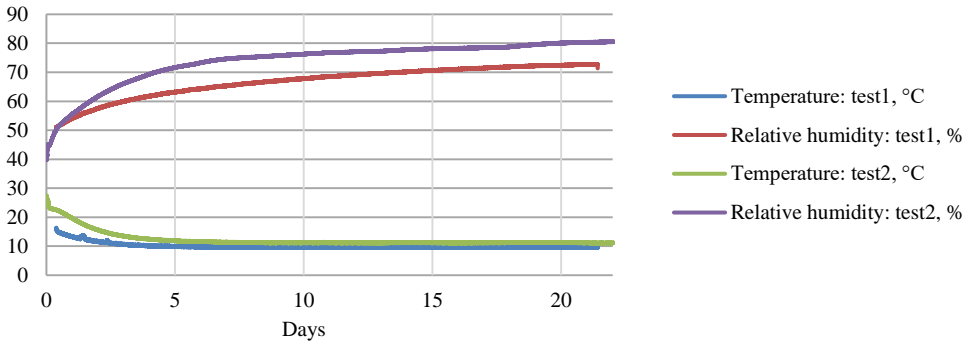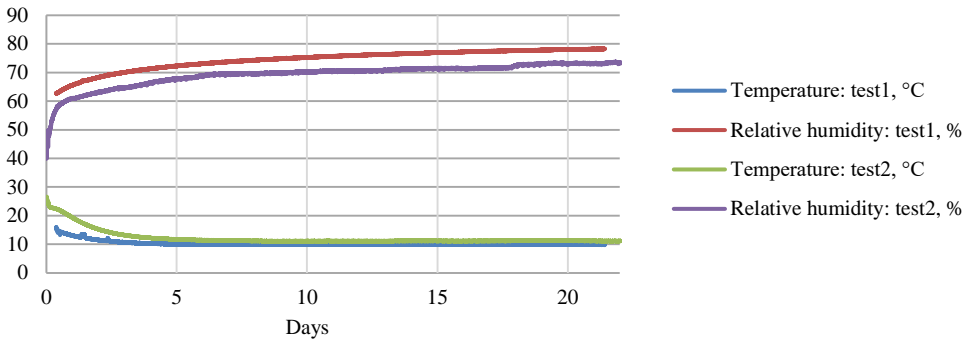

(a)
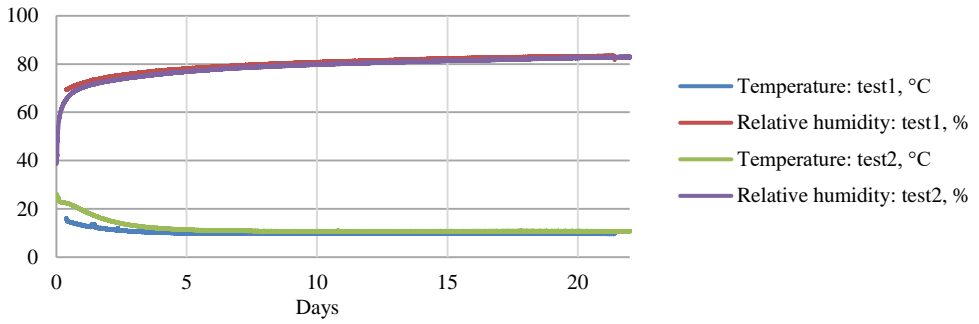
(b)

(c)

(d)

Fig. 5. Measured temperature and relative humidity between masonry and insulation layer: a) wood fiber,
b) mineral wool, c) EPS, d) granulated aerogel.

4.4. Mold Growth

Mold growth is one the major risks associated with internal insulation as the hygrothermal conditions are favourable for spore germination and further mycelium growth. If there are enough nutrients and time for germination, a high risk of mold growth exists. Fig. 6 illustrates development of the Lowest Isopleth for Mold from Isopleth of different species for both spore germination and mycelium growth.

(a)   (b)
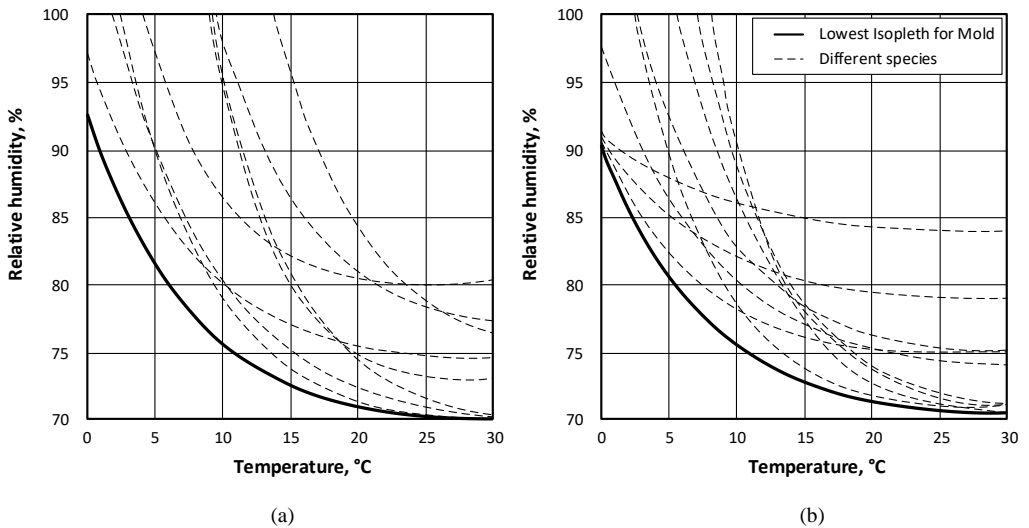
Fig. 6. The Lowest Isopleth for Mold of different species for spore germination (a) and mycelium growth (b) [29].

If the temperature is +10 °C and there are enough nutrients and time, spore germination and mycelium growth starts at 76 % relative humidity (see Fig. 6). In both test rounds temperature stabilized around +10 °C and relative humidity was above 76 % for all insulation materials. When the test wall was opened on the 22nd day after the beginning of the test, mold was discovered on one of the corners of the wood fiber mat. According to [5] wood fiber is substrate class I (biodegradable materials) with higher fungal growth rate and it 22 days was enough to

32

have visible fungal growth on the wood fiber. This corresponds to mold index level 3 by VTT Mold Growth model (visual findings of mold on surface, <10 % coverage) when new spores are produced [30]. Fig. 7 illustrates wood fiber affected by mold and magnified material with and without mold on it. After the second test round mold was discovered in the middle of the insulation material.
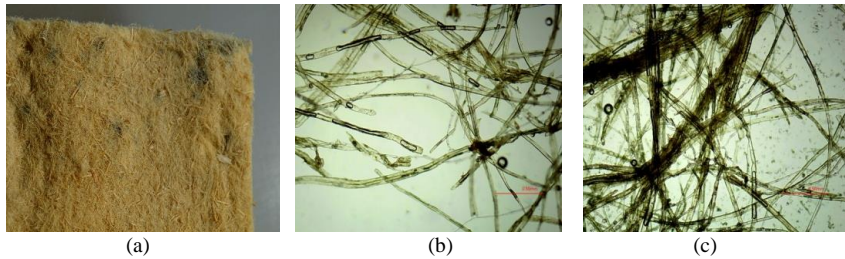

(a)   (b)   (c)

Fig. 7. Mold on wood fiber mat after test: a) mold on the top right corner, b) magnified wood fiber without mold, c) with mold.

4.5. Comparison of Experimental and Hygrothermal Simulation Results

Correlation analysis presented in Fig. 8 shows that satisfactory results are reached for temperature as correlation coefficient R^2 is in the range of 0.81 to 0.86. Correlation is good for simulated and measured results for relative humidity of wood fiber ($R^2 = 0.84$), but good correlation is not reached for relative humidity for EPS ($R^2 = 0.59$) and mineral wool ($R^2 = 0.54$).
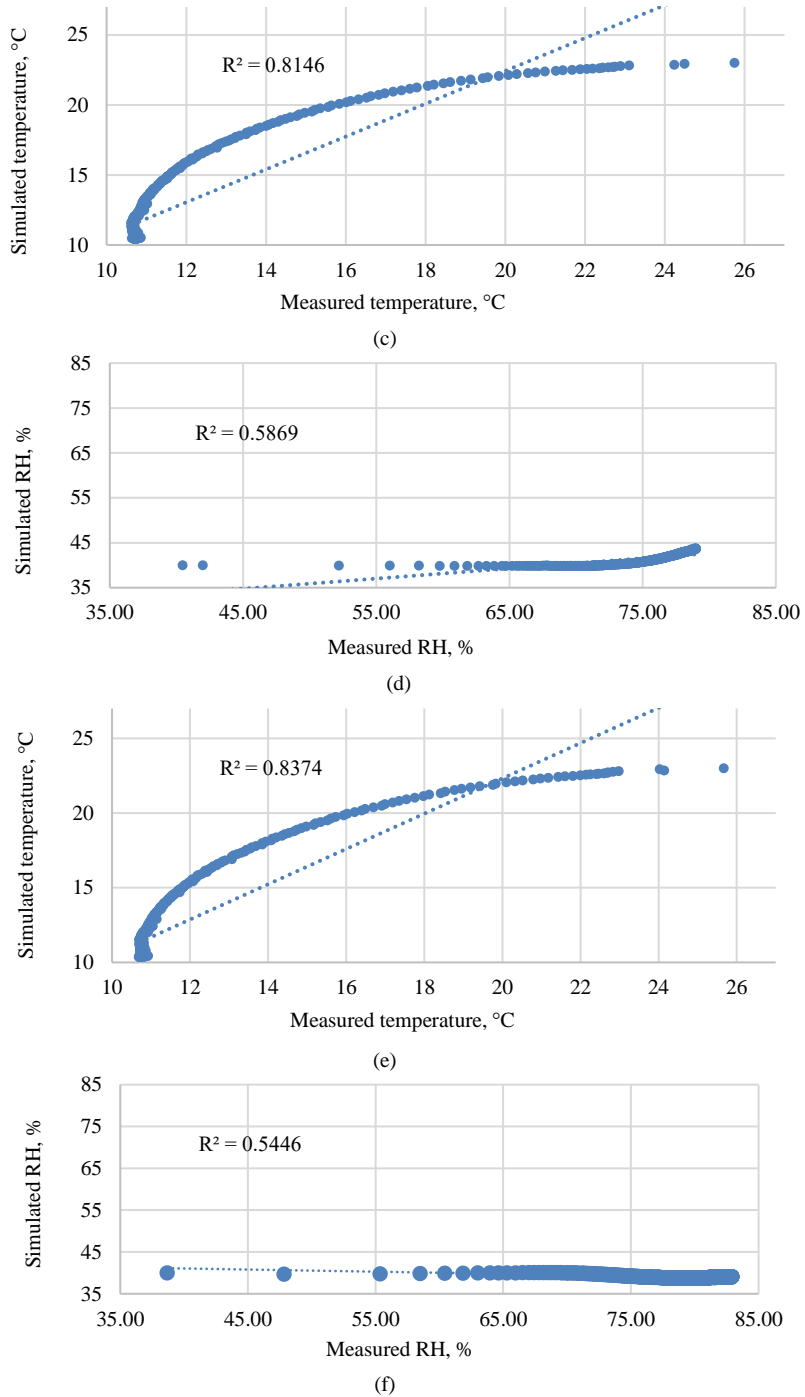

(a)

(b)

(c)

(d)

(e)

(f)
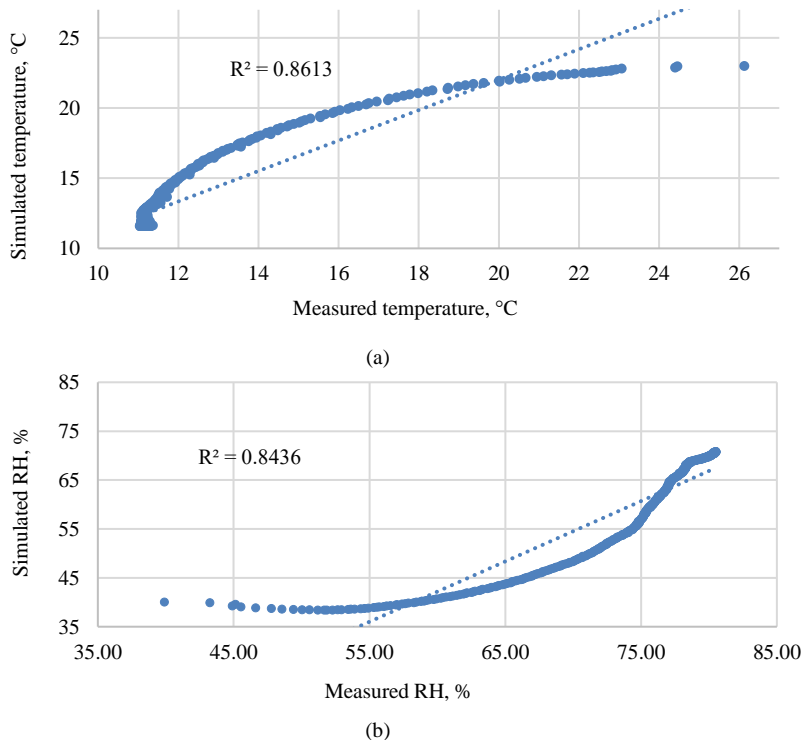
Fig. 8. Correlation between simulated and measured temperatures: a) wood fiber, c) EPS, e) mineral wool.
Relative humidity: b) wood fiber, d) EPS, f) mineral wool (between masonry and insulation layer).

34

Model fitting to measured data was improved by applying the parametric analysis. It was carried out by modifying parameters of masonry, mortar and insulation materials. Thermal conductivity, density of dry material, and water vapour diffusion resistance factor for insulation materials were changed to values supplied by material producers (see Table 1). For bricks and mortar thermal conductivity, specific heat capacity, liquid water conductivity at effective saturation, water uptake coefficient and initial relative humidity were adjusted. Adjusted values are presented in Table 5.

TABLE 5. PROPERTIES OF MATERIALS USED FOR PARAMETRIC ANALYSIS

		Brick	Mortar	Mineral wool	Wood fiber	EPS
Name of the material in *Delphin* database		Old building brick Dresden ZD	Lime cement mortar	Mineral Wool	Wood Fiber Insulation Board	Polystyrene Board – Expanded
Density of dry material, kg/m³		1619.51	1878.47	28 (–24 %)	50 (–67 %)	13.5 (–41 %)
Thermal conductivity, W/(mK)		0.482 (+20 %)	0.5 (–38 %)	0.036 (–10 %)	0.038 (–10 %)	0.039 (+8 %)
Specific heat capacity of dry material, J/kg		430 (–55 %)	470 (–38 %)	840	2000	1500
Water vapour diffusion resistance factor		10.4726	36.9113	1	2.1 (–30 %)	30 (–69 %)
Water uptake coefficient, kg/m²s$^{0.5}$		0.423587 (+11 %)	0,211622 (+486 %)	0	0.07	0.00001
Effective saturation (long term process), m³/m³		0.761043 (+111 %)	0.1 (–55 %)	0.9	0.6	0.92
Liquid water conductivity at effective saturation, s		2.59E–09 (+24 %)	3.52 E–10 (+3339 %)	0	2.16E–08	0
Sorption isotherm	Moisture content, m³/m³ RH 0 %	0.004030	2.83E–08		0.0000683	0.0000528
	RH 30 %	0.007003	0.004542		0.0048476	0.000455
	RH 50 %	0.007261	0.015729		0.0080606	0.000617
	RH 80 %	0.007720	0.027090		0.0176992	0.001078
	RH 95 %	0.023461	0.037559		0.0328964	0.009227
	RH 100 %	0.761043	0.1		0.6	0.92
Initial relative humidity within material, %		65 (+62 %)*	85 (+112 %)*	40	40	40
Initial temperature of material, °C		23	23	23	23	23

*Within the material starting from in the depth of 2.5...3.5 cm from the external surfaces of material.

Fig. 9 illustrates the changes of temperature and relative humidity during simulation before and after the experiment, and measured results in masonry with wood fiber without vapour barrier. The main gap between measured and pre-test simulation temperatures is observed during the first 10 days when the pre-test simulation temperature is decreasing at a slower rate than measured temperature. The post-test simulation results fit well with measured temperatures. The temperature at the equilibrium differs only 0.6 °C. To reach acceptable results for post-test

35

simulation fit, the values of the thermal conductivity, density of dry material, and the specific heat capacity have been changed (see Table 5).

The same tendency is observed for the relative humidity: the pre-test simulation has a much lower increase rate at the beginning hence it has not reached equilibrium during the simulation period. The post-test simulation and measured relative humidity fit well and both are stabilizing at around 80 %. To reach acceptable results for the post-test simulation, the water vapour diffusion resistance factor, the liquid water conductivity at effective saturation, water uptake coefficient and initial relative humidity of the brick and mortar have been changed (see Table 5).
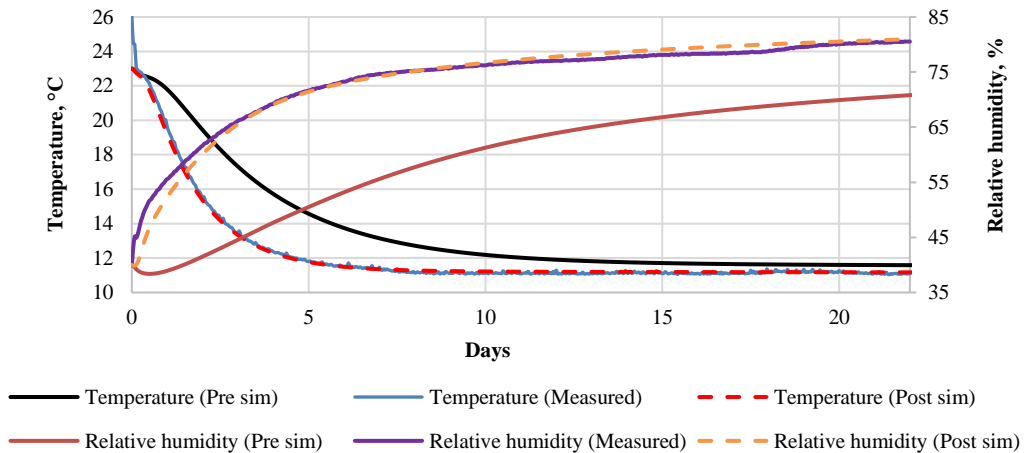
Fig. 9. Behaviour of temperature and relative humidity between masonry and wood fiber without vapour barrier insulation layer: simulation before and after experiment, and measured results.

Fig. 10 shows the changes of temperature and relative humidity during simulation before and after the experiment, and measured results between masonry and EPS insulation layer. The main gap between measured and pre-test simulation temperatures is observed during the first 10 days when the pre-test simulation temperature is decreasing at a slower rate than the measured temperature. The post-test simulation results fit well with measured temperatures. The temperature at the equilibrium fits well for all three graphs. To reach acceptable results for post-test simulation the values of the thermal conductivity, density of dry material, and the specific heat capacity have been changed (see Table 5).

The gap between measured and pre-test simulation results of relative humidity is significant. The relative humidity cannot gain the speed to increase the rate of change neither at the beginning nor during the rest of the pre-test simulation. The post-test simulation and measured relative humidity fit well and both are stabilizing around 81.5 % for measurements and 83 % for post-test simulation. To reach acceptable results for post-test simulation, the water vapour diffusion resistance factor, the liquid water conductivity at effective saturation, water uptake coefficient and initial relative humidity of the brick and mortar have been changed (see Table 4).
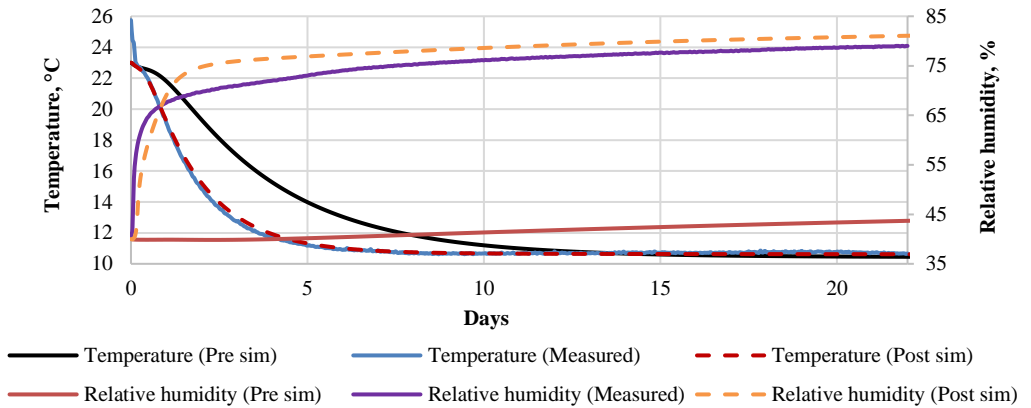
Fig. 10. Behaviour of temperature and relative humidity between masonry and EPS insulation layer: simulation before and after experiment, and measured results.

Fig. 11 shows the changes of temperature and relative humidity during simulation before and after the experiment, and measured results between masonry and mineral wool with vapour barrier ($s_d = 12$ m) insulation layer. The main gap between measured and pre-test simulation temperatures is observed during the first 10 days when the pre-test simulation temperature is decreasing at a slower rate than the measured temperature. The post-test simulation results fit well with measured temperatures. The temperature at the equilibrium fits well for all three graphs. To reach acceptable results for post-test simulation, the values of the thermal conductivity, density of dry material, and the specific heat capacity have been changed (see Table 5).

The gap between measured and pre-test simulation results of relative humidity is large. The relative humidity cannot gain the speed to increase the rate of change neither at the beginning nor during the rest of the pre-test simulation. The post-test simulation and measured relative humidity fit well and both are stabilizing around 83 % and 80.7 %. To reach acceptable results for post-test simulations, the water vapour diffusion resistance factor, the liquid water conductivity at effective saturation, water uptake coefficient and initial relative humidity of the brick and mortar have been changed (see Table 5).
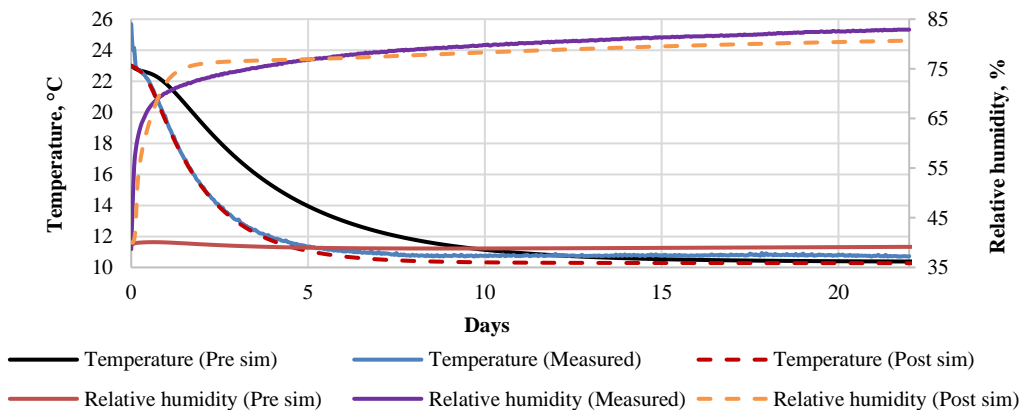

Fig. 11. Behaviour of temperature and relative humidity between masonry and mineral wool with vapour barrier ($s_d = 12$ m) insulation layer: simulation before and after experiment, and measured results.

37

5. DISCUSSION AND CONCLUSIONS

The goal of this research is to link hygrothermal simulation results with experimental results for internally insulated historic brick masonry to assess correlation between simulated and measured data as well as the most influential parameters.

We found the disagreement between measured and simulated hygrothermal performance of studied constructions. Test results showed that the relative humidity growth rate is high during the first test days for all materials and is slowing down when approaching equilibrium conditions. The temperature is decreasing at a slightly lower rate than relative humidity and is reaching equilibrium in about 5 days. The pre-test simulation showed a much lower growth rate of relative humidity and decrease rate for temperature compared to measured behaviour.

The parametric analysis that was carried out showed the most influential parameters on the hygrothermal behaviour of the whole construction. Parameters of all three insulation materials were adjusted to values supplied by material producers: thermal conductivity was increased by 8 % for EPS and reduced for mineral wool by 10 % and wood fiber by 10 %. Density was reduced for all three insulation materials to: mineral wool 24 %, wood fiber 67 % and EPS 41 %, and water vapour diffusion resistance factor which was reduced for wood fiber by 30 % and EPS by 69 %.

To reach acceptable results, thermal behaviour was changed by increasing thermal conductivity of bricks by 20 % while reducing for mortar by 38 %. Specific heat capacity was reduced significantly for both bricks (55 %) and mortar (38 %).

The highest influence on moisture transport growth rate has initial relative humidity of materials: it was increased by 62 % for bricks and 112 % for mortar compared to pre-test simulation values. Masonry was dried out for 10 days prior to tests and it was too short a period of time to dry it out, so the moisture level was still higher at the beginning of tests than predicted during pre-test simulation. Other parameters that have impact on the moisture transport are liquid water conductivity at effective saturation and it was increased by 24 % for bricks and mortar, and consequently water uptake coefficient has increased for bricks by 11 % and 486 % for mortar. Effective saturation was increased for about 111 % for bricks and reduced 55 % for mortar.

Material parameters as well as initial conditions of materials play an important role in the simulation but the latter is more influential in respect to material parameters.

Test results showed that under steady state conditions of an average outdoor climate of cold climate the highest relative humidity is reached by mineral wool (82.9 %), followed by wood fiber without vapour barrier (80.5 %), EPS (79 %), aerogel with vapour barrier (78.2 %), aerogel without vapour barrier (73.3 %) and wood fiber with vapour barrier (72.7 %). The temperature between the masonry wall and all insulation materials has stabilized on average at +10 °C.

Condensate tolerating wood fiber with vapour barrier reached 72.7 % relative humidity and 80.5 % in wood fiber without vapour barrier. Condensate limiting systems: EPS reached 79 % and mineral wool with vapour barrier reached 82.9 % relative humidity. In other insulation systems relative humidity has gone up to 73.3 % (aerogel without vapour barrier) and 78.2 % in aerogel with a vapour barrier.

There is no frost risk as relative humidity has not increased over 95 % which is the state when capillary saturation starts. This might change if outdoor boundary conditions are changed, e.g. wind driven rain and solar radiation is applied on the surface. However, there is a risk of mold

growth for insulation materials with biological origin such as wood fiber as it was detected during tests.

Considering all issues, our findings demonstrate that when internal insulation is applied to historic masonry in a cold climate, careful assessment of hygrothermal behaviour of combined historic masonry and insulation material wall construction has to be carried out. It is possible that simulation results will not conform precisely to actual measured data due to influence of values of initial moisture content of the wall as well as parameter value.

Future studies should include cyclic changes in boundary conditions, use of historic bricks and mortar with different properties.

ACKNOWLEDGEMENT

REFERENCES

[1] European Parliament and Council Directive 2010/31/EU on building energy efficiency. *The Official Journal of the European Union* 2010:153:13–35.

[2] Final energy consumption by end use in the EU-27. Available: www.eea.europa.eu/data-and-maps/indicators/energy-efficiency-and-energy-consumption-5/assessment/ [23.03.2017.]

[3] EU research project. RIBuild. Available: ribuild.eu [25.01.2018.]

[4] Miezis M., Zvaigznitis K., Stancioff N., Soeftestad L. Climate Change and Building Energy Efficiency – the key role of Residents. *Environmental and Climate Technologies* 2016. doi:10.1515/rtuect-2016-0004

[5] Ma Z., Cooper P., Daly D., Ledo L. Existing building retrofits: methodology and state-of-the-art. *Energy Build.* 2012:55:889–902. doi:10.1016/j.enbuild.2012.08.018

[6] Jerman M., Cerny R. Effect of moisture content on heat and moisture transport and storage properties of thermal insulation materials. *Energy Build.* 2012:53:39–46. doi:10.1016/j.enbuild.2012.07.002

[7] Zagorskas J., Paliulis G. M., Buriskiene M., Venckauskaite J., Rasmussen T. V. Energetic Refurbishment of Historic Brick Buildings: Problems and Opportunities. *Environmental and Climate Technologies* 2013. doi:10.2478/rtuect-2013-0012

[8] Purvins R., Biseniece E., Blumberga A. Laboratory investigation of Latvian historic brick and measurements of water movement in historic masonry walls. *Energy Procedia* 2017:113:327–332. doi:10.1016/j.egypro.2017.04.073

[9] Pasek J., Kesl P. Probabilistic assessment of failure risk of the building envelope thermally insulated from the inside. *Applied Mathematics and Computation* 2015:267:108–118. doi:10.1016/j.amc.2015.05.080

[10] Kass K., Blumberga A., Blumberga D., Zogla G., Kamenders A., Biseniece E. Pre-assessment method for historic building stock renovation evaluation. *Energy Procedia* 2017:113:346–353. doi:10.1016/j.egypro.2017.04.004

[11] *Delphin* software. Institute for Building Climatology. Available: www.bauklimatik-dresden.de/ [28.01.2018.]

[12] *WUFI* software. Fraunhofer institute for building physics. Available: wufi.de/de [28.01.2018.]

[13] Ibrahim M., Wurtz E., Biwole P. H., Achard P., Sallee H. (2014). Hygrothermal performance of exterior walls covered with aerogel-based insulating rendering. *Energy and Buildings*, 84: 241–251. doi:10.1016/j.enbuild.2014.07.039

[14] Haupl P., Fechner H. Hygric material properties of porous building materials. *Journal of Thermal Environment & Building Science* 2003:26(3):259–284. doi:10.1177/109719603032799

[15] Vereecken E., Roels S. A comparison of the hygric performance of interior insulation systems: A hot box–cold box experiment. *Building and Environment* 2014:80:37–44. doi:10.1016/j.enbuild.2014.04.033

[16] Pavlik Z., Cerny R. Experimental assessment of hygrothermal performance of an interior insulation system using a laboratory technique simulating on-site conditions. *Energy and Buildings* 2008:40:673–678. doi:10.1016/j.enbuild.2007.04.019

[17] Johansson P., Geving S., Hagentoft C.-E., Jelle B. P., Rognvik E., Kalagasidis A. S., Time B. Interior insulation retrofit of a historic brick wall using vacuum insulation panels: Hygrothermal numerical simulations and laboratory investigations. *Building and Environment* 2014:79:31–45. doi:10.1016/j.buildenv.2014.04.014

[18] Morelli M., Nielsen T. R., Scheffler G. A., Svendsen S. Internal Insulation of Masonry Walls with Wooden Floor Beams in Northern Humid Climate. ASHRAE, 2010.

[19] Biseniece E., Zogla G., Kamenders A., Purvins R., Kass K., Vanaga R., Blumberga A. Thermal performance of internally insulated historic brick building in cold climate: A long term case study. *Energy and Buildings* 2017:152:577–586. doi:10.1016/j.enbuild.2017.07.082

[20] Kloseiko P., Kalamees T., Arumargi E., Kallavus U. Hygrothermal Performance of a Massive Stone Wall with Interior Insulation: an In-Situ Study for Developing a Retrofit Measure. *Energy Procedia* 2015:78:195–200. doi:10.1016/j.egypro.2015.11.139

[21] Kloseiko P., Arumagi E., Kalamees T. Hygrothermal performance of internally insulated brick wall in cold climate: A case study in a historic school building. *Journal of Building Physics* 2015:38(5):444–464. doi:10.1177/1744259114532609

[22] Walker R., Pavia S. Thermal performance of a selection of insulation materials suitable for historic buildings. *Building and Environment* 2015:94:155–165. doi:10.1016/j.buildenv.2015.07.033

[23] Bianco L., Serra V., Fantucci S., Dutto M., Massolino M. Thermal insulating plaster as a solution for refurbishing historic building envelopes: First experimental results. *Energy and Buildings* 2015:95:86–91. doi:10.1016/j.enbuild.2014.11.016

[24] Galliano R., Ghazi Wakili K., Stahl T., Binder B., Daniotti B. Performance evaluation of aerogel-based and prelite-based prototyped insulations for internal thermal retrofitting: HMT model validation by monitoring at demo scale. *Energy and Buildings* 2016:126:275–286. doi:10.1016/j.enbuild.2016.05.021

[25] WTA Wissenschaftlich – Technische Arbeitsgemeinschaft für Bauwerkserhaltung und Denkmalpflege e.V. Innendämmung nach WTA I – Merkblatt 6-4: Planungsleitfaden. WTA Publications, 2014.

[26] DIN 4108-3:2014-11. Wärmeschutz und Energie-Einsparung in Gebäuden - Teil 3: Klimabedingter Feuchteschutz - Anforderungen, Berechnungsverfahren und Hinweise für Planung und Ausführung.

[27] EN 772-3:1998. Methods of test for masonry units. Determination of net volume and percentage of voids of clay masonry units by hydrostatic weighing.

[28] EN 772-13:2000. Methods of test for masonry units. Determination of net and gross dry density of masonry units (except for natural stone).

[29] Sedlbauer K., Krus M., Zillig W., Kunzel H. M. Mold growth prediction by computational simulation. Fraunhofer Institute for Building Physics, 2001.

[30] Viitanen H., Vinha J., Salminen K., Ojanen T., Peuhkuri R., Paajanen L., Lahdesmaki K. Moisture and bio-deterioration risk of building materials and structures. *Journal of Building Physics* 2010:33(3):201–224. doi:10.1177/1744259109343511

Edite Biseniece graduated from the Riga Technical University with professional bachelor degree in civil engineering and gained civil engineer qualification; in 2014 she obtained master degree in environmental engineering at Riga Technical University and at Vilnius Gediminas Technical University. In 2010 as an exchange student Edite studied in Technical University of Denmark.
Author has a background in civil engineering, and in environmental engineering. In 2012 she in master studies Edite has been focusing on indoor air quality and energy efficiency of renovated residential buildings. Work on residential building energy efficiency issues is continued in PhD studies.
ORCID: https://orcid.org/0000-0001-8301-2442
E-mail: edite.biseniece@rtu.lv

Ritvars Freimanis received B.sc. degree in Environmental Science at Environmental Science, Riga Technical University. His Bachelor thesis were about laboratory tests on internally insulated historic masonry walls. Now Ritvars continuous to study in Master program in Environmental Science.
Since 2017 he works as Scientific assistant at Institute of Environmental and Energy Systems in Riga Technical University, Riga. He is involved in EU research project *RIBuild* that develops guidelines on how to install thermal insulation on historic buildings.
E-mail: ritvars.freimanis_1@rtu.lv

40

Reinis Purvins received B.sc. degree in Environmental Science at Riga Technical University in 2016. Worked in Institute of Energy Systems and Environment from 2015–2017. His work in IESE was related to research projects such as EU research project *RIBuild*.
ORCID: https://orcid.org/0000-0001-5819-8601

Armands Gravelsins received Bachelor degree in Environmental Science at Riga Technical University in 2015. He received Master degree in Environmental Science by graduating both Riga Technical University and Vilnius Gediminas Technical University in 2017. Topic of the Master thesis was "Forest industry development towards bioeconomy: a system dynamics model". In 2017 he started Ph.D. studies in Riga Technical University.
Since 2014 Armands Gravelsins has been working at Institute of Energy Systems and Environment as a Researcher. He is an author of 11 scientific publications and conference papers indexed in SCOPUS and Web of Science, and a co-author of 3 scientific monographs. The main research areas are renewable energy, energy sector transition towards low carbon energy, bioeconomy, system dynamics modelling. In 2015 Armands Gravelsins received "Latvenergo" award for research in energy sector.
ORCID: https://orcid.org/0000-0002-4936-5233
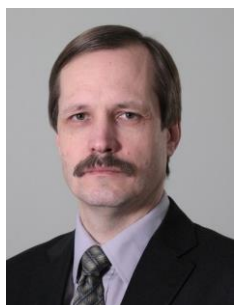
Aivars Pumpurs received a degree in electrical engineering from Riga Politechnical Institute in 1986. Since 2008 works at Department of Automatic electric drive in Riga Technical University as practical associate professor.
Author has worked in research projects regarding wind and hydrogen autonomous power system and energy efficiency.
ORCID: https://orcid.org/0000-0002-1593-8611
E-mail: Aivars.Pumpurs@rtu.lv

Andra Blumberga, Dr.sc.ing., professor, works for Institute of Energy Systems and Environments, Riga Technical university since 2001.
She has been working with energy efficiency since 1992. Her main research interest is energy efficiency both from technical and policy sides.
She has managed many national and international research and other projects since 1999, e.g. "Assessment on energy efficiency and use of renewable energy sources in Latvia by 2020", Climate Technology development modeling in energy sector", "Energy strategy 2030 for Latvia", "System Dynamics modeling for energy sector in Latvia".
She has been working as the World Bank energy expert for development of the Green Investment Scheme in Latvia. She is author of more than 80 publications and 14 monographs.
ORCID: https://orcid.org/0000-0002-4712-4794

Article

Hygrothermal Assessment of Insulation Systems for Internal Insulation of Solid Masonry Walls under Various Conditions

Ritvars Freimanis *[ID], Ruta Vanaga, Viesturs Balodis, Zigmars Zundans [ID] and Andra Blumberga [ID]

Institute of Energy Systems and Environment, Riga Technical University, LV1048 Riga, Latvia
* Correspondence: ritvars.freimanis@rtu.lv

Abstract: Energy efficiency renovation of building stock is an essential aspect of the climate change mitigation strategies in many countries. A large proportion of building stock is historical buildings. For this building stock, developing technology for safe internal insulation of external walls is crucial, preventing possible moisture damage to the building structures. Internal insulation is a risky technique as it has a high impact on the hygrothermal behavior of the wall. This study assesses the hygrothermal performance of massive masonry walls with 17 interior insulation systems exposed to different external boundary conditions, including a steady-state cycle, dynamic dry cycle, wind-driven cycle, and drying cycle. During the steady state cycle, the highest increase of moisture was observed under capillary active materials ranging from 39 to 119% increase in absolute moisture, with the exception of cellulose with an increase of only 7%. All the vapor-tight insulation systems showed no increase in absolute moisture during the steady-state cycle, with the exception being mineral wool in combination with a vapor barrier that showed a 30% increase in ablute humidity. In addition, relative moisture changes in masonry were measured. Results show that tested insulation systems exhibit similar thermal performance while having different moisture performance. Vapor-tight and vapor-open insulation systems exhibit different hygrothermal behavior under various test cycles depending on material vapor diffusion resistance. Numerical simulations are sensitive to the hygrothermal properties of materials.

Keywords: hygrothermal; DELPHIN; historical bricks; capillary-active; insulation

1. Introduction

The Sixth Assessment Report of the Intergovernmental Panel on Climate Change [1] urges the mitigation of climate change driven by anthropogenic impact. Many countries are committed to international climate mitigation goals and continually set new targets for GHG reduction in climate policy packages. Energy consumption in buildings accounts for 30% of total global final energy demand [2], and energy efficiency is essential to reduce the climate crisis.

Renovation of historic buildings is an essential aspect of the energy efficiency strategies in Europe [3]. Historic buildings are often located in historic centers of cities. They are facing various limitations for measures related to the reduction of thermal losses, e.g., heritage value of the facade and space limitation on the street for additional material layers on the exterior of the building. For this building stock, developing technology for safe internal insulation of external walls is crucial, preventing possible moisture damage to the building structures. This measure is a risky insulation technique as it has a high impact on the hygrothermal behavior of the wall, leading to the risk of mold growth, frost damage, and decay of embedded wooden beams [4,5].

When considering the application of internal insulation, hygrothermal evaluation is crucial. Detailed planning reduces the risk associated with changes in hygrothermal behavior [6,7]. Various factors must be considered during the planning, such as properties

of bricks in the original masonry, insulation materials, and outdoor and indoor boundary conditions.

Various studies have found that the hygrothermal properties of bricks are essential for the estimation of the impact of internal insulation; a single parameter is insufficient to estimate the hygrothermal impact of interior insulation, e.g., in a study [5], they found that the water absorption coefficient of a brick is not enough. The liquid water conductivity is more critical. A study by Johansson et al. (2014) [8] concluded that the thickness of the wall influences the moisture accumulation rate; the moisture content in the wall highly depends on the properties of the brick, and the drying rate depends on the mortar type.

Another vital factor is wind-driven rain [8–12]. Studies on the impact of the wind-driven rain load on the hygrothermal behavior of internally insulated wall show that under moderate rain protection, some insulation systems perform well at the normal indoor moisture load [13]. However, higher wind-driven loads have an influence on the magnitude of hygrothermal changes [5]. A study on a vapor-tight system showed that the rain load was the dominating factor determining the vapor and water transport in the wall and the relative humidity under insulation increased significantly during wind-driven rain [8]. Nielsen et al. (2012) stated that the effect of a vapor barrier and the thickness of the insulation is negligible, compared to wind-driven rain [14]. In vapor-open capillary active insulation systems, wind-driven rain can impact hygrothermal behavior by reducing thermal resistance or increasing indoor relative humidity [15]. High solar exposure on walls can contribute to drying [9]. However, it may cause inward solar-driven vapor flow.

A study [13] on the influence of indoor humidity on the performance of insulation systems showed that a high indoor moisture load can increase the risk of mold growth as it can lead to increased relative humidity behind calcium silicate and perlite insulation systems. For vapor-tight systems, a high risk of mold growth and interstitial condensation is predicted between masonry and the insulation and is mainly caused by outdoor boundary conditions [5].

Diffusion-open and diffusion-tight systems were compared in different studies [4,5,16–21]. When masonry is insulated internally, the moisture content in the masonry wall is higher for vapor-tight insulation materials [5]. Vereecken et al. (2014) [4] found that for the imposed quasi-steady-state winter condition, the increased stored moisture inside walls with a capillary active system is higher than for walls with a traditional vapor-tight system. The application of vapor-tight insulation materials prevents drying towards the inner surface [9,22]. Grunewald et al. (2006) [23] found that the moisture equilibrium of the original wall can reach up to three times higher moisture level when the moisture transport is driven by rain and evaporation. With calcium silicate insulation, the drying potential of the envelope walls is kept.

Vapor-open capillary active systems reduce the original wall's drying rate by allowing inward drying and buffer interstitial condensation. In capillary active systems, the temperature and vapor gradient induce an outward vapor transfer during the heating season. They have a high buffering potential and a large liquid conductivity in the capillary moisture range and can absorb the liquid water and redistribute it toward the room by a liquid flow that follows the inward capillary pressure gradient [24]. It is essential to ensure good contact between the masonry and insulation material since this guarantees that no interstitial condensations occur at the warm side of masonry and the capillary active material can redistribute it [25]. Other studies show that the relative humidity below insulation material can reach a high level [5,26,27]. Vereecken et al. (2016) [25] found that capillary active materials have disadvantages, such as the moisture storage having an adverse impact on the thermal performance, and the buffered moisture transported toward the room possibly affecting indoor relative humidity. Most bio-based materials such as grass, date palm wood, Alfa plant, straw, cork, hemp, and plant concrete are vapor-open capillary active because they are hygroscopic. However, they have a heterogeneous composition, which limits the assessment of their thermophysical properties [28]. Vegetal materials are more hygroscopic and their thermal performance is more sensitive to moisture accumulation [7]. In other natural-based materials, such as cork, the moisture transport phenomenon is limited to

the first layers of the expanded cork [29]. Analysis carried out by [30] showed that saw and wool exhibit dynamic response to hygrothermal changes to qualify as moisture buffers. The quantity of moisture accumulated is material-specific and dependent on the relative humidity and the temperature of the environment and by controlling these values, it is possible to accurately track the adsorption/desorption characteristics of bio-based materials [30]. Experimental data indicate that biotic and chemically hydrophilic (e.g., cellulosic) materials (wood, organic fibers, starches, earth and clay plasters, and plant derivatives) exhibit higher moisture buffer values than porous, abiotic (e.g., cementitious) materials (concretes, bricks, and gypsum, and other inorganics) [31].

When vapor-tight insulation systems are installed on the interior side of the wall, the drying capacity inwards is substantially reduced and the relative humidity in the wall increases substantially when exposed to driving rain [8]. Compared to the capillary active systems that are sensitive to small modifications of the wall structure (e.g., interior finishing coat, wall thickness), the hygrothermal behavior in vapor-tight systems exhibits minor differences [15]. Kloseiko et al. (2022) found that the vapor open solutions have lower frost damage and mold growth risks than the vapor-tight systems [32]. Hygrothermal behavior during winter conditions shows that if a capillary active system has risks of interstitial condensation due to high level of an accumulated moisture content in the wall and the glue mortar, a vapor-tight system is preferable [4]. Antolinc et al. (2021) found that in a room with very high indoor relative humidity, the capillary active interior insulation is not a suitable solution for improving the thermal insulation of buildings in a cold continental climate and vapor-tight insulation needs to be applied [33]. However, moist indoor air can diffuse outwards into the masonry due to mechanical damage to the vapor barrier or poor craftsmanship [34].

Many studies on the hygrothermal behavior of internal insulation are limited to pure simulation experiments, laboratory experiments in steady-state conditions, or in situ measurements in specific cases. Each of them faces limitations. Material properties are taken from the material database in simulation experiments, assuming perfect installation. Laboratory experiments with steady-state conditions do not account for the dynamics of real-world structures. In situ measurements are case-specific and general conclusions that can be applied to other cases and cannot be withdrawn. Various studies have obtained more evidence that wind-driven rain is a vital factor influencing the hygrothermal behavior of internally insulated walls, and other factors are less important. Insulation systems' laboratory and in situ tests are diverse with various boundary conditions, thicknesses, vapor barriers, heterogenous bricks, plasters, etc., and are difficult to compare. Simulations differ from measured data because they assume perfect installation and face uncertainty of parameter values and initial values. Many insulation systems have specific demands for installation quality, and if not correctly executed (e.g., vapor barriers, adhesive glue), it affects hygrothermal behavior. The application of biobased insulation materials as internal insulation is still uncertain due to hygrothermal behavior and failure modes related to mold growth.

This study will address these limitations by:

- Investigating the impact of dynamic outdoor climate on the internal insulation of solid masonry walls in a controlled environment
- Testing selected insulation systems and comparing them in the same boundary conditions
- Eliminating the impact of various bricks with heterogenous properties by applying commercially produced bricks
- Experimenting with internally insulated masonry walls with U-value as similar as possible (only limited by the material installation specifics)
- Eliminating the impact of external plaster by not applying it
- Assessing the effect of installation quality on the hygrothermal performance of the wall (various vapor barriers, adhesive glue)
- Using bio-based insulation materials.

This study aims to answer the following research question: What is the hygrothermal performance of a solid brick wall with various interior insulation systems with different moisture diffusion prevention levels under varying external boundary conditions?

The paper starts with a comprehensive literature analysis to define knowledge gaps in the research field of applying internal insulation on massive masonry walls. It is followed by describing tested materials and systems and applied methodology, including material characterization, experimental setup, and testing procedures for the laboratory and numerical experiments. The analysis of results from different test round results is presented, followed by conclusions.

2. Materials and Methods

2.1. Material Characterization

Eighteen insulation systems underwent testing across two rounds. These systems combined various insulation materials with or without vapor barriers and binders, some following manufacturer instructions (e.g., mineral wool with vapor barrier, EPS, XPS, PIR with Sika cement and glass fiber net, cork, expanded cork, aerogel blanket) and others intentionally deviating to assess hygrothermal behavior (e.g., vapor-open materials without vapor barriers such as rock wool, expanded clay, cellulose, various wood fiber plates, and planing chips plates without external finishes). Insulation materials came from diverse sources and included both vapor-tight and vapor-open options. Gypsum plaster results were excluded due to sensor failure. The tested insulation systems encompassed inorganic mineral-derived materials (mineral wool with vapor barrier, rock wool, expanded clay, gypsum plaster, aerogel blanket), organic fossil fuel-derived materials (EPS, XPS, PIR with various coverings, VIP), and organic plants/animal-derived materials (cellulose, wood fiber plates with different densities, cork, expanded cork, planing chips plates). An overview of insulation materials, finishing, and mounting technologies is provided in Appendix A Table A1. Material properties were obtained from the manufacturer's technical data sheets or directly contacting manufacturers. The information available was on the material's thermal properties, such as the thermal conductivity λ, but other parameters, such as the specific heat or the vapor resistance, were missing from the technical data sheets of some products.

Vapor-open insulation systems are designed to allow the passage of water vapor. They have a higher permeability to moisture, which means that water vapor can move relatively freely through these materials. These systems are often used when moisture needs to be managed and allowed to escape from the building envelope. They can help prevent moisture buildup and related problems such as condensation and mold growth. These insulation systems are condensate-tolerating insulation systems where the material itself gives the only vapor resistance in these insulation systems; therefore, they have very small vapor diffusion resistances (sd value < 0.5 m) [35]. Materials such as cellulose insulation, some types of wood fiberboard, and certain natural insulation materials are vapor-open. On the other hand, vapor-tight insulation systems are designed to block the passage of water vapor. They have low permeability to moisture, which means they resist the movement of water vapor. Vapor-tight systems are used to create a moisture barrier, often when preventing moisture from entering or leaving a particular area is essential. They help maintain controlled indoor humidity and temperature levels. They can be distinguished as condensate-preventing systems that disable vapor transfer from the room side into the construction by a vapor barrier (min sd value 1500 m), and condensate-limiting insulation systems include a vapor barrier with an sd-value of min. 0.5 m and max. 1500 m [35]. Materials such as extruded polystyrene (XPS) and foil-faced insulation boards are vapor-tight. In summary, vapor-open insulation systems allow water vapor to pass through, making them suitable for applications where moisture management and breathability are needed. On the other hand, vapor-tight insulation systems act as barriers to moisture, ideal for maintaining controlled indoor conditions and preventing moisture

intrusion. The choice between these systems depends on specific building requirements and environmental conditions.

In Appendix A Table A1, all materials and systems tested in this study are defined based on vapor tightness.

2.2. Experimental Setup and Testing Procedures

Two climate chambers (hot-box for indoor climate and cold-box for outdoor climate) were used to test insulation systems in a controlled environment (see Figure 1).
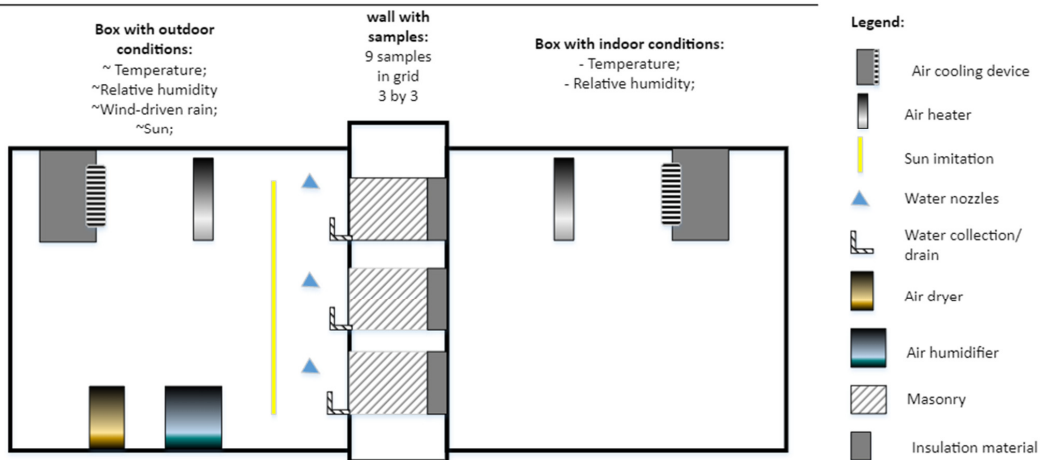

Figure 1. Testing setup for testing insulation systems in controlled environment.

The setup consisted of a test wall built from EPS (Figure 2). The wall had nine samples of single-leaf masonry wall (40 cm wide, 30 cm high, 25 cm deep each). Two test walls were built—each for one test round.
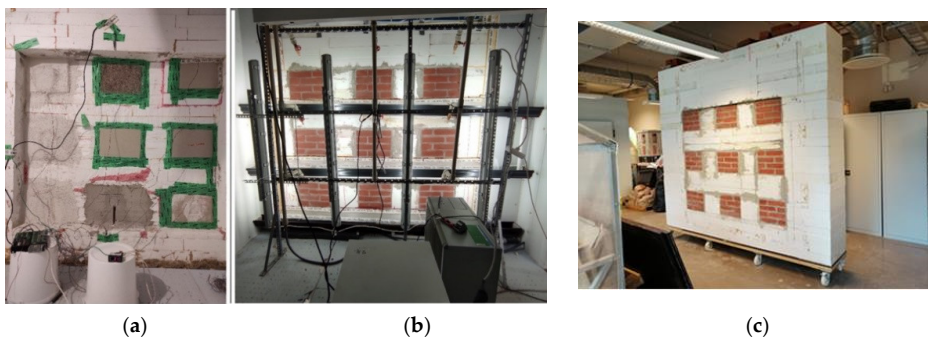

(**a**)   (**b**)   (**c**)

Figure 2. Test wall constructed for the laboratory experiment: (**a**) test wall from the hot-box side; (**b**) test wall from the cold box side; (**c**) test wall before insertion between hot-box and cold-box.

The test wall was installed between hot-box and cold-box climate chambers. The cold box simulates outdoor conditions by dynamically controlling the chamber's temperature, relative humidity, wind-driven rain, and solar radiation. Hot-box refers to indoor conditions; this chamber maintained a constant microclimate, maintaining constant relative

humidity and temperature. The cold-box chamber was equipped with a water spraying and collecting system on the outside side of the structure to replicate the effects of wind-driven rain (when rain is affected by wind, a large amount of water impacts vertical surfaces). The system consisted of 9 nozzles, one for each wall sample, a pump, plastic pipes for the water distribution system, and a water collection system (see Figure 2b). Solar radiation simulation lamps simulated exposure to the sun.

Each insulation system was attached to a single-leaf masonry sample built from industrially produced new bricks. New bricks were used to reduce the impact of uncertainty of material properties. Before starting the measurements, a conditioning period in the room condition was kept for the wall specimens to dry out. Figure 3 provides a simplified 2D model of the masonry sample in a cross-section from indoors to outdoors.
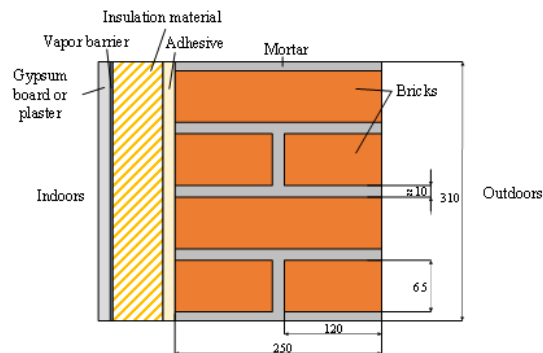

Figure 3. Two-dimensional model of the masonry sample (all measurements in mm).

Parameter values for the cold-box for all cycles were based on the weather data from 2014 to 2018 to mimic outdoor environmental conditions. They were obtained from the public observation database [36]. The decisive criterion for choosing the month for modeling the temperature fluctuation cycle was the highest amplitude of the daily temperature fluctuations. After the analysis, it was decided to model the temperature and relative humidity fluctuations according to the situation in May. Another critical selection criterion for the month was solar radiation on a vertical surface. The daily average hourly radiation profile for May was obtained. The average maximum amount of solar radiation was determined to be 607 W/m^2. On the south-facing wall, the maximum solar radiation was 432 W/m^2, and the total radiation received was 4037 Wh/day. With a constant solar simulator power (rounded to 450 W/m^2), the solar simulator should be operated for approximately 8 h daily to reach 4037 Wh/day. In addition to temperature, relative humidity, and solar radiation data, horizontal precipitation data were also analyzed. The average amount of precipitation over the days in May considered was 10.1 mm. Since the intensity of wind-driven rain depends heavily on wind speed, horizontal rainfall, and direction, it is impossible to provide 100% reality-imitating dynamic conditions affected by all these factors in the laboratory. Therefore, following an analysis of the amount of rainfall, it was decided to use a different approach to assess the flow of wind-blown rain on the wall. The estimated wind rain flow was estimated to be 0.278 l/(m^2 s). This amount of water was sprayed on the cold side of the wall for five minutes a day for two weeks during the rainy cycle of the test.

Eighteen insulation systems were tested in two rounds: 9 systems per round. The cycles were developed based on technical options, previous studies' experience, and weather data analysis. The experimental plan was based on the following conditions in chambers:

- Hot-box chamber temperature +20 °C, relative humidity 50%.
- old-box chamber temperature at the steady state conditions +10 °C and relative humidity 50%. For dynamic cycles, temperature and relative humidity followed outdoor

daily fluctuations in May (see Figure 4). Wind-driven rain was 0.278 l/m^2 s (5 min every day) and solar radiation 300 W/m^2 (8 h per day)
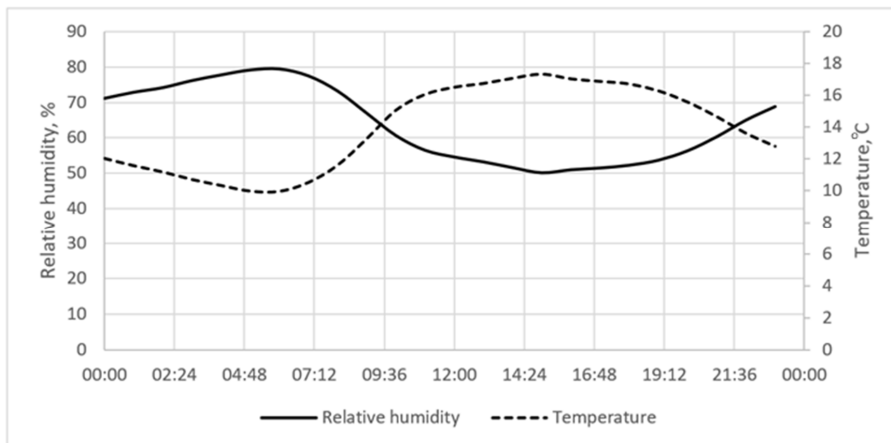

Figure 4. Daily fluctuations in relative humidity and temperature.

The relative humidity between the insulation layer and the masonry was measured using Honeywell HIH-4000 series humidity sensors. Humidity sensors were installed under the insulation layer together with K-type thermocouples. The sensors in each sample measured the conditions between the insulation layer and the masonry wall where there is a significant risk of condensation. The Campbell Scientific CR1000 data logger recorded the data on a computer. In addition to the measurements of relative humidity and temperature under the insulation, measurements of masonry humidity were performed with non-invasive measurement methods (dielectric and microwave probe). Non-invasive moisture measurements were taken before and after each test cycle, five times during the test. Trotec T3000 (Trotect GmbH, Heinsberg, Germany) was used for measurements. A microwave probe was used to measure moisture at a depth of 20 cm, and a dielectric probe was used to measure moisture at a depth of 2 cm.

2.3. Numerical Simulation

The simulations for the insulation systems from the first test round steady state conditions were carried out in the DELPHIN software by using similar materials from the existing material database. The materials were selected based on the specifications, which are provided by the manufacturers for the original materials used in the laboratory experiment. These simulations were carried out both according to the variable outdoor climate conditions as well as for constant conditions to obtain data and compare it to the measurement data acquired from the laboratory experiment. The initial temperature and relative humidity conditions of the simulations were set to comply with the ones measured at the beginning of the experiment and the outdoor relative humidity was increased to 93% to match the conditions maintained in the climate chamber. The time step for the simulations was set to 1 h. Each insulation system was also modeled in the DELPHIN 6 software (see Figure 5). The overview of insulation materials is given in Appendix A Table A2. A DELPHIN file was created for the hygrothermal properties of bricks used in the test walls. Material tests were performed at the laboratory and test results are presented in Appendix A Table A3.

(**a**)	(**b**)
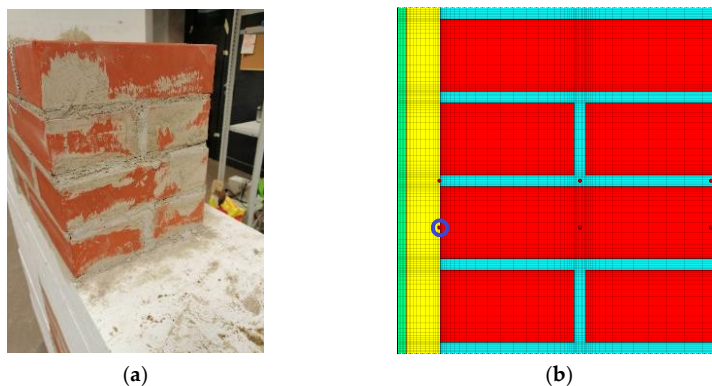
Figure 5. Test wall brick sample in laboratory (**a**) and in DELPHIN model (**b**). The data for further analysis were taken from the point circled in blue; (red-brick; yellow-insulation; green-plasterboard; blue-mortar; red dots-data points).

3. Results and Discussion

The first test round started with the first steady-state test for two weeks to gather data for numerical simulation. After that, the test wall was conditioned for 12 weeks in a room environment. That was followed by four cycles with various conditions. The second test round was designed differently from the first to better distinguish the impact of individual dynamic processes on measurement results, which is essential for drawing more accurate conclusions.

In all tests, temperature and relative humidity measurements between the insulation material and masonry look noisy. This is due to conditions in both climate chambers. This noise is in response to periodic fluctuations of air conditioning equipment working cycles (heater, humidifier, dehumidifier, refrigerator), and temperature and relative humidity oscillates in an amplitude of 1 °C. Both test rounds were carried out during the COVID-19 period, and laboratory access restrictions impacted the laboratory team's ability to react to issues related to malfunctioning air conditioning equipment in both chambers.

Two test rounds with various test conditions were carried out to simulate steady and unsteady/transient conditions. The first test round started with the steady-state conditions to be used as an experimental basis for numerical simulations with eight insulation systems (insulation systems (1–8) from Appendix A Table A1). Twelve weeks after the first steady-state test, the second steady-state test started, followed by dynamic conditions, wind-driven rain, and drying condition. Figure 6 presents measured cold- and hot-box temperatures and relative humidity during the first test round for each test cycle. Due to a malfunction of the data logger, cold-box temperature and relative humidity were not logged during the steady-state cycle.

Figure 7 presents the measured temperature between insulation material and masonry for tested insulation systems during the first test round. Oscillations followed temperature dynamics in the cold box. The temperature in all insulation systems followed the same trend. However, the temperature reached various levels.

Figure 8 illustrates the measured relative humidity between insulation material and masonry for tested insulation systems during the first test round. The relative humidity in each insulation system exhibited different behavior in terms of amplitude and value. The oscillation amplitude was determined by temperature changes in the cold-box relative to the hot-box temperature and the hygrothermal properties of the insulation system. The overall relative humidity trend followed the relative humidity in the hot-box based on the hygrothermal properties of the insulation system.
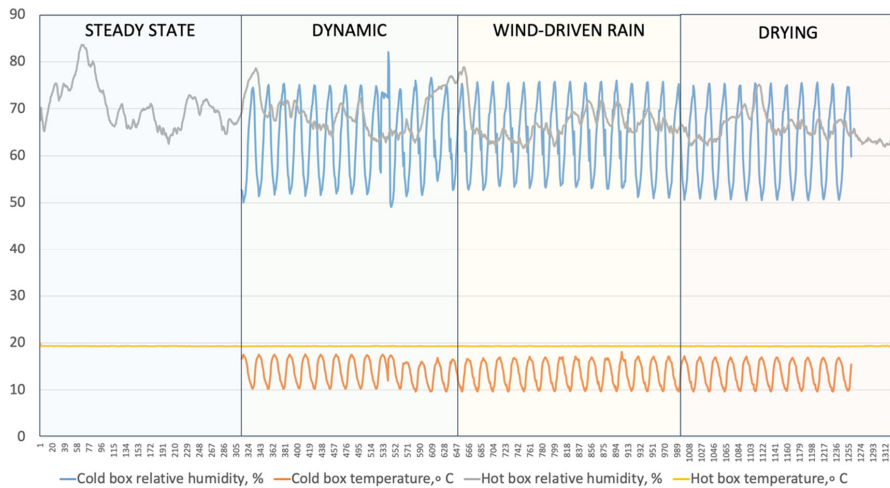
Figure 6. Measured cold- and hot-box temperature and relative humidity during the first test round.
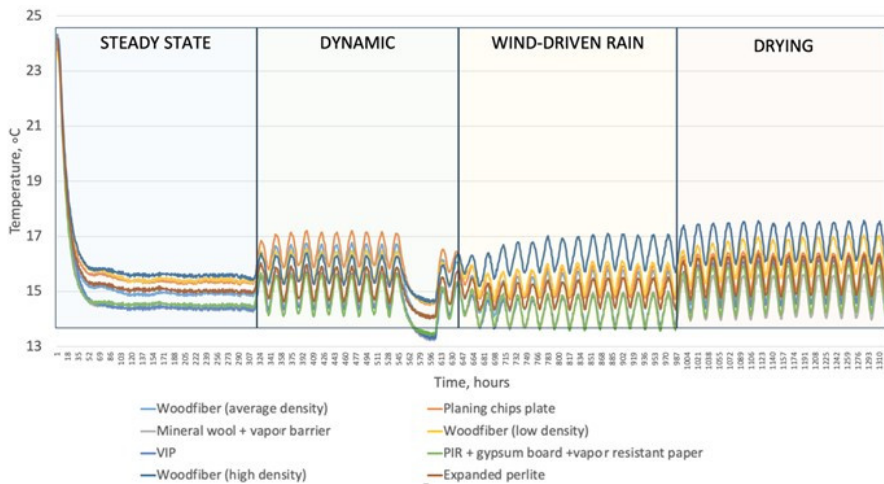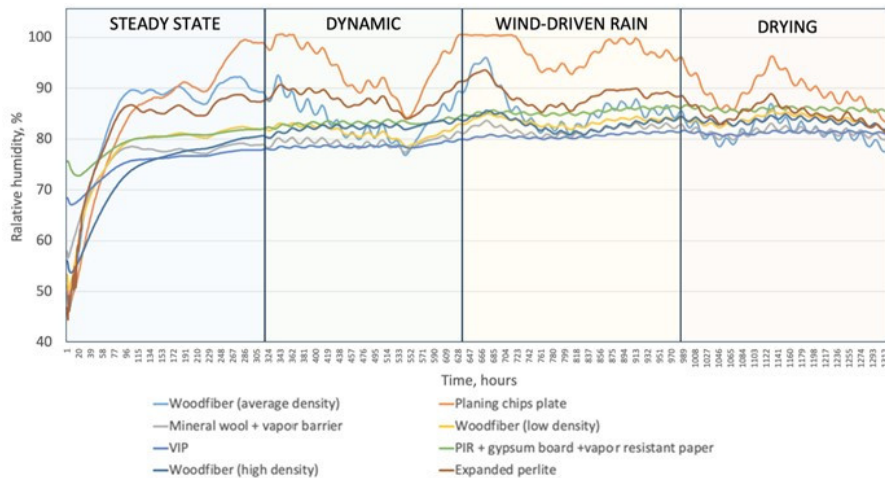

Figure 7. Measured temperature between insulation material and masonry for tested insulation systems during the first test round.

Figure 9 presents the results of non-invasive moisture measurements for all cycles. Measurements were carried out to determine relative changes in moisture at 2 cm depth and 20 cm depth from the exterior surface of the masonry (5 cm from the internal surface of the masonry). The change in moisture value relative to initial moisture at a 2 cm depth (Figure 9a) revealed that after two weeks of steady-state conditions, all insulation systems were in the range of ±10% change in moisture level. After two weeks of dynamic dry cycle, all masonry wall samples had an increase in moisture from 0% to 18% compared to initial conditions. An increase of 78% to 108% was obtained for masonry moisture change after a dynamic wind-driven cycle compared to initial conditions. Finally, initial moisture increased by 38% to 65% after a dynamic drying cycle. The amplitude of the change in the moisture at the depth of 20 cm (Figure 9b) was less than the 2 cm depth. The shift in moisture after steady-state conditions was between +3% and −20% relative to initial

conditions. After the dynamic dry cycle, changes in moisture were in the range of −8% to +10%. The highest changes occurred after a dynamic wind-driven cycle (5% to 60%). Finally, the dynamic drying cycle reduced the gap between initial moisture and actual to the range of −7% to 38%.

Figure 8. Measured relative humidity between insulation material and masonry for tested insulation systems during the first test round.
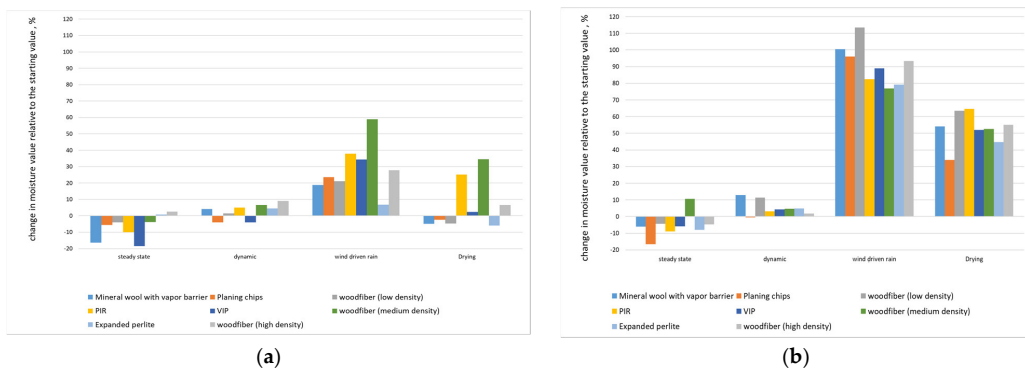
Figure 9. Change in moisture value relative to initial moisture at a depth (from the external surface of the masonry) of (**a**) 2 cm and (**b**) 20 cm.

The second test round with nine insulation systems (insulation systems (9–18) from Appendix A Table A1) started with steady-state conditions, followed by dynamic conditions, drying conditions, and wind-driven rain for spring conditions. Measured cold- and hot-box temperature and relative humidity during the second test round are presented in Figure 10.
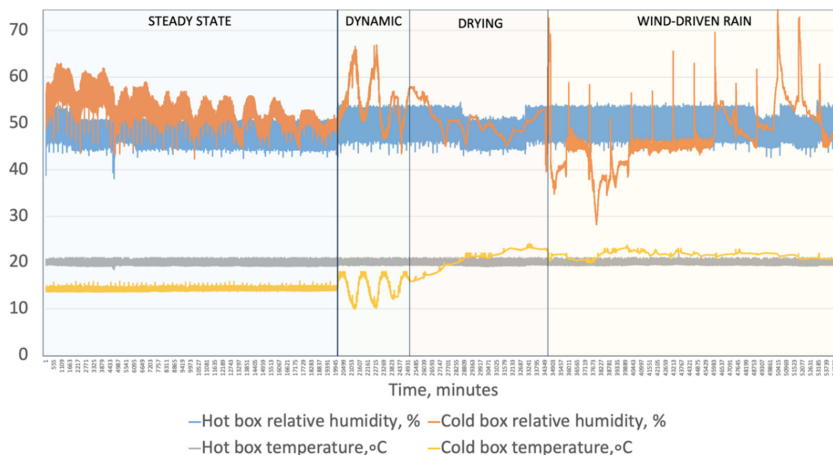
Figure 10. Measured cold- and hot-box temperature and relative humidity during the second test round.

Figure 11 presents the measured temperature between insulation material and masonry for tested insulation systems during the second test round. Similar to the first test round, the temperature in all insulation systems followed the cold-box temperature, and insulation systems exhibited various levels.

Figure 11. Measured temperature between insulation material and masonry for tested insulation systems during the second test round.

The measured relative humidity between insulation material and masonry for tested insulation systems during the second test round is presented in Figure 12. Similar to the first test round, relative humidity exhibited very different behavior for insulation systems, and it mainly depended on the vapor diffusion resistance of the insulation system.
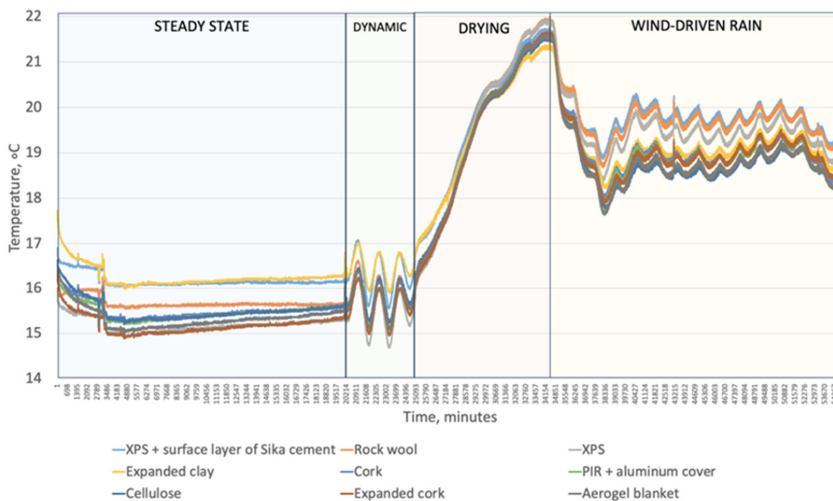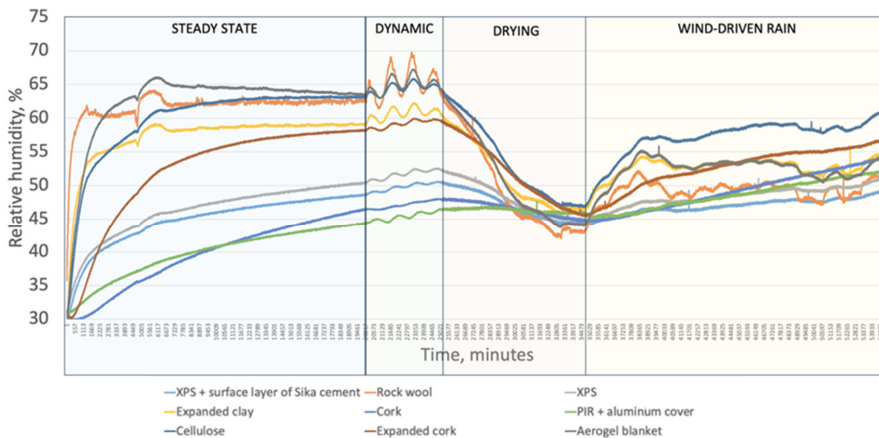
Figure 12. Measured relative humidity between insulation material and masonry for tested insulation systems during the second test round.

Measurements made with a dielectric probe at a depth of 2 cm maintained a relatively small dispersion after steady-state conditions (±5%). The same distribution was observed after the dynamic cycle. A significant increase in moisture changes was measured after a wind-driven rain cycle, ranging from 175% (XPS with the surface layer of Sika cement) to 215% (for PIR + aluminum cover). The average increase in moisture after a wind-driven rain cycle compared to initial conditions was 198%. In contrast to measurements at a depth of 2 cm, the dispersion between masonry samples was greater. After the first two weeks of constant conditions, moisture values in 20 cm depth in masonry samples begin to differ from +9% to −25% compared to initial conditions. The distribution of changes was the same after the dynamic cycle. After a wind-driven rain cycle, all masonry samples exhibited an increase in moisture level in the 10 to 35% range. Results are showed in Figure 13.
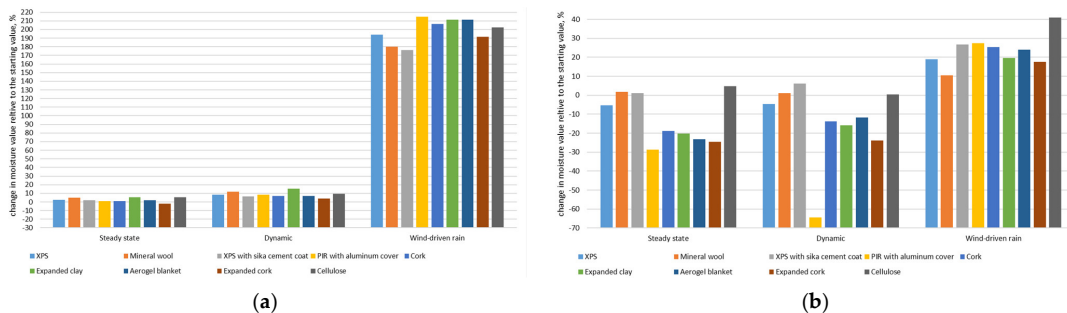
Figure 13. Change in moisture value relative to start moisture at a depth (from the external surface of the masonry) of (**a**) 2 cm and (**b**) 20 cm for the second test round.

3.1. Steady-State Conditions

- The first test round

Figure 14 shows the measured temperature and relative humidity profiles in hot- and cold-boxes during the first test of steady-state conditions. Relative humidity dropped in the hot-box from hours 49 to 150 due to the malfunctioning of the humidifier.
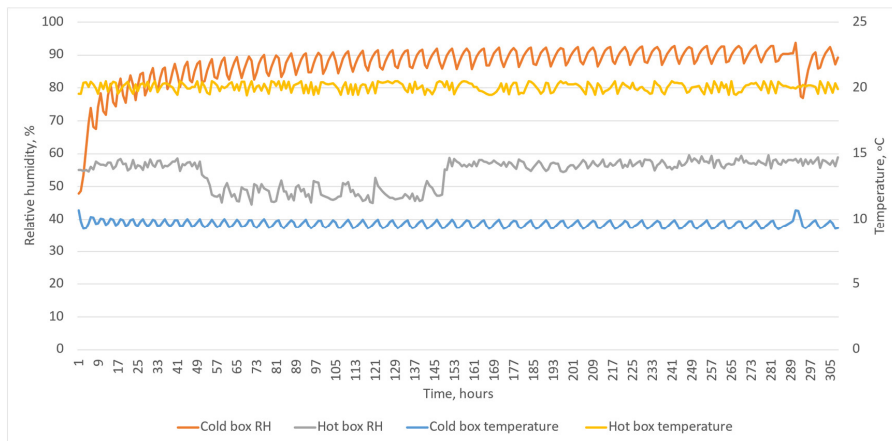
Figure 14. Measured temperature and relative humidity in hot- and cold-boxes during steady state conditions.

The measured and simulated temperature behavior for eight insulation systems tested in the first test round showed that the temperature rate of change was high at the beginning and reached steady-state conditions after approximately 72 h.

Figure 15 shows the zoomed-in measured (M) and simulated (S) temperature behavior between masonry and vapor-open insulation systems in the steady-state cycle. The highest temperature was measured behind vapor-open systems, while the lowest temperatures were reached in vapor-tight systems. For all insulation systems, the measured temperatures exceeded simulated temperatures and varied from 1 to 1.2 °C. For vapor-open systems, temperature stabilized at about +14 °C between masonry and planing chips plate, followed by high-density wood fiber and low-density wood fiber because their relatively low thermal resistance allows more heat flow from the hot-box. The temperature reached +13 °C for insulation systems with average-density wood fiber and expanded perlite. The simulated temperature behavior between these layers was also similar. However, the arrangement of the materials was slightly different. Similar to measurements, the lowest temperature was achieved by the mineral wool with a vapor barrier, followed by expanded perlite and average-density wood fiber. Moreover, the stabilization of temperatures was predicted to be at a slightly different range—from +12 to 13 °C. Vapor-tight insulation systems (PIR with gypsum board and vapor-resistant paper, VIP and mineral wool with vapor barrier) stabilized at lower temperatures than vapor-open systems.

The measured and simulated behavior of relative humidity between masonry and vapor-open insulation systems are illustrated in Figure 16. The internal side of the existing wall structure experienced reduced temperatures, resulting in the higher relative humidity levels between the wall and insulation system. The temperatures reached steady-state conditions after approximately 72 h while relative humidity still had not reached equilibrium after 13 days except for planing chips plate. The relative humidity increased faster for the vapor-open materials due to the vapor-open characteristic of these insulation systems. All vapor-open systems experienced a much higher increase of relative humidity at the beginning of the measurement compared to simulation. They also reached higher relative humidity levels compared to simulation results. The planing chips plate had the highest increase rate of relative humidity behind the masonry and reached equilibrium at 100% in 30 h. This is due to large and open pores, low vapor diffusion resistance, and lack of finishing material. In simulation, planing chips plate behavior is different: the trend increased at a slower rate and it did not reach 100% relative humidity. This material is suggested to be used as an internal finish because of its decorative nature. However, the application of this material without vapor barrier under the high indoor moisture load can result in mold

growth behind the insulation system. Average density wood fiber had the second highest relative humidity level and simulated behavior differed from measured. The third and fourth materials with the highest relative humidity were expanded perlite and low-density wood fiber. All these materials had low vapor diffusion resistance. The slowest increase of the relative humidity was observed for high-density wood fiber. The main reason for the discrepancy between measured and simulated behavior can be variations in material properties values in real material and simulation.
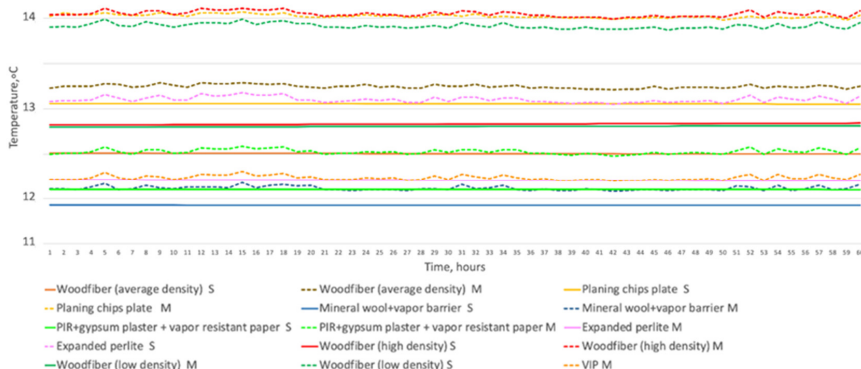
Figure 15. Measured (M) and simulated (S) behavior of temperature between masonry and vapor-open insulation systems in the steady state cycle (zoomed-in hours 245 to 305).
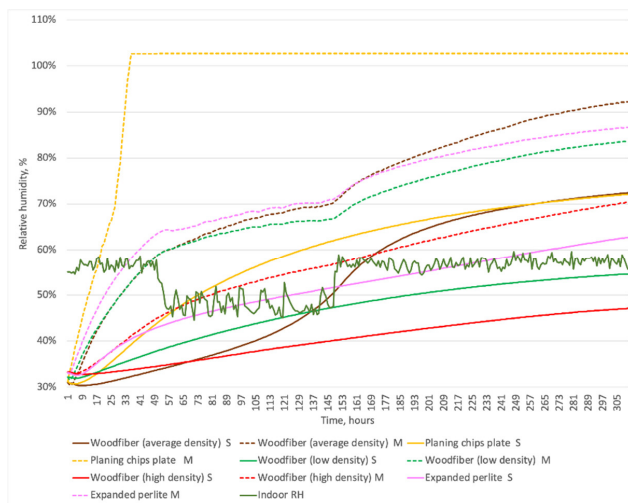
Figure 16. Measured (M) and simulated (S) behavior of relative humidity between masonry and vapor-open insulation systems.

The measured and simulated behavior of relative humidity between masonry and vapor-tight insulation systems (Figure 17) showed that measured and simulated trends were similar, but the values differed. The main cause might be the discrepancy in values of hygrothermal properties for actual materials and simulation. Mineral wool with a barrier exhibited similar behavior to vapor-open systems. This might be due to the low vapor resistance of the vapor barrier. The slowest increase in relative humidity was observed for the insulation systems with VIP, high-density wood fiber, and PIR with gypsum board and

vapor-resistant paper, which had the lowest increase in relative humidity. PIR with gypsum board and vapor-resistant paper exhibited the lowest growth of relative humidity on both simulations and measurements in the test stand. There is no risk of condensation behind any of these insulation systems. The hygrothermal behavior of VIP was not simulated due to a lack of material with similar properties in the DELPHIN database.
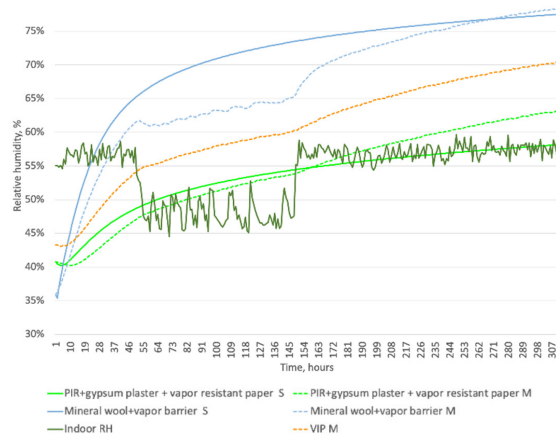
Figure 17. Measured (M) and simulated (S) behavior of relative humidity between masonry and vapor-tight insulation systems.

Figure 18 illustrates that vapor-open systems were sensitive to changes in indoor relative humidity when the cold-box temperature was stable. When indoor relative humidity fell between time 40 and 82 (Figure 18a), vapor-open materials with low Sd values (expanded perlite, average and low-density wood fibers) mimicked this behavior with an average time lag of one hour but with different trends. Vapor-tight mineral wool also mimicked it. This might be explained by the vapor barrier's low Sd value (7). Materials with higher Sd values did not imitate this behavior (VIP, high-density wood fiber, PIR with gypsum board, and vapor-resistant paper). The same reaction of insulation systems was observed when the hot-box relative humidity increased (Figure 18b). In both situations, mineral wool followed the trend closer than other materials, which might be explained by the limited moisture buffering capacity for this type of insulation, in contrast to the capillary active materials. The behavior of other materials followed the trend to a lesser extent because they have excellent MBV.

(**a**)

(**b**)
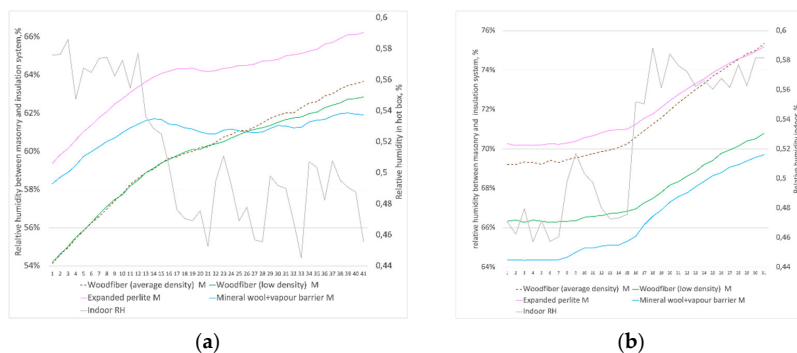
Figure 18. Behavior of vapor-open when hot box relative humidity (**a**) decreases (time 40–82 in Figure 17) and (**b**) increases (time 145–177 in Figure 17).

- The second test round

  Nine insulation systems were tested in the second test round. The vapor-open insulation systems were aerogel blanket, cellulose, and stone wool (without vapor barrier). The vapor-tight insulation systems were PIR with aluminum cover on both sides, expanded cork, cork, XPS with Sika cement layer, and XPS.

  Figure 19 shows the temperatures that reached steady-state conditions after approximately 58 h. Temperatures below each material gradually decreased and stabilized between 15.3 C and 16.3 °C (the values were higher than the first test round due to higher temperature in the cold-box). The lowest temperatures reached XPS and expanded cork, coinciding with the measured U-values at the laboratory. PIR with aluminum cover measured U-value coincided with the U-value of an expanded cork. Still, when comparing temperatures below these insulations, the temperature below the PIR with aluminum cover was on the same level as the cellulose, whose U-value was 0.07 W/m^{2}K higher. However, as these temperature differences were less than half a degree and fell within the error limits of temperature sensors, such small shifts were possible. Accordingly, expanded clay and XPS with the Sika cement layer, which had the highest U-values, also had the highest temperatures below these materials.

Figure 19. Temperature under insulation in steady state conditions for the second test round.

The relative humidity between masonry and insulation materials reached equilibrium after seven days for vapor-open materials, while others did not reach steady-state conditions even after 14 days (Figure 20).

The relative humidity level increased at a higher rate in vapor-open systems. In vapor-tight systems, a lower increase rate was observed. The relative humidity did not exceed 65% relative humidity. The highest relative humidity was under vapor-open insulation systems (stone wool without vapor barrier, aerogel blanket, cellulose, expanded clay). Vapor-tight systems had lower humidity levels: the highest level was reached by expanded cork, followed by XPS, XPS with Sika cement, cork, and PIR with aluminum cover. Vapor-open systems are sensitive to changes in indoor relative humidity. When indoor relative humidity fell or increased, vapor-open materials with lower Sd values (rock wool without vapor barrier, expanded clay, cellulose, aerogel blanket) mimicked this behavior but with different trends. Materials with higher Sd values did not imitate this behavior (VIP, high-density wood fiber, PIR with gypsum board, and vapor-resistant paper). In both situations, mineral wool followed the trend closer than other materials, which might be explained by the limited moisture buffering capacity for this type of insulation, in contrast to the capillary active materials. The behavior of other materials followed the trend to a lesser extent because they had excellent MBV.
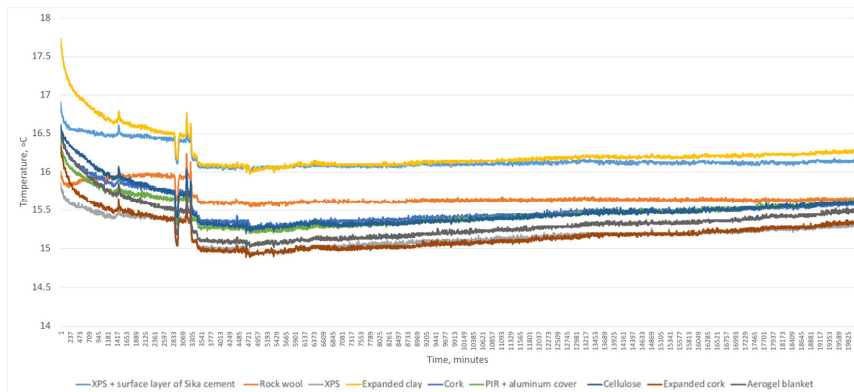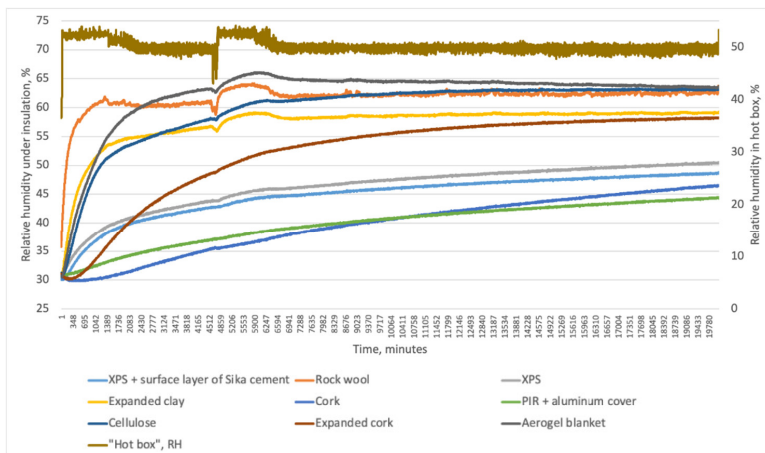
Figure 20. Relative humidity under insulation in steady-state conditions for the second test round.

- Changes in absolute humidity under the insulation materials

As the relative humidity was dependent on temperature, the absolute humidity in g/m^3 was used to compare the impact on moisture changes under different insulation materials (see Figure 21).
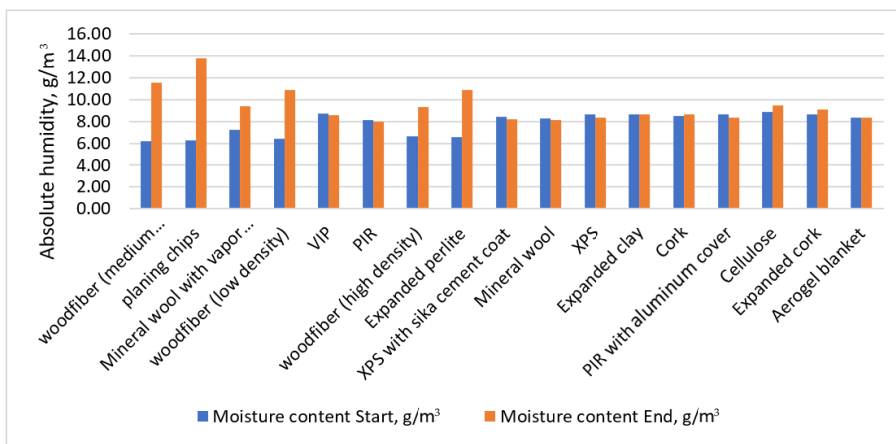
Figure 21. Absolute humidity under insulation materials at the start and end of steady state cycle.

The highest increase of moisture was evident under capillary active insulation materials (woofibers, planning chips, and expanded perlite). Two deviations were observed, the first being the mineral wool with vapor barrier (with sd value 12 m, could be considered as breathable wind barrier, not a true vapor barrier), that shows similar behavior to the capillary active insulation materials, and the second being capillary active cellulose that showed similar behavior to the vapor-tight insulation materials. The absolute moisture increase under insulation materials was as follows: Planing chips 119%, woodfiber (medium density) 85%, woodfiber (low density) 69%, expanded perlite 65%, woodfiber (high density) 39%, cellulose 7%, expanded cork 5%, cork 2%, aerogel blanket, and expanded clay 0%, and all the rest materials, all of which except for mineral wool are vapor-tight, had a negative absolute humidity change from −1 to −4%.

3.2. Unsteady State Conditions

3.2.1. Dynamic Cycle

The first test round showed that each insulation system comprises materials with different thermophysical properties, determining how the envelope responds to climatic conditions. The results showed that the temperature below the insulation materials followed the same daily cycle as the cold-box temperature with a visible time lag. The average time lag for the heat wave propagating from the inner surface to the outer surface for all insulation systems was 7–10 h. The decrement factor was the ratio of the heat wave amplitudes at the two surfaces of the wall, and the values were between 0.07 and 0.49. The lowest value of the decrement factor was exhibited by vapor-open systems with the lowest Sd value and increased with increased Sd value (the highest value is for PIR with aluminum cover).

Figure 22 shows the temperature behavior under insulation during the dynamic cycle in the second test round. Like the first test round, the temperature profile followed the cold-box temperature with delay. The time lag was between 9 and 11 h. The decrement factor correlated with the Sd value—the higher the Sd value, the higher the decrement factor. The most significant temperature amplitude was observed under rock wool, XPS, and XPS with Sika cement. The smallest temperature amplitude was observed under expanded clay. All other insulating materials were in the middle, with relatively similar temperature amplitudes. The ranges were from 1.21 °C to 1.67 °C.
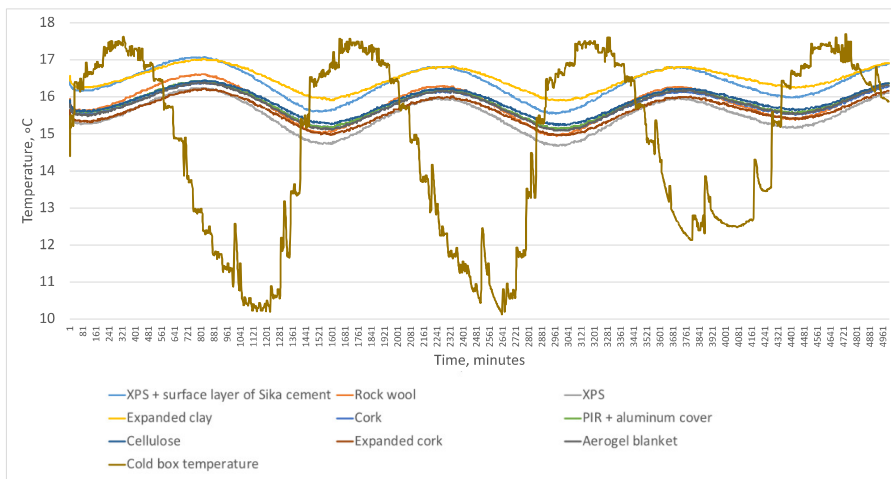
Figure 22. The temperature under insulation during dynamic cycle in the second test round.

The relative humidity dynamics under insulation during the dynamic cycle of the first test round revealed that relative humidity behavior under insulation material was less intuitive than temperature behavior. Each insulation system's initial relative humidity values were determined by the initial cold-box temperature at the beginning of the cycle. During this cycle, the cold-box average temperature was slightly higher than in the steady-state cycle. Similar to temperature, there was an effect of daily variation on relative humidity coupled with temperature fluctuations in the cold box. The time lag differed for the maximum and minimum values of temperature waves. For the maximum temperatures, the time lag was between 8 h (for vapor-open systems with low Sd values) and 17 h (for vapor-tight systems with high Sd values). The time lag for the minimum temperature values was more prolonged and varied from 10 to 19. However, the amplitude varied for insulation systems: vapor-tight systems had a lower amplitude, while vapor-open systems had a higher amplitude. The decrement factor was from 1.9 (for vapor-open systems with

low Sd) to 7 (for vapor-tight systems with high Sd value). The other difference from the temperature was the slope of relative humidity profiles. The vapor-tight system's relative humidity profiles were stable and increased only after the failure of the control system when the temperature in the cold-box decreased. Vapor-open systems had falling slopes, which meant the system was drying inwards. The steepest slope was exhibited by planing chips plate, followed by wood fiber with an average density, expanded perlite, and low-density wood fiber. After the failure of the control system, the same trend was present but in the opposite direction.

The relative moisture under insulation during the dynamic cycle in the second test round (Figure 23) behaved similarly to the first test round. The relative humidity followed temperature fluctuations because the hot-box relative humidity was steady, and the cold-box temperature oscillated. Vapor-tight systems had a lower amplitude, while vapor-open systems had a higher amplitude. When the amplitude of cold-box temperature decreased (starting at minute 3773), the relative humidity amplitude of the vapor-open insulation systems decreased after the time lag. The vapor-tight system's relative humidity profiles were slightly increasing.
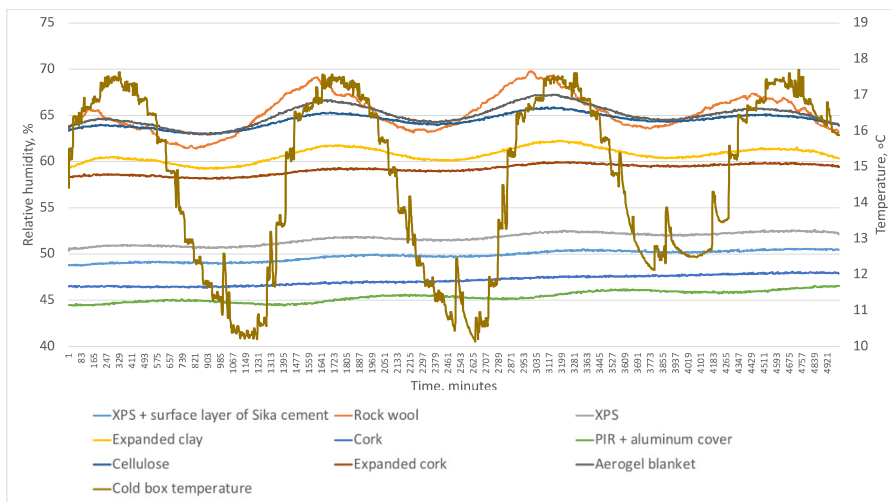
Figure 23. Relative humidity under insulation during dynamic cycle in the second test round.

Due to failure of the controller unit during the 1st test round, it was possible to compare the amplitudes of RH changes under insulation materials with the amplitude of RH change in hot-box, a response in % to those changes was observed as follows—woodfiber (medium density) 97%, planing chips 96%, expanded perlite 45%, woodfiber (low density) 23%, woodfiber (high density) 23%, mineral wool with vapor barrier 20%, PIR 1% and VIP 0%. For the second test round, such a comparison was not possible due to lack of dynamic indoor relative humidity conditions.

3.2.2. Wind-Driven Rain

As in the second cycle, the temperature continued to follow the outdoor temperature with an offset; the outdoor temperature is not plotted to make the graph easier to understand. As in the first/constant cycle, the lowest temperature was below PIR with gypsum board and vapor-resistant paper, VIP, and mineral wool with a vapor barrier, and the highest temperature was still below high-density wood fiber. The maintenance of the temperature distribution indicates that the thermal conductivity of the insulation materials was not significantly affected by moisture (see Figure 24).
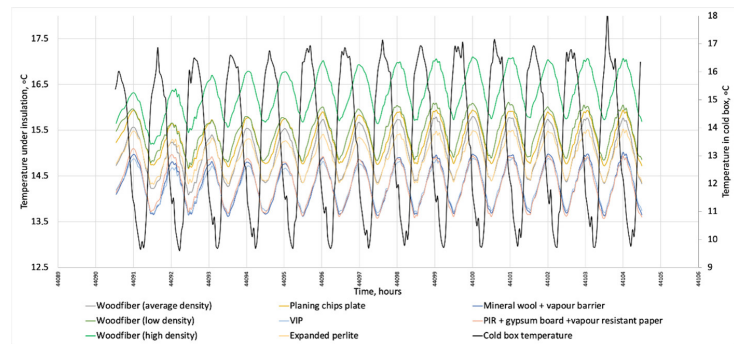
Figure 24. Temperature under insultation during wind-driven rain in the first test round.

When a dynamic cycle was complemented with wind-driven rain (regular peaks at the end of each cycle represent wind-driven rain injections in Figure 25), at the first part of the cycle, the relative humidity behavior was similar to a dry dynamic cycle where vapor-open systems exhibited a downward trend because systems with low Sd value followed an indoor relative humidity profile, and vapor-tight systems remained stable. After the seventh cycle, relative humidity profiles changed their slope upwards for both insulation systems. The rate of change was higher for vapor-open systems than for vapor-tight systems.
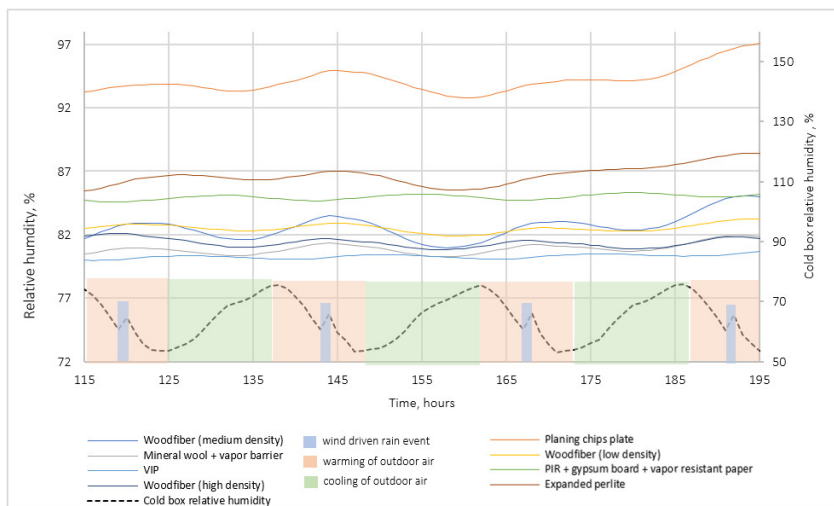
Figure 25. Relative humidity under insultation during wind-driven rain in the first test round.

- The second test round

During the second test round's wind-driven cycle, the cold-box conditions were not controlled but left to follow laboratory indoor conditions while hot-box conditions were controlled. This led to conditions similar to summer when the outdoor climate is warmer than indoors. Only wind-driven rain was controlled during this cycle. Temperature profiles for this cycle (Figure 26) show that temperatures between masonry and insulation systems followed the outdoor temperature profile with delay.
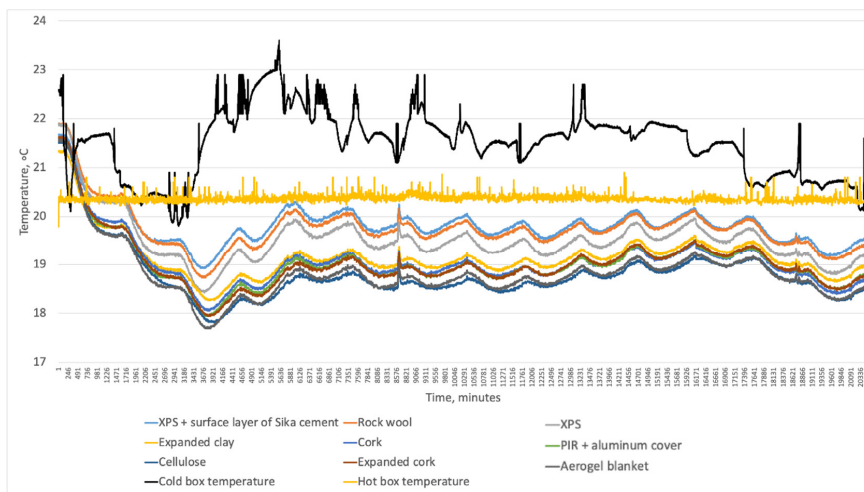
Figure 26. Temperature under insultation during wind-driven rain in the second test round.

The measurements of relative humidity under insulation during wind-driven rain in the second test round (Figure 27) show an increase in relative humidity under vapor-tight insulation systems with a μ-value of 10 or more (expanded cork, cork, PIR with aluminum cover, XPS, and XPS with the Sika cement layer). The increase in the relative humidity level in vapor-tight systems was likely caused by heat-driven vapor flow from the outside toward the inside (summer condensation). This can lead to condensing on the internal side of the masonry wall due to the tightness of these systems, indicating that seasonal drying out is not occurring behind the vapor-tight insulation. The relative humidity of the hot-box influenced the relative humidity under vapor-open materials with a μ-value of less than 10. The relative humidity behind the vapor-open insulation dropped in summer, indicating a seasonal drying out. Vapor-open systems such as rock wool without a vapor barrier, expanded clay, and aerogel blankets had high fluctuations behind insulation materials. Unlike cellulose with excellent moisture buffering capacity, which exhibited a flatter relative humidity profile at a higher value, they had negligible moisture buffering capacity.
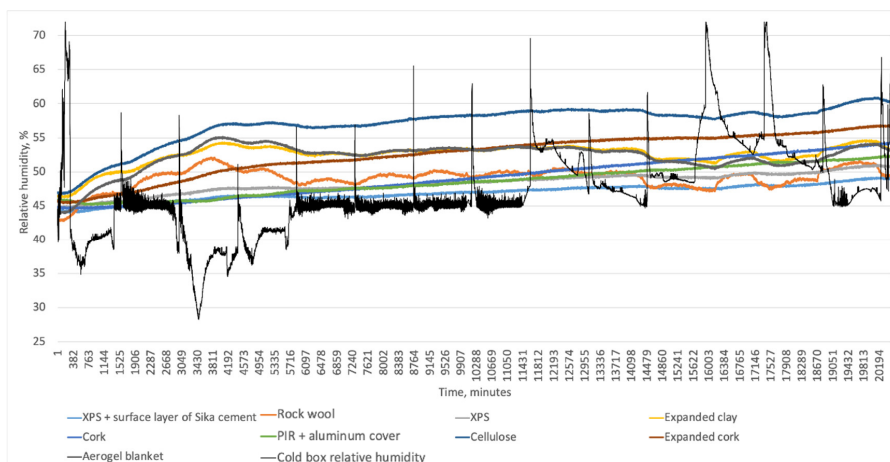
Figure 27. Relative humidity under insultation during wind-driven rain in the second test round.

For the 2nd test wall, the impact of wdr on the relative humidity under the insulation over 5 wdr cycles was observed as follows—cork 10%, expanded cork, mineral wool and PIR with aluminum cover 7%, aerogel blanket, cellulose and XPS 5%, expanded clay and XPS with Sika cement 4%.

3.2.3. Dry Dynamic Cycle with Heating

During the dry dynamic cycle, the temperature below the insulating materials increased, and new equilibrium states were acquired (see Figure 28).
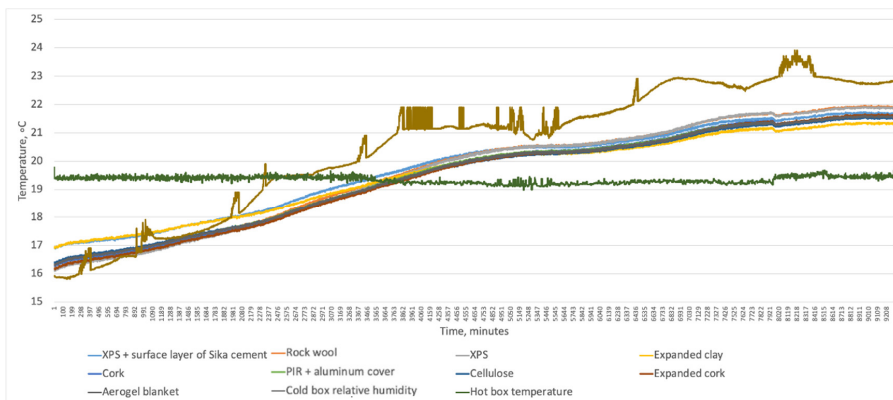
Figure 28. Temperature below insulation during the drying cycle.

Figure 29 presents relative humidity changes under insulation during the drying cycle. First, the relative humidity trend followed outdoor temperature because indoor relative humidity was constant. When indoor humidity fell, the insulation systems with low Sd values moved downwards faster than other materials. When indoor relative humidity increased at the last part of the cycle, vapor-open materials with low Sd values followed the trend.
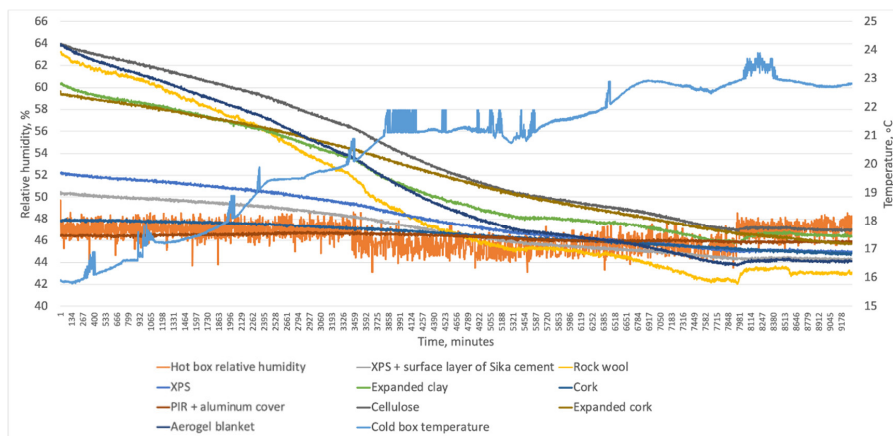
Figure 29. Relative humidity under insulation.

4. Conclusions

1. Internal insulation significantly impacts the hygrothermal behavior of masonry walls, leading to elevated relative humidity levels between insulation layers and an increased risk of frost damage and decay in embedded wooden components.

2. Tested insulation systems show similar thermal performance but distinct moisture performance, with temperature under insulation closely correlating with the insulation system's thermal conductivity.

3. The time lag for heat waves to propagate from the inner surface to the outer surface varies among insulation systems and depends on boundary conditions, particularly the temperature differential between indoor and outdoor environments. The temperature decrement factor also varies and correlates positively with vapor diffusion resistance.

4. Relative humidity beneath insulation is influenced by outdoor temperature fluctuations and indoor relative humidity changes. In systems with low vapor diffusion resistance, relative humidity tracks indoor humidity, while high-resistance systems are primarily influenced by outdoor temperature.

5. Under conditions of indoor humidity stability and outdoor temperature oscillation, vapor-open systems with low vapor diffusion resistance align their relative humidity behavior with temperature profiles. Vapor-tight systems exhibit reduced relative humidity amplitudes as vapor diffusion resistance decreases.

6. When both indoor relative humidity and outdoor temperatures oscillate, vapor-open systems with low vapor diffusion resistance resemble indoor humidity profiles more closely.

7. Wind-driven rain exacerbates relative humidity increase under insulation systems, with the impact being greater in materials with higher vapor diffusion resistance.

8. Vapor-open materials such as cork, expanded cork, and high-density fiberboard, even without vapor barriers, behave similarly to vapor-tight systems, being less sensitive to indoor relative humidity changes and more sensitive to outdoor temperature oscillations.

9. Longer test periods or mathematical model simulations based on short-term data are needed to detect and understand moisture accumulation effects on temperature and relative humidity under insulation.

10. Achieving accurate simulation results requires precise input data, including material properties such as insulation and mortar, which should closely match real-world values. The choice of brick type is also crucial, as different bricks with similar absorption coefficients can yield different results.

11. Internal insulation projects should be approached on a case-specific basis, considering various material parameters that can be challenging to determine, especially vapor and capillary conductivity as functions of moisture content. Detailed planning is essential to account for case-specific variables in hygrothermal simulations.

These conclusions underscore the complexity of hygrothermal behavior in internally insulated masonry walls and emphasize the need for careful material selection, long-term testing, and accurate simulation to ensure effective and durable insulation solutions.

Conflicts of Interest: The authors declare no conflict of interest.

Appendix A

Table A1. Thermal insulation systems used in the experiment.

No.	Insulation Material	Insulation Type	Mounting Mechanism/Glue	Vapor Barrier	Plaster Material	Type of Thermal Insulation System	Properties of Insulation Material Used in the Insulation System						
							δ, m	λ, W/mK	R_λ, m^{2}K/W	U, W/m^{2}K	μ	S_d, m	MBV Tested
1.	Planing chips plates	Organic plants/animal-derived	Glue	No	No	Vapor-open non capillary active	0.05	0.066	0.76	1.08	n/a	n/a	Yes
2.	Mineral wool	Inorganic mineral-derived	Carcass	Yes	Gypsum plaster	Vapor-tight (vapor-open with vapor barrier)	0.05	0.042	1.19	0.74	1	0.05	Yes
3.	PIR with gypsum board (indoors) and vapor-resistant paper (outdoors)	Organic fossil fuel-derived	Polyurethane glue	Embedded in material	Plasterboard embedded in the material	Vapor-tight	0.03	0.023	1.30	0.68	6400	256 *	Yes
4.	High density woodfiber	Organic plants/animal-derived	Clay plaster Two layers were glued with clay plaster to achieve similar U value to other woodfiber-based materials.	No	Special clay plaster	Vapor-open capillary active	0.044	0.048	0.92	0.92	5	0.22	Yes
5.	Average density woodfiber	Organic plants/animal-derived	clay plaster	No	Special clay plaster	Vapor-open capillary active	0.04	0.038	1.05	0.82	5	0.20	Yes
6.	Low density woodfiber	Organic plants/animal-derived	clay plaster	No	Special clay plaster	Vapor-open capillary active	0.05	0.038	1.32	0.67	2	0.10	Yes
7.	Expanded perlite	Inorganic mineral-derived	Special glue for expanded perlite	No	Gypsum plaster	Vapor-open capillary active	0.05	0.045	1.11	0.78	5	0.25	Yes
8.	VIP	Innovative	Polyurethane glue and carcass	No	Gypsum plaster	Vapor-tight	0.02	0.007	2.86	0.33	n/a	n/a	No
9.	XPS with the surface layer of Sika cement and a glass fibef net	Organic fossil fuel-derived		No	Gypsum plaster	Vapor-tight	0.02	0.035	0.57	1.75	133	2.66	Yes
10.	Rock wool	Inorganic mineral-derived		No	Gypsum plaster	Vapor-open non capillary active	0.05	0.045	1.11	0.9	1	0.05	Yes
11.	XPS	Organic fossil fuel-derived		No	Gypsum plaster	Vapor-tight	0.05	0.035	1.43	0.7	133	6.65	Yes
12.	Expanded clay	Inorganic mineral-derived	Loose fill	No	Gypsum plaster	Vapor-open	0.05	0.07	0.71	1.4	2	0.1	Yes
13.	Cork	Organic plants/animal-derived		No	Gypsum plaster	Vapor-open non capillary active	0.045	0.04	1.13	0.89	10	0.45	No
14.	Expanded cork	Organic plants/animal-derived		No	Gypsum plaster	Vapour-open non capillary active	0.05	0.04	1.25	0.8	10	0.5	No
15.	PIR with aluminum cover on both sides	Organic fossil fuel-derived		No	Gypsum plaster	Vapor tight	0.03	0.023	1.3	0.77	∞	99	No
16.	Cellulose	Organic plants/animal-derived	Loose fill	No	Gypsum plaster	Vapor-open capillary active	0.05	0.036	1.39	0.72	2	0.1	Yes
17.	Aerogel blanket	Innovative		No	Gypsum plaster	Vapor-open non capillary active	0.016	0.02	0.8	1.25	5	0.08	No

* Sd values were assigned to the entire insulation system because the manufacturer was unable to provide information on the insulation material separately.

Table A2. Properties of materials used for simulations to correspond with the laboratory experiment.

Material	Brick	Mortar	High Density Woodfiber	Low Eensity Woodfiber	Average Eensity Woodfiber	Planing Chips Plate	Expanded Perlite	PIR with Gypsum Board and Vapor-Resistant Paper	Clay Plaster for Woodfiber
Name of the material in the DELPHIN database	Old Building Brick Rote Kaserne Potsdam (inner brick 2)	Lime cement mortar	Wood Fiber Board	Wood Fiber Board indoor	Wood Fiber Insulation Board	Wood Wool Cement Board	TecTem Insulation Board Indoor 50 + 60 mm	Polyurethane boards	Light Clay Mortar
Density of the material, kg/m^3	2049	1878	300	119	161	180	100	35	900
Porosity, m^3/m^3	0.227	0.291	0.420	0.923	0.893	0.931	0.962	0.949	0.470
Water vapor diffusion resistance factor	19.0	36.9	5.0	1.1	3.4	4.9	8.0	100	30.0
Specific heat capacity of dry material, J/kg·K	847	758	1880	1000	1662	1470	1640	1500	1000
Thermal conductivity, W/m·K	0.861	0.803	0.050	0.040	0.039	0.060	0.046	0.028	0.230
Effective saturation (long term process), m^3/m^3	0.240	0.223	0.400	0.590	0.550	0.340	0.0770	0.949	0.450
Water uptake coefficient, kg/m^{2}s$^{0.5}$	0.3359	0.0360852	0.0674	0.00503591	0.00288593	0.0089	1.9809	1×10^{-7}	0.00367

Table A3. The brick properties acquired from laboratory tests and comparison with building brick from DELPHIN database used for initial simulations.

Brick	Bulk Density ϱ, kg/m^3	Specific Heat Capacity c, J/kg·K	Thermal Conductivity λ_{dry}	Total Porosity O$_{por}$, m^3/m^3	Capillary Saturation O$_{cap}$, m^3/m^3	Dry Cup Value μ_{dry}	Water Uptake A$_W$, kg/m^{2}s$^{0.5}$
Lode	2081.3	671	0.8809	0.1888	0.1492	24.04	0.0946
Old Building Brick Rote Kaserne Potsdam (inner brick 2)	2049	847	0.861	0.227	0.24	19	0.3359
Difference, %	+1.6%	−26.2%	+2.3%	−20.2%	−60.9%	+21.0%	−255.1%

Sorption isotherm and moisture retention curves were obtained from the performed tests (Figure A1).

The vapor permeability curves depending on relative humidity and moisture content were also determined (Figure A2).

The liquid conductivity curves depending on relative humidity and moisture content were also determined (Figure A3).

From the acquired data, a new material file, which could be used in the DELPHIN simulation software, was created.
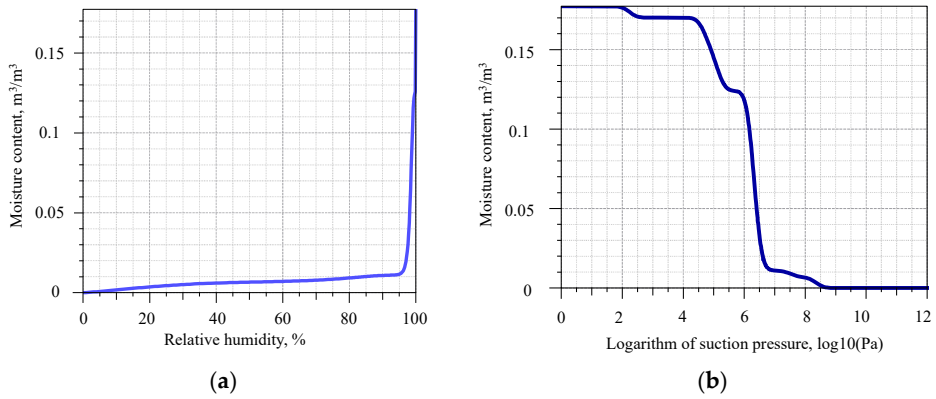
Figure A1. (**a**) Sorption isotherm and (**b**) moisture retention curves, of the brick used for the masonry sample.
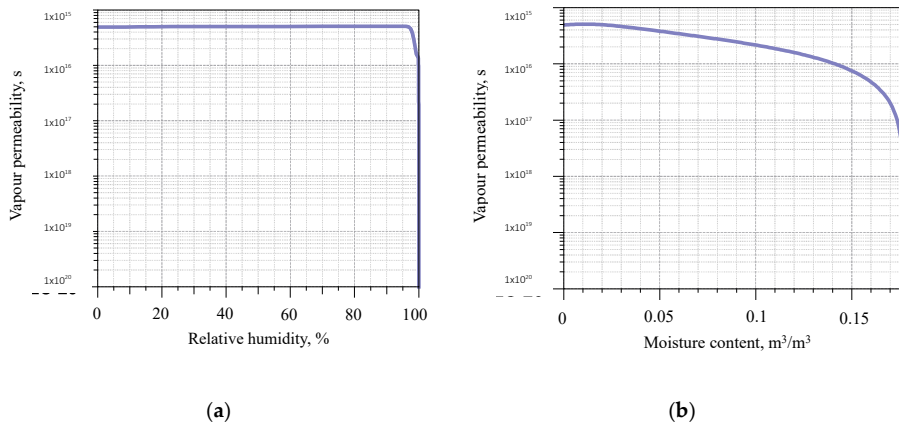

Figure A2. Vapor permeability curves of the brick rick used for the masonry sample depending on (**a**) relative humidity and (**b**) moisture content.
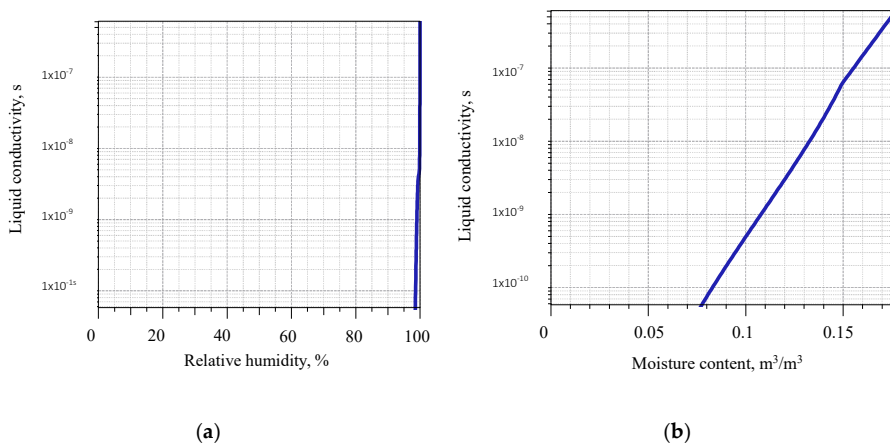

Figure A3. Liquid conductivity curves of the brick rick used for the masonry sample depending on relative humidity (**a**) and moisture content (**b**).

References

1. Calvin, K.; Lee, H.; Dasgupta, D. *IPCC, 2023: Climate Change 2023: Synthesis Report. Contribution of Working Groups I, II and III to the Sixth Assessment Report of the Intergovernmental Panel on Climate Change. Proceedings of the Intergovernmental Panel on Climate Change (IPCC), Geneva, Switzerland, 13–19 March 2023*; Core Writing Team, Lee, H., Romero, J., Eds.; IPCC: Geneva, Switzerland, 2023. [CrossRef]
2. Tracking Clean Energy Progress 2023—Analysis. IEA. Available online: https://www.iea.org/reports/tracking-clean-energy-progress-2023 (accessed on 6 September 2023).
3. Laaroussi, Y.; Bahrar, M.; Zavrl, E.; El Mankibi, M.; Stritih, U. New qualitative approach based on data analysis of European building stock and retrofit market. *Sustain. Cities Soc.* **2020**, *63*, 102452. [CrossRef]
4. Vereecken, E.; Roels, S. A comparison of the hygric performance of interior insulation systems: A hot box–cold box experiment. *Energy Build.* **2014**, *80*, 37–44. [CrossRef]
5. De Mets, T.; Tilmans, A.; Loncour, X. Hygrothermal assessment of internal insulation systems of brick walls through numerical simulation and full-scale laboratory testing. *Energy Procedia* **2017**, *132*, 753–758. [CrossRef]
6. Cornet: In2eurobuild–Consistent European Guidelines for Internal Insulation of Building Stock and HeritaGE. Available online: https://wufi.de/de/wp-content/uploads/sites/9/In2EuroBuild_Guideline-II_Internal-Insulation.pdf (accessed on 6 September 2023).
7. Bottino-Leone, D.; Larcher, M.; Herrera-Avellanosa, D.; Haas, F.; Troi, A. Evaluation of natural-based internal insulation systems in historic buildings through a holistic approach. *Energy* **2019**, *181*, 521–531. [CrossRef]
8. Johansson, P.; Geving, S.; Hagentoft, C.E.; Jelle, B.P.; Rognvik, E.; Kalagasidis, A.S.; Time, B. Interior insulation retrofit of a historical brick wall using vacuum insulation panels: Hygrothermal numerical simulations and laboratory investigations. *Build. Environ.* **2014**, *79*, 31–45. [CrossRef]
9. Straube, J.; Schumacher, C. Interior Insulation Retrofits of Load-Bearing Masonry Walls in Cold Climates. *J. Green Build.* **2007**, *2*, 42–50. [CrossRef]
10. Morelli, M.; Svendsen, S. Investigation of interior post-insulated masonry walls with wooden beam ends. *J. Build. Phys.* **2013**, *36*, 265–293. [CrossRef]
11. Nielsen, A.; Møller, E.B.; Rasmussen, T.V.; Jan de Place, E. Use of sensitivity analysis to evaluate hygrothermal conditions in solid brick walls with interior insulation. In Proceedings of the 5th International Building Physics Conference (IBPC), Kyoto, Japan, 28–31 May 2012; pp. 377–384.
12. Morelli, M.; Scheffler, G.; Nielsen, T.; Svendsen, S. Internal Insulation of Masonry Walls with Wooden Floor Beams in Northern Humid Climate. In Proceedings of the Thermal Performance of the Exterior Envelopes of Whole Buildings XI, Clearwater Beach, FL, USA, 5 December 2010.
13. Zhao, J.; Grunewald, J.; Ruisinger, U.; Feng, S. Evaluation of capillary-active mineral insulation systems for interior retrofit solution. *Build. Environ.* **2017**, *115*, 215–227. [CrossRef]
14. Freudenberg, P.; Ruisinger, U.; Stöcker, E.; Roles, S.; Feldt Jensen, N.; Odgaard, T.; Otiv, P.; Capener, C.-M.; Lång, L.; Peuhkuri, R.; et al. *Robust Internal Thermal Insulation of Historic Buildings Title of the Deliverable: 637268 Robust Internal Thermal Insulation of Historic Buildings RIBuild D3.1 Closed Technology Loop of Laboratory Experiments and Simulation Models in the Field of Internal Insulation Testing Contractual Date of Delivery to the CEC: 31.12.2017 Actual Date of Delivery to the CEC: Organisation Name of Lead Contractor for this Deliverable: TUD Work Package Contributing to the Deliverable: WP3 Nature: R Version: 2.0.*; European Commission: Brussels, Belgium, 2018.
15. Vereecken, E.; Roels, S. Capillary active interior insulation: Do the advantages really offset potential disadvantages? *Mater. Struct.* **2015**, *48*, 3009–3021. [CrossRef]
16. Vereecken, E.; Roels, S. Wooden beam ends in combination with interior insulation: The importance of an airtight sealing. *Energy Procedia* **2017**, *132*, 664–669. [CrossRef]
17. Hansen, T.K.; Bjarløv, S.P.; Peuhkuri, R.H.; Harrestrup, M. Long term in situ measurements of hygrothermal conditions at critical points in four cases of internally insulated historic solid masonry walls. *Energy Build.* **2018**, *172*, 235–248. [CrossRef]
18. Vereecken, E.; Van Gelder, L.; Janssen, H.; Roels, S. Interior insulation for wall retrofitting—A probabilistic analysis of energy savings and hygrothermal risks. *Energy Build.* **2015**, *89*, 231–244. [CrossRef]
19. Blumberga, A.; Freimanis, R.; Biseniece, E.; Kamenders, A. Hygrothermal Performance Evaluation of Internally Insulated Historic Stone Building in a Cold Climate. *Energies* **2023**, *16*, 866. [CrossRef]
20. Biseniece, E.; Freimanis, R.; Purvins, R.; Gravelsins, A.; Pumpurs, A.; Blumberga, A. Study of Hygrothermal Processes in External Walls with Internal Insulation. *Environ. Clim. Technol.* **2018**, *22*, 22–41. [CrossRef]
21. Biseniece, E.; Žogla, G.; Kamenders, A.; Purviņš, R.; Kašs, K.; Vanaga, R.; Blumberga, A. Thermal performance of internally insulated historic brick building in cold climate: A long term case study. *Energy Build.* **2017**, *152*, 577–586. [CrossRef]
22. Klõšeiko, P.; Arumägi, E.; Kalamees, T. Hygrothermal performance of internally insulated brick wall in cold climate: A case study in a historical school building. *J. Build. Phys.* **2015**, *38*, 444–464. [CrossRef]
23. Grunewald, J.; Ruisinger, U.; Häupl, P. The Rijksmuseum Amsterdam—Hygrothermal analysis and dimensioning of thermal insulation. In Proceedings of the 3rd International Conference in Building Physics–Research in Building Physics and Building Engineering, Montreal, QC, Canada, 27–31 August 2006; pp. 345–352.
24. Scheffler, G.; Grunewald, J. Material development and optimisation supported by numerical simulation for a capillary-active inside insulation material. In *Research in Building Physics*; CRC Press: Boca Raton, FL, USA, 2003; pp. 77–85.

25. Vereecken, E.; Roels, S. Capillary Active Interior Insulation Systems for Wall Retrofitting: A More Nuanced Story. *Int. J. Archit. Herit.* **2016**, *10*, 558–569. [CrossRef]

26. Odgaard, T.; Bjarløv, S.P.; Rode, C. Influence of hydrophobation and deliberate thermal bridge on hygrothermal conditions of internally insulated historic solid masonry walls with built-in wood. *Energy Build.* **2018**, *173*, 530–546. [CrossRef]

27. Scheffler, G.A. Hygric performance of internal insulation with light-weight autoclaved aerated concrete. In Proceedings of the 5th International Conference on Autoclaved Aerated Concrete, Bydgoszcz, Poland, 14–17 September 2011.

28. Bourbia, S.; Kazeoui, H.; Belarbi, R. A review on recent research on bio-based building materials and their applications. *Mater. Renew. Sustain. Energy* **2023**, *12*, 117–139. [CrossRef]

29. Fino, R.; Tadeu, A.; Simões, N. Influence of a period of wet weather on the heat transfer across a wall covered with uncoated medium density expanded cork. *Energy Build.* **2018**, *165*, 118–131. [CrossRef]

30. Romano, A.; Bras, A.; Grammatikos, S.; Shaw, A.; Riley, M. Dynamic behaviour of bio-based and recycled materials for indoor environmental comfort. *Constr. Build. Mater.* **2019**, *211*, 730–743. [CrossRef]

31. Kreiger, B.K.; Srubar, W.V. Moisture buffering in buildings: A review of experimental and numerical methods. *Energy Build.* **2019**, *202*, 109394. [CrossRef]

32. Klõšeiko, P.; Kalamees, T. Hygrothermal performance of a brick wall with interior insulation in cold climate: Vapour open versus vapour tight approach. *J. Build. Phys.* **2022**, *46*, 3–35. [CrossRef]

33. Antolinc, D.; Černe, K.; Jagličić, Z. Risk of Using Capillary Active Interior Insulation in a Cold Climate. *Energies* **2021**, *14*, 6890. [CrossRef]

34. Jensen, N.F.; Odgaard, T.R.; Bjarløv, S.P.; Andersen, B.; Rode, C.; Møller, E.B. Hygrothermal assessment of diffusion open insulation systems for interior retrofitting of solid masonry walls. *Build. Environ.* **2020**, *182*, 107011. [CrossRef]

35. RIBuild_D1.2_1.0.pdf. Available online: https://static1.squarespace.com/static/5e8c2889b5462512e400d1e2/t/5e9db814e1ea8b0e935c76d2/1587394584525/RIBuild_D1.2_1.0.pdf (accessed on 20 September 2020).

36. Latvijas Vides, Ģeoloģijas un Meteoroloģijas Centrs. Available online: https://videscentrs.lv (accessed on 6 September 2023).

Trilemma of historic buildings: Smart district heating systems, bioeconomy and energy efficiency

Andra Blumberga [*], Ritvars Freimanis, Indra Muizniece, Kriss Spalvins, Dagnija Blumberga

Institute of Energy Systems and Environment, Riga Technical University, Latvia

ABSTRACT

Today buildings become part of Smart Energy Systems. 4th generation district heating network requires buildings with low energy consumption. In Europe, historic buildings account for around 30% from total buildings stock with high energy consumption which has to be reduced. Many of them have heritage value and external insulation of walls is not possible. If internal insulation is applied, careful hygro-thermal assessment has to be carried out to avoid critical moisture conditions in the wall leading to failure modes. Insulation material market is dominated by petrochemicals or non-renewable natural materials. Yet development of bio-based thermal insulation materials is increasing and some of them successfully entered the market. EU Bioeconomy Strategy enhances use of bioresources to increase their added value. The main goal of this research is to assess applicability of innovative bio-based pine needles insulation material that is produced based on bioeconomy principles as internal insulation material for historic massive walls. Results show that studied material is highly porous, has high moisture transfer, storage capacity, and is good hygric regulator. Lime treated material has no mold growth at relative humidity 85%. Even if insulation material is treated with lime, heat savings have to be sacrificed to reduce critical conditions for mold growth.

© 2019 Published by Elsevier Ltd.

1. Introduction

Planet is facing climate change caused by high greenhouse gas emission rate. Energy used by the building stock is among the major pollution sources [1]. Today buildings become part of Smart Energy Systems that have integrated holistic view on different sectors with the main goal to integrate feasible solutions to the transformation towards sustainable energy solutions [2−5]. Energy efficiency measures carried out in building stock can have important impact on the district heating, e.g. simulation results for district heating in France shows that if heat demand decreases by 18%, relative heat losses in the network increases by 3%. It also has impact on heat production mix [6] The impact of demand reduction on the district heating shall be taken into account in due time before the renovation of buildings starts [7]. Current building stock comprises buildings built in different periods, including historic buildings built before 1945, buildings built between the Second World War and the Millennium, and low energy and nearly zero

energy buildings. In Europe, historic buildings account for 24−35% of total building stock area and can consume 27−42% from the nation final energy consumption [8]. Specific heating energy consumption of these buildings can be 8−10 times higher than in modern low energy buildings, and historic building users have higher energy bills, e.g. people living or working in historic buildings in England (UK) every year pay for energy on average £240 more [9]. Thus improvement of energy efficiency in historic buildings is among important issues. Yet many of these buildings have heritage value and external insulation cannot be applied. This technical solution has to be replaced with internal insulation which is among the most complicated energy efficiency measures. This is due to unfavorable changes in hydrothermal behavior of the wall leading to failure modes such as mold growth, algae growth, wood rot and freeze damage. Careful assessment has to be carried out prior to application of internal insulation [8].

Insulation materials dominating the market are produced from either petrochemicals (e.g.polystyrene) or non-renewable natural materials (mineral wools) [10]. Yet development of bio-based thermal insulation materials is increasing and some of them successfully entered the market while others are still at the development stage [11,12].

Bio-based insulation materials correspond to the goals of the European Bioeconomy Startegy which defines that "… the bio-economy covers all sectors and systems that rely on biological resources, their functions and principles. It includes and interlinks: land and marine ecosystems and the services they provide; all primary production sectors that use and produce biological resources; and all economic and industrial sectors that use biological resources and processes to produce food, feed, bio-based products, energy and services. To be successful, the European bioeconomy needs to have sustainability and circularity at its heart. This will drive the renewal of our industries, the modernisation of our primary production systems, the protection of the environment and will enhance biodiversity …. " [13].

Bio-based insulation materials have a number of advantages compared to conventional materials if used for internal insulation. They have lower embodied energy compared to conventional insulation materials [11,12]. In addition to that, they have high hygroscopicity which provides ability adsorb and desorb water vapor leading to higher Moisture Buffering Value [14,15]. Microstructure and high porosity of bio-based materials determine their hygroscopicity. These materials are characterized by a complex pore structure and low density. This also leads to low thermal conductivity. The size of pores and voids in bio-based materials can range from few nanometers to centimeters depending on type of material and processing. However determination of the porosity of bio-based materials is still challenging and either development of novel or adaptation of existing methods have to be carried out [16].

The amount of water vapor in the pores of a hygroscopic material has impact on both thermal and hygric properties of the material. During sorption processes heat energy in the amount of 2.5. kJ/g is either released or absorbed. Released heat diffuses through the material resulting in temperature changes [11]. Experimental hygrothermal tests of bio-based insulation boards alone show that bio-based materials have slower temperature change at the core of the sample compared to EPS due to higher thermal inertia and hygroscopicity. Temperature changes are also related to difference in absorbtion/desorption mechanisms. If Portland cement mortar plaster is applied to insulation boards, the differences are diminished [6]. Similar results are obtained by Ref. [17] who did tests on hemp-lime walls, and for mineral wool, wood fibre and hemp lime [18].

Nevertheless, hygroscopic properties of bio-based materials are not widely studied yet. Study on bio-based insulation materials [10] has found that only producers of commercialized bio-based insulation materials provide information on water vapor resistance. Authors guess that this parameter is not evaluated at an early development stage as additives or vapor barriers can be assessed during later stages.

Coniferous trees are widespread in the temperate zone. Their wood is in demand on the market, resulting in large amounts of logging residues, including the crown of coniferous trees (makes up to 25% from the total biomass volume of the tree). Fine coniferous branches up to 5 mm in diameter with greenery after logging are mostly not used. They are left in the forest, where they form nutrient base for the next generation of vegetation. On one hand, the greenery is important part of forest ecosystem, while on the other hand, not all the resources obtained during logging are fully utilized and maximum environmental and economic benefits are gained. The use of coniferous greenery for the production of products complies with the principles of bioeconomy, as the use of forest residues has so far been under-utilized. They do not occupy agricultural land, do not compete with agricultural crops and do not pose a threat to food safety. Production of this biomass does not include application of fertilizers, pesticides, and herbicides, as well as no watering and soil treatment is used, resulting in no additional

environmental and climate pressures. Use of forest residues also reduces the production of GHG emissions from biodegradation. They also temporarily accumulate carbon without allowing it to enter the atmosphere, thus reducing the amount of GHG emissions into the atmosphere through the use of greenery products. Finally, use of forest residues increases social and economic benefits from one managed forest unit, replacing fossil raw materials, creating environmentally and climate-friendly products that biodegradable at the end of their life cycle.

Scientific literature provides information on the use of coniferous greenery or needles for the production of various products. Coniferous needles are mainly studied and their value is related to the biologically active substances they contain [19,20]. Other products such as extracts and essential oils [21,22], antioxidants [23,24], biogas [25], nanofiber cellulose [26], nanosilicon [27], co-firing of biomass [28] have also been studied, cellulose [29,30], particle board [31,32], composite materials [33–35]. Current research on the use of coniferous needles or greenery products for the production of products shows a tendency to use only certain chemical elements of the product. The scientific community realizes that coniferous needles are a valuable resource and its wider use of high value added products is only a matter of time. As a result, the issue of using forest residues from the processing of coniferous trees would become increasingly relevant.

The thermal insulation material made from extracted or fresh coniferous wood is currently not commercially produced and is not commercially available anywhere in the world. It is known that in 1890, the United States patented a technology for obtaining fiber from pine needles [36]. So far, the composite materials produced from coniferous wood pellets have been manufactured with fossil-based binders, which have a higher thermal conductivity coefficient, do not naturally decompose and are more environmentally friendly over the life cycle than in the thermal insulation materials developed in this and previous articles by the authors. In India, for example, a similar pine cone composite material is used as a binder (isocyanate prepolymer) [37], but uses a more environmentally friendly binder and has a much lower thermal conductivity (0.136 W/m/K). Textiles, interior items, decorative panels and paper are produced from pine needles [38].

Our previous research was focused on reduction incomplete use of the forest residues by developing a bulk and slab-shaped thermal insulation material from the needles and greenery of pinaceae pine (Picea) and pine (Pinus) genus [39–42]. The results so far have shown that it is possible to produce thermal insulation material with a competitive thermal conductivity coefficient (0.035–0.075 W/m/K) from the coniferous greenery (see Table 1). Within the framework of this study, fibers from pine needles are obtained and thermal insulation material is made from them, thus searching for an alternative to fossil based and mineral wool insulation wool.

The main goal of this research is to assess applicability of innovative bio-based pine (Pinas Sylvestris) needles insulation material that is produced based on bioeconomy principles as internal insulation material for historic massive walls.

Paper starts with description of historic building which is used as the case study for historic stone walls. It is followed by description of pine needle insulation material, research methodology, description of results, discussions and finally, conclusions.

2. Original historic building wall

Original historic building selected as an example to be repeated in the laboratory tests for this study was built in 1893 (see Fig. 1). It is a single family house built for farmer's family and is located in Sece, Latvia. The building has massive walls built from dolomite

Table 1
Experimentally obtained thermal conductivity coefficients for coniferous greenery thermal insulation material.

Sample characteristic	Thermal conductivity, W/mK	Reference
Coniferous greenery granules	0,045	[41]
Coniferous greenery panels	0,061	[39]
Coniferous greenery panels with binder	0,065	[42]
Spruce needles	0,035	[40]
Pine needles	0,075	[40]

a)   b)

Fig. 1. Original historic building used as an example for the laboratory tests: a) the main façade of the building; b) outdoor surface of the stone wall.

stone that is available locally and has been popular building material in the region during previous centuries. Lime mortar has been used to bind the stones. Total thickness of the wall is 0.61 m in the ground floor and 0.45 m in the first floor.

3. Insulation material

Needles of *Pinus sylvestris* was used to make the samples. The raw material was collected in the winter 2018 from logging residues in a forest clearing in Olaine region, Latvia. Air dried pine needles are used, which were stored for about 1 month at ~25 °C. From scientific literature it is known that size of pine needles can be affected by various factors, such as lighting [43] and pollution [44,45], therefore pine needle length (5−70 mm) and thickness (0,35-1 mm) varies widely [46]. The length of pine needles used for insulation material was not defined and no specific size needles were selected. All size pine needles which have naturally grown on pine branches were used. The needles were manually removed from the twigs and assembled in glass containers with a lid. The containers are filled with water to cover the needles. Containers with needles were heated for 3 h in an autoclaveat +134 °C under 2 bar to make them softer. After cooling, the needles are separated from the liquid and mechanically broken, making the needles softer and breaking their natural structure, resulting in fibrous needle material. It was then dried in an Ecocell oven for 24 h at +105 °C. To avoid one of the major failure modes for internal insulation, mold growth, lime was considered as natural material to prevent mold growth at critical conditions (temperature and relative humidity). Two types of insulation material samples were prepared: needles treated with the lime and needles without lime additive (see Fig. 2).

Samples with lime were made by soaking dry needles (380 g) in lime-water solution (weight based ratio 1:4 (400 g lime and 1600 g water)) for 10 min. Xanthan gum (0.1% from total mass of the lime-water solution (2 g)) was added as the binder to provide better bonding of the lime to the needles. The proportion of this solution was chosen based on previous laboratory experiments. The needles were then separated from the liquid and dried in the oven for

24 h at +105 °C. Finally, needle fiber material treated with lime and without lime were filled in form and pressed to give a sample thickness of 0.03 m. Both types of material samples were made from equal amount of dry needles, thus the density of the sample with lime is higher.

4. Methodology

To assess application of pine needle insulation material as internal insulation material in historic buildings with massive walls, this study carries out tests of different properties of insulation material, critical conditions for mold growth, and hygrothermal behavior of the test wall in laboratory conditions.

4.1. Density, thermal conductivity and moisture content of insulation material

Thermal conductivity was determined for each sample using LaserComp device model FOX200 in accordance with ISO 8301:2012 [47]. The amplitude of the device temperature varies from −20 °C to +75 °C and the accuracy is 0.01 °C. Pine needle insulation material samples were measured within the temperature range from 0 °C to +20 °C. Measurements were carried out with 1% precision.

Moisture content was carried out according to LVS CENTS 14774-3 „Solid biofuels − methods for the determination of moisture content; Oven dry method − Part 3: Moisture in general analysis sample" [48].

The bulk density of insulation material was determined in accordance with BS EN 1602:2013 [49].

4.2. Moisture absorption of insulation material

Moisture absorption test of pine needle insulation material samples with and without lime as well as for sample with vapor barrier was carried out in the climate chamber TH-G-1000 with temperature range from +10 to +90 °C and relative humidity from

Fig. 2. Pine needle insulation material sample without lime (on the left) and with lime (on the right).

20 to 98%. Test was carried out in accordance with ISO 12572:2016 Annex B "Methods suitable for loose fills" [50]. Test containers were filled with desiccant (silica gel granules). Relative humidity in containers were 5% and in the climate chamber 35% at +23 °C. Vapor barriers Jutadach VB 120 (100% polypropylene; 180 g/m²; s_d value (EN 13501-1) 12 ± 5 m; water vapor permeability at RH 85% 23 C, 24 h > 420 g/m²) for all three samples were installed in lids of containers. Lids were sealed with wax and adhesive tape ISOVER Vario®KB 1. Insulation material samples with and without lime were filled on the top of the vapor barriers (see Fig. 3). Sample size was $66 \times 63 \times 30$ mm. Distance between desiccant and vapor barrier was 80 mm.

4.3. Mold growth tests

Pine needle insulation material was examined in order to determine the critical moisture level at which fungal growth would occur. During the initial development of the insulation material it was submerged in simple lime solution to cover the surface of the material in lime particles. Problem with this approach was that the final material created large amount of airborne lime dust particles whenever it was handled. Therefore, it was decided to use miniscule concentrations of xanthan gum (0.01%) as binder in order to attach more lime on the surface of the material and to reduce chance of smaller particles to detach and become airborne during handling. Even though treatment with xanthan gum improved the handling properties of final material there was a risk that mold growth would be promoted by the addition of the xanthan gum
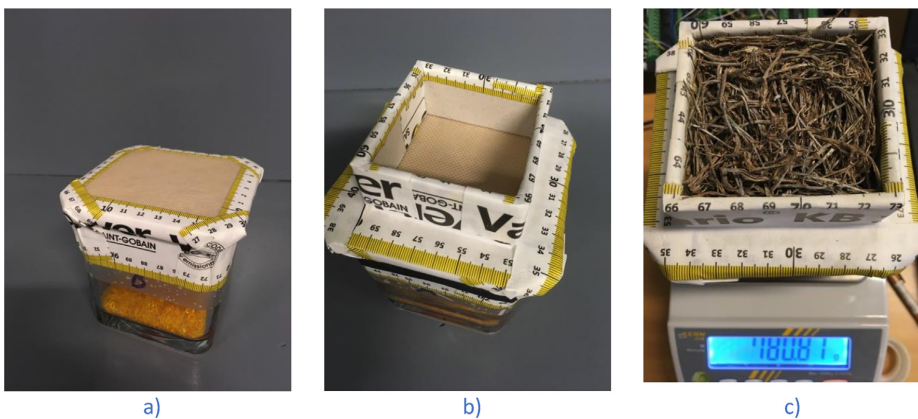

Fig. 3. Test samples for a) vapor barrier; b) pine needle insulation material (empty); c) pine needle insulation material (filled).

146

which is polysaccharide known to positively affect fungi growth [51]. Therefore, in order to determine if improved handling properties does not compromise material resistance to fungal growth, it was decided to test both treatment types - material treated with only lime and with lime and xanthan gum.

Material treated with lime (Treatment 1), with lime and xanthan gum (Treatment 2) and without lime (Control) were inserted in Petri dishes (⌀85 mm). Since treatment with lime and xanthan gum increased the total dry weight of the material by 30%, 5.2 g of treated materials were used in single replicate (Petri dish) and 4 g of control material per replicate. Three replicates of each differently treated material were incubated in each of the four relative humidity conditions (75%, 85%, 94%, 100%), thus a total of 12 replicates per untreated, 12 replicates per material treated with lime and 12 replicates per material treated with lime and xanthan gum were used.

• Fungal species and inoculation

Various species of fungi are found together on susceptible building materials [52–54]. A spore mixture of five fungi species was used in the experiment: *Mucor plumbeus*, *Penicillium chrysogenum*, *Cladosporium herbarum*, *Cladosporium cladosporioides*, *Trichoderma viride*. These species often grow on various building materials in damp houses [55–57]. Fungi strains on agar plates were kindly provided by Microbial Strain Collection of Latvia, University of Latvia. Fungi strains were cultivated and spore suspensions containing approximately 10^6 spores per ml were prepared for every fungi strain after which the five spore suspensions were mixed in equal volumes and 0.4 ml of the final suspension were sprayed onto surface of each of the samples. Cultivation, inoculum preparation and inoculation of samples were done according to Ref. [54] test for determination of critical moisture level for mold growth on building materials.

• Incubation conditions

After inoculation the samples were incubated in desiccators

with 0.30 m diameter and 0.37 m height, with porcelain platform. Desiccators had saturated salt solutions poured in the space below the desiccator platform. Saturated salt solutions were used to maintain particular values of relative humidity inside the desiccators (Table 2). Four Petri plates were placed inside each desiccator. Desiccators were placed in climate chamber CIBIN L32325B, (additional 1 kW heating element with ATR121-B thermostat was used) in the dark and temperature in the chamber was set up to +23 °C. Relative humidity was measured by HONEYWELL: HIH-4000-002 (accuracy 3.5%) and data was logged by Campbell CR1000.

• Assessment of mold growth

Samples were incubated for 40 days, after which measurements of the mold growth on the samples were taken. Most of the untreated samples were analyzed under stereo microscope Optika LAB-20 at 10-40× magnification, but since treated samples were covered with lime particles, it was difficult to assess fungal growth under stereo microscope, therefore light microscope Micros MC100LED at 100-400× magnification was used. Scale of the mold growth was assessed by using rating scale described by Ref. [54], with the ratings being as follows: 0 - no mold growth; 1 - initial growth; 2 - spare but clearly established growth; 3 - heavy growth; 4 - heavy growth over entire surface of the material.

4.4. Hygrothermal behavior tests of the test wall

For the hygrothermal behavior tests of the test wall a double climatic chamber in laboratory was used. Two test walls with irregular shape dolomite stones from the original historic building with lime mortar (40 × 55 × 50 cm) were built and inserted inside this chamber (see Fig. 4). Lime mortar was prepared from calcium lime CL80-S produced by *Krasnoselskstroimaterialy* and mixed with sand (weight based ratio 1:6). Stones are placed in the test walls as horizontal stylolites. Dolomite stone rubbles were used to fill in the space between stones. Each test wall has different fractions of stones, rubble stones and lime mortar: test wall A has 64.5% stones,

Table 2
Relative humidity and temperature conditions at which materials we incubated.

Relative humidity (%)	Saturated salt solution used	T (°C)	Incubation time (days)
75	NaCl	23	20
85	KCl		
100	Water only		
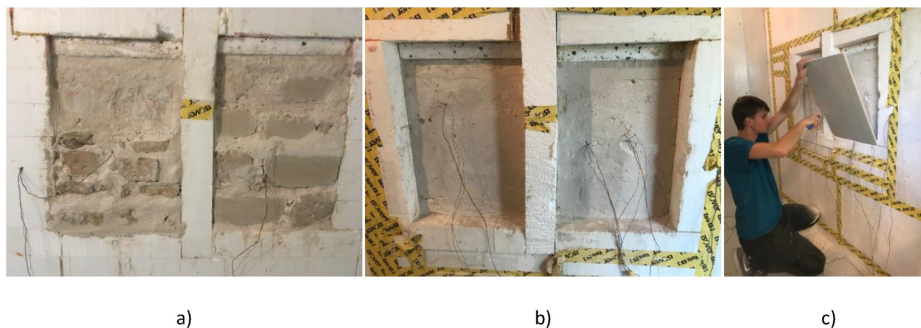
Fig. 4. Laboratory test stand with two historic stone walls from outdoor side (wall A on the right side and wall B on the left side) (a), indoor side (b), and applying pine needle insulation from the indoor side (c).

5.1% rubble stones and 30.4% lime mortar. Test wall B has 49.7% stone, 3.1% stone rubble and 47.2% lime mortar.

The indoor surface was covered with 0.01 m thick lime plaster, and 0.03 m thick insulation layers from pine needles treated with lime (wall A) and without lime (wall B) were installed on the indoor side. They were covered with gypsum plaster (0.125 m).

Relative humidity and temperature were measured between insulation and stone wall, and in the stone walls. 8 temperature sensors and 5 relative humidity sensors were installed in both climate chambers. Heat flow was measured in both wall samples with heat flow sensors HUKSEFLUX HFP01SC. Time step of measurements is 1 min. Data logger Campbell CR1000 with AM 16/32 multiplexer was used.

Two test rounds were carried out (see Table 3). The stone walls were dried out for 3 days prior to the first test round at $+43\,°C$ and 11 days prior to the second round at $+30\,°C$. The first test round was carried out for 10 days. The second test round took 20 days.

5. Results and discussions

5.1. Density and thermal conductivity of insulation material

The density of the sample without lime is 65.09 kg/m^3 while the density for the sample treated with lime is 84.34 kg/m^3. Thermal conductivity of the sample without lime is 0.05 W/m/K and for the sample with lime it is slightly higher and is 0.053 W/m/K. The difference is 6% and can be caused by addition of lime. This results coincides with findings in other studies, e.g. the binder in hemp-lime material is the most thermally conductive component and if a binder content increases, thermal conductivity increases as well [54].

Thermal conductivity of the lime used for this study was not available from the producer. Research carried out by Ref. [46] shows that the thermal conductivity of lime can vary depending on the

origin of the rock and is between 1.1 and 1.7 W/m/K at ambient temperature.

### 5.2. Moisture absorption of insulation material

Results of moisture absorption kinetics test of pine needle insulation without lime, pine needle insulation treated with lime and vapor barrier are presented in Fig. 5. When the test starts, moisture is increasing with higher rate in both samples of insulation material than in sample with single vapor barrier. It slows down and after 24 h moisture growth rate of both pine needle insulation samples have reached the same growth rate as the sample with vapor barrier. Moisture growth rate is the highest in the sample with lime additive as lime increases the pore surface space area and thus increasing ability to bind more molecules of water vapor.

These findings correspond to findings by Ref. [15] that bio-based insulation materials have high Moisture Buffering Value and are rated as "excellent". Similar results were obtained for hemp-lime materials [17]. They found that application of lime plaster on top of hemp-lime does not have significant impact on the Moisture Buffer Value.

The moisture transport rate and amount of accumulated moisture depends on many factors, such as surrounding air parameters (temperature, pressure, and relative humidity), needle fiber parameters (size of fibers, fiber components, degree of needle fiber beating etc.), and lime (water/lime ratio that determines the porosity of the lime-needle material) [55–59]. However, many studies have found that cumulative pore volume and pore size distribution is among the most important factors affecting the water vapor transmission properties [60] and materials with higher cumulative pore volume has higher Moisture Buffering Value [61]. Materials with smaller pore diameter has higher surface of the porous space area and therefore, better capability to bind molecules

Table 3
Test conditions in the climate chamber.

Test conditions	Test 1	Test 2
Preconditioning period, days	3	11
Preconditioning temperature/relative humidity	$+43\,°C$	$+30\,°C$
Length of the test, days	10	20
Test conditions:		
Indoor temperature/relative humidity	Variable conditions	$+19.5\,°C$ to $+20.5\,°C/53–56\%$
Outdoor temperature/relative humidity	Variable conditions	$+2.5\,°C$ to $+3.5\,°C/80–90\%$
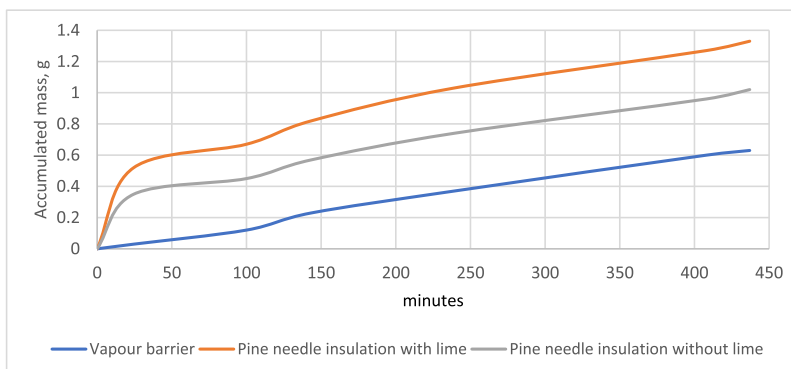
Fig. 5. Accumulated mass during adsorption test for three materials in minutes.

of water vapor and higher moisture buffering values [62–65].

5.3. Mold growth

Material treatments improved resistance to mold growth when compared to control (Fig. 6.), thus addition of lime has improved the mold resistance of the material, most likely through increased surface pH of the material which limits mold growth.

At 94% relative humidity material treated with lime performed better than material treated with lime and xanthan gum (Fig. 6.). This indicates that xanthan gum might promote mold growth even if used in miniscule concentrations.

After 4 month mold growth occurred on treated samples at 94% and 100% relative humidity (Fig. 6.), therefore critical moisture level of treated materials is somewhere between 85% and 94%. It has been previously observed for other building materials [53] that mold growth can occur later on, therefore longer test is required to more accurately determine the critical moisture level of this material.

Mold growth on samples without lime at 94% and 100% relative humidity was rated as 4 and on treated samples it was 2 and 3 (Fig. 7). Therefore, at 94% and 100% relative humidity all samples failed.

5.4. Hygrothermal behavior tests of the test wall

5.4.1. Steady state conditions test

Temperature and relative humidity behavior between stone walls and insulation materials treated and untreated with lime over time for the test with steady state conditions (Test 2) is presented in Fig. 8. Temperature decreases in both samples while relative

humidity increases. Temperature falls faster for the sample without lime and reaches equilibrium at lower value (+10.6 °C) compared to the sample with lime (+11.1 °C). The same trend is observed for relative humidity values as temperature changes correlate with relative humidity. Relative humidity for both samples reaches equilibrium at 100% which is critical moisture level for mold growth. The difference in equilibrium temperatures can be caused by different composition of both stone wall samples. The stone wall used for tests of needle insulation with lime has higher share of stones and is more homogenous while the other stone wall has higher share of lime mortar and is less homogenous. Another reason might be different sorption processes. Hygroscopic materials have ability to adsorb and desorb water vapor from the air. One of the most common is hygroscopic effects is physical adsorption when water vapor is adsorbed on both the surface of the masonry, and on the porous structure of the brick. During this process phase change of the vapor from gas to liquid and backwards happens and heat is released. The amount of energy released can be calculated in different ways, e.g. internal energy change, entropy and enthalpy. Moisture storage capacity has to be assessed by means of sorption isotherm. In dynamic system the moisture transport in the material also influences calculations. The sorption isotherm of used materials was not measured during this research and authors could not estimate impact of sorption processes on the temperature.

5.4.2. Variable conditions test

Temperature changes in both climate chambers and in both test walls (Test 1) are presented in Fig. 9. Outdoor temperature was kept at +2.5 °C for 46 h and then increased to +3.5 °C. Temperatures in both stone walls followed this trend with delay. After outdoor temperature was kept at +3.5 °C all temperatures in both test walls stabilized at equilibrium. Start conditions in both walls slightly differed at the beginning of the test and this difference can be observed throughout the test. High frequency variations of indoor and outdoor conditions are caused by the control system of climate chambers. The power of the cooling unit is too high and the air is cooled down very fast thus switching on and off very frequently.

Fig. 10. illustrates behavior of relative humidity in both climate chambers and within both test walls. Relative humidity was varied in outdoor chamber for the first 46 h and then kept constant for the rest of the test. The indoor relative humidity was changed during the length of the test. Results show that relative humidity inside the wall (both behind the gypsum board, and between insulation and the stone wall) follows the trend of indoor air relative humidity with delay. Although the start values of relative humidity for both insulation material samples differ, the insulation with and without
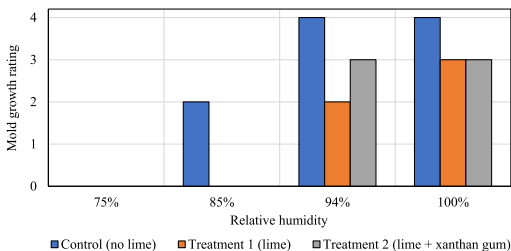

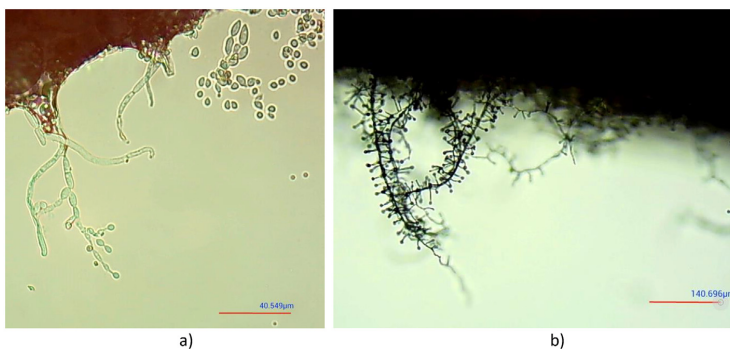**Fig. 6.** Mold growth on material samples at various relative humidity conditions.

Fig. 7. Mold growth on samples at 100% relative humidity: a) *Cladosporium* on surface of sample without lime; b) *Trichoderma viride* on surface of treated sample.
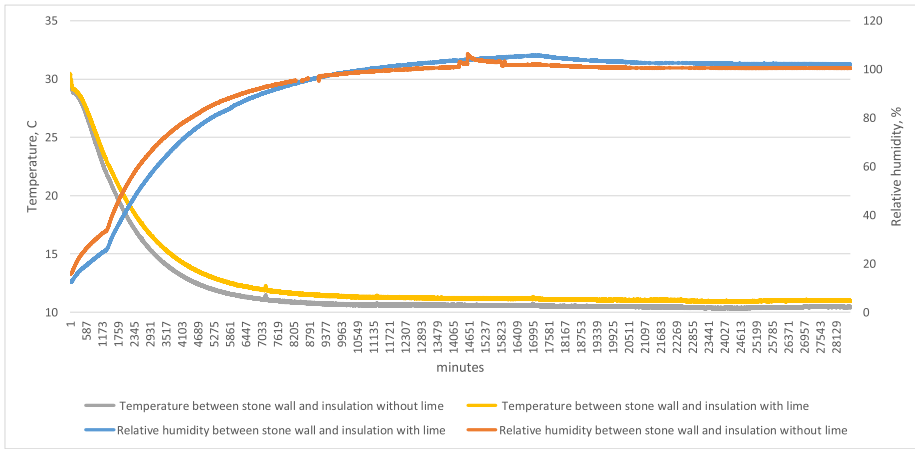
Fig. 8. Temperature and relative humidity between stone wall and insulation material during steady state test.
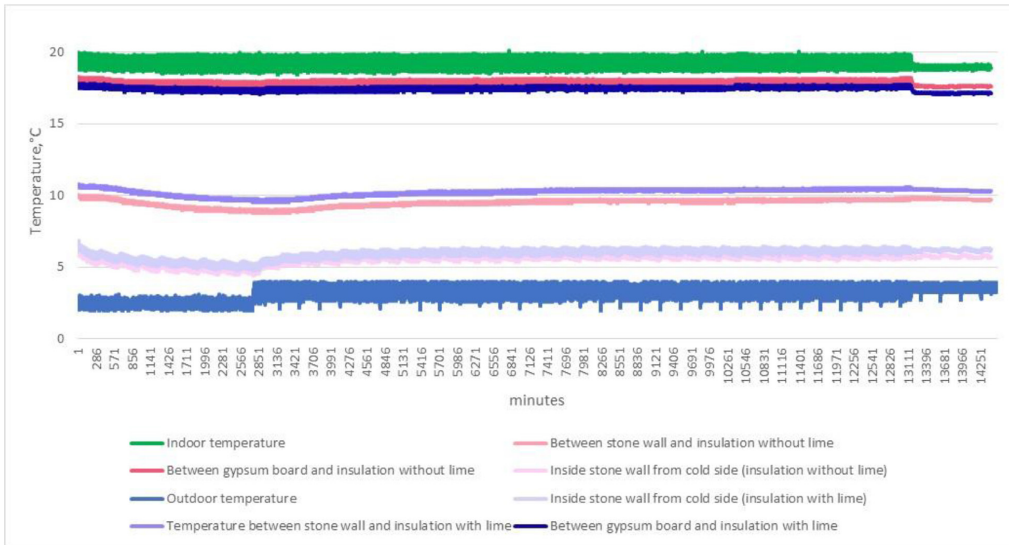
Fig. 9. Temperature during variable conditions test for both test walls.

lime display the same behavior and both samples react to changes in indoor relative humidity with slight delay. This behavior proves that needle insulation material has greater moisture buffering capacity even if it is covered with gypsum board. Both insulation samples are at higher relative moisture levels that can be critical for mold growth if no mold preventive material is applied.

Fig. 11 provides closer look on the behavior of relative humidity and temperature during variable conditions test between stone wall and needle insulation with and without lime. There is no correlation observed between temperature and relative humidity and the main driver for changes in relative humidity in the wall is indoor relative humidity due to high moisture absorption and desorption rates of pine needles and lime if added.

6. Conclusions

The main goal of this research is to assess applicability of innovative bio-based pine (Pinas Sylvestris) needles insulation material that is produced based on bioeconomy principles as internal insulation material for historic massive walls. The study was carried out to determine hygrothermal properties of needle insulation and to evaluate impact of temperature and relative humidity on moisture transport and accumulation, and critical conditions for mold growth. Needle insulation material was treated with lime to prevent mold growth and was compared with untreated material.

The novel bio-based insulation material was prepared based on bioeconomy principles and with reduced life cycle impact. High

Fig. 10. Relative humidity during variable conditions test for both test walls.

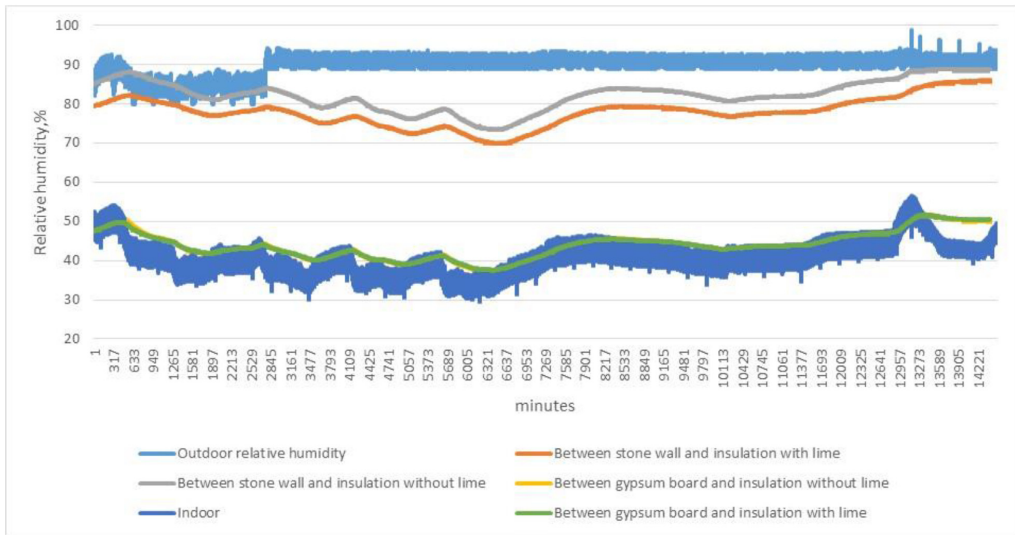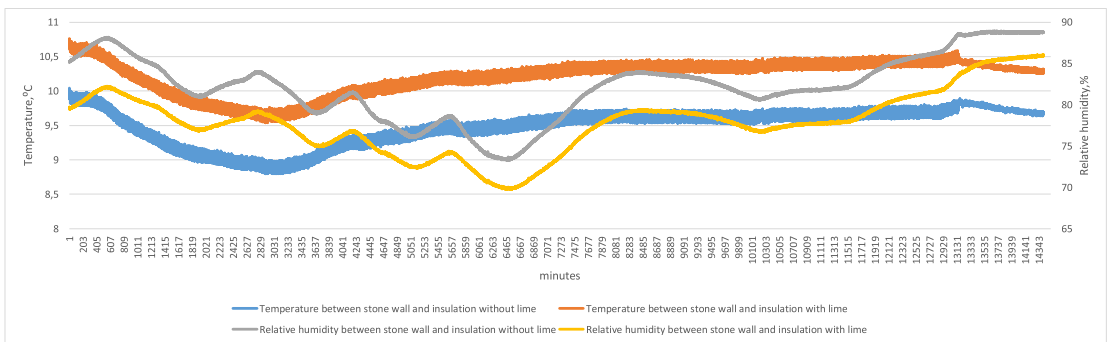**Fig. 11.** Relative humidity and temperature during variable conditions test between stone wall and needle insulation with and without lime.

added value product was created from pine needles from forest residues. They were mixed with lime and xanthan gum to avoid use of fossil based products with high environmental impact.

Obtained results show that studied material is highly porous and addition of lime increases moisture absorption rate of material due to increased area of pores. Needle insulation material has higher moisture transfer and storage capacity, and is good hygric regulator. This is important feature of insulation material used for internal insulation of historic buildings as it has ability to dry out quickly if relative humidity of surrounding air is reducing. Treatment of insulation material with lime has minor impact on thermal conductivity but has impact on mold growth reduction.

No mold growth for sample treated with lime was observed in 85% relative humidity while it was observed in 94% and 100% for all samples.

In steady state conditions lower temperatures leads to higher relative humidity level between the stone wall and needle insulation material and reaches critical value for mold growth. Variable condition test results show that the main driving force for relative humidity changes is indoor air relative humidity rather than temperature changes in the wall. Even if insulation material is treated with lime, heat savings have to be sacrificed to reduce critical conditions for mold growth.

Further research should focus on optimization of lime-insulation weight ratio to improve hygrothermal behavior and critical conditions for failure modes. In addition to that further tests to reduce compacting of the insulation material in the wall should be carried out. Other materials for reduction of dusting of lime should be tested.

Acknowledgements

References

[1] International Energy Agency. Modernising building energy codes. 2013.

[2] Lund H, Østergaard PA, Connolly D, Mathiesen BV. Smart energy and smart energy systems. Energy 2017;137:556–65.

[3] Lund H, Duic N, Ostergaar AP, Vad Mathiesen B. Future district heating systems and technologies: on the role of smart energy systems and 4th generation district heating. Energy 2018;165(A):614–9.

[4] Lund H, Ostergaar AP, Chang M, Werner S, Svendsen S, Sorknæs P, Thorsen JE, Hvelplund F, Mortensen BOG, Mathiesen B, Bojesen C, Duic N, Zhang X, Möller B. The status of 4th generation district heating: research and results. Energy 2018;164:147–59.

[5] Lund H, Ostregaard PA, Chang M, Werner S, Svendsen S, Sorknaes P, Thorsen JE, Hveplund F, Mortensen BOG, Mathiesen BV, Bojesen C, Duic N, Zhang X, Moller B. The status of 4th generation distric heating: research and results. Energy 2018;164:147–59.

[6] Andrič I, Fournier J, Lacarri B, Le Corre O, Ferrao P. The impact of global warming and building renovation measures on district heating system techno-economic parameters. Energy 2018;152:926–37.

[7] Ziemele J, Cilinskis E, Blumberga D. Pathway and restriction in district heating systems development towards 4th generation district heating. Energy 2018;152:108–18.

[8] Historical building types and combinations of structural solutions and main driving forces promoting renovation of historic buildings based on case studies. Report. EU project Robust Internal Thermal Insulation of Historic Buildings (RiBuild). 2015. project No. 637268.

[9] Hilber C, Palmer C, Pinchback EW. The costs of historic preservation. SERC Discussion Paper 217; 2017.

[10] Asdrubali F, D'Alessandro F, Schiavoni S. A review of unconventional sustainable building insulation materials. Sustainable Materials and Technologies 2015;4:1–17.

[11] Palumbo M, Lacasta AM, Giraldo MP, Haurie L, Correal E. Bio-based insulation materials and their hygrothermal performance in a building envelope system (ETICS). Energy Build 2018;174:147–55.

[12] Schiavoni S, D'Alessandro F, Bianchi F, Asdrubali F. Insulation materials for the building sector: a review and comparative analysis. Renew Sustain Energy Rev 2016;62:988–1011.

[13] European Comission. A sustainable bioeconomy for Europe: strengthening the connection between economy, society and the environment. Updated Bioeconomy Strategy; 2018.

[14] Rode C, editor. Moisture buffering of building materials. Department of Civil Engineering, Technical University of Denmark; 2005. Report R-126.

[15] Rode C, Peuhkuri R, Time B, Svennberg K, Ojanen T. Moisture buffer value of building materials. J ASTM Int (JAI) 2007;4(5):1–12.

[16] Lawrence M, Jiang Y. Bio-aggregates based building materials. Springer; 2017.

[17] Latif E, Lawrence K, Shea A, Walker P. Moisture buffer potential of experimental wall assemblies incorporating formulated hemp-lime. Build Environ 2015;93(P2):199–209.

[18] Latif E, Lawrence RMH, Shea AD, Walker P. An experimental investigation into the comparative hygrothermal performance of wall panels incorporating wood fibre, mineral wool and hemp-lime. Energy Build 2018;165:76–91.

[19] Polis O, Korica A, Daugavietis M. Bioloģiski aktīvo savienojumu saglabāšanās egles zaļenā uzglabāšanas procesā. Mežzinātne 2009;19(52):82–90.

[20] Daberte I, Barene I, Rubens J, Daugavietis M. Producing and determination of qualitative indices of ordinary pine needles thick extract. Eur J Pharm Sci 2007;32:S32–3.

[21] Hoai NT, Duc HV, Thao DT, Orav A, Raal A. Selectivity of Pinus sylvestris extract and essential oil to estrogen-dependent breast cancer cells Pinus sylvestris against cancer cells. Pharmacogn Mag 2015;11/2:290–5.

[22] Kelkar VM, Geils BW, Becker DR, Overby ST, Neary DG. How to recover more value from small pine trees:Essential oils and resins. Biomass Bioenergy 2006;30:316–20.

[23] Zeng WC, Zhang Z, Jia LR. Antioxidant activity and characterization of antioxidant. Carbohydr Polym 2014;108:58–64.

[24] Wu JP, Liang X, Liu XY, Zhong K, Gao B, Huang YN, Goa H. Cedrus deodara pine needle as a potential source of natural antioxidants: bioactive constituents and antioxidant activities. Journal of functional foods 2015;14:605–12.

[25] Tripathi AK, Kumari M, Kumar A, Kumar S. Generation of biogas using pine needles as substrate in domestic biogas plant. Int J Renew Energy Resour 2015;5(3):716–21.

[26] Xiao S, Gao R, Lu Y, Jian Li J, Qingfeng Sun. Fabrication and characterization of nanofibrillated cellulose and its. Carbohydr Polym 2015;119:202–9.

[27] Assefi M, Davar F, Hadadzadeh H. Green synthesis of nanosilica by thermal decomposition of pine cones. Adv Powder Technol 2015;26:1583–9.

[28] Kumar R, Singh RI. An investigation in 20 kWth oxygen-enriched bubbling fluidized bed. Fuel Process Technol 2016;148:256–68.

[29] Sharma N, Mahajan S, Sharma N. Evaluation of different forest wastes of Northern Himalayas. Journal of Agroalimentary Processes and Technologies 2012;18(4):324–35.

[30] Lal PS, Sharma A, Bist V. Pine needle - an evaluation of pulp and paper making potential. J For Prod Ind 2013;2(3):42–7.

[31] Nemli G, Aydin A. Evaluation of the physical and mechanical properties of particleboard made from the needle litter of Pinus pinaster Ait. Ind Crops Prod 2007;26:252–8.

[32] Nemli G, Yildiz S, Gezer ED. The potential for using the needle litter of Scotch pine (Pinus sylvestris L.) as a raw material for particleboard manufacturing. Bioresour Technol 2008;99:6054–8.

[33] Dong C, Parsons D, Davies JI. Tensile strength of pine needles and their feasibility as reinforcement in composite materials. J Mater Sci 2014;49: 8057–62.

[34] Chauhan M, Gupta M, Sungh B, Singh AK, Gupta VK. Pine needle/isocyanate composites: dimensional stability, biological resistance, flammability, and thermoacoustic characteristics. Polym Compos 2012:324–35.

[35] Bhandari L, Upadhyay CS, Mohite PM, Gupta Anirudh, Sarkar SC, Singh Panwar Vipin. Tensile test on pine needles and crack analysis of pine needles short fiber reinforced composites. Journal of Mechanical and Civil Engineering 2015;5:1–8.

[36] Berry J.B. Process of making pine-needle fiber. USA Patents US437555A, 1890.

[37] Chauhan M, Gupta M, Singh B, Bhattacharyya SK, Singh AK, Gupta VK. Pre-treatment of pine needles/wood particles and their composites with isocyanate prepolymer adhesive. Polym Eng Sci 2010;53/8.

[38] Material monday on scent in spaces - special edition: festive pines. Available: http://nirvanacph.com/2017/12/material-monday-scent-spaces-special-edition-festive-pines/. [Accessed 17 December 2018].

[39] Muizniece I, Blumberga D, Ansone A. The use of coniferous greenery for heat insulation material production. Energy Procedia 2015;72:209–15.

[40] Muizniece I, Lauka D, Blumberga D. Thermal conductivity of freely patterned pine and spruce needles. Energy Procedia 2015;72:256–62.

[41] Muizniece I, Vilcane L, Blumberga D. Laboratory research of granular heat insulation material from coniferous forestry residue. Agron Res 2015;13(2): 690–9.

[42] Muizniece I, Blumberga D. Thermal conductivity of heat insulation material made from coniferous needles with potato starch binder. Energy Procedia 2016;95:324–9.

[43] Kubinova Z, Janacek J, Lhatakova Z, Sprtova M, Kubinova L, Albrechtova J. Norway spruce needle size and cross section shape variability induced by irradiance on a macro- and microscale and CO2 concentration. Trees (Berl) 2018;32:231–44.

[44] Kozlov MV, Niemela P. Difference in needle length – a new and objective indicator of pollution impact on Scots pine (Pinus sylvestris). Water Air Soil Pollut 1999;116:365–70.

[45] Makarenko ES, Oudalova AA, Geraskin SA. Study of needle morphometric indices in Scots pine in the remote period after the Chernobyl accident. Radioprotection 2016;51(1):19–23.

[46] Ross J, Kellomaki S, Oker-Blom P, Ross V, Vilikainen L. Architecture of Scots pine crown: phytometrical characteristics of needles and shoots. Silva Fenn 1986;20(2):91–105.

[47] ISO 8301:2012. Thermal insulation — Determination of steady-state thermal resistance and related properties — Heat flow meter apparatus.

[48] LVS CENTS 14774-3. Solid biofuels – methods for the determination of moisture content; Oven dry method – Part 3: Moisture in general analysis sample.

[49] BS EN 1602. Thermal insulating products for building applications. Determination of the apparent density 2013.

[50] ISO 12572. Hygrothermal performance of building materials and products - Determination of water vapour transmission properties - Cup method. Annex B Methods suitable for loose fills 2016.

[51] Mahuku GS, Goodwin PH. Influence of sucrose, mucin and xanthan gum on spore germination of ten different fungi. Eur J Plant Pathol 1998;104(8): 849–52.

[52] Hyvärinen A, Meklin T, Vepsäläinen A, Nevalainen A. Fungi and actinobacteria in moisture-damaged building materials: concentrations and diversity. Int Biodeterior Biodegrad 2002:27–37.

[53] Andersen B, Frisvad JC, Søndergaard I, Rasmussen IS, Larsen LS. Associations between fungal species and water-damaged building materials. Appl Environ Microbiol 2011;77:4180–8.

[54] Johansson P, Ekstrand-Tobin A, Svensson T, Bok G. Laboratory study to determine the critical moisture level for mould growth on building materials. Int Biodeterior Biodegrad 2012;73:23–32.

[55] Walker R, Pavia S. Moisture transfer and thermal properties of hemp–lime concretes. Constr Build Mater 2014;64:270–6.

[56] Sandaka G, Al- Karawi J, Specht E, Silva M. Thermophysical properties of lime as a function of origin (Part 4): thermal conductivity. Cement, lime, gypsum: ZKG international - Gütersloh: Bauverl. BV, Bd. 2017;52(1):36–41.

[57] Thomson ML, Lindqvist J-E, Elsen J, Groot CJWP. Porosity of historic mortars. In: 13th international brick and block masonry conference Amsterdam; 2004. July 4-7.

[58] Češek B, Milichovský M, Potůček F. Kinetics of vapour diffusion and condensation in natural porous cellulosic fibre. ISRN Mate Sci 2011;2011:794306.

[59] Rode C, Grau K. Moisture buffering and its consequence in whole building hygrothermal modeling. J Build Phys 2008;38:333–60.

[60] Wu Y, Gong G, Yu CW, Huang Z. Proposing ultimate moisture buffering value (UMBV) for characterization of composite porous mortars. Constr Build Mater 2015;82:81–8.

[61] Collet F, Pretot S. Experimental investigation of moisture buffering capacity of sprayed hemp concrete. Constr Build Mater 2012;36:58–65.

[62] Polat R, Demirboga R, Karakoç MB, Turkmen I. The influence of lightweight aggregate on the physico-mechanical properties of concrete exposed to freeze-thaw cycles. Cold Reg Sci Technol 2010;60:51–6.

[63] Janssen H, Roels S. Qualitative and quantitative assessment of interior moisture buffering by enclosures. Energy Build 2009;41:382−94.
[64] Yang L, Fazio P, Rao J. An investigation of moisture buffering performance of wood paneling at room level and its buffering effect on a test room. Build Environ 2012;47:205−16.
[65] Fořt J, Doleželová M, Černý R. Moisture buffering potential of plasters for energy efficiency in modern buildings. In: Environmental engineering 10th international conference. Lithuania: Vilnius Gediminas Technical University; 2017. 27−28 April.

energies

Article

Hygrothermal Performance Evaluation of Internally Insulated Historic Stone Building in a Cold Climate

Andra Blumberga [ID], Ritvars Freimanis [ID], Edite Biseniece and Agris Kamenders *[ID]

Institute of Energy Systems and Environment, Riga Technical University, Azenes 12/1, LV-1048 Riga, Latvia; andra.blumberga@rtu.lv (A.B.); ritvars.freimanis@rtu.lv (R.F.); edite.biseniece@rtu.lv (E.B.)
* Correspondence: agris.kamenders@rtu.lv; Tel.: +371-2951-6506

Abstract: In most cases, internal insulation is the only solution to improve the energy efficiency of historic buildings. However, it is one of the most challenging and complex energy efficiency measures due to changes in boundary conditions and hygrothermal behavior of the wall, particularly in cold climates. This study presents the long-term monitoring of the hygrothermal performance of an internally insulated historic stone wall building. The study aimed to assess the hygrothermal behavior of the dolomite wall if mineral wool insulation is applied internally on the north-east wall in the rooms with and without high internal moisture load. The measurements included temperature, relative humidity, water content, and heat flux. Monitoring results are compared with 1D hygrothermal simulations and a building energy consumption simulation. The in situ measurement results and hygrothermal assessment shows energy consumption decreased by 55% with relative humidity under the insulation staying belove 60% for most of the time, with short periods of increase over 80%. Energy consumption simulation shows an energy saving potential of up to 72% in the case of proper energy management.

1. Introduction

The European Commission has set a target to reduce 40% of greenhouse gas emissions by 2030 [1]. It also aims to be climate neutral by 2050, in line with the objectives of the Paris Agreement [2]. The building sector is Europe's single largest energy consumer, accounting for 40% of EU energy consumption and 36% of greenhouse gas emissions [3]. Space heating takes a 67% share of the end-use in the residential sector [4].

A significant renovation of existing buildings, regardless of their size or retrofit of building elements, provides the opportunity to take a cost-effective measure to improve the energy performance of the existing building stock. According to the European Commission, the annual renovation rate of the building stock varies from 0.4 to 1.2% in the Member States. However, this rate will need to at least double if targets set by the European Commission are to be met [5]. Moreover, a life cycle cost analysis [6] shows that costs are higher for the demolition and rebuilding of older dwellings compared to retrofitting to the same energy standards without even considering the apparent increase in emissions associated with demolition and rebuilding [7,8].

More than 40% of European residential buildings were built before 1960 [9], and many of these buildings are considered to have cultural heritage value. These buildings were built when energy efficiency requirements were non-existing or non-demanding, and most of these buildings will still be actively used in 2050 [10]. The most significant challenges of the renovation of buildings occur in retrofitting heritage buildings where the facade cannot be modified as the building's unique architectural appearance, and integrity

needs to be maintained [11–13]. In addition, it is hard to evaluate the building's energy performance, as the technical documentation of old buildings often needs to provide adequate documentation of the present conditions or is not available at all [14]. For example, data from 2011 show that in Latvia, annual heating energy consumption in historical buildings (built before 1945) is estimated at approximately 31% of the total final heating energy consumed by residential and non-residential building sectors [15].

The most common approach to improve the buildings' thermal performance is installing external insulation on walls, window replacement, and insulation of basement ceilings and the building's roof [16–19]. Implemented simultaneously, these are by far the most efficient measures [20,21]. However, for buildings with historically valuable facades, only a few of these measures can be applied, such as insulation of the basement and roof, which alone do not produce the desired energy savings. In these cases, external insulation is not an option as it covers the historical heritage of the facade. The only other option is internal insulation of the walls, which allows reducing a building's operational energy and its associated negative impact on the environment [22,23].

Internal insulation, however, changes the hygrothermal conditions of the building envelope. This may negatively impact the hygrothermal performance of the building's wall [13,24,25]. Moisture control of the walls is different in modern buildings and historic buildings. Modern buildings protect external walls from impermeable membranes, wall cavities, and damp-proofing. In historic buildings, walls are built from locally sourced heterogeneous materials, using traditional craftsmen methods, controlling moisture by allowing the building fabric to wet and subsequently dry through materials and assemblies that both adsorb moisture and allow it to evaporate quickly [26]. If internal insulation is applied, the original wall remains on the structure's cold side, which reduces any potential drying of the wall. Hence, internal insulation may increase the risk of interstitial condensation, frost damage, decay of embedded wooden beams, and mold growth [25,27–33]. Moreover, internal insulation does not eliminate thermal bridges [23,34].

Water transport properties and anisotropy depend on a material's porosity, pore structure, textural characteristics, and mineralogy [35]. One of the stones used in historic buildings is dolomite rock or dolostone. It is a sedimentary carbonate rock with a high percentage of the mineral dolomite. These stones have been used as building materials for centuries because they are easy to work with, are easily accessible, and have a high aesthetic value at a relatively low cost [36]. Different studies have investigated the use of dolomite rock as a construction product in historic buildings, their decay, and conservation treatments [35,37–39]. Numerous papers report in situ heat transfer and moisture transport measurements in internally insulated masonry walls, both successful and unsuccessful examples. One study reports the flawless hygrothermal performance of an internally insulated 19th Century brick building in Prague that was insulated using hydrophilic mineral wool without a vapor barrier; during the 4-year in situ study, there was no interstitial water condensation [40]. Another study was carried out for internally insulated brick walls with different insulation materials (calcium silicate (CaSi), aerated concrete (AAC), polyurethane board with active capillary channels (IQ-T), and polyisocyanurate (PIR)); in the study, they found that IQ-T and PIR were performing similar regardless the capillary activity of IQ-T, both had high relative humidity (over 80%) under the insulation, CaSi and AAC showed a similar pattern of RH behind the insulation. CaSi maintained an Rh under 80%, while AAC exceeded 90%, but as mentioned by the authors, the hygrothermal performance of an insulated wall only partially depends on insulation material, properties, and thickness of the original wall, which also influences the performance and the built-in moisture [41]. Moreover, a holistic energy renovation (moisture safety and energy efficiency are balanced) approach has been studied, and 47% energy reduction was achieved in the case study building; in this study, one of the main conclusions was that a more detailed study over a longer period is necessary to decrease the uncertainty of results [31]. In a study about the rehabilitation of historical façade buildings, the full utility of AAC as internal insulation was confirmed, and the authors pointed out the important role of simulations

in predicting the long-term hygrothermal state of the internally insulated buildings [42]. One of the leading research institutes of the Technical University of Denmark performed hygrothermal measurement in four case-study buildings with different internal insulation materials, they concluded that vapor-open insulation systems overall performs better than vapor-tight systems, but they also concluded that other parameters, such as insulation thickness, surface treatment, and the external hygrothermal loads, have a high impact on the performance [43]. Moreover, our research institute has a previous experience in this field of study [44].

However, reviewing the research papers demonstrated a need for more research on hygrothermal performance and energy savings of internally insulated dolomite stone buildings.

This study aims to answer the following two research questions: (1) What is the impact of internally insulated natural stone buildings on the hygrothermal behavior of walls in a cold climate? (2) What energy savings can be reached by internal insulation of natural stone buildings in a cold climate? In comparison to existing research papers in our research, we monitored on-site indoor and outdoor climate, including solar radiation, and in addition to the relative humidity and temperature measurements in between the layers of internal insulation, we monitored volumetric moisture content of the external wall and performed mathematical simulations of the monitored building.

The paper starts with an introduction, followed by a description of the case study building, applied methodology, analysis of results, discussion, and finally, conclusions.

2. Case Study Building

2.1. Background Information

The case study building is a single-family home in the countryside in Sece parish, Aizkraukle county, Latvia. It was built in 1893 as a farmhouse. During the period after the second world war until the 21st century, the building was poorly maintained; the basement was used as a cattle shed which led to severe damage to the wooden beams and ground floor cover. In 1992, the building was denationalized, and the ownership of the building was retrieved by the family of the building's original owner.

The building has two floors with a total heated area of 339 m^2 and a volume of 870 m^3. The basement (floor area 68 m^2 and volume 130 m^3) occupies half of the building's floor area on the south-east façade and is not heated. The facade has a total area of 274 m^2, including windows and doors but excluding the basement part.

The external walls are constructed from locally sourced dolomite stone embedded in mortar. For basement walls, granite stones are used as well. Granite chips are also used to cover mortar joints between dolomite stones (Figure 1).
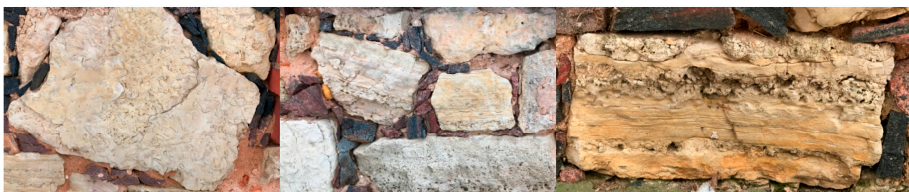
Figure 1. Structural patterns of dolomite stones in the external wall of the building.

The walls have a thickness of 0.60 m (ground floor and basement) and 0.45 m (1st floor). Brick columns are built in the corners and around the windows as a frame. The interior side of the external walls has an originally installed plaster layer. In 2006, after full-scale roof reconstruction, two dormers were added on the west and east sides of the house (see Figure 2).
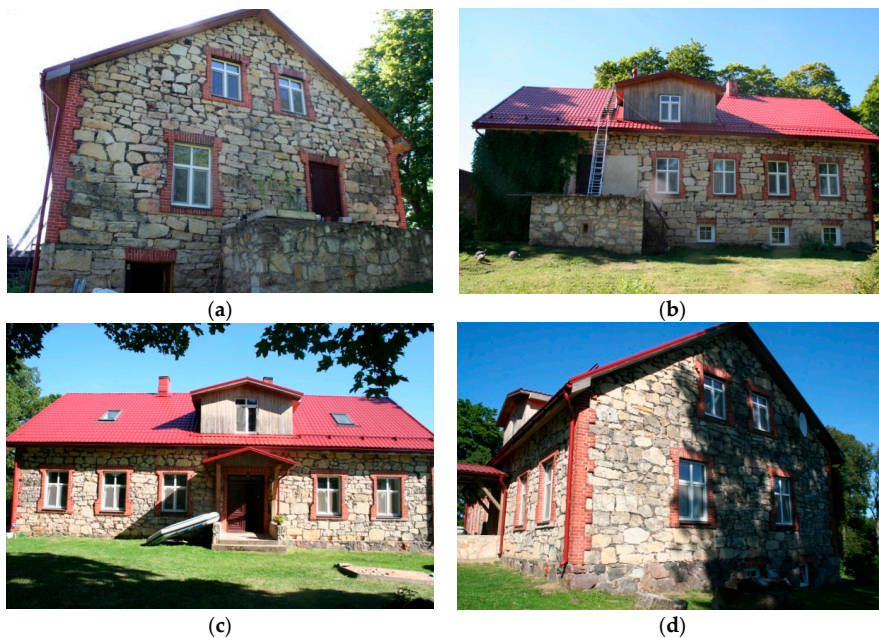
Figure 2. Facades of the case study building: (**a**) north-east, (**b**) south-east, (**c**) north-west, (**d**) south-west.

2.2. Energy Efficiency Measures

Two rounds of energy efficiency renovation were made. The main goal of both renovations was to decrease firewood consumption by decreasing heat loss through the building envelope. In 2006, the following measures were carried out:

- Internal insulation of the building walls on the ground and first floor with 0.15 m of mineral wool and installation of Ruberoid as a vapor barrier between the dolomite and insulation (moisture diffusion resistance equivalent of still air (Sd) = 15 m)
- Insulation of the basement ceiling with 0.25 m of expanded clay;
- Insulation of the roof with 0.30 m of mineral wool;
- Change of windows (U = 1.26 W/m^{2}K);
- Installation of wood boiler and water heating system with radiators;
- Installation of a hot water supply with a heat accumulation tank;
- Installment of cold water supply and sewage system.

Nine years later, based on the building residents' observations, the ground floor premises seemed colder, and firewood consumption had increased compared to the situation before the first round of the renovation. In 2015, the walls and floors of the ground floor rooms occupied all year were inspected (see Figure 3). The inspection revealed that the mineral wool was heavily inhabited by martens and rats, which had created a system of burrows within the walls. It was also discovered that in the bathroom located in the north corner of the building (see Figure 3, red line), the dolomite stone walls behind the mineral wool were covered with a black layer of mold. In 2015, the second round of renovation was carried out, and the old insulation was replaced with a new internal insulation system:
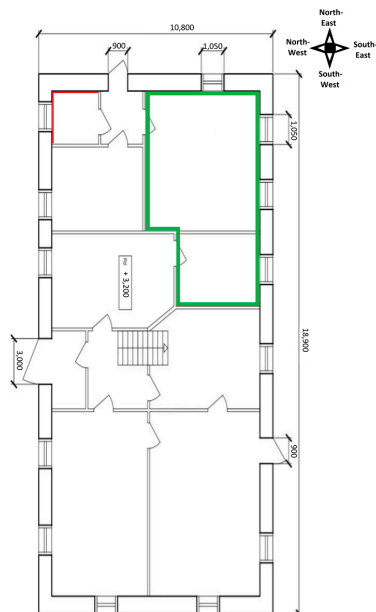
Figure 3. Inspected insulation on the ground floor in 2015: damaged floor and external wall insulation by martens (green) and a black layer of mold between the dolomite stone wall and mineral wool (red).

Insulation of the basement ceiling with expanded clay (0.25 m, λ = 0.11 W/mK) in the green part in Figure 3.

Mineral wool insulation (0.15 m in the rooms and 0.2 m in the bathroom, λ = 0.04 W/mK) in combination with an expanded clay layer (0.15 m thickness, 0.2 m from the ground) in both the green and red parts in Figure 3.

The vapor barrier was installed between mineral wool and plasterboard.

The cross-section of the living room's wall and the floor is presented in Figure 4.
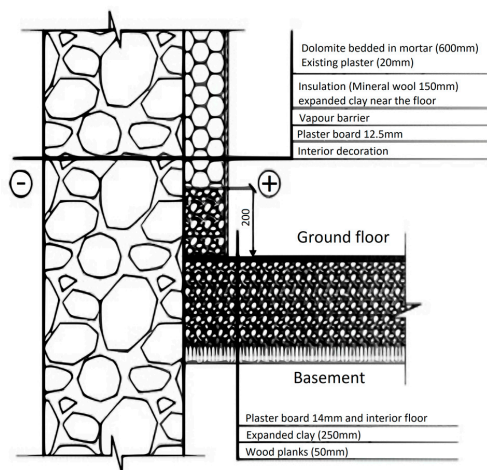
Figure 4. The cross-section of the living room's wall and floor construction after renovation in 2015.

After the renovation in 2015, external walls were divided into four types (see Figure 5).
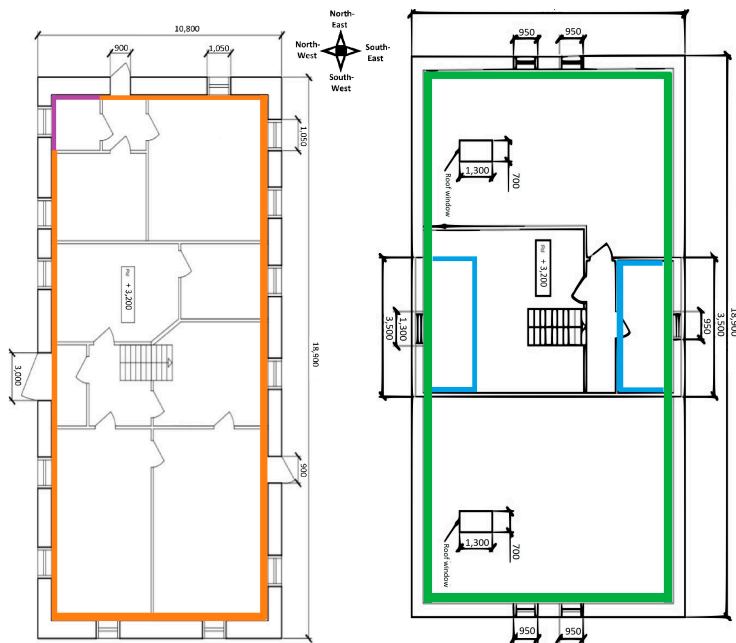
Figure 5. Location of four wall construction types in zones A2 after renovation in 2015, on the left 1st floor, on the right 2nd floor: type 1(purple), type 2 (orange), type 3 (green), and type 4 (blue).

Tables 1–4 contain detailed information about the different types of external walls.

Table 1. Facade construction after retrofit in 2015: Type 1.

Material	Thickness (mm)	Thermal Conductivity (λ, W/mK)	Density (kg/m³)	Area (m²)	Heat Transfer Coefficient (U, W/m²K)
Dolomite	600	2.2	2400		
Existing plaster	20	0.87	1800		
Mineral wool	200	0.035	60	149.54	0.208
Vapor barrier					
Plasterboard	12.5	0.21	680		
Interior decoration					

Table 2. Facade construction after retrofit in 2015: Type 2.

Material	Thickness (mm)	Thermal Conductivity (λ, W/mK)	Density (kg/m³)	Area (m²)	Heat Transfer Coefficient (U, W/m²K)
Dolomite	600	2.2	2400		
Existing plaster	20	0.87	1800		
Mineral wool	150	0.035	60	149.54	0.211
Vapor barrier					
Plasterboard	12.5	0.21	680		
Interior decoration—painted wallpaper					

Table 3. Facade construction after retrofit in 2015: Type 3.

Material	Thickness (mm)	Thermal Conductivity (λ, W/mK)	Density (kg/m^3)	Area (m^2)	Heat Transfer Coefficient (U, W/m^{2}K)
Dolomite	450	2.2	2400		
Existing plaster	20	0.87	1800		
Mineral wool	150	0.035	60	29.62	0.212
Vapor barrier					
Plasterboard	12.5	0.21	680		
Interior decoration—painted wallpaper					

Table 4. Facade construction after retrofit in 2015: Type 4.

Material	Thickness (mm)	Thermal Conductivity (λ, W/mK)	Density (kg/m^3)	Area (m^2)	Heat Transfer Coefficient (U, W/m^{2}K)
Wood planks	25	0.2			
Mineral wool	150	0.035	60		
Vapor barrier				22.78	0.215
Plasterboard	12.5	0.21	680		
Interior decoration—painted wallpaper					

2.3. Energy Consumption

The building has a central heating system with a 40 kW firewood boiler integrated with a hot water storage tank. There are no mechanical ventilation or air conditioning units used in the building. The building has a natural ventilation system with air exchange through the building envelope. Room temperature can be regulated based on the occupancy with radiator thermostats. Residents maintain the comfort temperature of +20 °C in the inhabited rooms while reducing the temperature in rooms that are not occupied. The north-east side of the ground floor is occupied all year; the rest of the building is inhabited only on weekends, holidays, and during the summer.

3. Research Methodology

3.1. Construction Material Analysis

Dolomite stones used in the building have different structural patterns (see Figure 1). The study on lithological morphological types of dolomite historically used for the construction of stone buildings in Latvia predominantly is mechanically resistant marble-like dolomite [45]. Dolomite samples from the building were obtained and tested in the laboratory of the Riga Technical University to determine their main properties—density, specific heat capacity, thermal conductivity, total porosity, capillary saturation, water vapor resistance factor, water uptake coefficient, and moisture storage. These values were further used as input data to characterize the material's properties in the simulation program DELPHIN [46].

Laboratory data were determined through a series of tests. Depending on the test, three to twenty-two specimens were prepared (cut, pre-conditioned) to obtain information on the properties' variance and minimize irregularity effects. In addition to the standard test methods [47–51], other methods [52,53] were also used. The test methods are summarized in Table 5.

Table 5. Test methods for the properties of the dolomite stone.

Name of the Material Property	Name of the Corresponding Experiment
Bulk density	Via dimensions and weight of the sample [41]
Open porosity	Calculated from density [48,52]
Thermal conductivity	Heat flux measurement (plate apparatus) [52]
Heat storage capacity	Calorimeter experiment [52]
Dry-cup vapor diffusion	μ dry-cup measurement [49]
Wet-cup vapor diffusion	μ wet-cup measurement [49]
Water uptake coefficient	Water uptake experiment [51]
Capillary saturation moisture content	The final value of the water uptake experiment [52]
Sorption moisture content	Exicator/desiccator [52]

3.2. Energy Consumption Simulation

The dynamic simulation tool TRNSYS Type 56 (2016) [54] was used to calculate the building's energy balance. For the simulation, the building was divided into zones A1—basement and A2—above-ground floors (See Figure 5). The primary input data are shown in Table 6.

Table 6. Main input data about the case study building.

|	Orientation				Heat Transfer Coefficient U, W/m^{2}K	
	North	**East**	**West**	**South**	**Before Renovation**	**After Renovation**
Facade walls (m^2)						
Basement	9.14	18.9	-	5.08	2.259	2.259
Basement in contact with soil	-	15.12	34.02	4.06		
Ground floor	32.4	56.7	56.7	32.4	2.147	0.208
1st floor (3rd type)	17.28	-	-	17.28	2.515	0.211
1st floor (4th type)	4.32	8.47	8.47	4.32	-	0.215
Windows (m^2)						
Basement	-	1.68	-	1.12	2.83	2.83
Ground floor	1.68	8.4	8.4	3.36	2.83	1.26
1st floor (3rd type)	2.47	-	-	2.47	2.83	1.26
1st floor (4th type)	-	1.24	1.57	-	-	1.26
Doors (m^2)						
Basement	1.44	-	-	-	2.83	2.83
Ground floor	1.98	1.98	2.86	-	2.83	2.83
Floor area on the ground		108.11			2.395	2.395
Basement ceiling		96.01			0.668	0.34
Roof area	-	141.4	141.4	-	1.087	0.110

Three scenarios were simulated:

- The baseline: the building before both renovations;
- The building with internal insulation on the walls of the ground and 1st floor;

- The building with additional energy-saving measures (insulation of basement ceiling and roof, replacement of windows).

The simulations for all scenarios were based on the following assumptions: (1) climatic data of Latvia defined by the software used as an input file in the TRNSYS were used; (2) indoor temperature +20 °C in zone A2 when the building is in use, e.g., workdays in the morning (6 am to 8 am) and in the evening (4 pm to 11 pm) and full days on weekends, and +18 °C the rest of the time; (3) indoor relative humidity 50%; (4) infiltration 0.05 h^{-1}, with additional natural ventilation during the opening of windows for zone A2—0.5 h^{-1}; (5) heat gains are based on values defined in EN ISO 13790:2008 [55], all heat gains are scheduled.

3.3. In Situ Measurements

In December 2017, temperature, relative humidity, volumetric water content, and heat flux sensors were installed within the external walls on the north-east facade. One set of sensors was installed in the living room wall, and the other in the bathroom wall (see Figure 6b). Both walls were retrofitted in 2015. Additionally, the pyranometer Campbell CMP3 060271 with sensitivity 11.72 $\times$ 10^{-6} V/Wm^{-2} was installed on the north-east facade. Figure 6 shows the sensors' setup and their connections to the data loggers used in the setup. The setup of sensors is the same for the living room and bathroom, except for the solar radiation sensor. One solar radiation sensor was installed 5 m from the ground level. Indoor temperature measurements were performed by twisted pair T-type thermocouples—Labfacility XE-2342. Temperature sensor t1 measures the temperature between the dolomite wall and the insulation layer, and t2 measures the temperature between the insulation layer and the vapor barrier (see Figure 6a). These sensors were installed at the 1.8 m height from the floor, corresponding to 4 m from the ground level. RH1-2 measures relative humidity at the same places as temperature sensors. Honeywell HIH-4000-002 measures RH had an accuracy of ±3.5%. Heat flow in walls was measured with Hukseflux heat flux sensors. Volumetric water content is measured using the time domain (TDR) reflectometer Campbell CR616, with an accuracy of ±2.5% of volumetric water content (VWC) and operational temperature from 0 to 70 °C. The CR616 has been installed 3.5 m from the ground level.
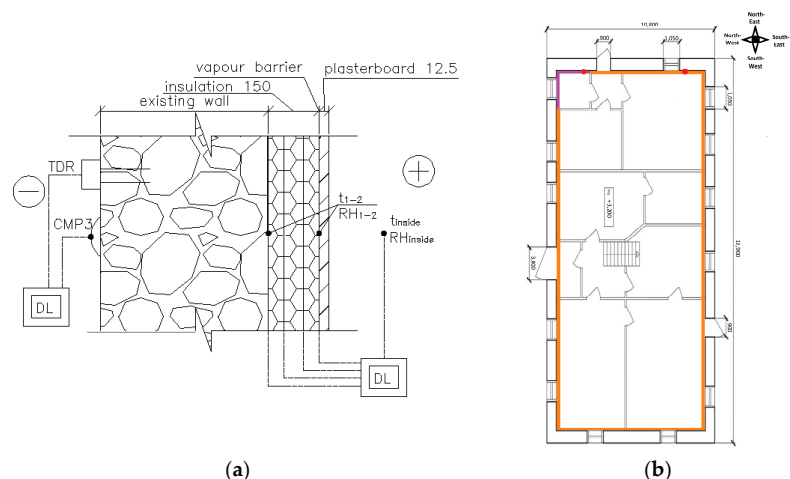
Figure 6. (**a**) Measurement setup (t—temperature; RH—relative humidity; CMP3—sun radiation, DL—data logger, TDR—volumetric water content.); (**b**) Measurement points: heat flow, temperature, and relative humidity sensors in the walls (the red dots).

Before installation, CR616 rods were shortened from the original 16 cm length to 10 cm length (due to restriction in drilling depth). Therefore, these sensors were recalibrated

afterward by using a sample dolomite stone from the case study building. During the calibration, the water-saturated dolomite sample mass and readings of the CR616 sensor were monitored. Based on that, a graph of water content vs. response time of the CR616 sensor specifically for dolomite stone was obtained (see Figure 7).
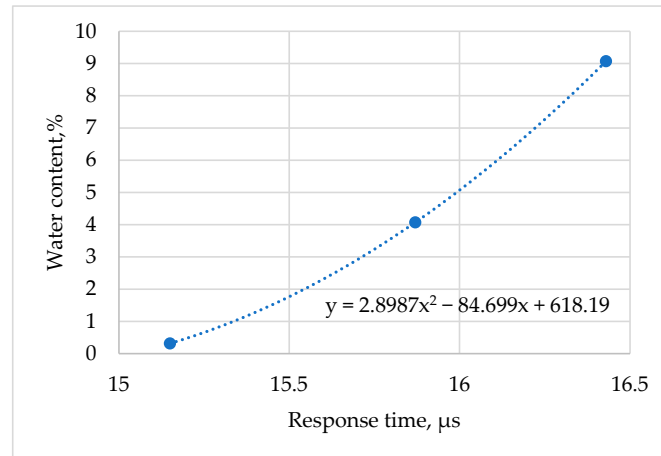
Figure 7. Calibration graph for TDR sensors.

Three data loggers were used for data logging: two Campbell Scientific CR1000 data loggers (one in the living room, one in the bathroom); one Campbell Scientific CR800 data logger (outside). A time step of 30 min for all measurements was taken. Data from data loggers were periodically collected.

3.4. Hygrothermal Calculations

The simulation tool DELPHIN 6.1. [46] and Glazer method was used to evaluate the hygrothermal behavior of the building's external walls with internal insulation. DELPHIN software is a simulation program for homogeneous layers to simulate heat and moisture mass transport and storage within the materials. The Glazer method is used for determining the conditions within the different layers of the wall at specific indoor and outdoor conditions. The simulation used climatic data entered by the software user. For indoor boundary conditions (temperature and relative humidity), data gained from in situ measurements were used. Weather data, such as outdoor temperature, relative humidity, wind speed and direction, hourly rain sum, and air pressure, were taken from weather station Skrīveri, located 20 km from the case study building, while sun radiation data were taken from the weather station Rīga—Universitāte located 100 km from the case study building. Both weather stations are operated by the state limited liability company "Latvian Environment, Geology and Meteorology Centre" (LEGMC) [56].

Material properties for plasterboard and mineral wool were imported from the DELPHIN material database. A vapor barrier was added as the resistance between material layers (sd = 2.3 m). Properties of dolomite were imported into the model as a new material file, using values obtained during the laboratory tests (Section 4.1). However, it should be noted that the load-bearing part of the walls is made from inhomogeneous natural materials. The results of laboratory tests also provide evidence of this during this research (Tables 5 and 6). For example, the density of the dolomite stone ranged from 1696.8 to 2949.5 kg/m^3, but the water vapor resistance factor from 26.67 to 77.83. Moreover, other research [56,57] about the properties of historical materials in Latvia showed a broad diversity in results.

4. Results

4.1. Construction Material Analysis

The results of the dolomite stone sample tests are summarized in Tables 7 and 8.

Table 7. Determined properties of the dolomite and corresponding test methods.

Name of the Material Property	Symbol (Unit)	Mean Value	Standard Deviation	Min Value	Max Value	Coefficient of Variance
Bulk density	ρ_b (kg/m^3)	2346.5	447.8	1696.8	2949.5	0.191
Open porosity	Θ_{por} (m^3/m^3)	0.1602	0.0224	0.1299	0.2008	0.140
Thermal conductivity	λ_{dry} (W/mK)	2.0478	0.0108	2.0362	2.0574	0.005
Heat storage capacity	c (J/kgK)	779.2842	5.1457	774.3023	784.5794	0.007
Dry-cup vapor diffusion	μ_{dry} $(-)$	44.14	29.18	26.67	77.83	0.661
Wet-cup vapour diffusion	μ_{wet} $(-)$	2113.88	943.36	1192.82	3078.06	0.446
Water uptake coefficient	A_w $(Kg/m^2\sqrt{s})$	0.0599	0.0110	0.0477	0.0691	0.184
Capillary saturation moisture content	Θ_{cap} (m^3/m^3)	0.1079				

Table 8. Sorption moisture content.

RH (%)	t (°C)	$\Theta_1 (\varphi) (m^3/m^3)$			
		Mean Value	Standard Deviation	Min Value	Max Value
84.7	23	0.009524	0.000570	0.008907	0.01026
53.5	23	0.004830	0.000284	0.004553	0.00514
32.9	23	0.001787	0.003670	-9.982×10^{-5}	0.00926

4.2. Energy Consumption

The simulated annual heat consumption for space heating in the first scenario is 66.1 MWh/year or 194.4 kWh/m^2; in the second, it is 42.8 MWh/year or 125.8 kWh/m^2 (35% energy saving compared to the first scenario), and in the third, it is 18.3 MWh/year or 53.9 kWh/m^2 (72% energy saving compared to the first scenario).

The wood log consumption is not precisely registered and accounted for by the building residents because they directly cut part of the wood logs in the forest. Based on the data provided by the residents, around 30 m^3 (adjusted for empty spaces between individual firewood logs with a coefficient of 0.61) of two years of dried firewood has been used in the 2017/2018 heating season. By assuming that the moisture content of the firewood after two years of drying is 20% and the 40 kW burner's efficiency of η = 75%, the calculated annual energy consumption per heated area should be 87 kWh/m^2, which is higher than calculated in the third scenario (53.9 kWh/m^2). Various reasons can cause the difference, including:

- Poor quality of construction works;
- Inaccurate assumption of indoor temperature and relative humidity;
- An inaccurate pattern of heat gain schedule in the calculation model;
- Inaccurate climatic input data in the model;

- Inaccurate assumptions about the volume and moisture content of firewood;
- Inaccurate assumption of efficiency of the biomass boiler.

Other researchers [26,58–60] pointed out the issue of result diversity using different building simulation programs to simulate energy consumption or hygrothermal performance of historic buildings. Moreover, used software may need to capture the physical phenomena in historic buildings adequately. For example, heat flux measurements performed later in the case study building showed that the heat transfer coefficient of the living room wall is 0.21 W/m^{2}K (Section 4.3.2). It corresponds to the values entered into the model 0.208–0.2115 W/m^{2}K (see Table 6).

4.3. In Situ Measurement Results

The measurement period was from 13 December 2017 to 4 January 2019. However, due to failures in data logging equipment, gaps in collected data are present.

4.3.1. Measured Climatic Conditions

The monthly average outdoor temperature and relative humidity are presented in Figure 8. The most significant temperature shifts were observed during the winter months (December, January, and February), with February being the coldest month, e.g., the lowest registered temperature was −23.6 °C. The highest relative humidity was observed during late autumn and winter, falling over the spring months and increasing again during summer.
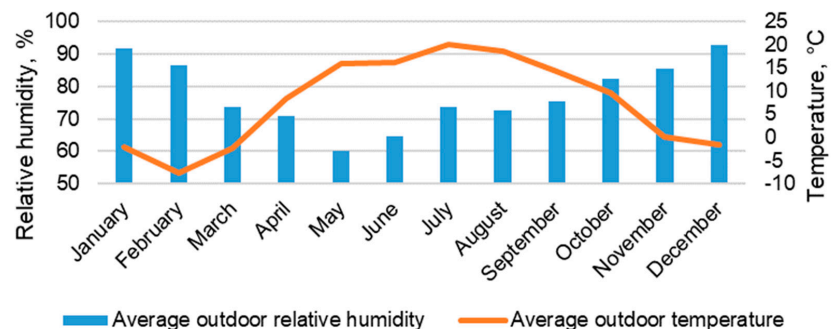
Figure 8. The monthly average outdoor relative humidity and temperature (data from the weather station "Skriveri").

The manual operation of the boiler causes fluctuations in the indoor air temperature. Monitoring results of the indoor temperature show that the residents try to maintain a constant room temperature during the day, letting it fall to +16 °C in the evening and then increasing the temperature before the night. Temperature increase from +16 to +22 °C takes around 2 to 3 h. During the winter months (December to March), the average indoor air temperature was +22 °C in the living room and +20.8 °C in the bathroom. The average indoor relative humidity was 35.7% in the living room and 40% in the bathroom. During spring months (April and May), the average temperature was +21.4 °C in the living room and +21.2 °C in the bathroom, and the average relative humidity was 47% in the living room and 50.4% in the bathroom. During the summer, relative humidity increased to 70% in the living room and over 80% in the bathroom. High relative humidity in the bathroom is expected as higher moisture loads are present in this room. During the monitored period, 2% of the time, relative humidity reached over 80%. After the relative humidity spike ends, it takes around 2–3 h for the relative humidity to drop from over 80% to under 70%.

4.3.2. Measured Conditions in the Wall

TDR measurement results show that water content mostly stays below 2% at both measurement points, and even after the rainfalls, when moisture content spikes appear, the wall does not reach saturation (see Figure 9).
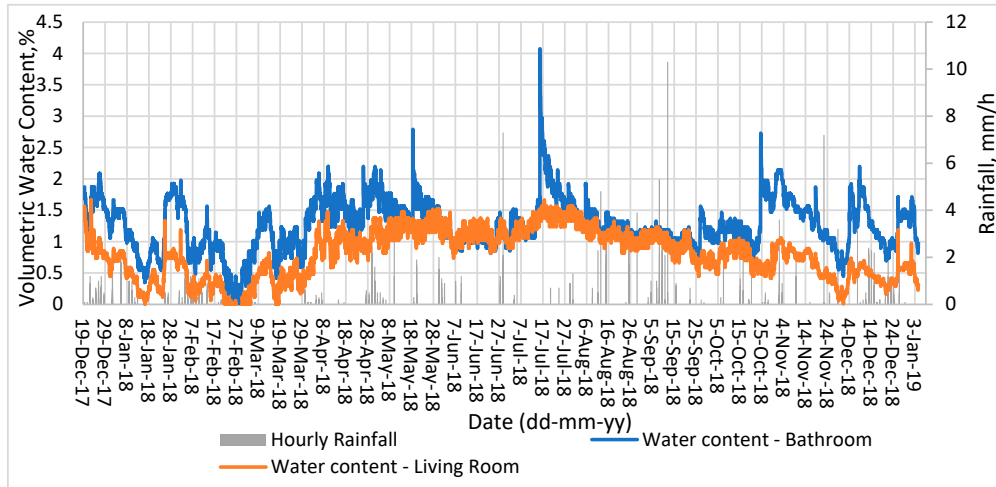
Figure 9. Results of water content measurements and rainfall (mm).

From the heat flux measurement and calculated indoor/outdoor temperature difference, a U-value of 0.21 W/(m^{2}K) for the living room wall and U = 0.19 W/(m^{2}K) for the bathroom wall was calculated.

4.4. Hygrothermal Calculation Results

Evaluation of the hygrothermal conditions with the Glazers method and 1D simulations in the DELPHIN 6.1 were performed. The eight months were chosen for the simulations to correspond to the available measurement data. For the Glazers method, average climatic conditions for Latvia were used (see Table 9).

Table 9. Average indoor and outdoor conditions for Latvia.

	Temperature, °C	Relative Humidity, %
Indoor	20	50
Outdoor	0	80

4.4.1. Measured and Simulated Conditions in the Wall

For wall type 1, the water vapor diffusion ratio of the cold and warm sides is 2.85, which is lower than the normative value (ratio > 5). Therefore, the saturated and partial pressure calculation for all planes of the type 1 wall was performed utilizing the Glazers method. For the calculations, the indoor temperature of 20 °C and outdoor temperature of 0 °C, outdoor humidity of 80%, and indoor humidity of 50% was used. Interstitial planes under the insulation material were found to be most prone to condensation (see Figure 10).
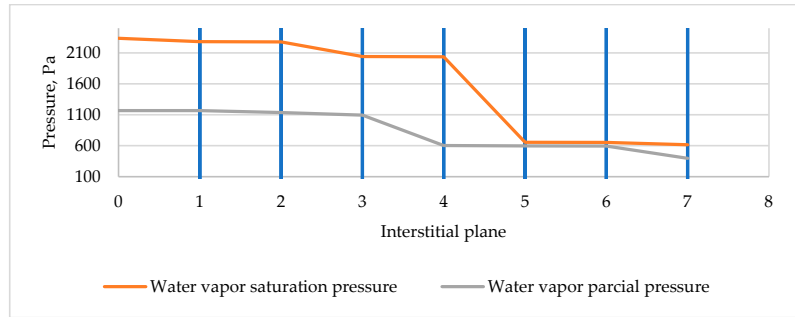
Figure 10. Partial and saturation pressures in interstitial planes for wall type1 (1. interior surface; 2. wallpaper/plasterboard; 3. vapor barrier/plasterboard; 4. mineral wool/vapor barrier; 5. plaster/mineral wool; 6. dolomite/plaster; 7. exterior wall surface).

Therefore, relative humidity calculations for interstitial planes on both sides of the vapor barrier and planes under the insulation material were performed for the range of outdoor temperatures (from +20 to −20 °C). The calculation results indicate the risk of interstitial condensation in the layer between wood planks and insulation (under the insulation) when the outdoor temperature drops below −5 °C. In the other high condensation-risk planes, there is no condensation risk within the given temperature range. (see Figure 11).
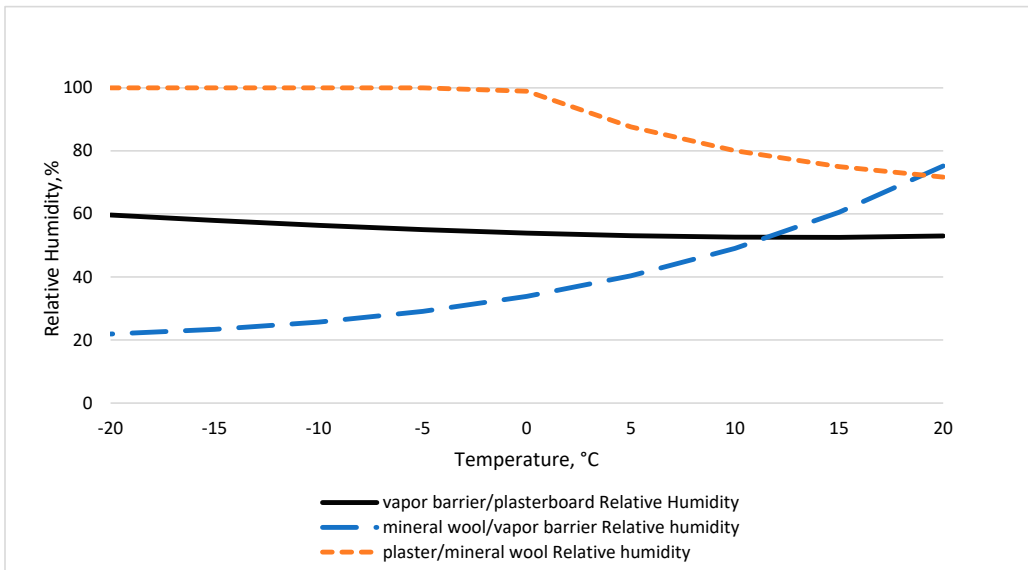
Figure 11. Calculated relative humidity at different interstitial planes for wall Type 1.

All three other wall types also did not reach the minimum normative warm/cold side ratio (type 2 = 2.85; type 3 = 3.78; type 4 = 1.74); therefore, the saturated and partial pressure calculation for all planes of all wall types was performed. As for wall type 1 and all the other wall types, the interstitial planes under the insulation material were found to be most prone to condensation. Therefore, the same relative humidity calculations for wall type 1 were performed for all the other wall types. The results for all the other wall types were very similar to those for wall type 1, with condensation risk under the insulation when the

temperature drops belove −5 °C and no condensation risk in other planes within the given temperature range.

4.4.2. Measured and Simulated Conditions in the Wall

The measured RH between the insulation layer and vapor barrier never exceeds 80%, mostly staying below 40% during winter and below 60% during the spring and summer. The exception was on 8 March 2018, when water leakage from the first-floor water supply system was detected. On that date, the RH between insulation and vapor barrier rapidly rises from 25% to 60% and then slowly decreases within the next two weeks (see Figure 12).
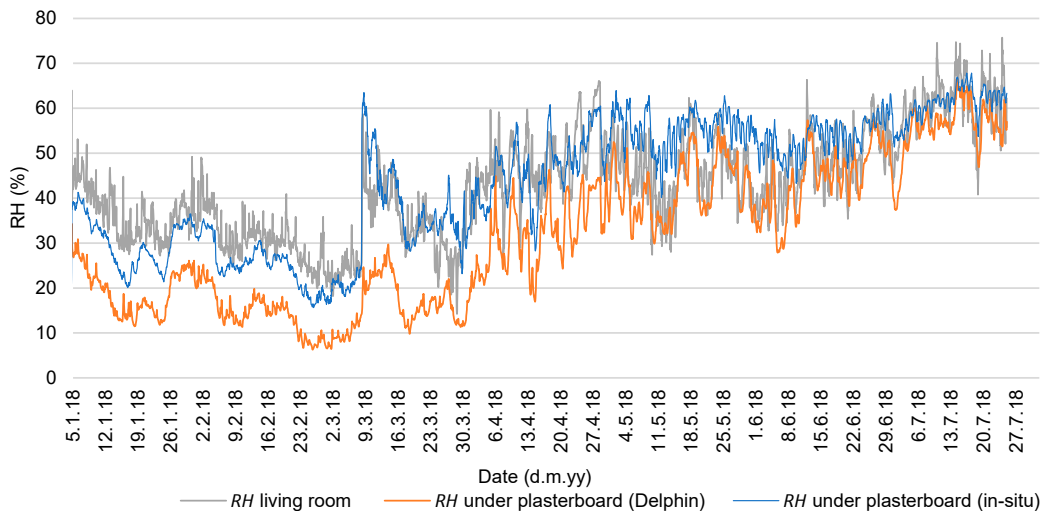
Figure 12. Relative humidity of the living room wall between the insulation and vapor barrier: measured RH (blue line), simulated RH (orange line), and indoor RH (grey line).

Simulated RH between the insulation and vapor barrier follows the trend of the indoor RH, although it is 5 to 10% lower than the level measured during the heating season (see Figure 12).

Simulated temperatures between the insulation and vapor barrier closely follow indoor temperature changes, with the difference in absolute values during winter. Differences between simulated and measured temperatures at the interface of the insulation and vapor barrier are most likely caused by the placement of room temperature sensors—off the wall and on the side of a closet (see Figure 6b). At that point, the temperature is higher than on the wall's surface. Moreover, measured temperatures are impacted more by fluctuations in the outside temperature. At the same time, simulated data follows room temperature, which in the simulation model was indicated as the climate data of the room (see Figure 13).
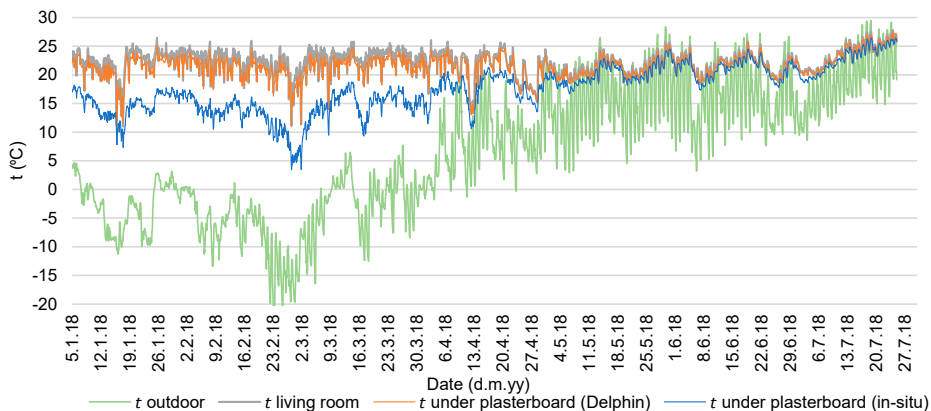
Figure 13. The temperature of the living room wall between the insulation and vapor barrier: measured T (blue line), simulated T (orange line), indoor T (grey line), and outdoor T (green line).

RH under the insulation mostly stays between 60 and 80%. Measured RH exceeded 90% in March during the water leakage incident when RH between the dolomite wall and insulation layer rapidly increased to 100% and then slowly dried out during the spring and summer (see Figure 14).
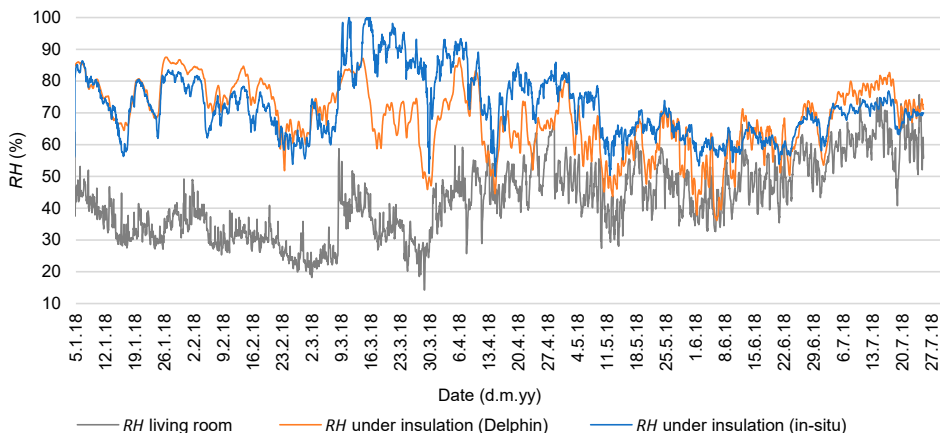
Figure 14. Relative humidity of the living room wall between dolomite and the insulation layers: measured RH (blue line), simulated RH (orange line), indoor RH (grey line), and outdoor RH (green line).

In the living room, the measured and simulated temperatures under the insulation follow a similar trend, but the simulated temperatures are around 1 degree lower than the measured. When the outside temperature drops below $-5\ °C$, the temperature between the dolomite wall and insulation layer drops below $0\ °C$. However, there are no risks related to frost damage as the moisture content in the materials of the wall never reaches capillary saturation (see Figure 15).

Figure 15. The temperature within the living room wall between dolomite and the insulation layers: measured T (blue line), simulated T (orange line), indoor T (grey line), and outdoor T (green line).

The bathroom RH between the insulation layer and vapor barrier never exceeds the critical level of 80%, mostly staying below 40% during the cold season and below 70% during the spring and summer (see Figure 16).

Figure 16. Relative humidity measurements of the bathroom wall between the insulation and vapor barrier: Measured RH (blue line), simulated RH (orange line), indoor bathroom RH (grey line).

Temperature between the insulation and vapor barrier in the bathroom shows similar data for measured and simulated data, with simulated data being slightly higher and closer to the measured indoor air temperature (see Figure 17).
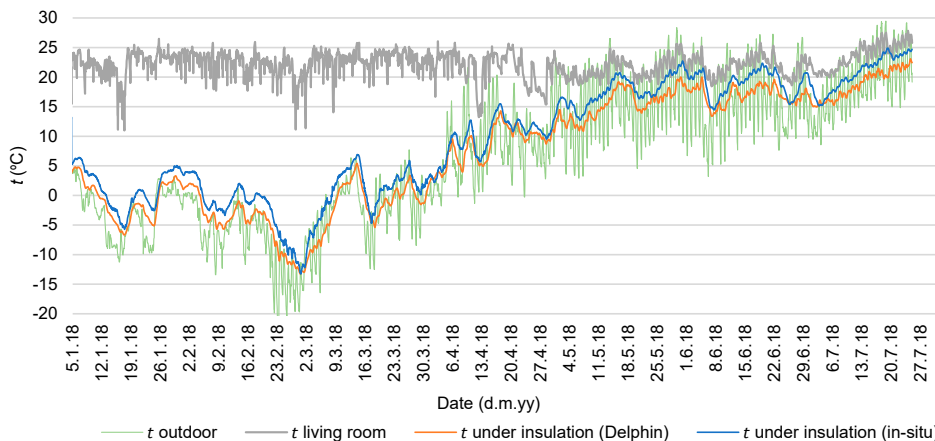
Figure 17. The temperature of the bathroom wall between the insulation and vapor barrier: measured T (blue line), simulated T (orange line), and indoor bathroom T (grey line).

The bathroom measured RH between dolomite and insulation mostly stays below 80% during autumn, winter, and spring and below 70% during summer. The simulated data for the same plane shows a higher RH of up to 90% (see Figure 18).
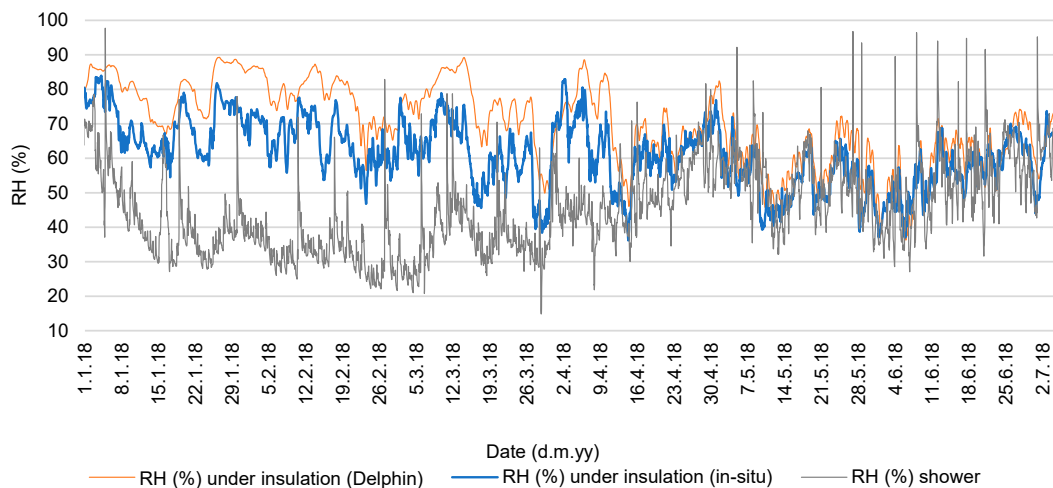
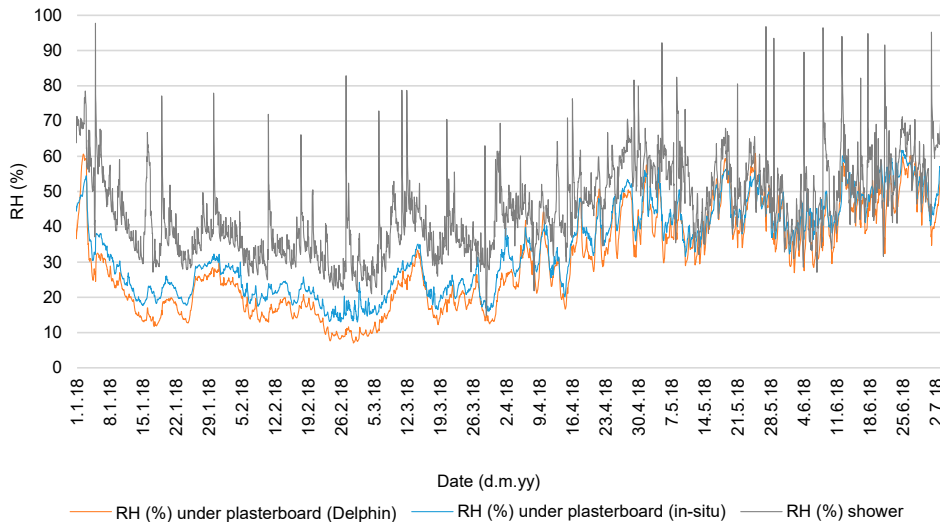**Figure 18.** Relative humidity of the bathroom wall between dolomite and insulation layers: measured RH (blue line), simulated RH (orange line), indoor RH (grey line), and outdoor RH (green line).

Measured temperatures between dolomite and insulation follow outside temperatures during the heating season and are between outdoor and indoor temperatures outside the heating season (see Figure 19).
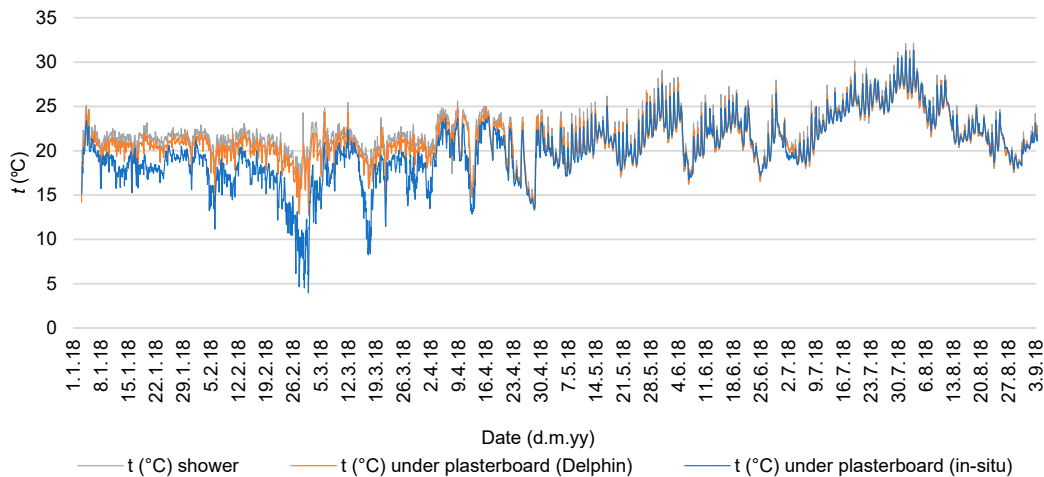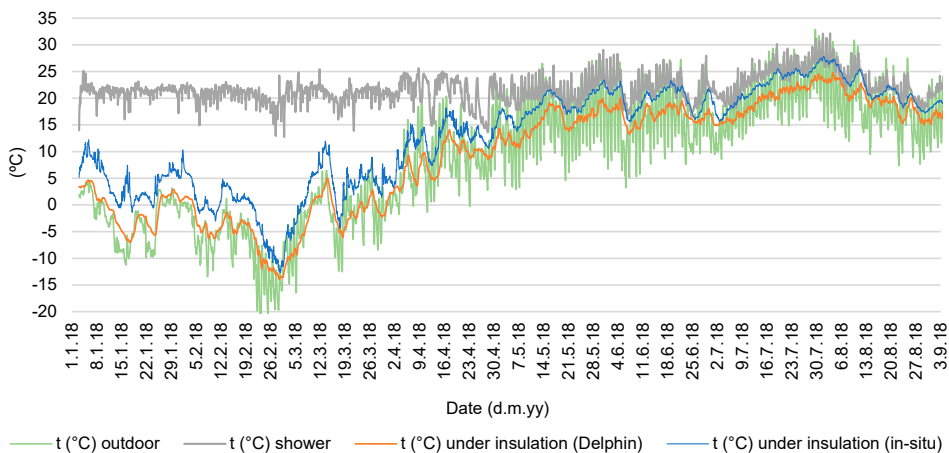
Figure 19. The temperature of the bathroom wall between dolomite and insulation layers: measured T (blue line), simulated T (orange line), indoor T (grey line), and outdoor T (green line).

4.4.3. Comparison of Experimental and Hygrothermal Simulation Results

The living room temperature correlation between dolomite and insulation (t under insulation) is strong ($R^2 = 0.9789$). However, the correlation between the insulation and vapor barrier is considerably lower ($R^2 = 0.4003$). The RH correlation is strong ($R^2 = 0.9047$) between the insulation and vapor barrier, and the correlation is weaker ($R^2 = 0.4775$) between dolomite and insulation (see Figure 20).
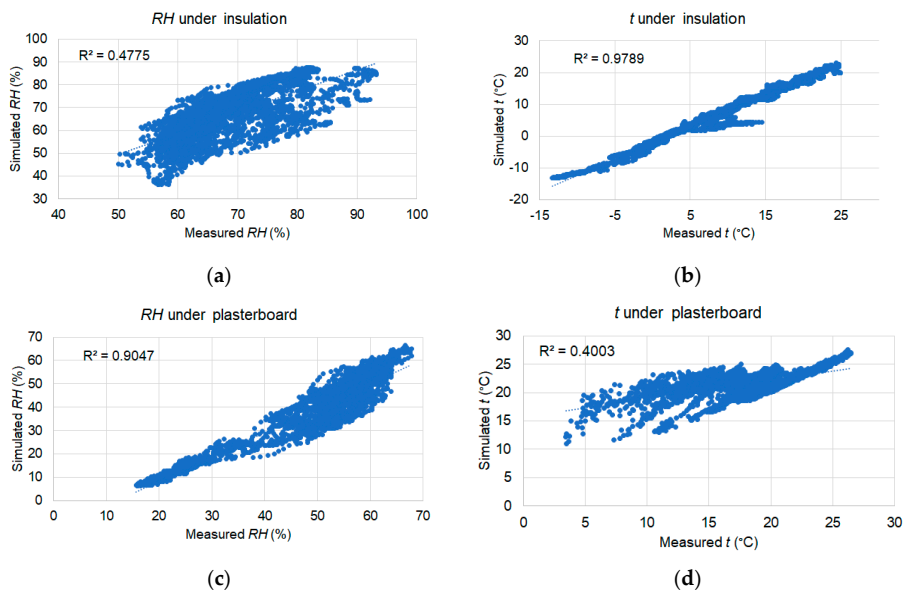
Figure 20. Correlation between simulated and measured RH and t in the living room wall: (**a**) RH between dolomite and insulation; (**b**) t between dolomite and insulation; (**c**) RH between the insulation and vapor barrier; (**d**) t between the insulation and vapor barrier.

The bathroom temperature correlation between dolomite and insulation (t under insulation) is strong ($R^2 = 0.9778$), and the insulation and vapor barrier correlation is also

strong (R^2 = 0.7876). The simulated and measured RH correlation between dolomite and insulation is moderate (R^2 = 0.633). In the case of RH between the insulation and vapor barrier, the correlation between measured and simulated data is strong (R^2 = 0.9694) (see Figure 21).
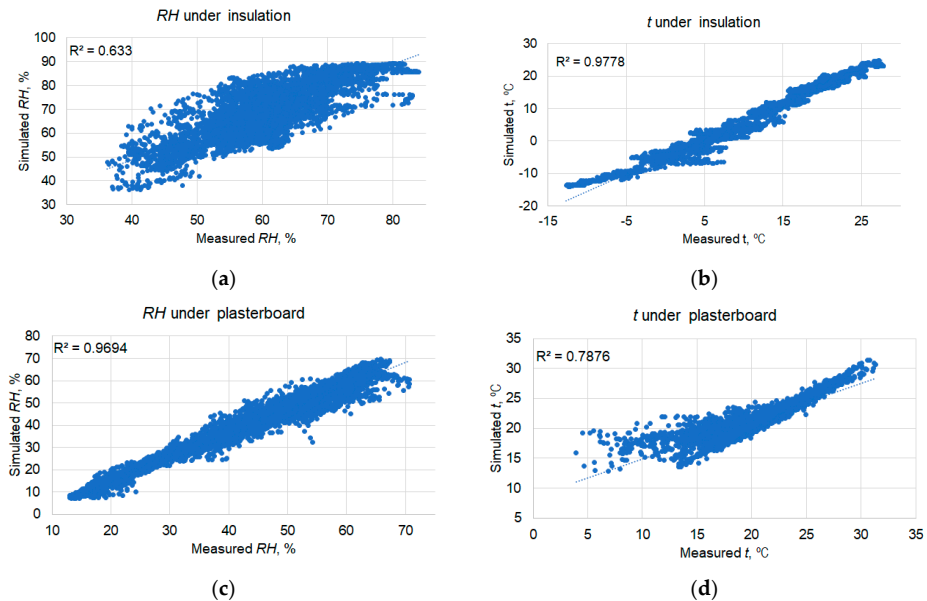
Figure 21. Correlation between simulated and measured RH and temperature in the bathroom wall: (**a**) RH between dolomite and insulation; (**b**) t between dolomite and insulation; (**c**) RH between the insulation and vapor barrier (**d**) t between the insulation and vapor barrier.

This correlation analysis does not include possible deviation of measurement accuracy, and three-week data following the water leakage accident were not used in the correlation analysis for the living room wall. Furthermore, outside temperatures and relative humidity data are taken from the weather station Skriveri, which is located 20 km away from the case study building.

The gap between the measured and simulated hygrothermal performance of internally insulated masonry walls was also seen in the previous study, where experimental results obtained in the controlled laboratory environment were compared to simulated results [28]. The research [61] showed that temperatures had a satisfactory correlation (R^2 in the range of 0.81 to 0.86), but walls insulated with mineral wool had the lowest correlation for measured and simulated RH (R^2 = 0.540). This corresponds to the research findings that the correlation for measured and simulated temperatures between masonry and insulation is strong but lower for relative humidity.

5. Discussions and Conclusions

This study aimed to answer two research questions. The first question was: what is the impact of internally insulated natural stone buildings on the hygrothermal behavior of walls in a cold climate? In situ measurements and hygrothermal simulations were carried out to evaluate the impact of internal insulation on the hygrothermal behavior of historic stone buildings in a cold climate. The assessment was performed for two occupied rooms located in the north-east facade. One of the rooms has a high indoor moisture load, while the other has an average moisture load. The results showed acceptable hygrothermal conditions within the wall. As the relative humidity between the insulation layer and vapor barrier and in the room stays relatively low (below 60%), excluding water

leakage accidents, the external wall does not indicate risks related to mold growth. Relative humidity reaches above critical 80% between the dolomite wall and insulation layer only for short periods. However, temperatures are lower than needed for spore germination (initial mold growth) at these moments and at this location. According to the literature review by Isaksson et al. [62], mold growth can occur at 80% high relative humidity if the temperature is at least 20 °C for porous materials. However, given that during the renovation in 2015, the tenants found mold on the bathroom wall, there is good potential for mold growth if appropriate conditions (high relative humidity and temperature) remain long enough as wall materials contain mold spores. In situ temperature measurements show that the outer part of the dolomite wall undergoes repeated freeze–thaw cycles. However, the risk of frost decay is minimal as the dolomite does not reach saturation [63]. Results of hygrothermal modeling validate the reliability of the prediction of hygrothermal conditions and risks of mold growth and frost damage in internally insulated historic buildings.

The second research question was: what energy savings can be reached by internal insulation of natural stone buildings in a cold climate? The simulated annual heat consumption for space heating in the baseline scenario can be reduced by 35% if internal insulation is applied on the ground and first-floor walls. If the significant energy efficiency renovation (internal wall insulation, basement ceiling, roof insulation, replacement of windows) is carried out, baseline energy consumption can be reduced by 72%. Actual energy consumption is calculated based on the data provided by the residents who count for primary energy resources—firewood which is partly supplied directly from the forest and dried on site. If the wood log consumption is converted into final energy, the annual energy consumption per heated area should be 87 kWh/m^2. Energy savings are 17% less than calculated in the simulation model. Several reasons could cause this difference, such as uncertainty of the quality of construction works and remaining thermal bridges, input data of the model, including factors related to occupancy frequency (heat gains, room temperature, and ventilation frequency). Simulation results are sensitive to the quality of input data, such as room temperature, relative humidity, ventilation, and material properties. In historic buildings, there is a lack of detailed information on wall cavities, ratio and typology of stones and mortar, construction defects, and specific properties of materials. On the other hand, the uncertainty of actual primary energy consumption, including the amount and quality of firewood efficiency of energy transformation technologies, significantly impacts the final energy consumption values.

References

1. Directive (EU) 2018/844 of the European Parliament and the Council of 30 May 2018 amending Directive 2010/31/EU on the energy performance of buildings and Directive 2012/27/EU on energy efficiency. *Off. J. Eur. Union* **2018**, *156*, 75–91.
2. European Commission. *A Clean Planet for All—A European Strategic Long-Term Vision for a Prosperous, Modern, Competitive and Climate Neutral Economy, COM*; European Commission: Brussels, Belgium, 2018.
3. Factsheet: Energy Performance in Buildings Directive. European Commission, January 2019. Available online: https://ec.europa.eu/energy/content/factsheet-energy-performance-buildings-directive_en?redir=1 (accessed on 2 December 2022).
4. Gynther, L.; Lapillonne, B.; Pollier, K. Energy Efficiency Trends and Policies in the Household and Tertiary Sectors—An Analysis Based on the ODYSSEE and MURE Databases. Available online: http://www.odyssee-mure.eu/publications/br/energy-efficiency-trends-policies-buildings.pdf (accessed on 2 December 2022).
5. Communication from the Commission: The European Green Deal. Brussels 11.12.2019. Available online: https://eur-lex.europa.eu/legal-content/EN/TXT/?qid=1576150542719&uri=COM%3A2019%3A640%3AFIN#footnote6 (accessed on 2 December 2022).

6.   La Fleur, L.; Rodin, P.; Moshfegh, B. Energy renovation versus demolition and construction of a new building—A comparative analysis of a Swedish multi-family building. *Energies* **2019**, *12*, 2218. [CrossRef]

7.   Gaspar, P.L.; Santos, A.L. Embodied energy on refurbishment vs. demolition: A southern Europe case study. *Energy Build.* **2015**, *87*, 386–394. [CrossRef]

8.   Berg, F.; Fuglseth, M. Life cycle assessment and historic buildings: Energy-efficiency refurbishment versus new construction in Norway. *Archit. Conserv.* **2018**, *24*, 152–167. [CrossRef]

9.   Economidou, M.; Laustsen, J.; Ruyssevelt, P.; Staniaszek, D. Europe's Buildings under the Microscope. Available online: http://bpie.eu/publication/europes-buildings-under-the-microscope/ (accessed on 2 December 2022).

10.   European Commission, An EU Strategy on Heating and Cooling, COM. 2016. Available online: https://eur-lex.europa.eu/LexUriServ/LexUriServ.do?uri=COM:2016:0051:FIN:EN:PDF (accessed on 2 December 2022).

11.   Mazzarella, L. Energy retrofit of historic and existing buildings. The legislative and regulatory point of view. *Energy Build.* **2015**, *95*, 23–31. [CrossRef]

12.   Murgul, V.; Pukhkal, V. Saving the Architectural Appearance of the Historical Buildings due to Heat Insulation of their External Walls. *Procedia Eng.* **2015**, *117*, 891–899. [CrossRef]

13.   Claude, S.; Ginestet, S.; Bonhomme, M.; Escadeillas, G.; Taylor, J.; Marincioni, V.; Korolija, I.; Altamirano, H. Evaluating retrofit options in a historical city center: Relevance of bio-based insulation and the need to consider complex urban form in decision-making. *Energy Build.* **2019**, *182*, 196–204. [CrossRef]

14.   Johansson, P.B.; Adl-Zarrabi, A.S. Kalagasidis, Evaluation of 5 years' performance of VIPs in a retrofitted building façade. *Energy Build.* **2016**, *130*, 488–494. [CrossRef]

15.   Blumberga, A.; Kašs, K.; Kamendere, E. A review on Latvian historical building stock with heavy walls. *Energy Procedia* **2016**, *95*, 17–21. [CrossRef]

16.   Ozel, M. Thermal performance and the optimum insulation thickness of building walls with different structure materials. *Appl. Therm. Eng.* **2011**, *31*, 3854–3863. [CrossRef]

17.   Salvalai, G.; Sesana, M.M.; Iannaccone, G. Deep renovation of multi-story multi-owner existing residential buildings: A pilot case study in Italy. *Energy Build.* **2017**, *148*, 23–36. [CrossRef]

18.   Pasichnyi, O.; Levin, F.; Shahrokni, H.; Wallin, J.; Kordas, O. Data-driven strategic planning of building energy retrofitting: The case of Stockholm. *J. Clean. Prod.* **2019**, *233*, 546–560. [CrossRef]

19.   Belaïd, F.; Ranjbar, Z.; Massié, C. Exploring the cost-effectiveness of energy efficiency implementation measures in the residential sector. *Energy Policy* **2021**, *150*, 112112. [CrossRef]

20.   van den Brom, P.; Meijer, A.; Visscher, H. Actual energy saving effects of thermal renovations in dwellings—Longitudinal data analysis including building and occupant characteristics. *Energy Build.* **2019**, *182*, 251–263. [CrossRef]

21.   Cholewa, T.; Balaras, C.A.; Nižetić, S.; Siuta-Olcha, A. On calculated and actual energy savings from thermal building renovations— Long term field evaluation of multifamily buildings. *Energy Build.* **2020**, *223*, 110–145. [CrossRef]

22.   Walker, R.; Pavía, S. Thermal performance of a selection of insulation materials suitable for historic buildings. *Build. Environ.* **2015**, *94*, 155–165. [CrossRef]

23.   Odgaard, T.; Bjarløv, S.P.; Rode, C. Interior insulation—Characterisation of the historic, solid masonry building segment and analysis of the heat saving potential by 1d, 2d, and 3d simulation. *Energy Build.* **2018**, *162*, 1–11. [CrossRef]

24.   De Mets, T.; Tilmans, A.; Loncour, X. Hygrothermal assessment of internal insulation systems of brick walls through numerical simulation and full-scale laboratory testing. *Energy Procedia* **2017**, *132*, 753–758. [CrossRef]

25.   Vereecken, E.; Van Gelder, L.; Janssen, H.; Roels, S. Interior insulation for wall retrofitting—A probabilistic analysis of energy savings and hygrothermal risks. *Energy Build* **2015**, *89*, 231–244. [CrossRef]

26.   Webb, A.L. Energy retrofits in historic and traditional buildings: A review of problems and methods, Renewable and Sustainable. *Energy Rev.* **2017**, *77*, 748–759.

27.   Vereecken, E.; Roels, S. A comparison of the hygric performance of interior insulation systems: A hot box–cold box experiment. *Energy Build.* **2014**, *80*, 37–44. [CrossRef]

28.   van Aarle, M.; Schellen, H.; van Schijndel, J. Hygro Thermal Simulation to Predict the Risk of Frost Damage in Masonry; Effects of Climate Change. *Energy Procedia* **2015**, *78*, 2536–2541. [CrossRef]

29.   Bjarløv, S.P.; Finken, G.R.; Odgaard, T. Retrofit with interior insulation on solid masonry walls in cool temperate climates—An evaluation of the influence of interior insulation materials on moisture condition in the building envelope. *Energy Procedia* **2015**, *78*, 1461–1466. [CrossRef]

30.   Zhao, J.; Meissner, F. Experimental investigation of moisture properties of historic building material with hydrophobization treatment. *Energy Procedia* **2017**, *132*, 261–266. [CrossRef]

31.   Harrestrup, M.; Svendsen, S. Full-scale test of an old heritage multi-story building undergoing energy retrofitting with focus on internal insulation and moisture. *Build. Environ.* **2015**, *85*, 123–133. [CrossRef]

32.   Bottino-Leone, D.; Larcher, M.; Herrera-Avellanosa, D.; Haas, F.; Troi, A. Evaluation of natural-based internal insulation systems in historic buildings through a holistic approach. *Energy* **2019**, *181*, 521–531. [CrossRef]

33.   Tijskens, A.; Janssen, H.; Roels, S. A simplified dynamic zone model for a probabilistic assessment of hygrothermal risks in building components hygrothermal risks in building components. *Energy Procedia* **2017**, *132*, 717–722. [CrossRef]

34. Cuce, E.; Cuce, P.M. The impact of internal aerogel retrofitting on the thermal bridges of residential buildings: An experimental and statistical research. *Energy Build.* **2016**, *116*, 449–454. [CrossRef]
35. Cueto, N.D.; Benavente, J.; Martínez-Martínez, M.A. García-del-Cura, Rock fabric, pore geometry and mineralogy effects on water transport in fractured dolostones. *Eng. Geol.* **2009**, *107*, 1–15. [CrossRef]
36. Vázquez, P.; Alonso, F.J.; Carrizo, L.; Molina, E.; Cultrone, G.; Blanco, M.; Zamora, I. Evaluation of the petrophysical properties of sedimentary building stones intostablish quality criteria. *Constr. Build. Mater.* **2013**, *41*, 868–878. [CrossRef]
37. Lucchi, E. Thermal transmittance of historical stone masonries: A comparison among standard, calculated and measured data. *Energy Build.* **2017**, *151*, 393–405. [CrossRef]
38. Varas-Muriel, M.J.; Pérez-Monserrat, E.M.; Vázquez-Calvo, C.; Fort, R. Effect of conservation treatments on heritage stone. CCharacterizationof decay processes in a case study. *Constr. Build. Mater.* **2015**, *95*, 611–622. [CrossRef]
39. Benavente, D.; Martínez-Martínez, J.; Cueto, N.; García-del-Cura, M.A. Salt weathering in dual-porosity building dolostones. *Eng. Geol.* **2007**, *94*, 215–226. [CrossRef]
40. Toman, J.; Vimmrova, A.; Cerny, R. Long-term on-site assessment of the hygrothermal performance of interior thermal insulation system without a watevapourur barrier. *Energy Build* **2009**, *41*, 51–55. [CrossRef]
41. Kološeiko, P.; Arumagi, E.; Kalamees, T. Hygrothermal performance of internally insulated brick wall in a cold climate: A case study in a historic school building. *Build. Phys.* **2015**, *38*, 444–464. [CrossRef]
42. Wójcik, R.; Kosiński, P. On the rehabilitation of buildings with historical facades On the rehabilitation of buildings with historical façades. *Energy Procedia* **2017**, *132*, 927–932.
43. Hansen, T.K.; Bjarløv, S.P.; Peuhkuri, R.H.; Harrestrup, M. Long term in situ measurements of hygrothermal conditions at critical points in four cases of internally insulated historic solid masonry walls. *Energy Build.* **2018**, *172*, 235–248. [CrossRef]
44. Biseniece, E.; Žogla, G.; Kamenders, A.; Purviņš, R.; Kašs, K.; Vanga, R.; Blumberga, A. Thermal performance of internally insulated historic brick building in cold climate: A long term case study. *Energy Build.* **2017**, *152*, 577–586. [CrossRef]
45. Hodireva, V.; Sidraba, I.; Purviņš, E. Augšdevona dolomīta litoloģiski morfoloģiskie tipi Rīgas Kultūrvēsturiskajos pieminekļos [Lithological morphological types of Upper Devonian dolomite in Riga Cultural Heritage Monuments]. *Mater. Sci. Appl. Chem.* **2010**, *22*, 105–113.
46. Simulation Tool DELPHIN. Available online: http://bauklimatik-dresden.de/delphin/index.php?aLa=en (accessed on 4 December 2022).
47. *EN 772-13:2000*; Methods of Test for Masonry Units. Determination of Net and Gross Dry Density of Masonry Units (Except for Natural Stone). BSI: London, UK, 2000.
48. *EN 772-3:1998*; Methods of Test for Masonry Units. Determination of Net Volume and Percentage of Voids of Clay Masonry Units by Hydrostatic Weighing. BSI: London, UK, 1998.
49. *EN ISO 12572:2001*; Hygrothermal Performance of Building Materials and Products—Determination of Water Vapour Transmission Properties. ISO: Geneva, Switzerland, 2001.
50. *EN ISO 12571:2013*; Hygrothermal Performance of Building Materials and Products—Determination of Hygroscopic Sorption Properties. ISO: Geneva, Switzerland, 2013.
51. *ISO 15148:2002*; Hygrothermal Performance of Building Materials and Products—Determination of Wa ter Absorption Coefficient by Partial Immersion. ISO: Geneva, Switzerland, 2002.
52. Project RIBuild. Available online: https://www.ribuild.eu/research-measurements/#10 (accessed on 4 December 2022).
53. Project RIBuild Deliverable D2.1 Report on the Material Properties. 2018. Available online: https://static1.squarespace.com/static/5e8c2889b5462512e400d1e2/t/5e9db81f43530a16d2f3fecf/1587394609561/RIBuild_D2.1_v1.0.pdf (accessed on 2 December 2022).
54. Simulation tool TRNSYS. Available online: http://www.trnsys.com (accessed on 4 December 2022).
55. *EN ISO 13790:2008*; Energy Performance of Buildings—Calculation of Energy Use for Space Heating and Cooling. ISO: Geneva, Switzerland, 2008.
56. State limited Liability Company Latvian Environment, Geology and Meteorology Centre. Available online: https://meteo.lv/meteorologija-datu-meklesana/?nid=461 (accessed on 2 December 2022).
57. Purviņš, R.; Kamendere, E.; Blumberga, A. Laboratory investigation of Latvian historic brick and measurements of water movement in historic masonry walls. *Energy Procedia* **2017**, *113*, 327–332. [CrossRef]
58. Kamendere, E.; Grava, L.; Zvaigznitis, K.; Kamenders, A.; Blumberga, A. Properties of bricks and masonry of historical buildings as a background for safe renovation measures. *Energy Procedia* **2016**, *95*, 119–123. [CrossRef]
59. Robertu, F.; Oberegger, U.F.; Gasparella, A. Calibrating historic building energy models to hourly indoor air and surface temperatures: Methodology and case study. *Energy Build.* **2015**, *108*, 236–243. [CrossRef]
60. Coelho, G.B.A.; Silva, H.E.; Henriques, F.M.A. Calibrated hygrothermal simulation models for historical buildings. *Build. Environ.* **2018**, *142*, 439–450. [CrossRef]
61. Biseniece, E.; Freimanis, R.; Purviņš, R.; Graveslins, A.; Pumpurs, A.; Blumberga, A. Study of Hygrothermal Processes in External Walls with Internal Insulation. *Environ. Clim. Technol.* **2018**, *22*, 22–41. [CrossRef]

62. Isaksson, T.; Thelandersson, S.; Ekstrand-Tobin, A.; Johansson, P. Critical conditions for onset of mould growth under varying climate conditions. *Build. Environ.* **2010**, *45*, 1712–1721. [CrossRef]
63. Litti, G.; Khoshdel, S.; Audenaert, A.; Braet, J. Hygrothermal performance evaluation of traditional brick masonry in historic buildings. *Energy Build.* **2015**, *105*, 393–411. [CrossRef]

In-Situ Moisture Assessment in External Walls of Historic Building using Non-Destructive Methods

Ritvars FREIMANIS[1]*, Rasa VAISKUNAITE[2], Tereza BEZRUCKO[3], Andra BLUMBERGA[4]

[1,3,4] *Institute of Energy Systems and Environment, Riga Technical University, Azenes iela 12/1, Riga, LV-1048, Latvia*

[2]*Department of Environmental Protection and Water Engineering, Vilnius Gediminas Technical University, Sauletekio al. 11, Vilnius, LT-10223, Lithuania*

Abstract – **In-situ measurements of a case study building located in Riga old town near the river Daugava has been carried out in this work. Performed measurements are moisture level of historic masonry, and interstitial monitoring of temperature and relative humidity between the layers of internal insulation and external wall. Obtained results are compared with outdoor weather data. Results show that during the cold months of the year no rising damp problem. No interstitial condensation under the internal insulation, and no risk of mold growth occur. However, the façade of the building tends to be highly influenced by the outdoor weather, and the moisture of the masonry increases during the rain load events.**

Keywords – **Dielectric measurement; internal insulation; interstitial relative humidity; masonry deterioration; microwave measurement; wind-driven rain**

1. INTRODUCTION

High greenhouse gas emissions rate is driving climate change. One of the main causes is high energy demand from existing building stock [1], [2]. In Europe, historic buildings still account for as many as 24 to 35 % of the entire building stock. Moreover, the building stock of historic buildings composes from 27 to 42 %, of the final energy demand in Europe – depending on the country [3]. It is estimated that about 36 % of CO_2 emissions in the European Union (EU) comes from the building sector [4], [5].

The main reasons for the high energy consumption in the buildings depends on the physical elements, thermal properties and climate conditions [6]. The main reason for high energy consumption in historic buildings is poor thermal properties of the building envelope, in terms of high thermal transmittance or U-Value. In theory U-value can be calculated if the thermal conductivity of the material and boundary conditions are known, but in reality, this value can be influenced by moisture, cracks, etc. [7]. Nevertheless, moisture-caused problems are present in many historic buildings, that leads to degradation of building materials, unsuitable indoor air conditions and poor thermal properties of exterior walls [8]. Unhealthy indoor air quality can affect general senses of the human, reducing their work abilities and leading to health risks [9]. Jimenez-Besecos et al. in their research, concluded, that healthy indoor air quality (IAQ) can be achieved when retrofit of a historic building is done. Healthy IAQ in the study is defined as 19 to 20 °C temperature, 40 to 70 % relative humidity and CO_2 concentration below 1000 ppm [10].

As most of the thermal energy losses are through the opaque building envelope (exterior walls), insulation of exterior walls, can reduce energy consumption of the building and thereby reduce

---

* Corresponding author.
E-mail address: ritvars.freimanis_1@rtu.lv

greenhouse gas emissions [11]. External walls can be insulated either from the outside or from the inside. To avoid exacerbation of moisture-related problems in the building, it is recommended to insulate the building from the outside. But almost in all cases insulation of historic buildings from the outside is not possible due to preservation of heritage value of the historic façade, or other limitations, such as space restrictions. Therefore internal insulation of exterior walls becomes the single best solution to reduce energy consumption of the historic building and thereby reduce greenhouse gas emissions [11]. At the same time, the renovation should not compromise the structural integrity and indoor air quality of the renovated building.

If the masonry moisture content exceeds 3 % of mass moisture content, there is a need to undertake action in order to reduce this moisture content before the renovation [12]. Moreover, if moisture sources in the masonry are not eliminated, further renovation is not recommended, considering masonry decay and other moisture-caused problems will reappear in a short period of time [8]. However, the situation that only one moisture source is present in the historic building is very rare, and many factors affecting the moisture content in the masonry makes it hard to clearly distinguish among the main moisture sources in the historic building. Therefore, to find a non-harmful renovation method a hygrothermal performance and moisture content of a historic masonry must be assessed. And to avoid oversized, inadequately expensive and ineffective interventions, preliminary monitoring of a building is recommended [13]. There are six main groups of moisture sources in the buildings: Raising dump, Wind-driven rain, Built-in moisture, Hygroscopic phenomena, Surface condensation, Damages in water systems, i.e. piping and gutter [14].

With new non-destructive moisture assessment technologies emerging and improving for moisture content assessment in-situ, the measurements are becoming more applicable to historic buildings, cause destructive methods such as drilling holes and inserting probes are mostly not preferable in historic facades. Test results obtained in-situ through the systematic surveys can be very helpful for the moisture source determination [8].

The main goal of this research is to study the application of internal insulation in historic buildings by assessing the possible moisture sources in the external wall and their impact on moisture content and moisture transport in the wall.

2. MATERIALS AND METHODS

2.1. Case Study Building

The case study building at Biskapa gate 6 in Riga, Latvia was selected for the in-situ measurements. This particular building was selected, because of complaints from building residents about the discomfort, in the form of increased indoor humidity levels. Another reason for choosing this building was the visible deterioration of the façade (Fig. 1).
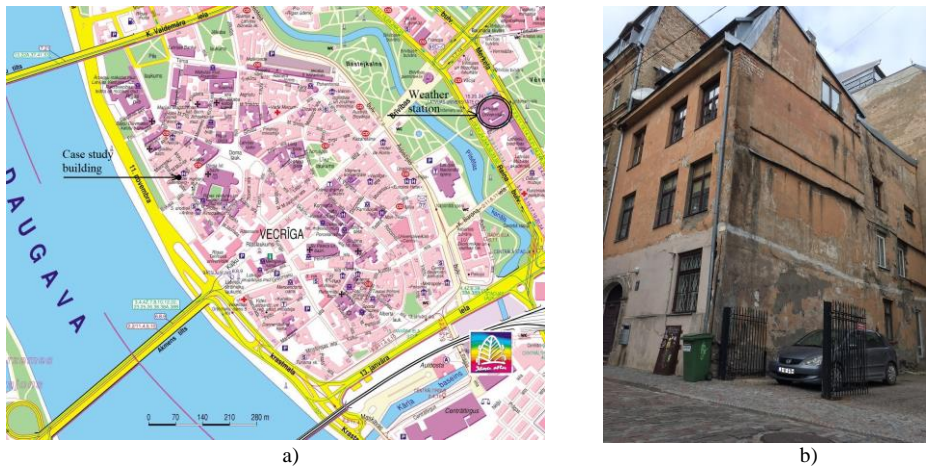
Fig. 1. Case study at Biskapa gate 6: a) location of building and weather station in map; b) façade of the building [15].

The building is a three-story residential building with additional attic floor and one underground floor (basement). Building was built in 1880 and is located in the historic center of Riga, approximately 150 m from the river Daugava (Fig. 1). The building area is 120.9 m² with a 1511 m³ of construction volume. The building has two adjacent buildings, one on the North-West (NE) and another on the North-East (NE) side of the building. Both adjacent buildings are 1 story higher than the case study building. The South-West (SW) side of the building is the main façade, with the entrance from the street (Biskapa gate). The SE facing façade is the largest open area to the outdoor weather, such as wind driven rain, sun radiation and wind. The free space between the SE façade and next building in this direction is 15 meters, this adjacent building has the same height as the case study building. About 10 years ago the ground floor flat owner has installed internal insulation of glasswool (0.05 m) on the SE wall.

2.2. Methodology

Qualitative and quantitative methods have been used for determination of the possible moisture sources in the external wall masonry.

Qualitative analysis includes direct observation of the building to identify existing signs of decay and moisture caused damages.

Quantitative method includes moisture distribution evaluation of the building exterior wall in relative scales. Moisture of the wall was measured from the outside. Wall moisture measurements from the inside were limited due to applied internal insulation. The moisture assessment was carried out in two depths – 2 cm and 20 cm deep in the masonry (including plaster). For these measurements a multifunction measuring device *Trotec T*3000 was used [16]. *Trotec T*3000 was used with two types of measurement probes for different measurement depths:

- Dielectric probe *TS* 660 *SDI* for 2 cm depth;
- Microwave probe *TS* 610 *SDI* for 20 cm depth.

Dielectric and microwave probe are both used for moisture distribution measurements in relative scale and cannot be directly compared with each other. Meaning that the same readings from both probes does not indicates same moisture contents.

For monitoring purposes, the measured South-East facing wall was divided into smaller squares forming a grid, approximately 0.4 m to 0.4 m each (Fig. 4). The same grid was used for the repeated moisture measurements over a period of time. Wall moisture measurements were started

124

in the autumn (September 21st of 2018) and were continued until the spring (March 5th of 2019). During the monitoring period, wall moisture was measured 5 times.

From the interior side of the wall, the monitoring system was installed, floor plan showing the measurement points are presented in Fig. 2.
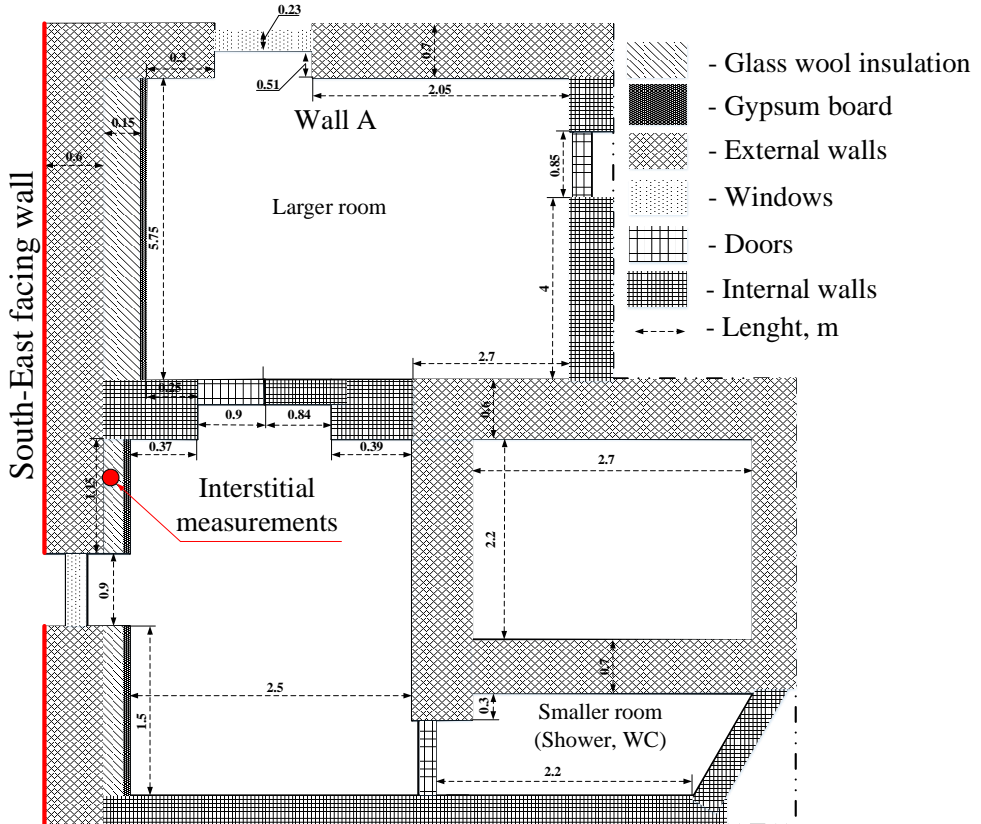
Fig. 2. Cross section of monitored wall with measurement points.

The monitoring system started to collect data on 20th November 2018. Monitoring system included relative humidity and temperature monitoring in between the layers of the insulation of the external wall. Monitoring of the relative humidity and temperature in between the layers of the insulation was done using the *Honeywell HIH* 4000-002 and type T PFA insulated twin twisted pair thermocouple cable. Data logger *Campbell CR*1000 was used for data logging of these sensors. For the insertion of the monitoring system, a small hole with a diameter of 27 mm was drilled in the internally insulated wall. In total, two relative humidity and two temperature sensors were installed in the insulation layers. The sensors were installed in pairs (relative humidity sensor combined with temperature sensor). The sensor pairs were installed 20 cm below the hole, one pair between the wall and insulation and the other pair between the insulation and gypsum board. Additionally, temperature and relative humidity was measured near the interior surface of the insulated wall. After the insertion of the relative humidity and temperature sensors, the hole was refilled with mineral wool and gypsum board. To avoid extra moisture addition to the insulation system through the cut and to retain access to the sensors, no plaster was used to cover the hole.

Instead the gypsum board was sealed in place with masking tape, and additionally covered with vapor tight aluminium adhesive tape.

Weather data from the closest weather station were used. The weather station is located at the University of Latvia (Fig. 1) and the data are managed by the "*Latvian Environment, Geology and Meteorology Centre*" (LEGMC) [17].

3. RESULTS AND DISCUSSIONS

Visual inspection of the façade revealed severe material loss, i.e. plaster and reduced masonry thickness at the ground level. Moreover, multiple cracks and poor-quality craftsmanship was noticeable. Algae growth was also evident on some parts of the façade. However, no sign of efflorescence was noticed. There was also an observation of some repair jobs carried out, where some of the lost material (plaster, bricks) had been replaced with cement. Near the ground level on the west-facing wall, a loss of building material was observed. Material loss was most severe on the edges of the wall and under the window but was almost undetectable on the front facing wall (Fig. 3).

a)

b)

c)

d)

Fig. 3. Façade of the building: a) South-West façade; b) South corner; c) right corner of South-East façade; d) South-East façade.

Fig. 4 shows the moisture measurements for both the 2 cm and 20 cm depths. The obtained values indicate moisture in relative scale, from drier to more wet area, where 0 signifies the most-dry and 250 the most-wet value.

126

| ☐ - Top | ☐ - Middle | ☐ - Bottom |

	134	147	149	128	125	159	181	155	147	82	128	153	168			142	116	82	143
	131	146	149	148	120	186	170	164	155	110	124	124	118			130	96	92	140
250	183	77	161	183	134	185	126	143	128	144	124	137	138			80	97	130	129
225	184	130	151	173	137	172	161	129	176	175	187	111	94			92	127	139	166
200	168	168	164	150	150	159	130	131	158	159	140	147	146	118	75	95	98	99	105
175	152	132	105	141	153	116	134	131	139	175	160	155	158	111	108	126	147	133	104
150										**2 cm depth**									
125	52	45	45	52	39	43	45	67	63	38	44	34	47			37	52	41	43
100	57	47	47	44	33	55	79	59	67	33	52	35	53			54	57	54	57
75	64	48	48	54	45	44	80	61	74	65	47	53	63			54	46	32	43
50	60	57	57	62	39	42	47	54	75	38	61	30	65			64	56	46	69
25	63	72	72	76	61	41	53	57	58	65	44	55	52	35	47	68	44	37	49
0	50	43	43	55	64	52	40	41	56	72	50	60	58	50	47	70	55	40	36

20 cm depth

Fig. 4. Moisture distribution in the wall, March 5th, year 2019.

The average moisture values for 20 cm depth of the external wall of all the measurement dates are presented in Table 1. The measurement difference between highest and lowest measured value varies from 45 in November to 65 in February.

TABLE 1. AVERAGE VALUES OF 20 CM DEPTH MEASUREMENTS

	21st September	22nd November	19th January	12th February	5th March
Average	48.35	48.56	49.24	50.45	52.30
Max value	79	78	83	89	80
Min value	28	33	30	24	30
Mode	39	50	44	49	47
Median	48	47	48	49	52
Standard deviation	10.85	9.46	9.18	11.28	11.41

TABLE 2. AVERAGE VALUES OF 2 CM DEPTH MEASUREMENTS

	21st September	22nd November	19th January	12th February	5th March
Average	99.84	123.95	107.12	119.58	137.59
Max value	182	190	161	161	187
Min value	49	13	14	16	75
Mode	126	126	100	125	147
Median	99	126	108.5	126	139
Standard deviation	28.87	30.98	26.44	21.21	26.99

For better understanding of moisture distribution in the wall and how it corresponds to the changing weather, the measurement area was divided in three sections (Fig. 7). The sections are

127

bottom section from ground up to 0.8 m, middle section from 0.8 m to 1.6 m and top section from 1.6 m to 2 m.

In Fig. 5 changes of average values in top, middle and bottom sections, for 20 cm depth measurements are presented. There has been an upward trend at the bottom section of the wall, during the measurement period. Likewise, the top section follows the upward trend, with the slight decrease from 1st to 2nd measurement. The moisture measurements of the middle section had a drop of average moisture value in January, but afterwards they start to follow an upward trend.
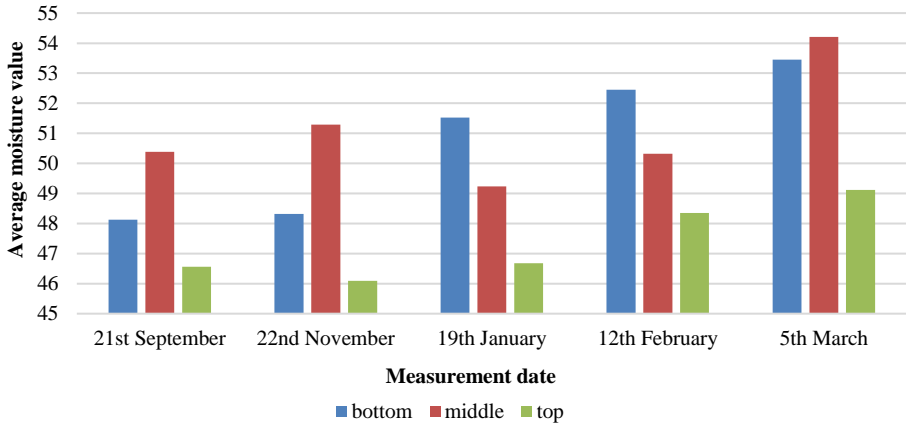
Fig. 5. Average moisture value changes for 20 cm depth measurements.

In Fig. 6 changes of average values in top, middle and bottom sections, for 2 cm depth measurements are illustrated. The 2 cm depth measurements follow a very similar trend as the 20 cm depth measurements in the middle section, with an increase in the period from the September to November, followed by a drop and then continuing an upward trend.
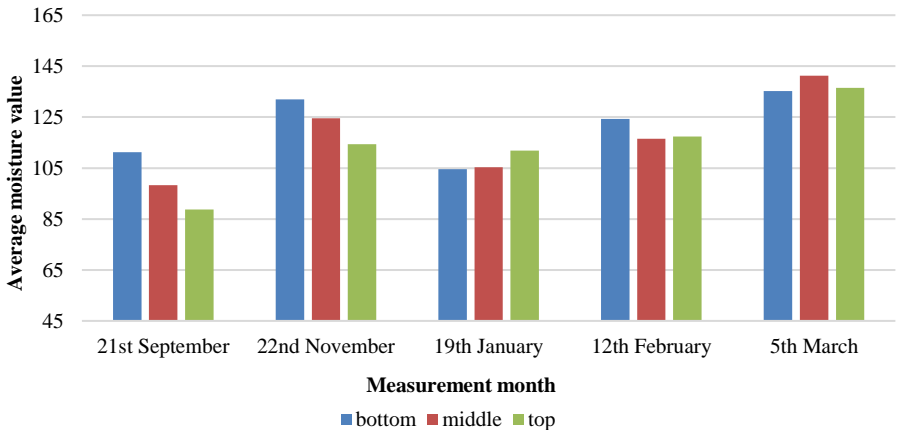
Fig. 6. Average moisture value changes for 2 cm depth measurements.

In Fig. 7 the average moisture measurement values are compared to each other and to average relative humidity period of 24-hours, prior to the measurements. It can be seen that 2 cm depth measurements, that represent moisture values near the surface, are more than two times greater

128

than 20 cm depth measurements that represent moisture values 20 cm inside the masonry. During the measurement period, average 20 cm depth measurements change only by 3.5 during the whole period, but maintain the upward trend. 2 cm depth measurements on the other hand fluctuate and change by a total of 37.75 during the measurement period.
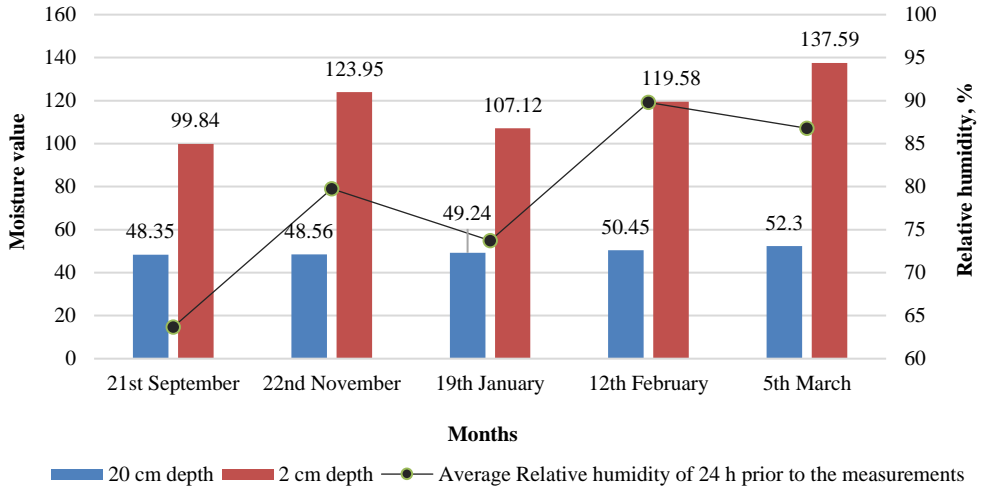
Fig. 7. Average values of the wall moisture measurements and outdoor relative humidity

In Fig. 8 the correlation between the outdoor relative humidity and wall moisture is presented. The correlation observed is good for 2 cm depth and little less for 20 cm depth.

a)   b)
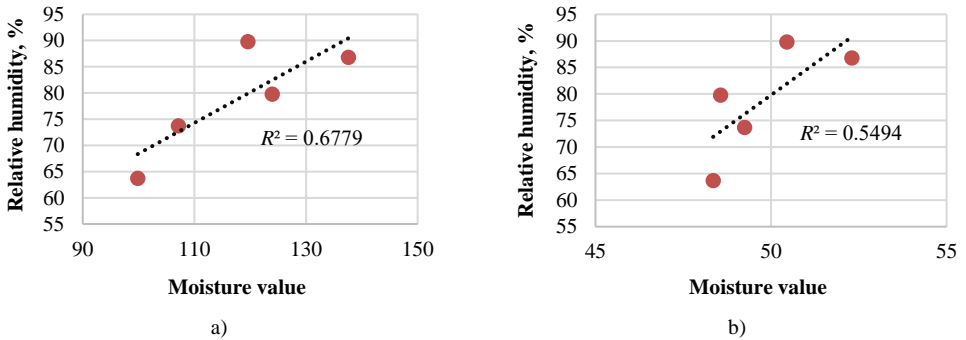
Fig. 8. Correlation between outdoor relative humidity and: a) 2 cm depth measurement values; b) 20 cm depth measurement values.

Rain load events with the total amount of rain 1 mm or greater are shown in Fig. 9. Total rain event is greater between 1st and 2nd measurement, than between the 2nd and 3rd measurements. That could explain the sudden drop of average moisture values in the 3rd measurements (in 19th January). Moreover, the 4th and 5th measurements, that have shown the highest average moisture values, are made right after the rain event.
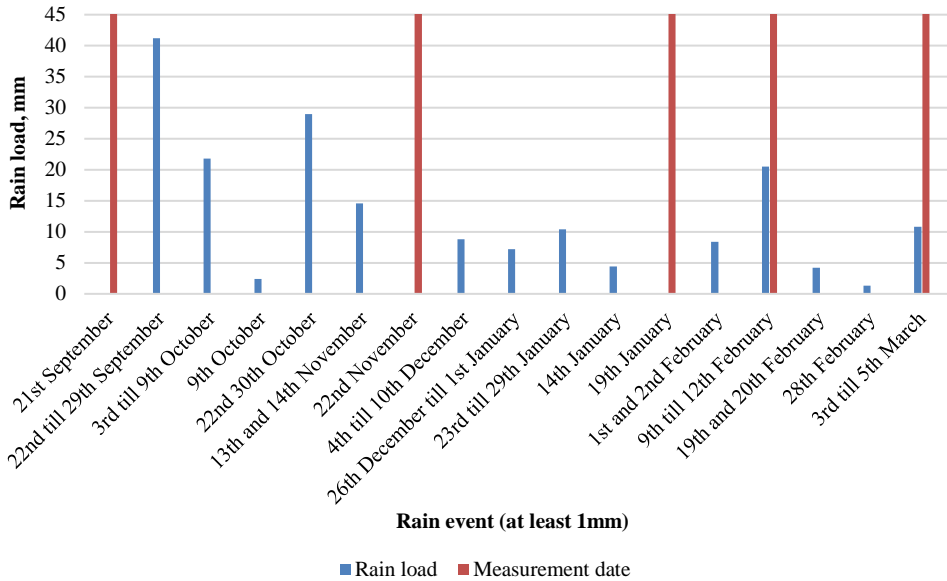
Fig. 9. Rain load event during the monitoring period.

24-hour cumulative rain events of three consecutive days prior to the measurements are presented in Fig. 13. When comparing Fig. 7 with Fig. 10, it can be seen that on the 12th February when the total rain load is higher (by 9.5 mm), the average 2 cm depth measurement is slightly lower (by 18.01) than on March 5th. However, the rain load during March 5th is higher (by 4.9 mm) than on February 12. After comparing average moisture values of 2 cm depth measurements with the rain event from Fig. 10, it can be seen that the average moisture value is affected more by the rain load event 24-hours before the measurement, rather than total rain load event of the 3-day period prior to the measurement.
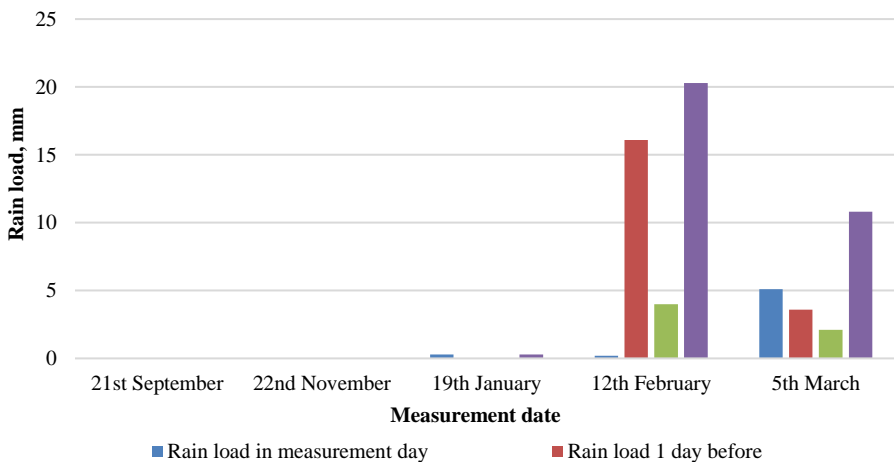
Fig. 10. Rain load of three days prior to the measurement.

130

The dominant winds and wind speeds during the monitoring period are shown in Fig. 11. Over the period of three days prior to the measurements on 12th February and 5th March, the following wind conditions were observed:

- 12th February 58.46 % of wind comes from the South, followed by 13.58 % from South-West with a dominant speed of 5 m/s;
- 5th March 47.69 % of wind comes from the South west followed by 18.6 % from South, with a dominant speed of 3 to 5 m/s.
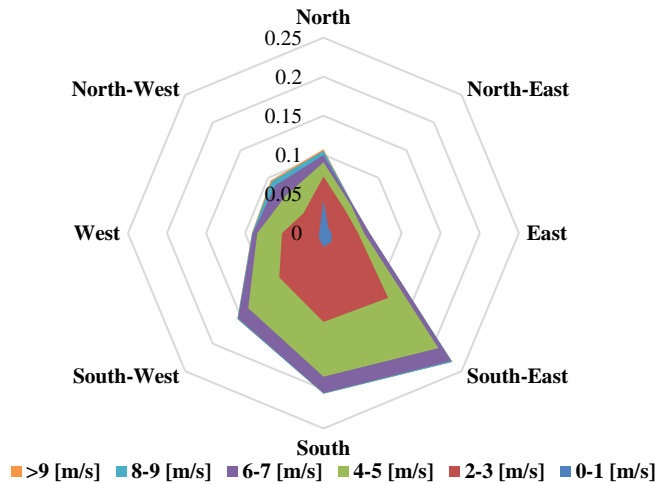
Fig. 11. Wind direction and speed during the monitoring period.

Fig. 12 present relative humidity and temperature measurements during the monitoring period. It can be seen that relative humidity under the insulation material stays mainly below 80 % that has been considered as the critical moisture when the mold growth would occur. Relative humidity fluctuates during the monitoring period from 58.85 % to 83.9 % and on the average is 74 %. It also can be seen that temperature under the insulation material stays above 0 °C that reduces the risks of freeze thaw cycles to occur. During the monitoring period temperature fluctuates from 5 °C to 11.5 °C and on the average is 8.4 °C.
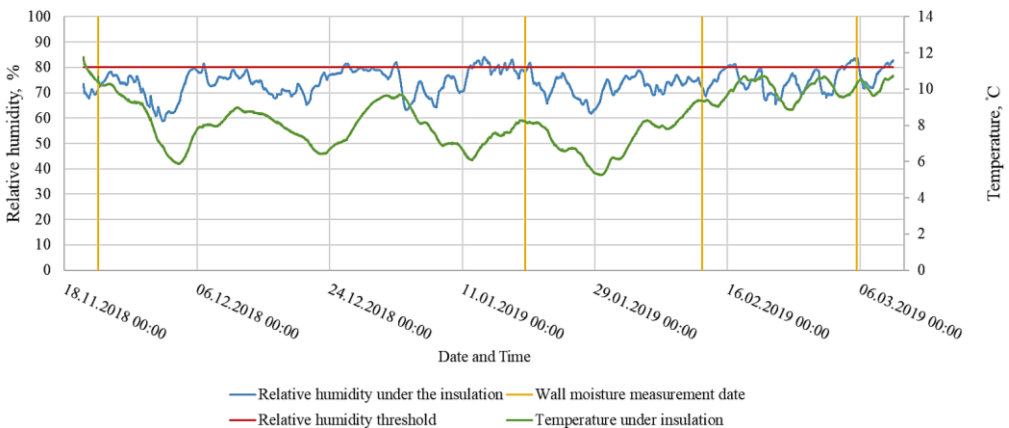
Fig. 12. Relative humidity in the insulation system.

4. CONCLUSIONS

The main goal of this research is to study application of internal insulation in historic buildings by assessing the possible moisture sources in the external wall and their impact on moisture content and moisture transport in the wall.

Obtained results show the loss of external plaster is obvious in many areas of the façade, combined with cracks, and cuts. These open areas allow outdoor moisture i.e. wind driven rain, to easily penetrate the wall. Algae growth on the façade indicates that rain water has been present on the walls' surface.

Measurement results also show that moisture content is building up during the autumn and winter periods. This is strongly influenced by outdoor moisture, both relative humidity and rain load events. The dominating wind during the monitoring period was from the same direction as the assessed façade is facing (SE), indicating that wind driven rain could be the reason for the accumulation of moisture in the masonry.

Outdoor weather conditions also have an effect on the interstitial conditions between the layers of the insulation and the external wall. But no interstitial condensation has been observed during the monitoring period. Highest relative humidity beneath the insulation material during the monitoring period reaches 84 % and for most of the time relative humidity stays under 80 %. Such moisture conditions do not cause high risk of mold growth. Results from biological assessment of insulation sample taken from the wall show no signs of mold presence.

No clear signs of rising damp problem were observed during the monitoring period. But as the monitoring period took place only seven months in the cold period of the year, rising damp problem could still be a problem during the spring and warm months of the year.

It must be considered that the non-homogeneity of the façade could be the reason for the fluctuations of the measurements, especially the 2 cm depth measurements close to the surface.

For more conclusive results, monitoring should be continued for at least one full year. Wind driven rain measurements on the façade and continuous moisture monitoring at different heights of the masonry will be performed.

ACKNOWLEDGEMENT

REFERENCES

[1]   Policy Pathways Modernising Building Energy Codes. Int. Energy Agency, 2013. [Online]. [Accessed: 01.02.2019] Available:
      https://cleanenergysolutions.org/sites/default/files/documents/2013-08-20-modernising-building-energy-codes.pdf
[2]   Albatayneh A., Alterman D., Page A., Moghtaderi B. The significance of building design for the climate. *Environmental and Climate Technologies* 2018:22:165–178. doi:10.2478/rtuect-2018-0011
[3]   Historical building types and combinations of structural solutions and main driving forces promoting renovation of historic buildings based on case studies. Report. EU project Robust Internal Thermal Insulation of Historic Buildings (RiBuild), project No. 637268: 2015.
[4]   De Rosa M., Bianco V., Scarpa F., and Tagliafico L. A. Heating and cooling building energy demand evaluation; a simplified model and a modified degree days approach. *Applied Energy* 2014:128:217–229. doi:10.1016/j.apenergy.2014.04.067
[5]   European Commission. Directive 2010/31/EU Of The European Parliament And Of The Council of 19 May 2010 on the energy performance of buildings (recast). *Official Journal of the European Union* 2010:153.
[6]   Ratnieks J., Jakovics A., Gendelis S. Wall assemblies U-value calculation in test buildings using constant power heating. *Energy Procedia* 2018:147:207–213. doi:10.1016/j.egypro.2018.07.061
[7]   Albatayneh A., Alterman D., Page A., Moghtaderi B. The Significance of Temperature Based Approach Over the Energy Based Approaches in the Buildings Thermal Assessment. *Environmental and Climate Technologies* 2017:19:39–50. doi:10.1515/rtuect-2017-0004

132

[8]   Franzoni E. Rising damp removal from historical masonries: A still open challenge. *Constr. Build. Mater.* 2014:54:123–136. doi:10.1016/j.conbuildmat.2013.12.054

[9]   Krawczyk D. A., Wadolowska B. Analysis of indoor air parameters in an education building. *Energy Procedia* 2018:147:96–103. doi:10.1016/j.egypro.2018.07.038

[10]   Jimenez-Bescos C., Prewett R. Monitoring IAQ and thermal comfort in a conservation area low energy retrofit. *Energy Procedia* 2018:147:195–201. doi:10.1016/j.egypro.2018.07.055

[11]   Adhikari R., Lucchi E., Pracchi V. Experimental measurements on thermal transmittance of the opaque vertical walls in the historical buildings. PLEA2012 Conf. Oppor. Limits Needs Towar. an Environ. responsible Archit., 2012.

[12]   Hola A. Measuring of the moisture content in brick walls of historical buildings – the overview of methods. *IOP Conf. Ser. Mater. Sci. Eng.* 2017:251:012067. doi:10.1088/1757-899X/251/1/012067

[13]   Rosina E. When and how reducing moisture content for the conservation of historic building. A problem solving view or monitoring approach? *J. Cult. Herit.* 2018:31:S82–S88. doi:10.1016/j.culher.2018.03.023

[14]   Barreira E., Almeida R. M. S. F., Delgado J. M. P. Q. Infrared thermography for assessing moisture related phenomena in building components. *Constr. Build. Mater.* 2016:110:251–269. doi:10.1016/j.conbuildmat.2016.02.026

[15]   Jana seta [Online]. [Accessed 15.03.2019]. Available: https://www.kartes.lv/lv/

[16]   Practice handbook for multifunction measuring meter T3000 (EN) [Online]. [Accessed: 01.02.2019] Available: https://uk.trotec.com/fileadmin/downloads/Multifunktion/T3000/TRT-PH-T3000-WM-001-EN.pdf

[17]   LEGMC [Online]. [Accessed: 10.03.2019] Available: https://www.meteo.lv/

Ritvars Freimanis received M. sc. degree in Environmental Engineering by graduation both Riga Technical University and Vilnius Gediminas Technical University in 2019.
Since 2017 he works as a scientific assistant at Institute of Environmental and Energy Systems at Riga Technical University, Riga. He is involved in EU research project *RIBuild* that develops guidelines on how to install thermal insulation on historic buildings.

Rasa Vaiskunaite defended dissertation in the field of Technological Sciences (Environmental Engineering Sciences Field, 04T), Vilnius Gediminas Technical University (VGTU), 2004. Master of Natural Sciences (Ecology), Vilnius University (VU), 2000. Bachelor of Natural sciences (Biology), Vilnius Pedagogical University (VPU), 1998.
Work experience. Doctoral student (Ph. D.) of Technical Sciences (from 2000) in the Vilnius Gediminas Technical University (VGTU, formerly VTU); Assistant of the Environment Protection Department (from 2002) in VGTU; Associate Professor of the Environment Protection Department (from 2004) in the VGTU; Vice-Dean of the Environmental Engineering Faculty (from 2005) in VGTU; Professor of the Environment Protection and Water Engineering Department (from 2015) in VGTU.
Author prepared more than 73 scientific publications: 1 monograph, 1 handbook, 3 training books, 68 publications, 1 patent. Author participated in 16 conferences (7 of them international – in Sweden, Greece, Russia, Bulgaria etc.), Chairman of the Organizing Committee in 4 International Conferences "Environmental Engineering".

Tereza Bezrucko, Senior expert and project administrative manager at Riga Technical University, Institute of Energy Systems and Environment. Since 2008 Tereza Bezrucko is working at Riga Technical University. The main research area of the Author is analysis and planning of economic processes at local and international levels. She has been involved in more than 40 EU and national research projects.

133

Andra Blumberga, Dr.sc.ing., professor, works for Institute of Energy Systems and Environments, Riga Technical University since 2001.

She has been working with energy efficiency since 1992. Her main research interest is energy efficiency both from technical and policy sides.

She has managed many national and international research and other projects since 1999, e.g. "Assessment on energy efficiency and use of renewable energy sources in Latvia by 2020", "Climate Technology development modelling in energy sector", "Energy strategy 2030 for Latvia", "System Dynamics modelling for energy sector in Latvia".

She has been working as the World Bank energy expert for development of the Green Investment Scheme in Latvia. She is author of more than 80 publications and 14 monographs.
ORCID ID: https://orcid.org/0000-0002-4712-4794

Is the High Quality *Baukultur* a Monkey Wrench in the Global Climate Challenges?

Andra BLUMBERGA[1]*, Ruta VANAGA[2], Juris ANTUZS[3], Ritvars FREIMANIS[4],
Edgars BONDARS[5], Sandra TREIJA[6]

[1–4]*Institute of Energy Systems and Environment, Riga Technical University, Azenes iela 12/1, Riga, LV-1048, Latvia*

[5–6]*Faculty of Architecture, Riga Technical University, Kipsalas iela 6, Riga, LV-1048, Latvia*

Abstract – **The EU 2030 climate package calls for raising energy efficiency, increasing usage of RES and decreasing the carbon footprint. There are stringent requirements for new buildings, but the energy efficiency potential in the existing building stock is still not fully explored. The latest trend in urban energy efficiency is the Positive Energy Block (PEB) strategies for new developments. It includes raising building energy efficiency, optimizing energy flow and implementing renewable energy sources (RES). Transforming all existing blocks in a city centre to a PEB would radically change the pattern of energy supply and consumption. European cities have historic centres with great architectural and cultural value. Any urban regeneration strategies must respect and preserve historic values. This paper describes double multi-criteria analysis evaluating urban blocks from both the energy efficiency and cultural heritage perspective with the goal to select the sample block for a "Smart urban regeneration – transition to the Positive Energy Block" case study. Proposed criteria for multi-criteria analysis to evaluate cultural heritage, liveability and energy efficiency potential describes specific qualities of the urban block. The obtained results show that blocks with higher cultural value show less energy efficiency potential and *vice versa*. It is recommended to apply cultural value and liveability qualities in the Smart urban regeneration process to those blocks with high energy efficiency potential.**

Keywords – **Building energy efficiency; cultural heritage; Davos declaration; energy community; historic city centre; liveable city; multi-criteria analysis (MCA); Positive Energy Block (PEB); smart urban regeneration**

Nomenclature	
PEB	Positive energy block
MCA	Multi-criteria analysis
nZEB	Nearly Zero energy building
RHC	Riga Historic Centre
GHG	Greenhouse gases

---

* Corresponding author.
E-mail address: andra.blumberga@rtu.lv

1. INTRODUCTION

1.1. Climate Change Mitigation

Frequent extreme weather occurrences, irreversible loss of biodiversity, animal species migrating to new habitats misbalancing local ecosystems, even humans are migrating or being displaced facing extreme weather or related scarce resources/nutrition are the effects of climate change we have to face. The climate change is present and very likely driven by anthropogenic impact (raising GHG levels due to human activities) [1]–[5]. To mitigate climate change, the Paris Agreement has set the goal to restrict anthropogenic impact on climate systems by decreasing GHG emissions and limiting global temperature increase to 1.5 ℃ [6], [7].

The EU is fully committed to international climate mitigation goals and continually sets new targets for GHG reduction in climate policy packages developed by the European Climate Change Programme and each member state contributes to the common goal [8]. The 2030 climate and energy framework is currently in force and it aims to cut GHG, to increase the use of renewables and to raise energy efficiency [9].

1.2. Dilemma – Building Energy Efficiency in Historic City Centre vs Preservation of Cultural Heritage

Buildings and construction account for 36 % of global final energy [10], cities account for around 75 % of CO_2 emissions from final energy use [11], [12] and this makes the building sector and urban areas a target of energy efficiency policies [13]–[16]. There are stringent requirements for new developments – all new buildings must be nearly zero energy buildings (nZEB) and the latest EU Directive 2018/844/EU stresses the necessity of reaching nearly zero energy building benchmarks in building renovations and decarbonizing the existing building stock.

There are a number of techniques developed for energy efficiency measures for buildings built in the post-WWII era. Thus pre-WWII buildings demand more skilled renovations, preserving possible cultural heritage values [17]–[19]. Especially in dense urban environments, new energy efficiency techniques for renovation of culturally valuable building stock are urgently necessary to fulfil the plans of decarbonising the existing building stock.

Energy efficiency driven refurbishment often is accused of not respecting the aesthetic needs and surrounding context and prioritizing technological and economic issues. To trigger changes in building processes and understanding of the importance of the built environment, Davos declaration (2018) calls to reinforce the traditions of high quality "*Baukultur*" and reminds us that the built environment is one of essential cultural values – it creates a scene for habitat and is essential to the quality of life. The Davos declaration emphasizes the importance of liveable surroundings and preservation of cultural values [20], [21]. On one hand there lies big energy efficiency potential in existing building stock, but on the other hand cultural values must be preserved. Will the Davos declaration requirements limit local and global energy efficiency and climate goals? To what extent? Is there a compromise possible?

Research project "Smart urban regeneration – transition from traditional urban block to the Positive Energy Block in Riga Historic Centre" will evaluate the possibilities and limits of energy efficiency driven smart urban regeneration in valuable historic environment.

1.3. Positive Energy Blocks

Research launched matches to the European Strategic Energy Technology Plan (SET-Plan) aiming to reduce GHG emissions accelerating the deployment of low-carbon technologies and specifically addresses smart cities and communities as the target group by introducing positive energy blocks/districts [22]. In the scope of building a low-carbon, climate resilient future, the concept of smart cities has been developed to promote energy transition in cities – *"Positive Energy Blocks (PEB)/districts consist of several buildings (new, retro-fitted or a combination of both) that actively manage their energy consumption and the energy flow between them and the wider energy system. PEB/Districts have an annual positive energy balance. They make optimal use of elements such as advanced materials, local RES, local storage, smart energy grids, demand-response, cutting edge energy management (electricity, heating and cooling), user interaction/involvement and information and communications technologies (ICT)"* [23], [24]. In a symbiotic approach combining all buildings within one block in a single energy system can be beneficial to every building unit and the overall building energy efficiency goals can be easier to achieve.

1.4. Smart Urban Regeneration – Transition to a Positive Energy Block Respecting the High Quality of Baukultur

The research has two equally important goals – to reach a positive yearly energy balance and to apply high quality *Baukultur* requirements to energy-driven, smart urban regeneration. The result of this research will demonstrate to what extent preservation of cultural values might limit energy efficiency goals. The first step of the study and the scope of this paper is the selection of Riga's Historic Centre urban block with the greatest potential to reach a positive yearly energy balance.

2. METHODOLOGY OF THE STUDY

Proposed methodology of selection of the urban block with the greatest potential to reach the positive yearly energy balance is applicable to any densely built urban environment.

The aim of the first step of the study is to select a RHC block for smart urban regeneration. Since there are two equally important goals for the study, the selection of the block is considered from two perspectives – its energy efficiency potential and the high quality *Baukultur* and liveability in urban blocks.

The selection of the block will be based on multi-criteria analysis (MCA) where possible alternatives are evaluated according to the set of criteria important for the goal [25], [26]. MCA has been used in numerous sustainable development studies [27]–[34].

Research is carried out in three phases (Fig. 1). In PHASE 1 – the decision-making context is identified, goals are set and a decision-making hierarchy is created. In PHASE 2 multiple sets of MCA are performed according to the number of stakeholders involved. In the scope of this research "Energy efficiency" and "Cultural heritage and liveability" are considered. The alternatives are ranked according to the sub-goals of each analysis, and the best alternative for each stakeholder is determined. In PHASE 3 results are compared and final decisions made based on PHASE 2 findings and summarized in conclusions.

Fig. 1. Methodology of the study.

MCA is carried out in three steps. The 1st step is to define outranking criteria that are essential for the goal, so the blocks missing essential criteria are excluded from further study. The 2nd step is to define and weight criteria using Analytical Hierarchy Process methodology. In the 3rd step TOPSIS is used for ranking the alternatives [25].

3. CASE STUDY: URBAN BLOCK SELECTION RIGA HISTORIC CENTRE FOR SMART URBAN REGENERATION

3.1. PHASE 1 – Identifying the Context, Setting the Goal

Context. Fig. 2 illustrates the average age of buildings in Riga city [35]. The city centre comprises of the oldest buildings (more than 80 years), but the outskirts of the city are dominated by buildings of less than 50 years illustrating the expansion waves of Riga city. The launched study focusing on Historic Centre of Riga will provide new knowledge for energy efficiency driven intensive refurbishments in dense urban areas carrying cultural values.

233
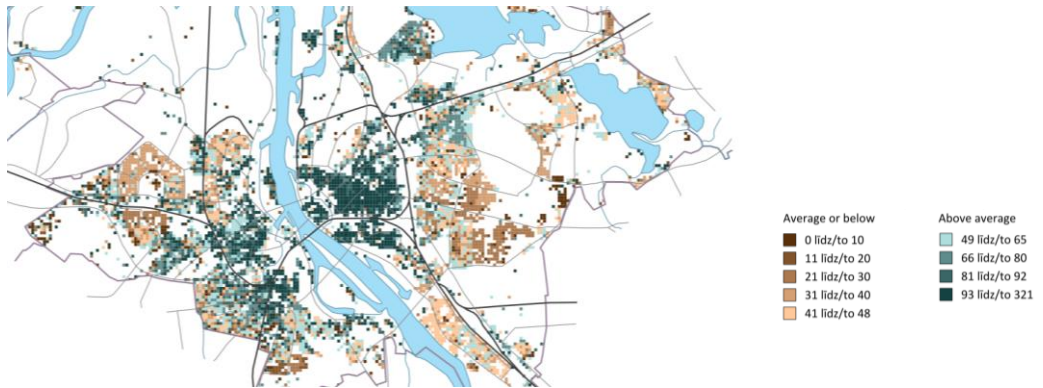
Fig. 2. Average age of inhabited dwellings in Riga [32].

The special value of the Riga Historic Centre RHC (Fig. 3) is its unique architecture – Art Nouveau buildings, wooden buildings and industrial architectural heritage. Historical values coexist with multifunctional use. RHC is a town-constructive monument with a unique landscape consisting of the multifunctional character of the city centre and its unique architecture. Preserving the cultural heritage while implementing the new developments to the historical environment is the vision set out in the ''Riga Sustainable Development Strategy 2030'' [38].
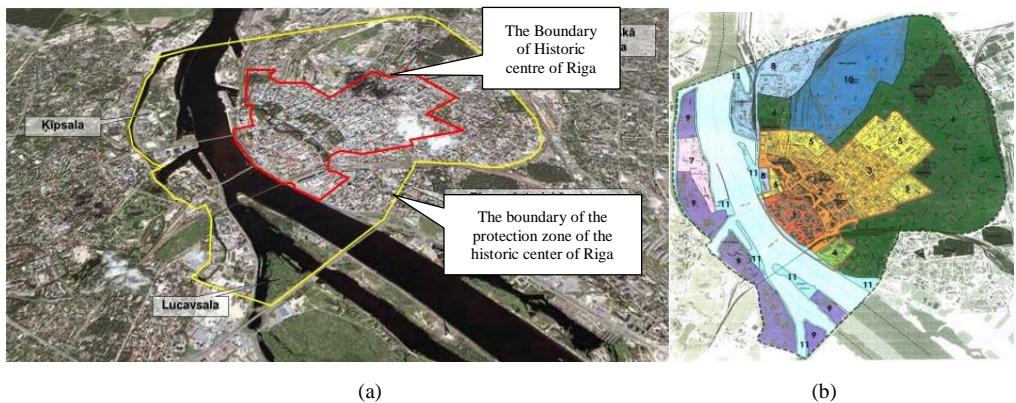
Fig. 3. (a) Riga Historic Centre in the context of the city [36]; (b) zoning in Riga Historic Centre and its protection zone [37].

The status of the UNESCO World Heritage Site [39], [40] puts the city of Riga in the context of global urban competition. The rich cultural background makes RHC a perfect scene for Smart urban regeneration – transition to a PEB respecting the high quality *Baukultur*.

The goal. The first step in the Smart urban regeneration research project is to select the RHC urban block that reflects energy efficiency capacities and high quality *Baukultur* and cultural heritage values.

The RHC and its protection zone are subdivided in 11 characteristic territories (Fig. 3(b)). This research is focusing on the densest territories of RHC – its core (No. 3) and the outer parts of the core (No. 5). The first screening of RHC shows that blocks with energy efficiency capacities are located at the outer perimeter of RHC, but blocks with higher cultural value are

234

concentrated in the central parts of RHC, therefore two sub-goals are defined in decision making hierarchy 1) to find the RHC urban block with the highest energy efficiency potential and 2) to find the RHC urban block representing the highest qualities of cultural heritage and urban liveability.

3.2. PHASE 2 – Selection of Alternatives from Various Perspectives

3.2.1. Multi-Criteria Analysis, Selecting the "Cultural Heritage Block"

The unique values of RHC – listed buildings of national importance, Art Nouveau buildings and wooden buildings – are defined as the outranking criteria for further selection of "Cultural heritage block". Map overlay method [41], [42] was used in this step – colouring blocks comprising each outranking criterion. Blocks that comprise all three criteria are the subject of the next step of the evaluation process. 15 blocks were selected (Fig. 4).
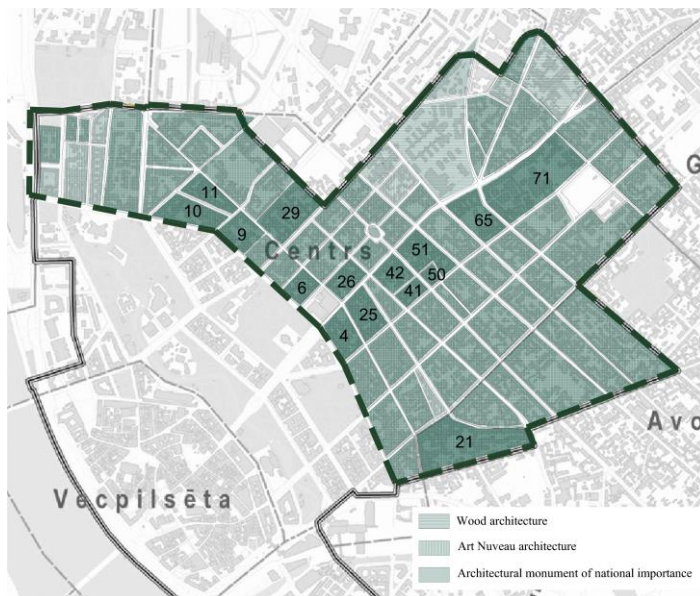
Fig. 4. Overlay map of architectural values in RHC.

Criteria. The presence of cultural heritage or buildings of high architectural value is just one component essential for habitable environment. The space between the buildings is another important component – it can upgrade if it is human-oriented or downgrade the living environment if human needs are disregarded. Jacobs [43], Whyte [44], [45] were the frontiers of the human-oriented approach in urban planning. The term liveability is introduced to describe the quality of life in living environment integrating physical and social wellbeing parameters. There are different methods of evaluating urban liveability ranging from socio-economic oriented methods designed for expatriates, businessmen, investors, corporations to more urban planning related criteria designed for residents and city population [46]–[64]. In the scope of this study, urban planning parameters are found to be more suitable. Following the path of the human-oriented approach, influential urban design consultant Jan Ghel has defined 12 liveable city criteria divided in three categories [65], [66]:
  – Protection – protection against traffic and accidents, protection against crime and

          violence and protection against unpleasant sensory experiences;
- Comfort – opportunity to walk, to stand/stay, to see, to talk, to play and exercise;
- Delight – human scale design, opportunities to enjoy local climate, and to gain positive sensory experiences – fine views, plants, trees and water presence.

RHC is a rather homogenous environment and most of these criteria are relevant to all the RHC urban blocks – some of those are developed equally well (walking opportunities and human scale for instance); some are equally disregarded (exercising opportunities).

Liveability of cities is a dynamic process – it involves a lot of participants and holds the unstable character of human decisions. Defined criteria and evaluation of urban blocks is the attempt to capture RHC situation in one moment of time. To compare building blocks following criteria are used combining cultural heritage and liveability aspects.

TABLE 1. "CULTURAL HERITAGE AND LIVEABILITY BLOCK" CRITERIA

Criteria	Definition
Cultural heritage	
Cultural and historical significance	Evaluates diversity of values in an urban block. RHC comprises Art nouveau and wooden buildings, national and local cultural monuments, as well as buildings with a specific cultural and historical value. RHC urban blocks vary in their cultural heritage capacity
Variety of construction periods	More construction periods show a wider spectrum of the development periods of city, believes and values of different times and create richer background for further developments
Protection	
Protection against crime and violence	Most important criteria for liveable cities
Protection against unpleasant sensory experiences	Air pollution and noise problems are directly related to the intensity of the traffic of street adjacent to the urban block. More intensive streets create more pollution and noise. Blocks not directly connected to the main arteries of the city are considered more liveable despite the fact that over the years the greatest architectural achievements and treasures were on display facing the most important routes of the city
Comfort	
Opportunity to stay and sit	There are several parks at the central part of the RHC that are accessible to any urban block within a walking distance (15 min), but public spaces along the streets are poorly developed. None of RHC urban blocks are privileged to comprise a pedestrian street or public recreational spaces. In this criteria street cafes are recognized as an added value to the streetscape and urban environment
Landscaped courtyard	Municipal decisions to support and develop car infrastructure has led to private initiatives to explore their properties as parking lots for cars. Car infrastructure in inner spaces of urban blocks prevails over space for leisure, exercise and recreational functions. Landscaped courtyards add qualities to the urban liveability
Delight	
Positive sensory experiences	Positive sensory experiences among other aspects are provided by the presence of trees, plants and water. Trees along the street add a positive sense to the urban environment
Renovation cycle of buildings	High quality *Baukultur* should not stop with handing the key to the owner. Not only buildings should be built following high standards but respectfully maintained as well. Jan Gehl`s criteria are complemented with the criterion evaluating the condition of the buildings – are the buildings well preserved improving the environment or deteriorated degrading the environment

The weights of the criteria are obtained in a pairwise comparison matrix according to Analytical Hierarchy Process methodology [25]. Fig. 5 reflects the criteria weight. Cultural

significance and a variety of construction periods are defined as the most important criteria for "Cultural heritage block". From the liveability perspective, the most important is protection against crime, good sensory experience and the renovation of buildings. Weighted criteria reflect the priorities of the authors.
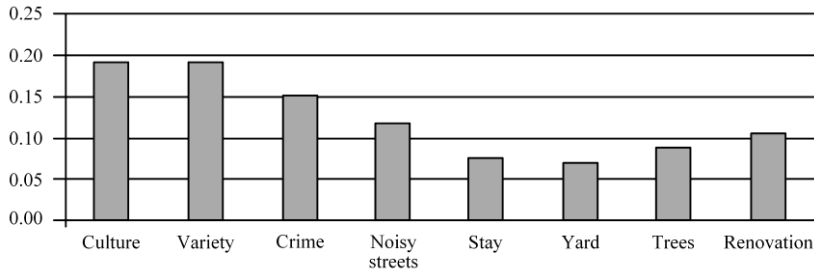

Fig. 5. Cultural heritage and liveability criteria weight.

Indicators. Each criterion is evaluated with the relevant indicator best describing the qualities and the essence of the criterion summarized in Table 2.

TABLE 2. "CULTURAL HERITAGE AND LIVEABILITY BLOCK" CRITERIA EVALUATION INDICATORS

Criteria	Definition
Cultural heritage	
Cultural and historical significance	For each architectural monument of national importance 3 points, 2 points for the local monument and 1 point for each other building with a historical value. Specific indicator was obtained dividing the total number of points by the number of plots in the block [64], [67]
Variety of construction periods	7 construction periods were defined – 1) prior to 1884; 2)1885–1923; 3)1924–1944; 4) 1945–1960; 5) 1961–1991; 6) 1992–2000; 7) 2001 – up until nowadays. 1 point for each decade of the construction period was awarded. Specific indicator was obtained dividing the total number of points by number of plots in the block [68]
Protection	
Protection against crime and violence	Number of crimes over last 3 years committed in urban block and adjacent streets were counted. Specific indicator was obtained dividing the total number of crimes by the total area of the block [69]
Protection against unpleasant sensory experiences	Each adjacent street of the block was evaluated. 0 points if the street is a part of route of national importance; 2 points for city magisterial street; 3 points for secondary street; 4 points for small by-street was awarded. Specific indicator was obtained dividing the total number of points by number of adjacent streets in the block [64]
Comfort	
Opportunity to stay and sit	Meters of the street length occupied by seasonal street cafes bars were evaluated. Specific indicator was obtained dividing the total meterage of cafes by total perimeter of the block
Landscaped courtyard	In the scope of this study, it was determined that publicly accessible parking lots serve the cars, not the people residing in the city. Plot in an urban block comprising public parking lot is penalized with –2 points. –1 point if inner courtyard serves just for cars. 0 points if courtyard is left empty, with no landscaping elements. 1 point if there is vegetation in courtyard with cars. 2 points landscaped courtyard without cars. Specific indicator was obtained dividing the total number of points by number of plots in the block

Delight	
Positive sensory experiences	Street landscaping is evaluated in this criterion. Each adjacent street is considered –1 point if there are no trees along the street and cars are occupying part of the sidewalk. 0 points if there are no trees on any side of the street and cars are parked on the road. 1 point if there are trees along one side of the street. 2 points if there are trees along both sides of the street. Specific indicator was obtained dividing the total number of points by number of adjacent streets in the block [64]
Renovation cycle of buildings	0 points for abandoned and deteriorating buildings long past the necessary renovation cycle; 2 points for un-renovated building closely past the renovation cycle and 3 points for renovated buildings are awarded. Specific indicator was obtained dividing the total number of points by number of buildings in the block

Ranking the alternatives. There are two distinctive blocks among others. Block No. 11 and Block No. 50. First one located at a border of RHC comprises outstanding cultural heritage values – the most remarkable Art Nouveau examples in Riga Historic City. The second block ranking the highest overall ranking of alternatives from cultural heritage and liveability perspective is a small urban block in the inner part of RHC. Block No. 50 gains this predominance ranking high both in terms cultural heritage and in the top 3 in terms of liveability criteria (crime, unpleasant sensory experiences and renovation of buildings).
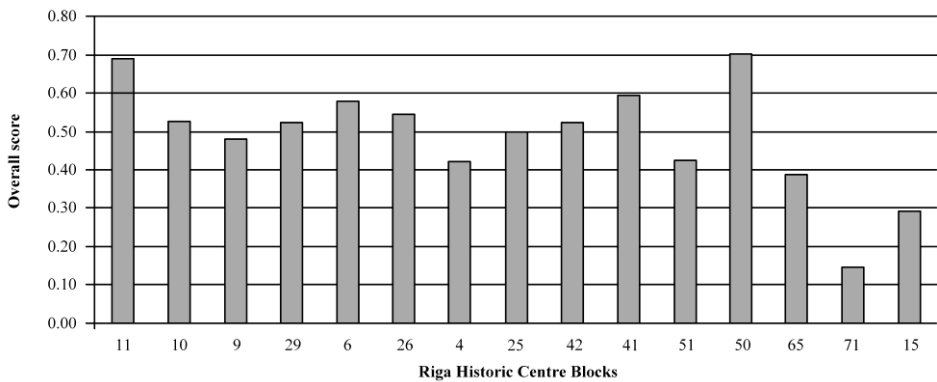
Fig. 6. Ranking the "Cultural heritage and liveability" alternatives.

3.2.2. Multi-Criteria Analysis, Selecting the "Energy Block"

Multi-criteria analysis goal from the energy perspective is to select the Riga Historic Center urban block with the greatest potential for transformation into a Positive Energy Block.

There are two phases for selecting the most appropriate urban block for transition to the PEB. In the first phase outranking criteria are defined. The urban block is processed for further research if: 1) there is an energy intensive enterprise located in the block; 2) the block has a residential function of at least 10 %; 3) there is an undeveloped plot in the urban block for highly efficient development. The medieval part of the RHC and the boulevard circle was excluded from further study since those are areas of special cultural value and distinctive character. The research area is marked with a blue dotted line (see Fig. 7). Map overlay method was used to visualize the shortlisted urban blocks. The darker the block (multiple layers) – the more qualities it carries. From the 82 RHC urban blocks in Riga Historic Centre, 12 blocks are suitable for more detailed research and multi-criteria analysis.

Fig. 7. Shortlisted "Energy blocks".

TABLE 3. "ENERGY BLOCK" CRITERIA

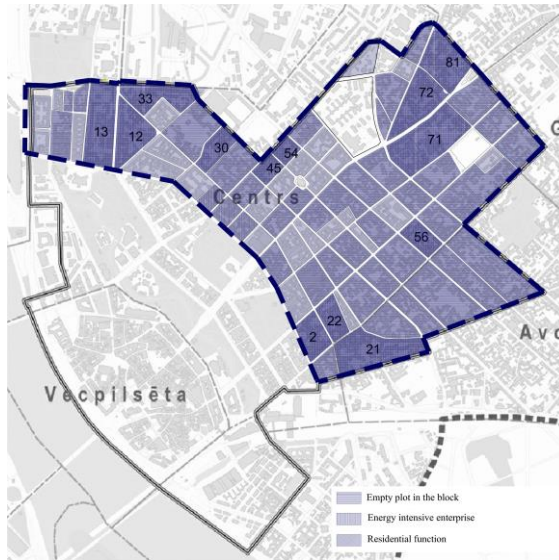| Criteria	Definition
Building density	Density of an urban block indicates the percentage of built footprint from total area. Free area for new development would be desirable and for allocating RES technologies. High density could limit these possibilities. Low density indicates poor development of the block
Proportion of residential function	It is important that residential and non-residential functions are represented in the urban block, because, typically, these functions share different times of day. If one function strongly prevails over the other, a misbalance occurs the can lead to energy demand and supply jams
Future development, new buildings	Every possibility for nZEB development in PEB would lower the overall average energy demand in a block. In new development advanced energy production and exchange technologies could be widely implemented
Possible intensive refurbishment	In the historic city centre there are a number of listed buildings where energy efficiency improvement measures are limited. This criterion encounters the amount of buildings where the intensive energy efficiency driven refurbished can be applied. The more there are buildings the can be intensively refurbished – the lower the overall energy demand of the block
Energy intensive function	To develop efficient and advanced energy exchange concepts energy intensive consumer within the block is needed in PEB. Energy intensive consumer can become waste heat source and surplus energy produced should not be transmitted to the grid. There are 5 energy intensive functions recognized in RHC: 1) production; 2) data centres; 3) office buildings; 4) hotels; and 5) libraries with strict indoor climate regulation demand. Cafes, restaurants are not considered energy intensive in the scope of this study
Type of energy intensive function	Defined Energy intensive functions vary in their intensity. Since there is no energy consumption data available for each building "type of energy intensive function" estimates the differences between functions

Criteria. MCA method TOPSIS for selecting the energy block is chosen. Six criteria are defined to evaluate urban blocks and their capacities for transition to a Positive energy block.

Criteria weights are obtained in a pairwise comparison matrix following the Analytical Hierarchy Process methodology [25]. Selected criteria are applicable worldwide in dense urban areas. Selected alternatives are local.

The most important criteria within the scope of this study are the presence of energy intensive enterprise in the urban block and its type. There are a lot of strategies widely applicable to building thermal envelope. But the energy efficiency strategies dealing with the optimization of energy exchange are the next generation in transition to Positive Energy Blocks. Therefore, criteria "Energy intensive function" and "Type of function" are strongly prevailing over the other criteria. Fig. 8 reflects the overall criteria weight. All the selected criteria are important for further study. Criteria with less significant importance in selection of urban block are the "Building density" and "Residential function".
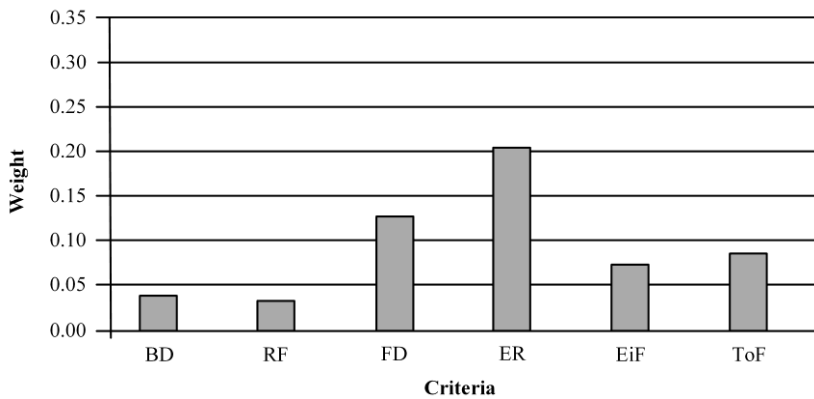

Fig. 8. "Energy block" criteria weight.

Indicators. Each criterion is evaluated with the relevant indicator best describing the qualities and the essence of criterion summarized in Table 4.

TABLE 4. "ENERGY BLOCK" CRITERIA INDICATORS

Criteria	Definition
Building density	Building footprint is divided by the overall area of the selected block. As the optimum 50 % of building density is defined Distance from 50 % is calculated [67]–[71]
Proportion of residential function	As the optimum 50 % of residential function proportion in urban block is defined. Distance from 50 % is calculated [67]–[72]
Future development, new buildings	Possible new development building footprint in every plot is evaluated. Total new development footprint in all plots of the block is divided by the overall area of the block [73]
Possible intensive refurbishment	Buildings 1960–2000 are designated for intensive energy efficiency refurbishment. Criterion expressed as the building footprint divided by the overall area of the block
Energy intensive function	Criterion expressed as the energy intensive building footprint divided by the total area of the building footprint in the block including new development
Type of energy intensive function	The most energy intensive function is the industrial enterprises awarded with 5 points. Less intensive (and less waste heat expected) functions are data centres – 4 points. Data office buildings – 3 points, hotels – 2 points and libraries (conditioned) – 1 point

Since the data obtained have incomparable dimensions, data normalization is carried out according to Weitendorf linear normalisation [74]. Eq. (1) for maximised values and Eq. (2) for minimised values:

$$b_{ij} = \frac{a_{ij} - \min_{ij}}{\max_{ij} - \min_{ij}} ,$$
(1)

$$b_{ij} = \frac{\max_{ij} - a_{ij}}{\max_{ij} - \min_{ij}} .$$
(2)

Ranking the alternatives. The alternative with the highest ranking (Fig. 9) is average size urban block that scored high in three most important criteria – it comprises a data centre that occupies about half of building footprint of urban block "22", the type of function is the second most intensive and it carries big potential for intensive energy efficiency refurbishment. Urban block "45/54" ranking second, comprises a significant footprint of the data centre as well. Urban block "72" ranking third comprises the most intensive function – industry, but it covers proportionally less of the overall building footprint in the urban block.
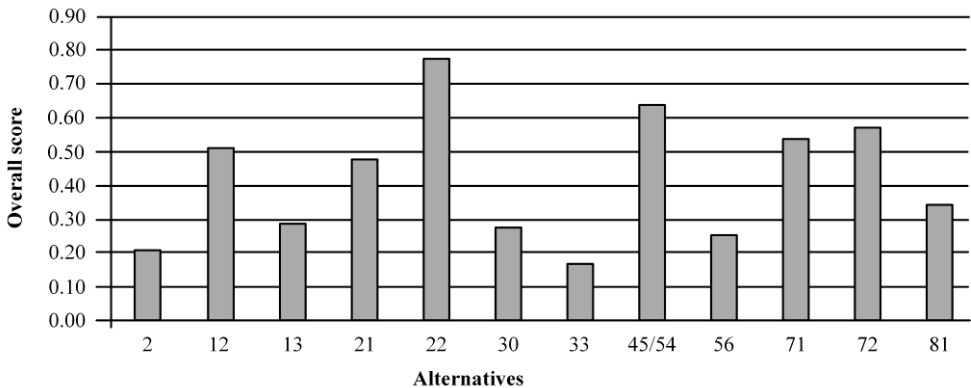
Fig. 9. Ranking "Energy block" alternatives.

3.3. PHASE 3 – Comparison of the Results, Decision Making

The study shows that higher quality architecture carrying more significant cultural value is concentrated in the central areas of Riga Historic Centre along the main routes, where once it had a representative function – to exhibit the technological achievements and conceptually new ideas. Unfortunately, over time the main routes have lost their role to showcase new architectural concepts and ideas and have turned into transportation infrastructure. Cars prevail over humans and the culturally most valuable areas are losing their liveability to traffic. It is found that the blocks with higher liveability capacity are located a bit away from the main streets but still in central areas of the RHC. These blocks have a lower cultural value, but higher liveability qualities.

"Energy blocks" are mostly situated in areas at the edges of the RHC. Most of the identified energy intensive units are built after WWII. In post-war planning, public spaces where injected in the existing urban pattern. Post-war/Soviet-period buildings have not been evaluated yet, none of these buildings are listed. In outranking phase of multi-criteria analysis creating the shortlist of potential urban blocks suitable for the research only two blocks No. 21 and No. 71 were on both lists "Energy" and "Heritage". Neither of those ranked high in overall ranking of alternatives and were not discussed for further research.

Energy perspective multi-criteria analysis has highlighted urban block with significant deep decarbonisation potential. Cultural heritage and liveability MCA have highlighted two outstanding Riga Historic Centre blocks – one carrying cultural heritage values, but the other – representing urban liveability qualities. The decision has been made to select block No. 22 for Smart Urban regeneration and implement the liveability and cultural qualities of blocks No. 11 and No. 50 to create a vibrant city centre block.

4. DISCUSSION

In this paper an attempt of quantifying and measuring cultural heritage, urban liveability and energy efficiency potential of urban bocks is described. The proposed methodology on selecting the urban block for transition to Positive Energy Block with defined criteria adequately reflects energy efficiency potential and cultural heritage intensity and liveability qualities of urban blocks and can be used worldwide. Further steps of the launched research will be to develop: 1) intensive energy efficiency refurbishment strategies; 2) renewable energy strategies; 3) energy supply-demand strategies for culturally valuable urban block. In addition, further research will be to 1) implement identified urban liveability strategies within the design of the city and 2) evaluate the impact of historical heritage preservation on energy efficiency measures.

ACKNOWLEDGEMENT

REFERENCES

[1] Díaz S., Settele J., Brondízio E. Summary for policymakers of the global assessment report on biodiversity and ecosystem services of the Intergovernmental Science-Policy Platform on Biodiversity and Ecosystem Services. IPBES, 2019.
[2] IPCC. Global Warming of 1.5 °C. Special Report. Intergovernmental Panel on Climate Change, 2018.
[3] World Meteorological Organization. Statement on the State of the Global Climate in 2018. Geneva: WMO, 2018.
[4] Tong S., Ebi K. L. Preventing and mitigating health risks of climate change. *Environmental Research* 2019:174:9–13. doi:10.1016/j.envres.2019.04.012
[5] Seneviratne S. I., et al. The many possible climates from the Paris Agreement's aim of 1.5 °C warming. *Nature* 2018:558:41–49. doi:10.1038/s41586-018-0181-4
[6] UNFCC. Adoption of The Paris Agreement. UNFCCC, 2015.
[7] UNFCCC. Paris Agreement. UNFCCC, 2015.
[8] ECCP. Second ECCP Progress Report. Can we meet our Kyoto targets? ECCP, 2003.
[9] A policy framework for climate and energy in the period from 2020 to 2030. Brussels: European Commission, 2014.
[10] Abergel T., Dean B., Dulac J. Global Status Report. Towards a zero-emission, efficient, and resilient buildings and construction sector. International Energy Agency, 2017.
[11] Gouldson A., et al. Exploring the economic case for climate action in cities. *Global Environmental Change* 2015:35:93–105. doi:10.1016/j.gloenvcha.2015.07.009

[12] ICPP. Climate Change 2014 – IPCC Fifth Assessment Report. Intergovernmental Panel on Climate Change/Cambridge University Press. Cambridge: Cambridge University Press, 2014.

[13] Mi Z., et al. Cities: The core of climate change mitigation. *Journal of Cleaner Production* 2019:207:582–589. doi:10.1016/j.jclepro.2018.10.034

[14] Mata E., et al. Economic feasibility of building retrofitting mitigation potentials: Climate change uncertainties for Swedish cities. *Applied Energy* 2019:242:1022–1035. doi:10.1016/j.apenergy.2019.03.042

[15] Dent C. M., Bale C. S. E., Wadud Z., Voss H. Cities, energy and climate change mitigation: An introduction. *Cities* 2016:54:1–3. doi:10.1016/j.cities.2015.11.009

[16] Gouldson A., et al. Cities and climate change mitigation: Economic opportunities and governance challenges in Asia. *Cities* 2016:54:11–19. doi:10.1016/j.cities.2015.10.010

[17] Biseniece E., Freimanis R., Purvins R., Gravelsins A., Pumpurs A., Blumberga A. Study of Hygrothermal Processes in External Walls with Internal Insulation. *Environmental and Climate Technologies* 2018:22(1):22–41. doi:10.1515/rtuect-2018-0002

[18] Albatayneh A., Alterman D., Page A., Moghtaderi B. The Significance of Building Design for the Climate. *Environmental and Climate Technologies* 2018:22(1):165–178. doi:10.2478/rtuect-2018-0011

[19] Bajcinovci B., Jerliu F. Achieving Energy Efficiency in Accordance with Bioclimatic Architecture Principles. *Environmental and Climate Technologies* 2016:18(1):54–63. doi:10.1515/rtuect-2016-0013

[20] Davos Declaration. Presented at the Conference of Ministers of Culture, Davos, Switzerland, 2018.

[21] How to measure Baukultur – Save the Date! Presented at the International Conference on How to measure Baukultur, Geneva, Switzerland, 2019.

[22] European Commission. The Strategic Energy Technology (SET) Plan. Luxembourg: Publications Office of the European Union, 2017.

[23] European Commission. SET Plan delivering results: The Implementation Plans. Luxembourg: Publications of the European Union, 2018.

[24] European Commission. Horizon 2020. Work Programme 2018–2020. European Commission, 2018.

[25] Ishizaka A., Nemery P. Multi-Criteria Decision Analysis: Methods and Software. John Wiley & Sons, 2013.

[26] Malczewski J. Multicriteria Analysis. Comprehensive Geographic Information Systems. Elsevier, 2018:197–217.

[27] Wang J.-J., et al. Review on multi-criteria decision analysis aid in sustainable energy decision-making. *Renewable and Sustainable Energy Reviews* 2009:13(9):2263–2278. doi:10.1016/j.rser.2009.06.021

[28] Tsoutsos T., et al. Sustainable energy planning by using multi-criteria analysis application in the island of Crete. *Energy Policy* 2009:37(5):1587–1600. doi:10.1016/j.enpol.2008.12.011

[29] Campos-Guzmán V., et al. Life Cycle Analysis with Multi-Criteria Decision Making: A review of approaches for the sustainability evaluation of renewable energy technologies. *Renewable and Sustainable Energy Reviews* 2019:104:343–366. doi:10.1016/j.rser.2019.01.031

[30] Baumann M., et al. A review of multi-criteria decision making approaches for evaluating energy storage systems for grid applications. *Renewable and Sustainable Energy Reviews* 2019:107:516–534. doi:10.1016/j.rser.2019.02.016

[31] Yang K., et al. Multi-criteria integrated evaluation of distributed energy system for community energy planning based on improved grey incidence approach: A case study in Tianjin. *Applied Energy* 2018:229:352–363. doi:10.1016/j.apenergy.2018.08.016

[32] Murrant D., Radcliffe J. Assessing energy storage technology options using a multi-criteria decision analysis-based framework. *Applied Energy* 2018:231:788–802. doi:10.1016/j.apenergy.2018.09.170

[33] Prodanuks T., Blumberga D. Methodology of municipal energy plans. Priorities for sustainability. *Energy Procedia* 2018:147:594–599. doi:10.1016/j.egypro.2018.07.076

[34] Trotter P. A., Cooper N. J., Wilson P. A multi-criteria, long-term energy planning optimisation model with integrated on-grid and off-grid electrification – The case of Uganda. *Applied Energy* 2019:243:288–312. doi:10.1016/j.apenergy.2019.03.178

[35] Centrālā statistikas pārvalde. Apdzīvoto mājokļu vidējais vecums Rīgā un Jūrmalā [Online]. [Accessed 2.05.2019]. Available: https://www.csb.gov.lv/lv/statistika/statistikas-temas/iedzivotaji/tautas-skaitisana/meklet-tema/143-apdzivoto-majoklu-videjais-vecums-riga-un (in Latvian)

[36] Šaršūne I. S. Rīgas pilsētas pašvaldības Pilsētas attīstības departamenta Pilsētvides attīstības pārvaldes Vēsturiskā centra plānošanas nodaļa [Online]. [Accessed 2.05.2019]. Available: https://www.slideserve.com/jesse/r-gas-v-sturisk-centra-un-t-aizsardz-bas-zonas-teritorijas-pl-nojums (in Latvian)

[37] Legal Acts of Republic of Latvia. Law on Preservation and Protection of the Historic Centre of Riga [Online]. [Accessed 4.02.2019]. Available: https://likumi.lv/ta/en/en/id/76001-law-on-preservation-and-protection-of-the-historic-centre-of-riga

[38] Rīgas domes Pilsētas attīstības departaments [Online]. [Accessed 4.02.2019]. Available: http://www.rdpad.lv/wp-content/uploads/2014/11/ENG_STRATEGIJA.pdf (in Latvian)

[39] World Heritage Committee. Convention Concerning the Protection of the World Cultural and Natural Heritage. Report. United Nations Educational, Scientific and Cultural Organization, Naples, 1997.

[40] The International Council of Monuments and Sites. Advisory Body Evaluation (ICOMOS). UNESCO World Heritage Centre, 1996.

[41] Bolstad P. *GIS Fundamentals: A First Text on Geographic Information Systems*. Acton: Eider Press, 2016.

[42] DeMers M. N. *Fundamentals of Geographic Information Systems*. John Wiley & Sons, 2008.

[43] Jacobs J. *The Death and Life of Great American Cities*. New York: Random House, 1961.

[44] Whyte W. H. City. Rediscovering the Center. Philadelphia: University of Pennsylvania Press, 1988.

[45] Whyte W. H. The Social Life of Small Urban Spaces. New York: Project for Public Spaces Inc, 1980.

[46] The IEU. The Global Liveability Index 2018. A free overview. The Economist Intelligence Unit, 2018.

[47] Mercer. Mercer's 21st annual Quality of Living survey. Mercer, 2019.

[48] OECD. How's Life? 2017. Measuring Wellbeing. Paris: OECD Publishing, 2017.

[49] Marshall W. E. An evaluation of livability in creating transit-enriched communities for improved regional benefits. *Research in Transportation Business & Management* 2013:7:54–68. doi:10.1016/j.rtbm.2013.01.002

[50] Ding X., et al. An inclusive model for assessing the sustainability of cities in developing countries Trinity of Cities' Sustainability from Spatial, Logical and Time Dimensions (TCS-SLTD). *Journal of Cleaner Production* 2015:109:62–75. doi:10.1016/j.jclepro.2015.06.140

[51] Marsal-Llacuna L.-M., Colomer-Llinàs J., Meléndez-Frigola J. Lessons in urban monitoring taken from sustainable and livable cities to better address the Smart Cities initiative. *Technological Forecasting & Social Change* 2015:90(B):611–622. doi:10.1016/j.techfore.2014.01.012

[52] Norouzian-Maleki S., Bell S., Hosseini S.-B., Faizi M. Developing and testing a framework for the assessment ofneighbourhood liveability in two contrasting countries: Iran and Estonia. *Ecological Indicators* 2015:48:263–271. doi:10.1016/j.ecolind.2014.07.033

[53] Silva A. N. R., et al. A comparative evaluation of mobility conditions in selected cities of the five Brazilian regions. *Transport Policy* 2015:37:147–156. doi:10.1016/j.tranpol.2014.10.017

[54] Zanella A., Camanho A. S., Dias T. G. The assessment of cities' livability integrating human wellbeing and environmental impact. *Annuals of Operations Research* 2015:226(1):695–726. doi:10.1007/s10479-014-1666-7

[55] Zhou J., Shen L., Song X., Zhang X. Selection and modeling sustainable urbanization indicators: A responsibility-based method. *Ecological Indicators* 2015:56:87–95. doi:10.1016/j.ecolind.2015.03.024

[56] Zhan D., et al. Assessment and determinants of satisfaction with urban livability in China. *Cities* 2018:79:92–101. doi:10.1016/j.cities.2018.02.025

[57] Reis I. F. C., et al. An evaluation thermometer for assessing city sustainability and livability. *Sustainable Cities and Society* 2019:47:101449. doi:10.1016/j.scs.2019.101449

[58] Kashef M. Urban livability across disciplinary and professional boundaries. *Frontiers of Architectural Research* 2016:5(2):239–253. doi:10.1016/j.foar.2016.03.003

[59] Okulicz-Kozaryn A. City life: Rankings (livability) versus perceptions (satisfaction). *Social Indicators Research* 2013:110(2):433–451. doi:10.1007/s11205-011-9939-x

[60] Faria P. A. M., et al. Combining cognitive mapping and MCDA for improving quality of life in urban areas. *Cities* 2018:78:116–127. doi:10.1016/j.cities.2018.02.006

[61] PPS (Project for Public Spaces). How to Turn a Place Around. New York: Project for Public Spaces Inc, 2000.

[62] Ghasemi K., Hamzenejad M., Meshkini A. The spatial analysis of the livability of 22 districts of Tehran Metropolis using multi-criteria decision making approaches. *Sustainable Cities and Society* 2018:38:382–404. doi:10.1016/j.scs.2018.01.018

[63] Stanislav A., Chin J. T. Evaluating livability and perceived values of sustainable neighborhood design: New Urbanism and original urban suburbs. *Sustainable Cities and Society* 2019:47:101517. doi:10.1016/j.scs.2019.101517

[64] Yassin H. H. Livable city: An approach to pedestrianization through tactical urbanism. *Alexandria Engineering Journal* 2019:58(1):251–259. doi:10.1016/j.aej.2019.02.005

[65] Ghel J. Cities for People. Washington: Island Press, 2010.

[66] Ghel J. Life Between Buildings: Using Public Space. Washington:Island Press, 2011.

[67] Riga Municipality City Development Department. Historic Centre of Riga urban planning documentation graphical annexes [Online]. [Accessed 4.02.2019]. Available: http://www.rdpad.lv/rtp/rvc/

[68] Rīgas Jūgendstila centrs. Jūgendstila arhitektūras objekti Rīgā [Online]. [Accessed 8.03.2019]. Available: http://www.jugendstils.riga.lv/lat/JugendstilsRiga (in Latvian)

[69] Latvijas Ģeotelpiskās aģentūra. Karšu Pārlūks [Online]. [Accessed 8.03.2019]. Available: https://kartes.lgia.gov.lv/karte/ (in Latvian)

[70] Kultūrvēsturiskie ansambļi un kultūras pieminekļi RVC un tā aizsardzības zonā. Rīgas domes Pilsētas attīstības departaments [Online]. [Accessed 8.03.2019]. Available: http://www.rdpad.lv/wp-content/uploads/2014/12/11_Pieminekli_6000_konsolidets_042017.pdf (in Latvian)

[71] Riga Municipality City Development Department GIS information.

[72] The Information Centre of the Ministry of the Interior. Registered criminal offenses on a digital map (GIS) [Online]. [Accessed 25.04.2019]. Available: http://www.ic.iem.gov.lv/gis/index.php

[73] State Land Service of the Republic of Latvia [Online]. [Accessed 2.05.2019]. Available: https://www.kadastrs.lv/#

[74] Migilinskas D., Ustinovichius L. Normalisation in the selection of construction. *Management and Decision Making* 2007:8:297–313. doi:10.1504/IJMDM.2007.013422

Transition from traditional historic urban block to positive energy block

Andra Blumberga [a, *], Ruta Vanaga [a], Ritvars Freimanis [a], Dagnija Blumberga [a], Juris Antužs [a], Artūrs Krastiņš [a], Ivars Jankovskis [a], Edgars Bondars [b], Sandra Treija [b]

[a] Riga Technical University, Institute of Energy Systems and Environment, Āzenes iela 12/1, Riga, LV 1048, Latvia
[b] Riga Technical University, Faculty of Architecture, Ķīpsalas iela 6–407, Rīga, LV 1048, Latvia

ABSTRACT

Optimizing energy consumption in the cities might present a significant impact on decarbonization strategies approaching carbon neutral future in 2050. Positive Energy Block initiative is targeted particularly to densely build environments promoting shared on-site renewable energy production and storage, using smart grids, internet and communication technologies, Internet of Things and other highly advanced energy efficiency technologies within the neighborhoods. Research presented focuses on transition from traditional urban block to Positive Energy Block in valuable environment of historic city center exploring possibilities of waste heat regeneration and on-site renewable energy technologies. Energy consumption data is analyzed and the conception for possibilities of on – site renewable energy generation and waste heat recovery from data centers and cooling units in selected urban block is drawn. The results indicate that very ambitious targets for energy efficiency improvement are needed to achieve positive energy block – 65% and 60% for electricity and heating consumption, respectively. Possible savings of CO_2 emissions are 45–50 kg/m^2 per year.

© 2020 Published by Elsevier Ltd.

1. Introduction

Climate change causes health risks [1], extreme weather [2] conditions and reduces biodiversity [3]. To mitigate the climate change that is recognized to very likely be driven by anthropogenic impact [4] Paris Agreement has set the goal to decrease anthropogenic GHG emissions and to limit global temperature increase to 1.5 °C [5]. The set goal should guide policy makers and industry to come up with new solutions – social [6] and technological [7].

Cities that occupy only 2–3% of the world's land are responsible for 70% of world's greenhouse gas emissions causing the global warming [8]. Therefore energy efficiency measures should target entire energy systems in the cities. Smart cities and communities are at the core of action of European Strategic Energy Technology Plan (SET-Plan) aiming to reduce GHG emissions decarbonizing city energy systems and introducing positive energy blocks/districts to local communities [9]. The Positive Energy Blocks often faces challenges that should be resolved. Among these challenges [10] are political, economic, technical, spatial, etc. that might be resolved by establishing communication between all the involved parties.

It is characterized [11] that eventually Positive Energy Blocks will lead to Positive Energy Districts and Energy Positive Neighborhoods, thus approaching low carbon society in the cities. Overall, it is expected [12] that PEBs will stimulate the usage of Renewable Energy Sources (RES) and also support the improvement of energy efficiency within mentioned PEBs. Thus, by means of RES usage PEB goal might be achievable.

Research has been launched in the light of cutting CO_2 emissions in the cities focusing on decarbonizing existing building stock in a densely built urban historic city center. To reach the goal, a transition from traditional energy block to PEB is needed.

The novelty of the research project is to combine several energy efficiency improvement technologies – nZEB refurbishment strategies, waste heat regeneration, smart energy systems – including on – site RES technologies and Positive Energy Block principles – to a historic urban block. In this paper, the results of preliminary evaluation of potential to reduce CO_2 emissions are presented.

The paper describes 1) overall methodology of the study; 2) methodology of the holistic design in transition from traditional

Nomenclature		LCA	Life cycle analysis
		MCA	Multi-criteria analysis
a	Annum	nZEB	Nearly Zero energy building
AI	Artificial intelligence	PEB	Positive Energy Block
DHW	Domestic hot water	PED	Positive Energy District
DC	Data center	PEN	Positive Energy Neighborhood
GHG	Greenhouse gases	PV	Photo − voltaic panels
HP	Heat pump	PVT	Photo − voltaic panels/thermal
HVAC	Heating Ventilation Air conditioning	RES	Renewable energy source
ICOMOS	The International Council of Monuments and Sites	RHC	Riga Historic Centre
ICT	Information and communications technologies	SES	Smart energy systems
IoT	Internet of Things		

historic urban block to Positive Energy Block; and 3) preliminary calculation of potential decarbonization level of selected urban block.

2. Literature review. Transition from traditional to positive energy block

Potential energy savings in transition from traditional to Positive Energy Block can be divided into three main groups: 1) building related; 2) introducing smart energy systems including waste heat utilization and renewable energy sources and 3) social energy savings via energy communities and other behavioral energy savings.

2.1. Building related energy savings

Building thermal envelope. Buildings are responsible for 36% of the global final energy and ~40% of energy - related carbon dioxide emissions according to 2018 Global Status Report [13]. There lies a great potential for energy consumption reduction. Latest amendments of the existing legislation on building energy efficiency, Directive 2010/31/EU calls for decarbonization of existing building stock via deep renovations aiming for nZEB level [14].

Intensification of building density. Building highly efficient buildings within the block in empty plots or adding extra m^2 to existing structures would lower the overall specific indicator in kWh/m^2. Added structures have to be designed thoroughly in order not to diminish the existing urban qualities of a historic urban block.

2.2. Energy savings implementing smart energy systems

In the scope of this study smart energy systems are considered in the broadest sense of the term not only focusing on smart grid and ICT solutions, but as a holistic view on a system including all energy carriers [15] within defined boundaries (the whole urban block in the scope of this study). A s mart energy system will allow the concept described above to operate with its fullest potential, avoiding losses, and ensuring an ongoing optimization process via constant monitoring and analysis of the demand side of energy system. Smart energy systems that will be developed at later stages of this research at the urban block level would be scalable to the Smart City level thus contributing to the wider decarbonization goals [16].

Smart grid, ICT, IoT. There are several definitions of smart grids [17]. In the scope of this study the one defined already in 2006 by European Technology Platform [18] is considered: "*Smart grid is an electricity network that can cost efficiently integrate the behavior and actions of all users connected to it − generators, consumers and those*

that do both − in order to ensure economically efficient, sustainable power system with low losses and high levels of quality and security of supply and safety." Smart grid operates using smart metering systems and intelligent appliances using IoT technology which allows to optimize energy flows − reducing peak loads by shifting the operation of smart appliances to the low demand periods and simultaneously reducing the cost for energy; allows to avoid unnecessary losses; ensures demand responsiveness, analyses historic data and manages prediction based on self-learning algorithms under different uncertainties and offers demand − response flexibilities [17,19]. Smart grid systems would take over the human dependent behavioral energy savings due to its reliable, precise and intelligent consistency.

Smart grid is mainly referred to the electricity sector, but it can be applied to the thermal energy systems as well [20].

Capturing waste heat or cold. "*Waste heat is equivalent to the energy load that is not extracted otherwise and requires external cooling*" as stated in Annex IV of European Commission recommendation on the content of the comprehensive assessment of the potential for efficient heating and cooling under Article 14 of Directive 2012/27/EU. Heat generated in technological systems and utilized within the same site/energy unit is not considered to be waste heat.

In mixed use historic center blocks there are different load patterns for every function daily and seasonally − residential parts of the block are usually occupied from 18:00−8:00, but office buildings in a period from 8:30−17:30. Waste heat sources in historic urban block could be such facilities as bars/cafes/restaurants and data/telecommunication centers. The data centers are producing the biggest amount of waste heat and are operating 24/7. Incorporating the waste heat in energy in heating or DHW system would lower both − peak load and overall energy consumption.

Renewable energy sources and energy storage. Since buildings in Europe account for about 40% of the total energy use [21] and more than 70% of said buildings are built before 1980 [22] it is crucial to employ on − site renewable energy and energy storage possibilities in the urban environment and cut down CO_2 emissions, in order to comply with the directive EU 2018/2001 of the European Parliament [23].

EU directive on the energy performance of buildings [24] suggests that low amount of energy needed for nZEB buildings should be produced on site or nearby. Deep renovation of existing building stock should aim nZEB level according to decarbonization strategy [23]. Implementing renewable energy sources should aim to cover the energy needed for deeply renovated urban blocks, although nZEB level might not be achieved due to the prevailing restrictions in valuable historic urban center. Restrictions are applicable not only to buildings themselves but to placing renewable energy sources in the historic urban landscape as well − there are

landscape restrictions as well as aesthetic requirements for facades. Restrictions would apply to all renewable sources that change the landscape or façade appearance — wind and solar. To use biomass in an urban block would face technological restrictions — space both indoors and outdoors in existing structures have their limitations; installation in densely build environment could encounter limitations as well.

These restrictions limit the choice of possible RES technologies — models (aesthetics and geometry), performance capacity (the size limitations or type of technology; for example — flat film or mono/poly crystal solar PV panels), possible location due to aesthetic, functional and geolocation restrictions of dense urban surroundings.

The availability of solar and wind renewable energy does not always match the consumption pattern both on daily and seasonal scale. To compensate these fluctuations in energy generation incorporation of energy storage technologies in smart energy systems would allow to use more RES produced energy on site — without forwarding it to grid and avoiding energy jams.

Lately 100% renewable scenarios have been studied in order to draw future development strategies in smart grid and SES technologies, including energy storage. Lund et al. compares different alternatives — 100% individual building electric heating, HP heating and combined version of DH and HP (smart energy systems) — and concludes that the latter is the most promising, where sectors would make integrated system working beneficially, thus creating a pathway to 100% renewable energy [20]. Looking at the smart energy systems, energy storage plays an important role; and to make the most profitable solution cross-sector approach in energy conversion technologies combined with different types of energy storage is preferable [25,26]. Energy storage plays an even more important role in continental and northern climate countries dealing with demand variabilities [27]. The 100% renewable energy scenario 2050 for Germany stresses the need for energy savings in the transition process [28].

2.3. Social energy savings

Energy community. By the European Union it is considered [23,29] that energy communities are a powerful instrument in fighting climate change. It is defined [30] that if energy community annually generates at least 75% of the necessary energy by employing technologies that are located within said community, it is treated as the energy community.

Mainly, energy communities are founded with purpose of RES production — it does not directly save energy but it decarbonizes the energy needed. Inhabitants can share both electricity (PV panels) and thermal energy generation (solar collectors) or hybrid systems. It is the most effective to place RES technologies on site. Inhabitants of historic urban block would thus turn from consumers to prosumers.

Energy communities in urban block might ensure more efficient waste heat capture making use of the waste heat amount, that is not necessary in the unit it has been primarily generated. Founding energy community could help in financing energy efficiency measures within a block and optimize costs due to the scale of the regeneration project.

Behavioral energy savings does not take any financial investment, but calls for active energy management on a daily basis — introducing and maintaining energy saving patterns. Behavioral energy savings can be supplemented by smart algorithms, so energy savings are not dependent on human daily activity, but smart demand-responsive algorithms.

2.4. Challenges of energy efficiency measures in densely populated historic urban center

Designing PEBs in new developments is a challenging and, complex task. Applying it to the existing building stock makes it even more challenging. Performing PEB concept in a densely built historic urban center meets many more obstacles to deal with and overcome. Table 1 summarizes the specific challenges in historic urban environment.

Main restrictions are 1) historic substance to be preserved (its authenticity) and building structure in listed buildings, which limits application of energy efficiency measures — thermal insulation, intervention in internal structures when dealing with optimization of building services; 2) historic landscape to be preserved restricts both building thermal envelope measures and introduction of renewable energy technologies in historic urban block; 3) technical obstacles which includes outdated infrastructure less flexible to changes and physical limitations of the space; and 4) legal restrictions in terms of existing legislation and forms of ownership.

2.5. Impact of energy efficiency measures on historic heritage values and decarbonization of existing building stock

There are two contradicting sides in the historic urban regeneration. One the one hand, latest alarming global warming evidences and low carbon society vision puts *energy efficiency first* (Directive (EU) 2018/2002 of the European Parliament and of the Council (December 11, 2018) amending Directive 2012/27/EU on energy efficiency), and, on the other hand, the fear of losing cultural heritage over reckless energy efficiency solutions might make preservation requirements even more stringent.

International Council of Monuments and sites (ICOMOS) recognizes both the threatening impact of climate change to the world heritage sites and the need to update heritage preservation practices. New models should be developed to evaluate conservation and adaptation measures from the perspective of Circular Economy processes, such as Life Cycle Assessments (LCA), which center on materials, energy and waste minimization [31].

Cultural heritage will be impacted by climate change and therefore adaptation strategies are needed to manage the Risks. Selection and implementation of adaptation measures will require the integration of Cultural Significance assessments (both relative Significance and impacts to Significance from adaptation actions) together with Risk/Vulnerability Assessments, and feasibility studies. Adaptation activities are likely to require additional resourcing; however knowledge, understanding and the provision of sectoral leadership are possibly more crucial in the early stage of the process.

Historic urban regeneration is a cyclic process. Over time new ideas on improvement of the quality of life are being introduced constantly in routine urban regeneration. Historic urban centers carry evidences of dilemmas of the past — modern movement against preservation of cultural values. Historic cultural heritage has survived modern movement, de-urbanization, re-urbanization, intensification of traffic serving to the needs of its inhabitants and trying to keep testimonies of the past to the next generation [32].

Now, the actual dilemma is between energy efficiency and preservation of cultural heritage. Moving towards carbon-free economy, new borders will have to be drawn — to what extent energy efficiency measures can interfere with historic buildings? the important values to be preserved to the next generations will have to be redefined; how much this preservation costs in terms of CO_2 emitted over the lifetime of the building? The next step is to find consensus in optimal decarbonization level of historic urban

Table 1
Challenges of energy efficiency measures in densely populated historic urban center.

Type of energy efficiency measures	Energy efficiency measure	Challenges in historic urban environment
Buildings	Building thermal envelope energy efficiency (Walls, roofs, floors, windows)	Historic substance to be preserved (Listed buildings)
		Legal restrictions
		Technical restrictions
	Building services energy efficiency (Ventilation, hot water, distribution)	Historic structures to be preserved (Listed buildings)
	Intensification	Technical state of building and services systems
		Preservation of street views and landscape
		Structural (load bearing) restrictions
		Solar insolation
Smart energy systems	Smart grid, ICT, AI	Aged infrastructure, amount of necessary investments
	Waste heat, energy cycle	Legal issues among owners
		Data sensitivity
	Renewables	Preservable historic landscape
		Old grid systems non - flexible
	Energy storage	Technical restrictions
Social energy savings	Energy community	Mixed ownership, mixed use
	Behavioral energy savings	The pattern of usage in offices energy bill might be the smallest portion of expenses
		The same with economically well situated inhabitants.

centers. Using innovative approaches of energy management, possibilities of IoT and AI advanced materials and energy communities using RES.

Table 2 illustrates the impact of described above energy efficiency measures in the transition to the Positive Energy block to both the level of decarbonization of a chosen historic urban block and the risks of losing its historic values.

The highest rating energy saving strategies that deal with energy efficiency measures in building thermal envelope has the highest risk of losing historic heritage values. Both parties should reach a consensus to ensure the progress towards low-carbon society. In order to do it − 1) built heritage practices has to be updated, and 2) innovative solutions are needed for rising thermal resistance of historic building's thermal envelope and both traditional and innovative approaches has to be handled with deep understanding of cultural values.

Research described in the paper is a holistic approach to decarbonization strategy including high and low impact on historic substances energy efficiency strategies.

3. Methodology of the study

Historic built structures carry multiple layers and dimensions of nationally and globally significant cultural values. Therefore, the task to transform historic urban block into positive energy block will be as complex as the urban fabric itself. Methodology of this extensive research is organized in six sequent steps (see Fig. 1):

Decarbonization strategy of urban block in historic center via Positive Energy Block concept will be developed considering two aspects − energy efficiency and cultural heritage. Perspective of both parties will be taken into account in each step of research methodology. Usually energy efficiency scenarios are weighted using cost benefit analysis and CO_2 life cycle analysis. In this study, the evaluation will be supplemented with evaluation of energy efficiency measures' impact on cultural heritage. Raising the comfort in historic buildings and adding new features are considered an intrusion into historic built structure. For further discussion, it is important to evaluate if the proposed design raises the quality of life in the urban block and what is it's impact on historical heritage values. Three different evaluation analysis methods will illustrate

Table 2
Impact of energy efficiency measures on historic heritage values and decarbonization of existing building stock.

| Type of energy efficiency measures	Energy efficiency measure	Loss of historic heritage values	Decarbonization
Buildings	Building thermal envelope energy efficiency	High	High
	Building services energy efficiency	High	High
	Intensification	Medium	Medium
Smart energy systems	Smart grid, ICT	Low	Medium
	Waste heat, energy cycle	Low	Medium
	Renewables	Medium	High
	Energy storage	Low	Medium
Social energy savings	Energy community	Low	Medium
	Behavioural energy savings	Low	Medium

Low impact   High impact
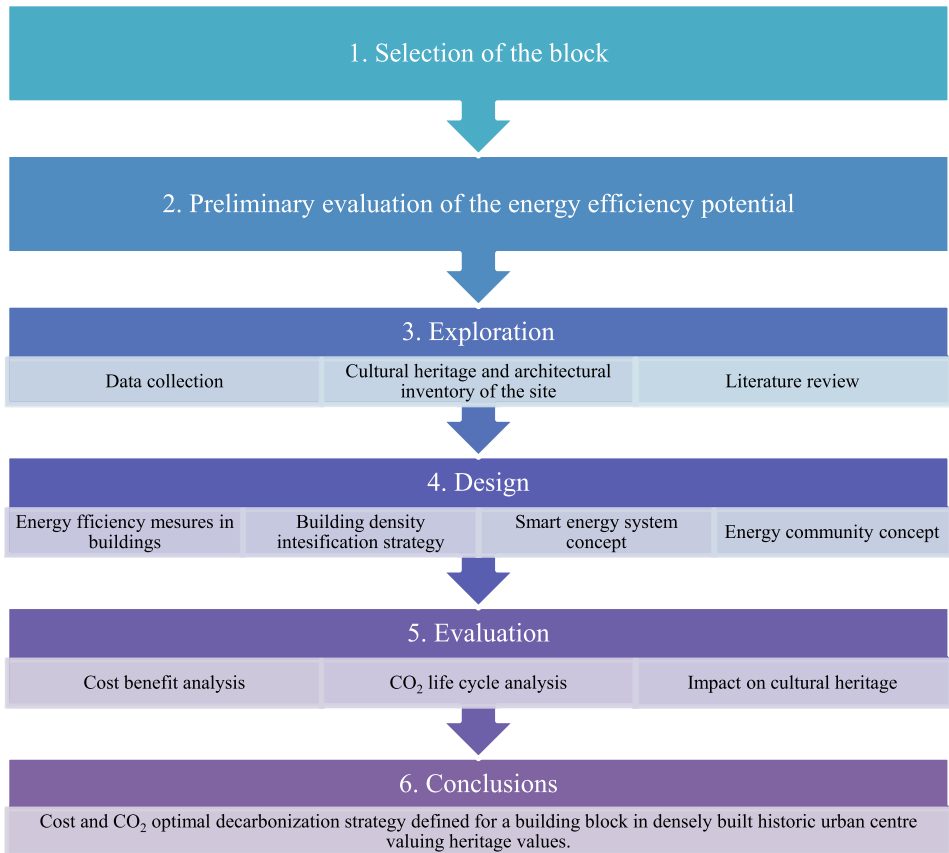
Fig. 1. Methodology for research study - transition from traditional historic center block to the Positive Energy Block.

different possible perspectives, and will serve as a basis for the discussion among professionals: environmental engineers, architects, local city planners and authorities, as well as the general public, on how to find a balance in climate change mitigation actions and cultural heritage preservation in the way to low-carbon society.

One of the most complex phases in this research will be the 4th step − design phase. Additional methodology was created to the design phase for transition from traditional historic urban block to Positive Energy Block and it consists of three main steps − preliminary exploration, conceptual design and overall energy balance calculation (see Fig. 2).

Each of the design steps is a complex task and carries different sequential modules. Developing the overall concept for PEB, two stakeholders are taken into consideration as well. The design process itself will be driven by the question − is the positive energy block level achieved? If not, adjustments in the design (both demand and supply side) will be made in the framework of the defined architectural limitations. Such spiral of optimization continues until the PEB level is reached.

The overall concept of energy savings is based on three pillars:

1) Energy demand is reduced in deep renovation of existing buildings using advanced energy efficiency technologies approaching energy savings (both − thermal envelope and building services);
2) Energy supply from RES technologies and storage is estimated based on available roof and facade surfaces. It is assumed that combined photo − voltaic/thermal and photo − voltaic systems are used. Thermal energy generated would cover both heating system and DHW system;
3) Waste heat capture in local network within the block using heat pumps (powered by local RES). The amount of available waste heat is estimated based on the study [33].

The heat load graph (see Fig. 3) reflects conceptual scheme for decarbonizing selected urban block based on the three pillars described.

In each of six steps of research methodology massive research work will be done. This paper describes the 2nd step − preliminary evaluation of decarbonization potential of selected urban block. Preliminary energy consumption data analysis and evaluation of possible renewable energy concepts has been carried out and presented in next chapter.
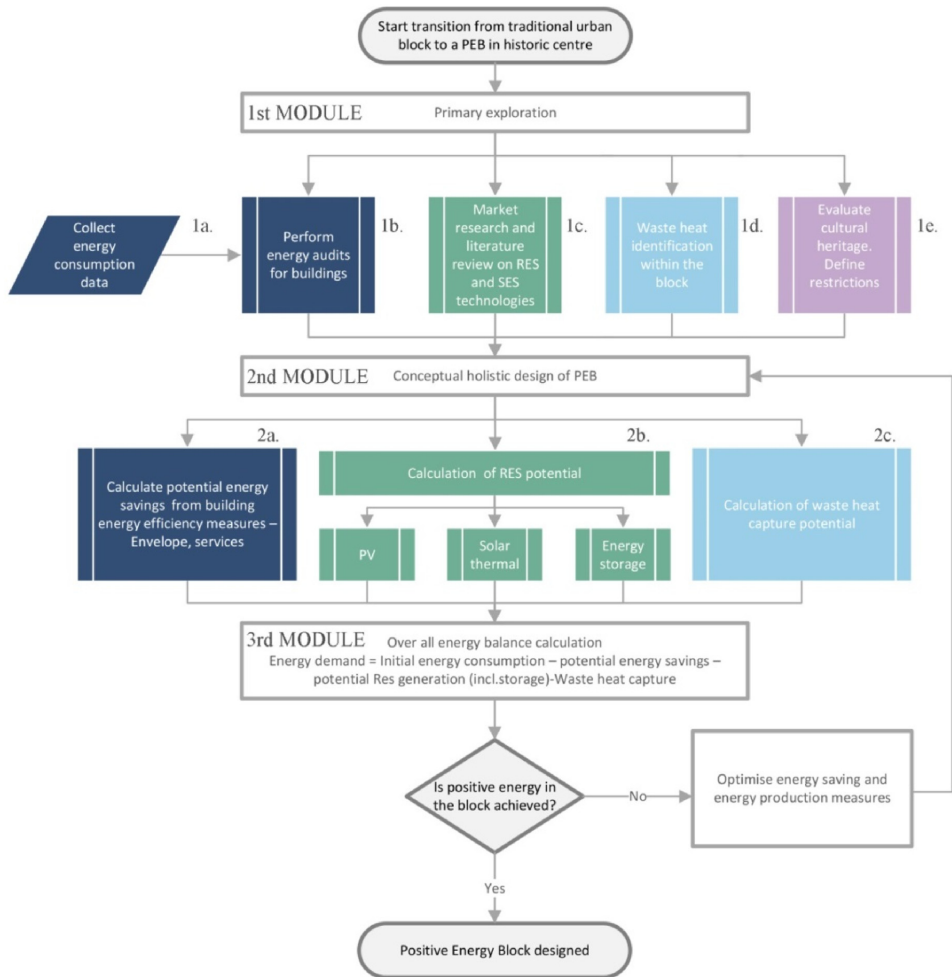
Fig. 2. Methodology for the design phase of transition from traditional historic urban block to Positive Energy Block.
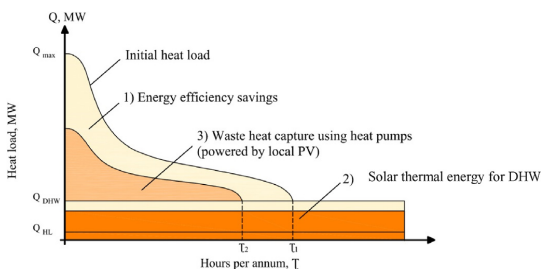

Fig. 3. Heat load graph reflecting in brief the transition phases.

4. Preliminary evaluation of the decarbonization potential of selected block

4.1. Previous study − selection of urban block in double multi-criteria analysis

For the case study in multi criteria analysis Riga Historic center (RHC) urban block was chosen for further research [34]. Double multi-criteria analysis (MCA) was performed − from energy and cultural heritage perspectives. First MCA evaluated the biggest potential for decarbonization and transition to PEB using two level ranking. At the first level outranking criteria were chosen − energy intensive enterprise should be located in the block, residential function at least 10% and empty plot for new development. All urban blocks were evaluated at the first outranking level of MCA. At second level shortlisted RHC blocks were evaluated according to six criteria - building density in the block (typical proportion), proportion of residential function (for fair share of mixed use),
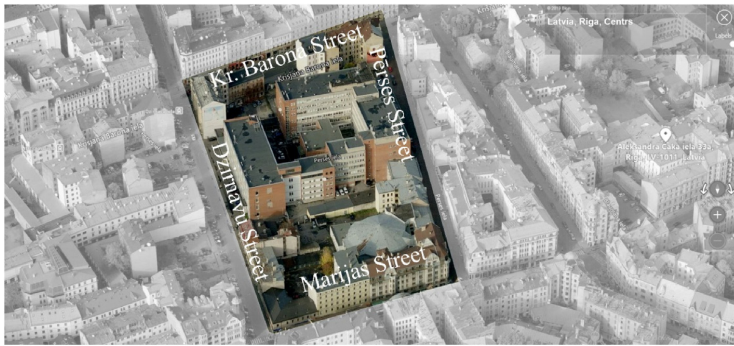
Fig. 4. Selected urban block in the landscape of Riga Historic centre.

availability for high performing future development, possible intensive refurbishment (as the amount of buildings that are not listed), energy intensive function (as important milestone for the energy flow optimization), type of energy intensive function (with the focus to data and telecommunication centers).

Second MCA evaluated the RHC urban blocks according to the highest architectural value. Two level ranking was used as well. At the first level, map overlay method was used. For further research, the selected blocks had to meet the chosen criteria: only the building blocks comprising three architectural typical RHC values — listed buildings of national importance, Art Nouveau buildings and wooden buildings. At the second level of MCA 4 criteria groups were used — cultural heritage and 3 city livability criteria — protection, comfort and delight according to Jan Ghel concept of livable city [35].

After the outranking level of both MCA from 82 RHC urban blocks 12 blocks were selected from energy perspective and 15 blocks were shortlisted from cultural heritage perspective only two urban blocks were on both lists, and none of those was the highest ranking at the second level of evaluation in neither of perspectives, therefore, the decision was made to proceed with the urban block, ranking the highest from the energy perspective and in conceptual design stage of the research livability qualities will be added to the block to improve its architectural and urban value.

4.2. Description of the selected Riga Historic center urban block

Selected Riga Historic center urban block is placed in the central part of RCH (see Fig. 4). It covers 2,12 ha and comprises16 plots and 25 buildings (including 6 technical buildings). City quarter is surrounded by two magisterial streets — Kr. Barona Street and Marijas Street, one secondary street Dzirnavu and one by-street Pērses Street. The numbers of floors of the buildings in block vary from 2 to 6 floors. The building density (building footprint to whole quarter ground surface area) is 60%, intensity (useful area to whole quarter ground surface area) is 250%. Compared to the adjacent blocks, in selected urban block the square footage of post war buildings is larger.

Buildings in the block are built in various periods — from 1870 till 1976. It is of mixed use and there are several functions present in the block — residential, small offices, small shops and cafes, medium size concert hall and energy intensive enterprise — telecommunication and data center of national importance. Buildings are of different styles and materials — wooden, masonry and prefabricated post-war buildings. There are two empty plots located in the block that cover a rather small portion of the block (see Fig. 5).

4.3. Energy consumption data analysis

Heating. Energy consumption data have been collected from district heating provider and are summarized in Fig. 6. Graph on the left shows specific energy demand of all the buildings connected to
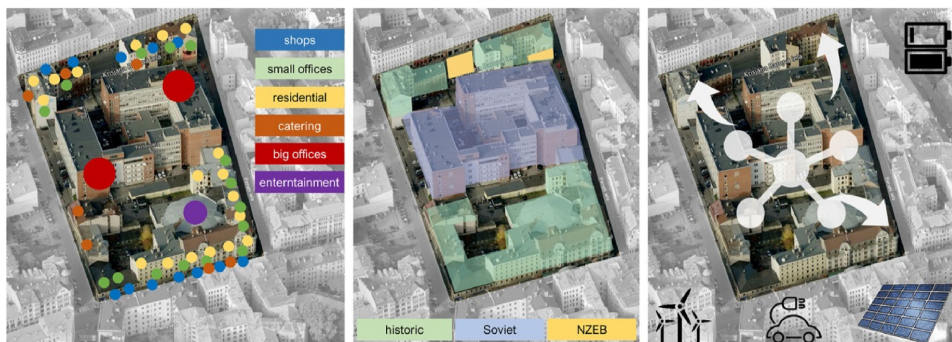

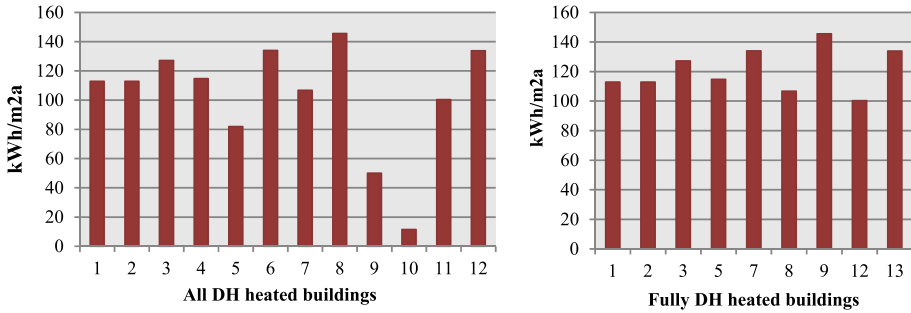**Fig. 5.** a) function mix in an urban block; b) building periods; c) conceptual sketch of smart energy systems in a block.

212

Fig. 6. Specific energy consumption for heating. All DH heated buildings in the block (left) and fully DH heated buildings.
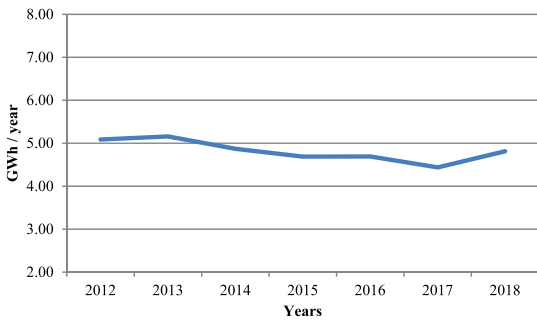

Fig. 7. Total annual electricity consumption in selected urban block.
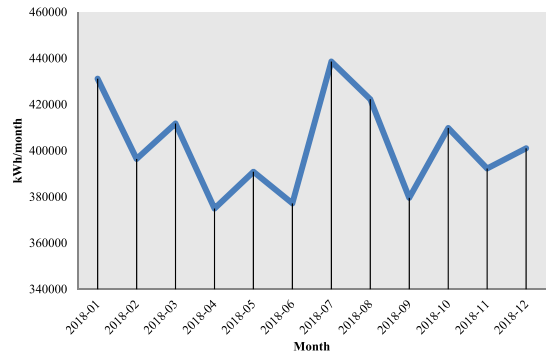

Fig. 9. Total monthly electricity consumption in selected urban block.

the DH and identifies buildings No.5, No.9 and No.10 far below average level for heating demand. Graph on the right illustrates energy consumption only in buildings fully heated by district heating, it shows values between 100 and 145 kWh/m^{2}a energy consumption for heating and gives an average 124 kWh/m^{2}a.

Besides, 4 unexploited buildings and 2 buildings heated with undefined energy source have been identified. Urban building block comprises 36 000 m^2 of utilized area. The area fully heated by district heating versus the area heated with other energy source,
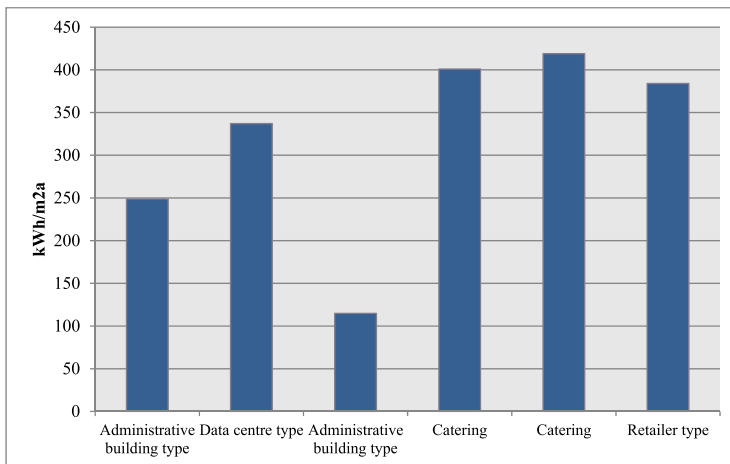

Fig. 8. Specific electricity consumption of the biggest electricity consumers in the selected urban block.
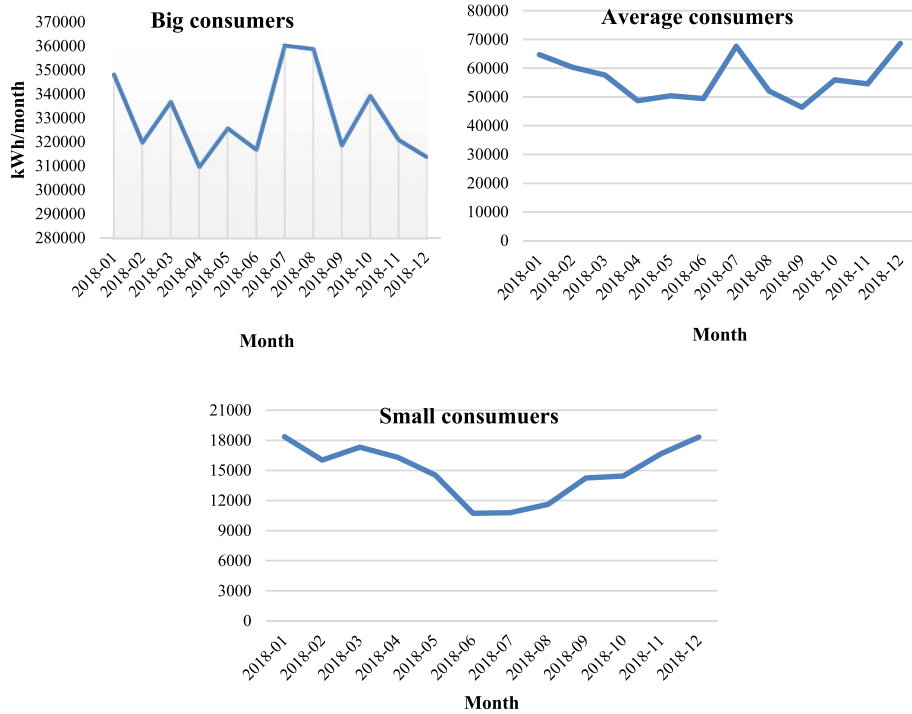
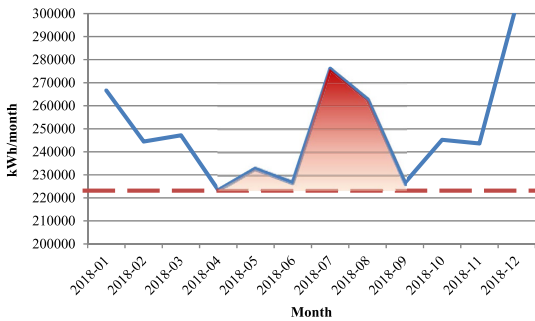Fig. 10. Monthly consumption — big, average, small consumers.

Fig. 11. Energy consumption above the baseline in May—August indicates energy consumption for cooling.

partially heated or unheated, makes proportion of 65/45. Applying the calculated average of the heating demand to all utilized area of the block makes the total annual energy consumption for heating in the block 4,5 GWh.

Electricity. Since the urban block used for the case study is a mixed use urban block, electricity consumers vary: there are small consumers, like households with average energy consumption 1,0—3,0 MWh per year; averagely small energy consumers such as smaller offices and services with energy consumption 5—10 MWh per year; averagely medium consumers, such as bigger offices with

energy consumption 13—40 MWh per year, averagely big consumer, like energy intensive services (small scale concert hall, for example), catering type and retailers with energy consumption 50—100 MWh per year, and big consumers, like 4000—7000 m^2 administrative building types and data center type consumers with energy consumption 500—1800 MWh per year. Total average annual electricity consumption in the selected urban block is 4,8 GWh over 7 year period. Fig. 7 shows total annual consumption differences. The highest consumption in the year 2013 differs from average level 7%, the lowest consumption in the year 2017 differs from average level 8%.

The gathered data indicates that 40% of consumers use electricity irregularly. Square footage occupied by these tenants is impossible to identify, therefore, the overall specific electricity consumption in the block does not reflect the true situation. From the available data it can be concluded, that 3 biggest consumers occupying 47% of square footage, consume 80% of total energy; 10 averagely medium and averagely big consumers occupying 10% of square footage consume 12% of total energy; and small and

Table 3
The temperature of heat extracted from data centers for different cooling technologies.

Cooling technology	The temperature of heat extracted from data centers
Air cooling	35—40 °C
Water cooling	60—70 °C
Two phase cooling	70—80 °C

Table 4
Calculation of data center's waste heat regeneration capacity in selected urban block.

|		
Installed power of data centre [45]	1	MW
Waste heat recovered [45]	5627	MWh/year
Installed power of data centre (case study)	0,06	MW
Waste heat recovered (based on [45])	338	MWh/year

averagely small consumers occupying 32% of square footage consume only 8% of total energy. 11% of total square footage is unexploited.

Specific energy consumption of the biggest consumers within the block can be identified – catering type and retailer type consumers are followed by data center type buildings and administrative building type. Thus, energy intensity per square meter in catering type and retailer stores as well as data center type are among the highest in densely built urban environment (see Fig. 8).

The overall electricity consumption profile per month (Fig. 9) coincides with the typical pattern: the highest electricity consumption is in December/January due to the necessity of lighting and partial electric heating and in June/July due to the necessity of cooling.

Splitting users by the consumption level (Fig. 10) electricity consumption data clearly illustrate the potential for average and big consumers for energy efficiency measures introducing smart energy systems coupling waste heat recovery from cooling systems and district heating. Small consumers in the summer season have smaller electricity consumption, but average and big consumers experience peak electricity demand during summer time. It indicates significant cooling loads.

The total building footprint in selected urban block is 12800 m^2.
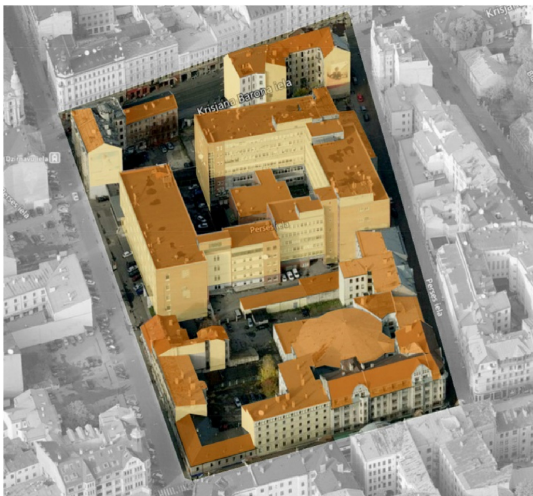
Fig. 12. Rooftops suitable for placement PVT and PV panels (colored orange). SE and SW facades (colored yellow, North is facing up) suitable for placement of BIPV (for buildings built between 1960 and 1980 and brand walls for buildings build before 1945). (For interpretation of the references to color in this figure legend, the reader is referred to the Web version of this article.)

4.4. Potential of energy savings in selected urban block. Preliminary calculation

To evaluate provisional potential of energy savings in selected urban block simplified calculation has been made estimating 1) building deep renovation energy savings; 2) RES production with conventional technologies PV and solar thermal; and 3) waste heat recovery technology.

Building related energy savings. The study suggests that in northern climate (Sweden) economically feasible deep renovation is 50% energy savings [36]. But Zangheri et al. comparing different refurbishment scenarios across Europe, have found 36–88% amplitude for net primary energy savings. An interesting outcome of this study is the conclusion that reaching for lower energy consumption often resulted in lower global costs over 30 years compared to base line scenarios [37]. To evaluate the possibilities to achieve PEB level in the selected urban block, it is assumed that electricity consumption can be reduced by 50%, but heating by 60%. Id est electricity demand would be 2,4 GWh/year, but heating demand 1,8G Wh/year (50 kWh/m^{2}a average).

Waste heat utilization from other cooling units. The cooling demand of the buildings in the block is extracted from electricity consumption data. Electricity consumption in April reflects basic electricity needs typical for summer months (lighting and equipment) and is denoted as baseline. Electricity consumption above base level indicates the energy consumed for cooling the premises during May–August (Fig. 11).

Monthly electricity consumption data shows that there is 110 MWh total surplus energy consumption above the baseline used for cooling the buildings (excluding data center). Waste heat could be extracted from cooling compressors with the efficiency rate of 75% using heat pump. Heat recovered could be used for preheating the domestic hot water within the block.

Waste heat utilization from data center. In the digital era, due to the need for data processing and storage, data centers have become energy intensive services [38]. Over the last two decades, energy efficiency technologies in data centers have been studied moving from removing the heat and optimizing air flow via active cooling chiller cooling systems [39] to 2) free cooling [40] and cooling with hot water instead of air, thus creating options for energy reuse for heating [41], and 3) sophisticated waste heat recovery strategies [42]. It has been calculated how much waste heat can be captured in small (40–100 kW power consumption), medium (400–1000 kW power consumption) and large scale data centers (4000–10,000 kW) power consumption [33]. Recovered energy can be supplied to the DH grid or shared with adjacent buildings using heat pumps. Different strategies for feeding DH grid are being developed to ensure minimal losses in energy transition process. One of crucial aspects is the temperature of waste heat [43].

The temperature of heat extracted from data centers as summarized by Ebrahimi et al. is dependent on the type of cooling system used in data center [44] (see Table 3). For each temperature range there is the most suitable waste heat utilization purpose. The lowest grade can be utilized at the building itself as a pre - heater, but for district heating higher temperatures are needed >60°. Two phase cooling system provides the highest temperature, thus providing more flexibilities for waste heat utilization, and allows to recover heat with higher efficiency rate as recognized by Huang et al. [42]. To ensure utilization of waste heat and transmit the heat captured to other energy carrier heat exchanger for lower temperatures and heat pumps for higher temperatures are needed.

Based on the findings of Lu [45] et al. identifying the amount of waste heat recoverable from 1 MW data center, a calculation was performed to evaluate possible energy recovery from data center in selected urban block. The installed power in data center is

Table 5
Energy and CO2 savings introducing PEB concept to historic urban block.

Technology used	Energy savings		m²	Energy generation		CO₂
	Heating	Electricity		Electricity	Thermal energy	CO₂ savings
	MWh	MWh	m²	MWh	MWh	tons
Building energy efficiency related energy savings	2686	2400	–	–	–	970
Waste heat utilization						
DC Waste heat	–	–	–	–	338	89
Utilized cooling energy demand - -			–	–	83	22
Energy production						
Usefull roftop area						
Rooftop area covered with PV	–	–	5965	1014	–	111
Rooftop area covered with PVT	–	–	3895	425	1380	411
Facades	–	–				
Useful area of South - East facades	–	–	1307	135	–	15
Useful area of South - West facades	–	–	835	89	–	10
				1663	**1800**	**1627**
Percentage from total energy demand of selected				69%	100%	

0,06 MWh. Based on Pärssinen et al. analysis of different sizes of data centers [33] proportional evaluation was carried out (Table 4).

19% of total heating demand could be covered by waste heat regenerated from 0,06 MWh data center situated in the middle of urban block.

Renewable energy technologies. RES technologies considered for energy generation are − photo-voltaic/thermal panels, photo-voltaic panels on rooftops, building integrated photovoltaic systems for South − East and South − West facades on buildings built after 1945 and on the exposed brand walls of historic buildings (Fig. 12). Total area available for RES technologies is summarized in Table 5.

In the scope of this study at the preliminary calculation phase it is assumed, that two phase cooling system is used to capture heat from data center and heat pumps for capturing heat from other cooling units supplying offices, administrative buildings, different shops, catering within the block for preheating the domestic hot water. At this − preliminary calculation phase, it is assumed, that all generated energy can be directly utilized within the selected urban block or fed into grid (both electric and DH) when there is surplus energy generated and extracted from the grid when RES technologies do not cover instantaneous energy demand.

5. Results − energy and CO2 savings

Eventual energy and CO_2 savings derived from preliminary evaluation are summarized in Table 5. For PVT electricity and thermal energy generation calculation Pakere et al. findings are used − 109 kWh/m^2 and 443 kWh/m^2, respectively [46]. The calculation suggests that all thermal energy needed to cover heating demand can be generated on site. Since there are energy intensive electricity consumers within the block, only 69% of electricity demand can be generated on site.

In Latvia, the CO_2 emission factor for district heating is 264 kg$_{CO2}$/MWh, whereas for electricity it is 109 kg$_{CO2}$/MWh. For existing situation within the selected block, CO_2 emissions from heating are 1188 tons and from electricity − 523 tons per year (1712 all together). Setting a goal of 50% electricity consumption savings and 60% of heating demand reduction, and introducing waste heat recovery systems and RES technologies in selected block gives overall CO_2 savings of 1627 tons per year.

To reach the Positive Energy block level even more ambitious energy saving target should be set. Reducing electricity consumption by 65% would allow achieving Positive Energy block level. However, with energy intensive consumer, such as data center, that might be a challenge due to the strict standards for the service.

To use generated energy more efficiently at periods when energy demand is lower than energy production level e − mobility would be one more sector to be included in smart energy system, to ensure efficient and flexible energy storage.

6. Discussions

Preliminary evaluation of possibilities to transform urban block in historic center to a positive energy block has revealed some limitations. Further challenges of this research will be:

- Since the preliminary calculation indicates that electricity demand cannot be covered by on - site generation, at the next research phase, while designing the overall smart energy system, all the possible waste heat amount shall be utilized at the full potential;
- Off - site renewable energy generation shall be considered;
- Historic urban structures are complicated: density of built structure is high, the distance between buildings is smaller than in newly built structures, and preservable historical value, which limits energy efficiency measures. Innovative technologies shall be considered;
- To find suitable and efficient energy efficiency improvement solutions for thermal envelope of historic buildings;
- Full potential of energy efficiency improvement measures in buildings built in 1960−1980 shall be explored to lower overall energy demand within the urban block;
- Economic feasibility might be a challenge. Innovative technologies might be more expensive and particular design for challenging historical structure might be energy and CO_2 intensive. The optimum between invested and saved money and CO_2 shall be found as well as initial building energy efficiency measures and on-site available energy production shall be well balanced.

In other urban blocks, where there are no energy intensive consumers and balance between historically valuable buildings and buildings built in 1960−1980 is in favor of historic buildings, there would not be or would be limited possibilities for waste heat recovery on one hand, but on the other hand, specific electricity demand per square meter most probably would be smaller.

Energy consumption data analysis highlighted sharp differences in energy consumption among units in selected urban block. Thus prior to developing energy sharing concepts the level of possible energetic independency of each building shall be evaluated.

To deeply understand the correlation of cultural preservation impact on decarbonization strategies and vice versa 3 design

concepts will be developed following 3 different pathways:

- *"Baukultur* first" would be the business as usual (BAU), following existing stringent requirements for preservation of architectural heritage, emphasizing the importance of authentic substance;
- "energy efficiency first", maximizing energy efficiency measures in deep renovation concept aiming to reach nZEB level and pushing boundaries of cultural heritage preservation boundaries;
- "Positive energy block" concept using state of art technologies and smart energy system advantages creating conceptually new approach to the urban regeneration in historic center.

The next steps of research methodology — exploration and design should incorporate:

1. Urban regeneration strategies performing deep renovation and. Innovative technologies of increasing thermal resistance of building thermal envelope respecting the cultural heritage values.
2. Cross - sectional inclusive smart energy systems taking account all energy carriers.
3. Up to date ICT, IoT, AI technologies for smart grids and smart energy systems.
4. Waste heat recovery technologies.
5. Renewable energy technologies in densely built urban environment.
6. Energy storage solutions — electric and thermal; short - term and seasonal.

7. Conclusions

Aiming for carbon neutral future in 2050, the focus shall be redirected to the existing building structures, since there lies a great potential for cutting CO_2 emissions.

Preliminary calculations of eventual CO_2 savings in transition from traditional historic urban block to Positive Energy Block show the potential of ~45 kg/m^2 CO_2 savings per year reducing from 50 to 5 kg/m^2 CO_2 emissions per year and 1627 tons per year overall. According to the calculated results, heating energy demand can be fully covered with the energy generated on site (using storage or feeding the district heating grid), but to cover electricity demand in case of energy intensive consumers off-site production is needed.

In Latvia, specific primary energy level for nearly zero energy buildings is 95 kWh/m^2 per year that results in 10—18 kg/m^2 CO_2 emissions. The proposed conceptual framework aims to lower the benchmark for energy efficiency and carbon footprint to move towards a carbon neutral future.

The overall methodology of this study can be used for building blocks in any other urban structure worldwide. However, each step demands a local expertise: 1) energy efficiency measures should be tailored to fit the local climate; 2) renewable energy technologies should take advantage of particular surroundings and climate conditions; 3) and preservable historic values are also local in nature.

To tackle climate change energy efficiency measures must be targeted to the most polluting structures — cities. Positive Energy Block initiative is one of the decarbonization tools used for cities. In the transition from traditional historic urban block to PEB two contradicting concepts should come to an agreement — the preservation of cultural heritage and "energy efficiency first" concept driving the climate action policies.

The methodology for transition from traditional historic urban block to PEB is presented in paper using cross — sectorial holistic approach in decarbonization concept. The preliminary calculation based on the milestones of the described methodology in case study exploring the urban quarter in Riga Historic center shows the potential of reaching very low energy demand in the block thus encouraging further research.

The findings of this and further research steps dealing with retrofitting to nZEB and plus level in historic city centers shall accommodate a discussion among environmental engineers, architects, local city planners, authorities and the general public, what our common future in the cities will be.

Declaration of competing interest

The authors declare that they have no known competing financial interests or personal relationships that could have appeared to influence the work reported in this paper.

References

[1] Tong S, Ebi K. Preventing and mitigating health risks of climate change. Environ Res Jul. 2019;174:9—13.
[2] Vogel MM, Zscheischler J, Wartenburger R, Dee D, Seneviratne SI. "Concurrent 2018 hot extremes across Northern Hemisphere due to human-induced climate change,". *Earth's Futur.*; Jun. 2019. 2019EF001189.
[3] Brondízio E, Settele J, Diaz S, Ngo TH. The global assessment Report on biodiversity and ecosystem services. 2019.
[4] IPPC. Special Report: global warming of 1.5 °C. 2018.
[5] UNFCC. "Paris Agreement; 2015.
[6] Seneviratne SI, et al. "The many possible climates from the Paris Agreement's aim of 1.5 °C warming. Nature Jun. 2018;558(7708):41—9.
[7] Gao Y, Gao X, Zhang X. "The 2 °C global temperature target and the evolution of the long-term goal of addressing climate change—from the united nations framework convention on climate change to the Paris agreement. Engineering Apr. 2017;3(2):272—8.
[8] UN. Hot cities: battle-ground for climate change CHANGE," *UN habitat. Glob. Rep. Hum. Settl.*, no. March 2011:2.
[9] Directorate-general for research and innovation (European commission); joint research centre (European commission), "strategic energy technology. ": SET) Plan; 2017.
[10] Alpagut B, Akyürek Ö, Mitre EM. Positive energy districts methodology and its replication potential. Proceedings 2019;20(1):8.
[11] Temporary Working Group of the European Strategic Energy Technology. "Set-plan Action no 3.2. Implementation Plan Europe to become a global role model in integrated , innovative solutions for the planning , deployment , and replication of Positive Energy Districts," no. 2018. June.
[12] Backe S, Crespo P, Tomasgard A. "Local flexibility markets in smart Cities : interactions between positive energy blocks, vol. 1; 2019. p. 25—9.
[13] Dean B, Dulac J, Petrichenko K, Graham P. Towards a zero-emission, efficient, and resilient buildings and construction sector. 2016.
[14] "EUR-Lex - 32018L0844 - EN - EUR-Lex.". https://eur-lex.europa.eu/legal-content/EN/TXT/?toc=OJ%3AL%3A2018%3A156%3ATOC&uri=uriserv%3AOJ.L_.2018.156.01.0075.01.ENG. [Accessed 16 May 2019].

[15] Lund H, Østergaard PA, Connolly D, Mathiesen BV. "Smart energy and smart energy systems," *Energy* Oct. 2017;137:556−65.

[16] O'Dwyer E, Pan I, Acha S, Shah N. Smart energy systems for sustainable smart cities: current developments, trends and future directions. Appl Energy Mar. 2019;237:581−97.

[17] Dileep G. A survey on smart grid technologies and applications. Renew Energy Feb. 2020;146:2589−625.

[18] European Commission. Definition, expected services, functionalities and benefits of smart grids 2012;66:37−9.

[19] Tsiatsis V, et al. Smart grid. " *Internet of Things*; Jan. 2019. p. 257−68.

[20] Lund H. Renewable heating strategies and their consequences for storage and grid infrastructures comparing a smart grid to a smart energy systems approach. Energy May 2018;151:94−102.

[21] Harrestrup M, Svendsen S. Changes in heat load profile of typical Danish multi-storey buildings when energy-renovated and supplied with low-temperature district heating. Int J Sustain Energy 2015;34(3−4):232−47.

[22] Pérez-Lombard L, Ortiz J, Pout C. A review on buildings energy consumption information. Energy Build 2008;40(3):394−8.

[23] EU. Directive (EU) 2018/2001 of the European Parliament and of the Council on the promotion of the use of energy from renewable sources," *off*. J. Eur. Union 2018;2018(328):82−209.

[24] European Parliament, Council of the European Union. Directive 2010/31/EU of the European Parliament and of the council of 19 May 2010 on the energy performance of buildings. Off. J. Eur. Union 2010;L 153(18.6.2010):13−35.

[25] Henrik Lund PS, Østergaard Poul Alberg, Connolly David. Iva ridjan, brian vad mathiesen, frede hvelplund, jakob zinck thellufsen, "energy storage and smart energy systems. Int. J. Sustain. Energy Plan. Manag. 2016;11:3−14.

[26] Hansen K, Breyer C, Lund H. Status and perspectives on 100% renewable energy systems. Energy May 2019;175:471−80.

[27] Bogdanov D, Toktarova A, Breyer C. Transition towards 100% renewable power and heat supply for energy intensive economies and severe continental climate conditions: case for Kazakhstan. Appl Energy Nov. 2019;253:113606.

[28] Hansen K, Mathiesen BV, Skov IR. Full energy system transition towards 100% renewable energy in Germany in 2050. Renew Sustain Energy Rev Mar. 2019;102:1−13.

[29] Dóci G, Vasileiadou E, Petersen A, Dóci G, Vasileiadou E, Petersen A. Renewable energy communities,". *Elsevier*; 2018. p. 1−21.

[30] Carlisle N, Otto A, Geet V, Pless S. "Definition of a "zero net energy" community,". November, 2009.

[31] ICOMOS. The Future of our Pasts: engaging cultural heritage in climate action. 2019.

[32] Eglė Navickienė LA. Edita Riaubienė, Vilnius Gediminas Technical University,

"Changes of approach to urban context in international guidelines and experiences in Lithuanian urban environment. Sci. J. Latv. Univ. Life Sci. Technol. 2018;13(13):7−17.

[33] Pärssinen M, Wahlroos M, Manner J, Syri S. Waste heat from data centers: an investment analysis. Sustain. Cities Soc. Jan. 2019;44:428−44.

[34] Blumberga A, Vanaga R, Freimanis R, Antužs J, Bondars E, Treija S. Is the high quality baukultur a monkey wrench in the global climate challenges? | enhanced reader. Environ. Clim. Technol. 2019;23(3):230−44.

[35] "Gehl-12-Criteria-EN.png (PNG image, 4135 × 5315 pixels) - scaled (17%).". https://mcconnellfoundation.ca/wp-content/uploads/2017/11/Gehl-12-Criteria-EN.png. [Accessed 16 May 2019].

[36] Dodoo A, Gustavsson L, Tettey UYA. Final energy savings and cost-effectiveness of deep energy renovation of a multi-storey residential building. Energy Sep. 2017;135:563−76.

[37] Zangheri P, Armani R, Pietrobon M, Pagliano L. Identification of cost-optimal and NZEB refurbishment levels for representative climates and building typologies across Europe. Energy Effic. Feb. 2018;11(2):337−69.

[38] Fakhim B, Behnia M, Armfield SW, Srinarayana N. Cooling solutions in an operational data centre: a case study. Appl Therm Eng Oct. 2011;31(14−15): 2279−91.

[39] Karlsson JF, Moshfegh B. Investigation of indoor climate and power usage in a data center. Energy Build Oct. 2005;37(10):1075−83.

[40] Lee KP, Chen HL. Analysis of energy saving potential of air-side free cooling for data centers in worldwide climate zones. Energy Build Sep. 2013;64:103−12.

[41] Zimmermann S, Meijer I, Tiwari MK, Paredes S, Michel B, Poulikakos D, Aquasar ". A hot water cooled data center with direct energy reuse. Energy Jul. 2012;43(1):237−45.

[42] Huang P, et al. A review of data centers as prosumers in district energy systems: renewable energy integration and waste heat reuse for district heating. Appl Energy 15-Jan;258. Elsevier Ltd.

[43] Capozzoli A, Primiceri G. Cooling systems in data centers: state of art and emerging technologies. In: Energy procedia. vol. 83; 2015. p. 484−93.

[44] Ebrahimi K, Jones GF, Fleischer AS. A review of data center cooling technology, operating conditions and the corresponding low-grade waste heat recovery opportunities. Renew Sustain Energy Rev 2014;31:622−38. Elsevier Ltd.

[45] Lu T, Lü X, Remes M, Viljanen M. Investigation of air management and energy performance in a data center in Finland: case study. Energy Build Dec. 2011;43(12):3360−72.

[46] Pakere I, Lauka D, Blumberga D. Solar power and heat production via photovoltaic thermal panels for district heating and industrial plant. Energy Jul. 2018;154:424−32.

Ritvars Freimanis dzimis 1988. gadā. Rīgas Tehniskajā universitātē ieguvis maģistra grādu vides zinātnē (2019). Paralēli tam absolvējis arī Viļņas Ģedimina tehnisko universitāti, iegūstot maģistra grādu vides inženierijā. Patlaban ir RTU Elektrotehnikas un vides inženierzinātņu fakultātes Vides aizsardzības un siltuma sistēmu institūta pētnieks un lektors. Institūtā nostrādāto sešu gadu laikā ir publicējis 21 zinātnisko publikāciju, ir viena patenta līdzautors. Ieguldījumu zinātnisko projektu īstenošanā sniedzis, darbojoties Eiropas Savienības īstenotā projektā *"RIBuild"*, kur asistējis Ēku energoefektivitātes laboratorijas izveidē. Turpina aktīvi darboties zinātniskajā pētniecībā, līgumdarbu īstenošanā un laboratorijas darbu praktiskās daļas vadīšanā Ēku energoefektivitātes laboratorijā.